
**Università degli Studi Roma Tre**

Dipartimento di Matematica e Fisica
Doctoral program in Physics – XXXIV cycle

A thesis presented for the degree of
Doctor of Philosophy in Physics

# The neutron proton mass difference in Lattice QCD+QED

*Author:*
**Simone Romiti**

*Supervisors:*
Prof. **Vittorio Lubicz**
Dr. **Silvano Simula**

*Doctoral Program Coordinator:*
Prof. **Giuseppe Degrassi**

October 2021

*To my mother and my sister,*
*for their love and invaluable support.*

# Declaration of authorship

I, Simone Romiti, declare that this thesis titled "The neutron proton mass difference in Lattice QCD+QED" and the work presented in it are my own. I confirm that:

- Where I have consulted the published work of others, this is always clearly attributed.
- Where I have quoted from the work of others, the source is always given. With the exception of such quotations, this thesis is entirely my own work.
- Where the thesis is based on work done by myself jointly with others, this is clearly stated.
- Parts of this thesis have appeared and should appear in the following papers:
  - Romiti S., Simula S., 2019. Extraction of multiple exponential signals from lattice correlation functions. Physical Review D, 100(5), p.054515.
  - Romiti S. *The neutron-proton mass difference*, PoS LATTICE 2021
  - Romiti S. *Leading Isospin Breaking effects in the nucleon and* $\Delta$ *masses*, PoS HADRON 2021
- This work was done within the period of my PhD fellow, namely from 1 November 2018 to the submission date of the present thesis, 31 October 2021.
- I have acknowledged all main sources of help.

Sign (Simone Romiti):

_____

Date:

_____

# Ringraziamenti

La fine del mio corso di dottorato rappresenta anche la conclusione di un lungo percorso qui a Roma Tre. Tra laurea triennale, magistrale e dottorato sono volati 8 anni. Guardandomi indietro rivedo momenti di intense emozioni, momenti di soddisfazione ma anche di difficoltà, nei quali le persone a me vicine hanno giocato un ruolo determinante. Sento quindi di dover ringraziare molte di loro, e spero di menzionarle tutte in questa sezione.
Ringrazio affettuosamente mia madre e mia sorella, alle quali dedico questa tesi.
A seguire, i miei ringraziamenti vanno naturalmente ai miei supervisori, Silvano e Vittorio. Con loro ringrazio anche tutti gli altri membri della nostra collaborazione di QCD su reticolo. In particolare Francesco, Cecilia e i professori G. Martinelli e N. Tantalo, per il loro prezioso supporto e i chiarimenti. Lo stesso dicasi per tutti gli altri miei ex insegnanti più stimati, ai quali spero di aver sempre trasmesso il mio senso di soddisfazione nei loro confronti.
Ringrazio poi i miei colleghi di dottorato, per i momenti di leggerezza nelle pause lavorative e i gustosi pranzi ad Ariccia! Grazie ad Alessio, Alessio Mattia, Chiara, Daniele, Laura, Lorenza, Marco, Maria Teresa, Martina e Lorenzo. Tra loro un posto speciale è riservato ad Alessio, Alessio Mattia, Chiara e Daniele, "fratelli e sorelle d'arme" dal mio primo anno a Roma Tre insieme a Camilla e Alessandro. Con loro ho passato molto tempo difficile da dimenticare. Dedico uno spazio anche ad Andrea e Giampiero, i portieri del nostro dipartimento e vicini di ufficio. È stato un piacere avervi alla porta accanto e condividere i nostri festeggiamenti in Acquario. Colgo anche l'occasione per augurare un buon proseguimento di dottorato agli studenti più giovani, in particolare ai miei compagni di stanza Raul e Sacha.
Ringrazio i miei amici più stretti che non ho già menzionato, per la loro partecipazione e i loro consigli in questo periodo di forti cambiamenti. Tra loro, il mio più caro e vecchio amico Francesco, per la sua preziosa amicizia e supporto. A seguire i miei cari amici Alex, Antonio, Emilia e Giorgia, per i felici momenti passati assieme come una famiglia.
Desidero ringraziare anche Valerio Vicari, lo stimato direttore artistico di Roma Tre Orchestra, per il suo costante e nobile impegno nel promuovere la cultura musicale attraverso questo ateneo. Non posso poi non menzionare Claudio Calvani, che ringrazio moltissimo per il suo supporto tecnico e disponibilità nei momenti di bisogno. Sempre tra il personale di dipartimento, rivolgo un ringraziamento alle splendide ragazze della nostra segreteria, in particolare a Filomena Foglietta, Marina Mongiorgi, Serena Macinetti e Valentina Feliciello.
Per ultimi, ma non per importanza, sono molto grato ai miei insegnanti di matematica e fisica del liceo, il professor Ferdinando Galdi e soprattutto la professoressa Costanza Mazzetti. Quest'ultima è stata fondamentale per la mia formazione e la scelta del mio percorso di studi universitario, che senza di lei sarebbe stato probabilmente molto diverso.

# Software

Here I list the software resources that played a significant role in the development of this thesis. This can serve as a reference list, but also as an acknowledgment to software developers. On my computer I installed the `GNU-Linux` Operating System `Ubuntu 20.04 LTS` . The numerical simulations needed to calculate the Lattice correlators of this work were done on the `Marconi` supercomputer of the `CINECA` . For that I used `nissa` , a set of `C++` libraries for $SU(N)$ algorithms hosted at the following repository: `https://github.com/sunpho84/nissa`. The analysis were carried out using a set of `C++` and `Python3` libraries of my creation: `https://gitlab.com/simone-romiti/silibs2.git`. The latter make use of the `Boost C++ Libraries` libraries, and of `Minuit2` for non-linear minimization in curve fitting. The code for plots and generic scripting were done in `Python3` , with heavy use of the `matplotlib` and `numpy` libraries. For symbolic calculations I found very useful the `simpy` library. I also used `Wolfram Mathematica` , for which I'm grateful to my University for having provided the license to PhD students. The present document was typeset using the LaTeX software system. All the Feynman diagrams were drawn using the `Jaxodraw2.0` software and the corresponding `axodraw4j` LaTeX package.

# Contents

# Introduction

In nature we observe a rich variety of phenomena, which we understand as interactions among different parts of the universe. Over the millennia scientists and philosophers have wondered on why these events happen, and how they can be understood in terms of fewer and fewer fundamental laws.
At present our picture is the following. There exist some elementary (i.e. null size) particles, which can join to form complicated structures: nuclei, atoms and molecules, living things, planets and solar systems, galaxies and so on.
Above the Plank scale ($\ell_P = \sqrt{\frac{\hbar G}{c^3}} \approx 1.6 \cdot 10^{-35}$ m), we understand their dynamics in terms of 4 fundamental interactions [1]. These are the gravitational, electromagnetic (EM), weak and strong nuclear forces.
The theory of General Relativity predicts the behavior of macroscopic systems at large distances, while the Standard Model (SM) is the best confirmed quantum field theory (QFT) so far. In this theory each particle is associated to a field, whose interaction with the others is responsible for particle creation and annihilation. The fundamental forces comes from symmetry principles and the masses are generated by the *Higgs mechanism*.
The SM has proven to be extremely effective, leading to unprecedented level of precision in particle physics. Despite its unquestionable success in precision, hints of its failure may come through the measure of the famous muon's $g_\mu - 2$, on which the debate is still open.
Moreover the SM can't be the end of the story in any case, for more than one reason. First of all it doesn't include gravity, which must be treated separately. Its interactions are not unified, we don't know what happens at the Plack scale, and it doesn't contain a valid candidate for Dark Matter (which accounts for the majority of the mass content of the Universe [2]). Moreover, it contains 18 free parameters whose values are not explained. We don't know the origin of mass hierarchies, and the violation of the $CP$ symmetry coming from them is not enough to account for the matter-antimatter asymmetry observed in nature.
It is clear that some New Physics (NP) is to be discovered, and the way to takle this problem is done from various sides. Theorists provide new models in which new particles may occur, and experimentalists try to reveal them in detectors. Typically, for heavy and short-lived particles we rely on high energy accelerators, while long-lived elusive candidates are searched through their interaction with ordinary matter.
In order to disprove a model, also indirect proofs are important. Phenomenological physicists work to improve the theoretical prediction of observables, jointly with the experimental measure. The aim is to find significative discrepancies between theory and experiment, in order to lead the model building to the right direction.
Flavour physics is a branch of phenomenology which studies the consequences of the

flavour structure in the SM. Of particular interest is quark flavour physics, which investigates the consequences of the quark parameters in the SM Lagrangian.
Quarks and gluons are the fundamental degrees of freedom of Quantum Chromo-Dynamics (QCD), the QFT describing hadronic processes. The former are not eigenstates of weak interactions too, but mix according to the Cabibbo-Kobayashi-Maskawa (CKM) matrix [3]:

$$V_{CKM} = \begin{bmatrix} V_{ud} & V_{us} & V_{ub} \\ V_{cd} & V_{cs} & V_{cb} \\ V_{td} & V_{ts} & V_{tb} \end{bmatrix} \quad . \tag{0.1}$$

Since this matrix is the only responsible for $CP$ violation in the SM (provided that the strong $CP$ parameter $\theta$ is exactly zero), the study of its properties is of interest in solving the puzzle of matter-antimatter asymmetry. The independent measure of its entries can be used to test the SM, searching for deviations from unitarity ($V^{-1} = V^{\dagger}$). A possible way is to consider the leptonic and semi-leptonic decay rates such as the neutron $\beta$ decay: $n \to pe\bar{\nu}_e$. In the latter the decay width contains $V_{ud}$ [4]:

$$\Gamma = \frac{G_F^2 m_e^5}{(2\pi^3)} |V_{ud}|^2 \left[1 + 3g_A^2\right] f^{p.s.}(1 + \Delta_R) \quad , \tag{0.2}$$

where $G_F$ is the Fermi constant, $m_e$ the mass of the electron and $g_A$ the nucleon-axial coupling. $f^{p.s.}$ is a phase space factor and $\Delta_R$ accounts for radiative corrections.
Currently the best determination of $V_{ud}$ comes from 14 super-allowed nuclear beta decays ($0^+ \to 0^+$) (see [3, 5]), and radiative corrections come from model-dependent assumptions (see e.g. [6]). If we had more precise information about the EM corrections to the $\beta$ decay, we could correct these nuclear decay widths and hopefully improve the testing of the SM through $V_{ud}$.
The problem is that hadronic scattering processes and decays are determined by the structure of hadrons. These effects are hard or often impossible to find analytically, given the intrinsic nature of strong interactions. QCD is non-perturbative at low energies, and analytical first principle calculations are unfeasible .
A solution to the latter on a discretized space-time lattice is provided by Lattice QCD (LQCD), a regularization of QCD which can be implemented numerically [7]. Moreover, at present, the latter is the only way to treat non-perturbative hadronic effects from the first principles of the theory without adding additional parameters besides those present in the QCD action.
The inclusion of EM effects in in leptonic and semi-leptonic decays from lattice calculations has been done only recently ([8], [9], [10], [11] ). The case of the neutron is of interest because from its $\beta$ decay we can measure $V_{ud}$. Apart from decay processes, the inclusion of electromagnetism in lattice calculations has now become mandatory in several of them. In fact, many lattice computations in pure QCD in the Isospin symmetry limit have reached the $O(1\%)$ precision. The two main Isospin Breaking (IB) effects are indeed $O(1\%)$ corrections, coming from $\hat{m}_d - \hat{m}_u$, the mass difference between the $u$ and $d$ quarks, and $\hat{\alpha}_{EM}$, the EM fine structure constant. IB modifies the spectrum of hadrons, also removing the degeneracy in hadronic multiplets.
In this thesis the effects of IB on the masses of mesons and baryons are investigated, focusing on the $N$ and $\Delta$ multiplets. The calculation was done at Leading Order (LO) in $\frac{\hat{m}_d - \hat{m}_u}{\Lambda_{QCD}}$ and $\hat{\alpha}_{EM}$ using the well established RM123 method [12]. The latter

consists in evaluating the observables in QCD+QED expanding at 1st order in these parameters. The quantities in the full theory (QCD+QED) are given by the sum of the isosymmetric part, i.e. evaluated in QCD with isospin symmetry, plus the IB contribution, namely the one given by $O(\alpha)$ and $O(\frac{\hat{m}_d - \hat{m}_u}{\Lambda_{QCD}})$ (neglecting higher orders). The slopes multiplying these factors can be evaluated in the isosymmetric theory, so that the IB correction is given by the combination of isosymmetric slopes with the appropriate charge factors and mass conterterms.
A purely hadronic renormalization scheme was adopted, using $\pi$s, $K$s and $\Omega^-$ masses as normalization parameters to set the scale, tune the counterterms and reach the physical point. We also define a scheme for the separation of the so called *strong IB* and *QED* contributions. The first represents the modification due to the mass difference between $u$ and $d$, while the remaining part stems from interaction of quarks with the photon field. The separation of these two effects is arbitrary but mantains some rather useful physical intuition.
The first aim was to determine $M_n - M_p$. The latter is the available phase space for the aforementioned $\beta$ decay. The fact that it's positive is the necessary condition for the decay to happen (in inertial frames). In this sense, finding this quantity is reasonably the first and preliminary step to face up to EM correction in neutron $\beta$ decay.
The other quantities of interest are the masses of the $\Delta$ resonances and their splittings. $\Delta$s are unstable and their spectrum is not completely determined yet experimentally. Masses and decay widths of these resonances are used in effective $\pi N$ interaction models, both for accelerator experiments as well for astrophysical models in the dynamics of compact objects.
The results found in this work are listed below. The uncertainties are statistical and obtained using the jackknife resampling technique.

$$M_N = 0.9549(97)\,\text{GeV} \quad , \tag{0.3}$$

$$\sigma_{\pi N} = 43.2(1.4)\,\text{MeV} \quad , \tag{0.4}$$

$$M_\Delta = 1.261(30)\,\text{GeV} \quad , \tag{0.5}$$

$$\sigma_{\pi\Delta} = 24.55(77)\,\text{MeV} \quad , \tag{0.6}$$

$$M_n - M_p = 1.73(69)\,\text{MeV} \quad , \tag{0.7}$$

$$(M_n - M_p)^{(QED)} = -1.16(25)\,\text{MeV} \quad , \tag{0.8}$$

$$(M_n - M_p)^{(QCD)} = 3.10(59)\,\text{MeV} \quad , \tag{0.9}$$

$$M_n = 0.961(20)\,\text{GeV} \quad , \tag{0.10}$$

$$M_p = 0.959(20)\,\text{GeV} \quad . \tag{0.11}$$

The masses of the $\Delta$ are reported in the following table.

| | $M$(GeV) |
|---|---|
| $\Delta^-$ | 1.251(40) |
| $\Delta^0$ | 1.247(39) |
| $\Delta^+$ | 1.245(39) |
| $\Delta^{++}$ | 1.244(39) |

Table 1: Our results for the masses of the 4 lightest $\Delta$ resonances.

In the following table are reported the mass splittings in the $\Delta(1232)$ quadruplet. As we'll see, at LO in IB the knowledge of only 2 of them is sufficient to determine the others.

| | $\Delta M$(MeV) |
|---|---|
| $\Delta^{++} - \Delta^+$ | -0.48(26) |
| $\Delta^{++} - \Delta^0$ | -2.06(38) |
| $\Delta^{++} - \Delta^-$ | -4.76(55) |
| $\Delta^+ - \Delta^0$ | -1.59(18) |
| $\Delta^+ - \Delta^-$ | -4.41(50) |
| $\Delta^- - \Delta^0$ | 2.85(35) |
| $(\Delta^{++} + \Delta^-) - (\Delta^+ + \Delta^0)$ | 2.41(51) |

Table 2: Our results for the mass splittings among the 4 lightest $\Delta$ resonances.

Using the values of the renormalization constants $Z_P$ in the $\overline{\text{MS}}$ scheme from [13] we also find the following renomalized values:

$$\hat{m}_\ell(\mu = 2\,\text{GeV}) = \frac{\hat{m}_u + \hat{m}_d}{2} = 3.781(76)\,\text{MeV} \tag{0.12}$$

$$\hat{m}_s(\mu = 2\,\text{GeV}) = 103.2(2.0)\,\text{MeV} \tag{0.13}$$

$$\Delta\hat{m}_{ud}(\mu = 2\,\text{GeV}) = \frac{\hat{m}_d - \hat{m}_u}{2} = 1.208(43)\,\text{MeV} \tag{0.14}$$

The thesis is structured as follows:

- In Chapter 1 the Lattice regularization of QCD is presented. We'll see how to quantize quarks and gluons on the lattice with the path integral formalism, how to build hadronic euclidean correlators and extract their properties. We'll briefly review the numerical issues involved, the twisted mass regularization used to simulate QCD in the present study, and renormalization.

  On the lattice hadronic masses and matrix elements have a dependence on the parameters in the Lagrangian, the lattice spacing and the volume size. We discuss how to take into account these effects, set the scale of the system and extrapolate observables to their physical values.

- Chapter 2 is devoted to the theoretical framework used to treat IB effects, i.e. the RM123 method. We show how to expand the path integral in a theory containing QCD and QED (QCD+QED) at LO in $\hat{m}_d - \hat{m}_u$ and $\hat{\alpha}_{EM}$. At LO, all calculations can be done on a Isospin symmetric background, finding the

slopes with respect to the perturbation parameters. The combination of these slopes with the correct counterterms and charge factors give the value of the observables in the full theory.

QED is a long-range interaction. This leads to Finite Volume Effects which are suppressed as power-laws (not exponentially like in QCD), which we take into account using the known theoretical results together with a fit over a number of different volumes. We also discuss in some detail how one can define a separation between *strong IB* and QED effects, and the intuition behind it.

- Chapter (3) describes the analysis of isosymmetric quantities. We give the definition of the hadronic renormalization scheme, with the discussion of the extrapolation technique. It is discussed how to treat finite size effects, discretization effects and dependence on the quark masses. We find the isoQCD limits of $M_N$ and $M_\Delta$, together with the sigma terms $\sigma_{\pi N}$. and $\sigma_{\pi\Delta}$.

- In Chapter (4) are shown the details of the calculation of IB effects at LO. We tune the critical mass counterterms from the PCAC Ward Identity (WI) in order to preserve the maximal twist (and so the $O(a)$ improvement on observables). We use 3 ratios in QCD+QED in order to tune physical mass countertems for each ensemble. We correct the masses from universal QED finite volume effects and extrapolate the physical values of the observables taking into account the residual rependence on $L$, $a$ and $M_\pi$.

# Chapter 1

# Introduction to Lattice QCD

A lattice field theory (LFT) is a Quantum Field Theory (QFT) in which space-time is bounded and discretized. In such a theory the universe is typically chosen to be an hyper-cubic lattice embedded in $\mathbb{R}^4$ of size TxLxLxL (where T is the time extension and L the length of the $3D$ cube's side), nearest neighbors are separated by a lattice constant $a$, and some specific conditions are given at the boundaries.
This technique is useful to deal with non-perturbative theories such as Quantum ChromoDynamics (QCD) for which the non-perturbative regime falls in the low-energy range[1]. In fact it's not possible to get a safe theoretical evaluation through perturbation theory of hadronic low-energy contributions. LQCD allows to calculate quantities of physical interest numerically without any expansion with respect to coupling constants.
The main idea is to simulate a lattice universe and, by using path integral formalism, evaluate some quantities which contain information about hadrons. Nevertheless, due to simulation constraints, lattice QCD is not a faithful description of the actual hadrons, for which one must recover the real-world values performing the *continuum limit* ($a \to 0$), the *infinite volume limit* ($L \to \infty$), and the *infinite temporal extension limit* ($T \to \infty$), named also the *0 temperature limit* [2]. The first limit recovers the continuity of spacetime, while the second and third ones remove the effects due to the imposition of boundary constraints.
Often one has to extrapolate also to the *physical point*, since the cost of the simulation may require to use quark masses different from the physical ones.
The structure of the chapter is the following.
In sec. (1.1) are discussed *Euclidean Correlators*. We derive the path integral representation for the simple case of a scalar field theory and shown the general structure of their spectral decomposition. In sec. (1.2) QCD on the lattice is presented. Some numerical aspects involved are also examined. Finally it is shown how to treat the extrapolation of hadronic observable and get physical predictions.
In sec. (1.3) we discuss how to build correlators and extract energies and matrix elements from them. In sec. (1.4) we present the leading systematic effects in the extracted quantities, and in sec. (1.5) some numerical aspects involved in lattice calculations.

[1] Experimentally this is found to be between 0 and $\Lambda_{QCD} \approx 200 - 300[MeV]$ [1].
[2] For more details about the thermodynamic terminology used here see sec. (1.1.1).

## 1.1 Correlators and fields on the lattice

Before entering the discussion on correlators and path integrals, it's useful to recap some algebraic properties of physical states and operators acting on them.
In Quantum Mechanics physical states are *rays* in a Hilbert space, a complex vector space $(\mathcal{V}, +, \cdot)$ equipped with a *sesquilinear* scalar product $\langle *; * \rangle$ which induces a norm $\|*\| = \sqrt{\langle *; * \rangle}$, and *complete* with respect to the latter. For $\mathcal{V}$ there exists a basis $\mathcal{B} = \{|e_1\rangle, |e_2\rangle, ...\}$ such that every $|\psi\rangle$ can be expanded, with respect to the above norm, as a linear combination of elements in $\mathcal{B}$:

$$|\psi\rangle = \sum_n c_n |e_n\rangle \quad . \tag{1.1}$$

The above basis may be chosen to be *orthonormal*, i.e. such that $\langle e_i | e_j \rangle = \delta_{ij}$ (every Hilbert space has an *orthonormal* basis). We'll assume that in the following unless explicitly stated.
The properties of such a Hilbert space are given by bounded linear operators [3]. The expectation value of an operator $\hat{A}$ on a state $|\psi\rangle$ is given by $\langle \hat{A} \rangle := \langle \psi | \hat{A} | \psi \rangle$.
The *hermitian conjugate* $\hat{A}^\dagger$ of $\hat{A}$ is defined via:

$$\langle \alpha | \hat{A} | \beta \rangle := \langle \beta | \hat{A}^\dagger | \alpha \rangle^* \quad \forall \alpha, \beta \in \mathcal{V}$$

An operator is *hermitian* when it coincides with its hermitian conjugate. In this case, the eigenvalues are real.
The identity operator $\hat{1}$ is the one which maps every vector into itself and, for an orthonormal basis, can be written as

$$\hat{1} = \sum_n |e_n\rangle \langle e_n| \quad .$$

The trace of an operator $\hat{A}$, always for an ortho-normal basis, is

$$tr[\hat{A}] = \sum_n \langle e_n | \hat{A} | e_n \rangle \quad .$$

Given the boundedness condition, operator functions are defined through their corresponding Taylor power series:

$$f(x) = \sum_n a_n x^n \quad \rightarrow \quad f(\hat{A}) = \sum_n a_n \hat{A}^n \quad .$$

The last two definition can be intuitively generalized to uncountable bases, with sums becoming integrals. To be precise however, the latter case requires some subtleties on the use of distributions (see [15]).
The Hamiltonian $\hat{H}$ of the system, assumed to be the generator of time translations, governs the evolution of the system. Its eigenvectors constitute a *complete* basis $\{|n\rangle\}_n$ for $\mathcal{V}$. In the following, we'll consider these states listed in ascending order according to the eigenvalues.
Each state can be described giving its quantum numbers: energy, spin, etc.

[3] In principle one has to consider also *antilinear* operators, but in the present work they won't be used. For a more in-depth analysis see [14].

Coherently with the indistinguishability of identical particles, in particle physics the state of the system is written in terms of the number of particles of each kind, with the creation and annihilation operators defined in order to satisfy Bose-Einstein or Fermi-Dirac statistics. Such a space is called the *Fock space*. The $|\psi\rangle$ is then a tensor product of many vectors, each of which corresponds to a given particle and characterized by the number of particles. Since elementary particles' quantum numbers are only 2, spin and momentum (or equivalently position), any state can be written as:

$$|\psi\rangle = |N_1, p_1, \sigma_1\rangle_{particle_1} \times ... \times |N_n, p_n, \sigma_n\rangle_{particle_n}$$

The vacuum, $|0\rangle$, is the state containing no particles:

$$|0\rangle_{particle_1} \times |0\rangle_{particle_2} \times ... \times |0\rangle_{particle_n} .$$

### 1.1.1 Path integral in QFT

Feynman's formulation of quantum mechanics consists in the interpretation of probability amplitudes as weighted sums (or integrals) over all possible configurations (*paths*). The dynamics of the system is governed by a Lagrangian $L$, and the expectation values can be rephrased as functional integrals over all configurations of the lagrangian variables [1]:

$$\sum_{(paths)} e^{iS/\hbar} \quad or \quad \int \mathcal{D}\{\eta\} e^{iS[\{\eta\}]/\hbar} \quad , \tag{1.2}$$

where the "paths" are the possible ways in which an event can occur and $\{\eta\}$ represents the degrees of freedom of the action. The classical limit is recovered through the stationary phase method when $\hbar$ is small.
In order to show how quantization works, let's now consider the simple case of the Klein-Gordon Lagrangian of a real scalar field, by constructing from the beginning the lattice version of the path integral.
In continuum space-time, the Lagrangian density $\mathcal{L}$ ($L = \int_{\mathbb{R}^3} d^3x\, \mathcal{L}$) for a spinless neutral field of mass $m$ is:

$$\mathcal{L} = \frac{1}{2}\left[(\partial_\mu\phi)(\partial^\mu\phi) - m^2\phi^2\right] - V(\phi) \quad . \tag{1.3}$$

with equations of motion,

$$\frac{\partial\mathcal{L}}{\partial\phi} = \partial_\mu\left(\frac{\partial\mathcal{L}}{\partial(\partial_\mu\phi)}\right) \quad , \tag{1.4}$$

The Hamiltonian density is given by the Legendre transform:

$$\mathcal{H} = \frac{\partial\mathcal{L}}{\partial(\partial_0\phi)}(\partial_0\phi) - \mathcal{L} = \pi\dot{\phi} - \mathcal{L} = \frac{1}{2}\left[\pi^2 + (\nabla\phi)^2\right] + V(\phi) \quad , \tag{1.5}$$

where $\pi = \frac{\partial\mathcal{L}}{\partial(\partial_0\phi)}$ is the canonical momentum field.

The second quantization procedure promotes $\phi$ and $\pi$ to operators satisfying the commutation relations [4]:

$$[\phi(\vec{x}), \phi(\vec{y})] = [\pi(\vec{x}), \pi(\vec{y})] = 0 \quad ; \quad [\phi(\vec{x}), \pi(\vec{y})] = i\delta(\vec{x} - \vec{y}) \quad . \tag{1.6}$$

The Hamiltonian density (operator) is the operator-promoted version of eq. (1.5). We now extend this to the lattice regularization. First, we replace the entire space with a cubic lattice $\Lambda_3$ with spacing $a$ and size $L = Na$, $N^3$ being the number of points. Positions become lattice points:

$$\vec{x} \quad \to \quad a\vec{n}, \quad \vec{n} \in \mathbb{N}^3 \wedge n_i \leq N \quad \forall i \quad . \tag{1.7}$$

Spatial derivatives are replaced by finite differences:

$$\partial_k \phi \quad \to \quad \Delta_k \phi(\vec{n}) = \frac{\phi(\vec{n} + \hat{k}) - \phi(\vec{n} - \hat{k})}{2a} \quad , \tag{1.8}$$

and the lattice Hamiltonian is:

$$H = a^3 \sum_{\vec{n} \in \Lambda_3} \left[ \frac{1}{2} \left( \pi(\vec{n})^2 + \sum_k \Delta_k \phi(\vec{n})^2 + m^2 \phi(\vec{n})^2 \right) + V\left(\phi(\vec{n})\right) \right] \quad . \tag{1.9}$$

The canonical commutation relations are:

$$[\phi(\vec{n}), \phi(\vec{m})] = [\pi(\vec{n}), \pi(\vec{m})] = 0 \quad ; \quad [\phi(\vec{n}), \pi(\vec{m})] = \frac{i}{a^3} \delta_{\vec{n}.\vec{m}} \quad . \tag{1.10}$$

Let's now contruct the path integral. The states $|\phi\rangle = |\phi(\vec{n}_1)\rangle \times |\phi(\vec{n}_2)\rangle \times ... \times |\phi(\vec{n}_{N^3})\rangle$ form a complete basis and are eigenvectors of the field, i.e.

$$\phi(\vec{n}) \, |\phi\rangle = \phi(\vec{n}) \, |\phi\rangle \quad .$$

From eq. (1.10) we see that in the space of $\phi$ wave functions a representation of the conjugate momentum $\pi$ is the derivative operator

$$\frac{-i}{a^3} \partial_\phi \quad .$$

Hence:

$$\langle \phi | \pi \rangle = \prod_{\vec{n} \in \lambda} \sqrt{\frac{a^3}{2\pi}} e^{i\pi(\vec{n})\phi(\vec{n})} \quad ; \tag{1.11}$$

Normalizing appropriately the eigenstates $|\pi\rangle$, the unit operator can be written as:

$$\hat{1} = \int \mathcal{D}\phi \, |\phi\rangle \, \langle\phi| = \int \mathcal{D}\pi \, |\pi\rangle \, \langle\pi| \quad , \tag{1.12}$$

where

$$\mathcal{D}\phi = \prod_{\vec{n} \in \Lambda_3} d\phi(\vec{n}) \quad \text{and} \quad \mathcal{D}\pi = \prod_{\vec{n} \in \Lambda_3} d\pi(\vec{n}) \quad ;$$

[4] To be fair one should use a distinctive symbol for operators, in order to not confuse them with classical fields. In general however there's no ambiguity in using the same symbol, since the two are used in different context. Operators are found in commutation relations, near bras and kets, etc. Fields appear inside the Lagrangian, path integrals, etc.

The Hamiltonian is the sum of two pieces, one depending on $\pi$ and the other on $\phi$:

$$\hat{H} = \hat{T}(\hat{\pi}) + \hat{U}(\hat{\phi}) \quad . \tag{1.13}$$

The exponentials appearing in the definition of Euclidean Correlators can be treated with the *Trotter* formula [16]:

$$e^{\alpha \hat{A}} = \lim_{N\to\infty} \left(e^{\frac{\alpha}{N}\hat{A}}\right)^N \quad . \tag{1.14}$$

Moreover we can write (for $\epsilon \to 0$):

$$e^{-\epsilon \hat{H}} = e^{-\epsilon \hat{U}} e^{-\epsilon \hat{T}} e^{-\epsilon \hat{U}} \quad . \tag{1.15}$$

At this point construction of the path integral is a matter of algebra. Fist of all we take the trace of operators as an integral over the field states:

$$\mathrm{Tr}(\hat{Q}) = \int \mathcal{D}\phi_0 \, \langle \phi_0 | \, \hat{Q} \, | \phi_0 \rangle \quad . \tag{1.16}$$

After that, we write all the exponentials of the type $e^{T\hat{H}}$ as a product of $N_T$ terms $e^{\epsilon \hat{H}}$ (with $T = N_T \epsilon$) and then insert $(N_T - 1)$ identity operators $\hat{1} = \int \mathcal{D}\phi_k \, |\phi_k\rangle \, \langle \phi_k|$. If we keep in mind the following formulas:

$$\hat{U} \, |\phi\rangle = U[\phi] \, |\phi\rangle \quad ,$$

$$\langle \phi_1 | \phi_2 \rangle = \delta(\phi_1 - \phi_2) \quad ,$$

$$\langle \phi_1 | \, e^{-\epsilon \hat{T}} \, | \phi_2 \rangle = \int \mathcal{D}\pi \, \langle \phi_1 | \, e^{-\epsilon \hat{T}} \, | \pi \rangle \, \langle \pi | \phi_2 \rangle = \int \mathcal{D}\pi e^{-\epsilon T} \prod_{\vec{n}\in\lambda} \sqrt{\frac{a^3}{2\pi}} e^{i\pi(\vec{n})(\phi_1(\vec{n}) - \phi_2(\vec{n}))} \quad ,$$

$$\int_{-\infty}^{+\infty} dx e^{-ax^2 \pm ibx} = \sqrt{\frac{\pi}{a}} e^{-\frac{b^2}{4a}} \quad ,$$

is easy to show that the limit $a, \epsilon \to 0$ and $N, N_T \to \infty$ of the correlator

$$C_T(t) = \langle O_2(t) O_1(0) \rangle = \frac{\mathrm{Tr}\left(e^{-TH} e^{tH} O_2 e^{-tH} O_1\right)}{\mathrm{Tr}\left(e^{-TH}\right)} \quad , \tag{1.17}$$

with $O_1$ and $O_2$ build from the field $\phi$, is equal to:

$$\frac{\int \mathcal{D}\phi \, e^{-S_E[\phi]} O_2(t) O_1(0)}{\int \mathcal{D}\phi \, e^{-S_E[\phi]}} \quad . \tag{1.18}$$

Here, with abuse of notation, we wrote $\mathcal{D}\phi = \prod_{n\in\Lambda} d\phi(n)$ . The time dependence of the fields is induced by the decomposition of the time intervals in many infinitesimal pieces,

$$\phi(\vec{n})_k = \phi(\vec{n}, n_k) \quad ,$$

having in mind now an hyper-cubic lattice

$$\Lambda = \{(\vec{n}, n_4) | \vec{n} \in \Lambda_3, n_4 = 0, ..., (N_T - 1)\} \quad ,$$

with periodic conditions on the fields. Note that this is valid for boson fields, whilst for fermions we must use anti-periodic conditions (see eg. Appendix A.2 of [17] for details).
The euclidean action $S_E$ is given by:

$$S_E = \epsilon a^3 \sum_{(\vec{n},n_4)\in\Lambda} \frac{1}{2}\left[\left(\frac{\phi(\vec{n},n_4+1)-\phi(\vec{n},n_4)}{\epsilon}\right)^2 + \sum_{j=1}^{3}\left(\frac{\phi(\vec{n}+\vec{j},n_4)-\phi(\vec{n}-\vec{j},n_4)}{2a}\right)^2\right] \tag{1.19}$$

$$+\frac{m^2}{2}\phi(\vec{n},n_4)^2 + V\left(\phi(\vec{n},n_4)\right). \tag{1.20}$$

The first thing one notices is that the discretization of derivatives is different for time and spatial arguments, with the $\epsilon \to 0$ and $a \to 0$ limits recovering the continuum correlator.
At this point we can decide to adopt a different quantization procedure. We directly use the form obtained for the correlator with the above slicing of the time interval $T$, set $\epsilon = a$, and forget about second quantization. In other words, in virtue of the equivalence of space and time, we say the action is simply given by the limit for $a \to 0$ of:

$$S_E[\phi] = a^4 \sum_{n\in\Lambda}\left[\frac{1}{2}\sum_{\mu=1}^{4}\left(\frac{\phi(n+e_\mu)-\phi(n-e_\mu)}{2a}\right)^2 + \frac{m^2}{2}\phi(n)^2 + V\left(\phi(n)\right)\right] \quad , \tag{1.21}$$

with $e_\mu$ being the unit vector in the $\mu^{\text{th}}$ direction.
For more general actions, correlators are given by averages on the degrees of freedom of the latter, weighted with the Boltzmann factor $e^{-S_E}$.
With an eye to the interacting case, a thing it's worth noting. In the lattice formulation of a QFT, there are no infinities in integrands coming from loop diagrams. There are two natural regulators: the lattice spacing $a$ in the Ultraviolet (UV), and the volume in the Infrared (IR) range of energies. This means that, in contrast to the usual continuum formulation of interacting QFT, we don't have to manually regulate our theory (e.g with dimensional regularization, Pauli-Villars, etc.). We still have to introduce counterterms, which could be divergent in powers of $a^{-1}$ and/or $\log a$, but everything we get from the simulation is finite.

### Connection with statistical mechanics

Thanks to the Feynman's interpretation of quantum mechanics, there's a close connection between statistical mechanics and QFT. This is of course important both from a philosophical and computational point of view. The former consist in a different perspective about phenomena occurring near the critical point of a macroscopic system, while the latter is the feasibility of numerical calculations with tested techniques such as Monte Carlo algorithms.
In order to see it explicitly, we can compare the expression of the partition functions for a LFT and the one for thermodynamical system at equilibrium in the canonical ensemble (CE):

$$Z_{LGT} = \int \mathcal{D}\phi e^{-S_E[\phi]} \quad \leftrightarrow \quad Z_{CE} = \mathrm{Tr}(e^{-\beta H}) \quad . \tag{1.22}$$

$Z_{CE}$ can be, with the same insertions of the identity operator presented before, written as an integral over some variables $\Phi$:

$$Z_{CE} = \int \mathcal{D}\Phi \exp\left[-\int_0^{\tilde{\beta}} d\tau \int_{\mathbb{R}^3} d\vec{x} L_E(\Phi, \partial_\mu \Phi)\right]$$

where $\tilde{\beta} = \frac{1}{\tilde{T}}$, with $\tilde{T}$ being the temperature of the system[5]. The variable $\tilde{\beta}$ plays the role of the time extension $T$ of the universe simulated in a LGT. Hence, in analogy with the above case, we say that a simulation of a LGT is made at *finite temperature* in the sense that the time $T$ is finite, and with *0-temperature limit* we mean $T \to \infty$.

**Euclidean and Minkowsky spacetimes**

To conclude the above discussion, let's see the connection between the Euclidean and Minkowsky metrics.
Consider a 2-point Green's function for a scalar field in Minkowsky spacetime [1]:

$$\langle\Omega|\,\mathcal{T}\left(\phi_{_H}(x)\phi_{_H}(y)\right)|\Omega\rangle = \lim_{T\to\infty(1-i\epsilon)} \frac{\langle 0|\,\mathcal{T}\left(\phi_I(x)\phi_I(y)e^{-i\int_{-T}^{T} dt \int_{\mathbb{R}^3} d\vec{x}\mathcal{H}_I^{(int)}}\right)|0\rangle}{\langle 0|\,\mathcal{T}\left(e^{-i\int_{-T}^{T} dt \int_{\mathbb{R}^3} d\vec{x}\mathcal{H}_I^{(int)}}\right)|0\rangle} \quad , \tag{1.23}$$

where the subscripts $_H$ and $_I$ correspond respectively to the *Heisenberg* and the *interaction* picture. $\mathcal{T}$ is the time-ordered product, $|\Omega\rangle$ is the vacuum in the interacting theory while $|0\rangle$ is the one for the free theory. $H^{(int)}$ is the interaction part of the Hamiltonian.
With the same procedure used previously, the path integral form one obtains is:

$$\langle\Omega|\,\mathcal{T}\left(\phi_{_H}(x)\phi_{_H}(y)\right)|\Omega\rangle = \lim_{T\to\infty(1-i\epsilon)} \frac{\int \mathcal{D}\phi\, e^{iS_T[\phi]}\,\phi(x)\phi(y)}{\int \mathcal{D}\phi e^{iS_T[\phi]}} \quad , \tag{1.24}$$

where is understood $S_T[\phi] = \int_{-T}^{T} dt' \int_{\mathbb{R}^3} d\vec{x}'\mathcal{L}$. The above expression represents the sum of all connected diagrams with two legs starting from the points $x$ and $y$:

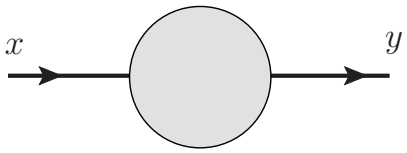


Now we consider the special case $x^0 = t$ and $y^0 = 0$, and apply an analytic continuation to the time variable. In absence of poles and assuming the fields vanish quickly enough at infinity, we can make a Wick rotation for the variable $t'$ (i.e $t' \to it'$), and recover the Euclidean correlator defined above. The metric $\eta_{\mu\nu}$ becomes *Euclidean*[6], that is:

$$\eta_{\mu\nu} \doteq \begin{pmatrix} 1 & 0 & 0 & 0 \\ 0 & -1 & 0 & 0 \\ 0 & 0 & -1 & 0 \\ 0 & 0 & 0 & -1 \end{pmatrix} \quad \to \quad (-\delta_{\mu\nu}) \doteq - \begin{pmatrix} 1 & 0 & 0 & 0 \\ 0 & 1 & 0 & 0 \\ 0 & 0 & 1 & 0 \\ 0 & 0 & 0 & 1 \end{pmatrix} \quad , \tag{1.25}$$

[5] We are adopting here the convention $k_B = 1$.
[6] From which the name *Euclidean* correlators.

and the above Green's function assumes the form found previously. This result is easily generalized to a generic $n$-point Green function. The reason why we use a Euclidean metric is numerical, because with that the integrand does not oscillate strongly in sign.

### 1.1.2 Spectral decomposition of Euclidean Correlators

*Correlation functions* (or *Correlators*) are expectation values of products of operators. They have a spectral decomposition coming from the operators used to build them, and admit a representation as averages over field configurations in the path integral formalism. Combining the information allows to extract matrix elements and masses of the asymptotic states of the theory.
The generalization of eq. (1.17) defines a generic *euclidean correlator* at finite $T$:

$$C_T(t) = \langle O_2(t) O_1(0) \rangle = \frac{\mathrm{Tr}\left(e^{-TH} e^{tH} O_2 e^{-tH} O_1\right)}{\mathrm{Tr}\left(e^{-TH}\right)} \quad , \tag{1.26}$$

where $O_1$ and $O_2$ are functionals of the degrees of freedom of the theory. In the literature the operator at $t = 0$, $O_1$, is called *source* and the one at $t$, $O_2$, is the *sink*. $C_T$ can be expressed in terms of path integrals analogously to eq. (1.18) and we now derive the form of the spectral decomposition. Using the eigenstates of $H$, by definition of trace the numerator and the denominator of such expression are then given by:

$$\begin{cases} \mathrm{Tr}\left(e^{-(T-t)H} O_2 e^{-tH} O_1\right) = \sum_n \sum_m e^{-(T-t)\widetilde{E}_n} \langle n | O_2 | m \rangle \langle m | O_1 | n \rangle e^{-t\widetilde{E}_m} \\ \mathrm{Tr}\left(e^{-TH}\right) = \sum_n e^{-T\widetilde{E}_n} \end{cases} , \tag{1.27}$$

Factoring out $e^{-\widetilde{E}_0 T}$ ($\widetilde{E}_0$ is the energy of the ground state, i.e. the vacuum) we get the energies $E_n = (\widetilde{E}_n - \widetilde{E}_0)$ in the exponentials:

$$C_T(t) = \frac{\sum_m \left(e^{-E_m t} \langle 0 | O_2 | m \rangle \langle m | O_1 | 0 \rangle + \sum_{n \geq 1} e^{-(T-t)E_n} \langle n | O_2 | m \rangle e^{-E_m t} \langle m | O_1 | n \rangle\right)}{1 + \sum_{n \geq 1} e^{-TE_n}} \quad . \tag{1.28}$$

Note that these are indeed the energies of states we find in experiments. We then have:

$$\lim_{T \to \infty} C_T(t) = \sum_n \left[e^{-E_n t} \langle 0 | O_2 | n \rangle \langle n | O_1 | 0 \rangle + e^{-E_n (T-t)} \langle 0 | O_1 | n \rangle \langle n | O_2 | 0 \rangle\right] \quad , \tag{1.29}$$

where the second terms comes from the region of $t \gg 1$ (and $T \gg 1$ from the limit), but $(T - t)$ finite.
The above statement has a central role in LFT data analysis. It basically says, once $C_T(t)$ has been calculated in some way, that its time behavior is given by a linear combination of exponentials. It follows that considering larger and larger times restricts the attention on the first contributions, since the others are quickly suppressed (and drowned in the noise). In other words, for small times all states contribute significantly, but as $t$ increases one can extract the contribution of the lightest states.

A noteworthy case of the latter decomposition is when whe consider an operator $O = O_2 = O_1^\dagger$. In this case the above limit is given by:

$$C_T(t) \sim \sum_n \langle 0|O|n\rangle \langle n|O^\dagger|0\rangle e^{-E_n t} + \sum_{\bar{n}} \langle 0|O^\dagger|\bar{n}\rangle \langle \bar{n}|O|0\rangle e^{-E_{\bar{n}}(T-t)} \quad , \tag{1.30}$$

where in the second term the contributions comes from the anti-particles $|\bar{n}\rangle$.
From $CPT$ theorem [18] we have $E_n = E_{\bar{n}}$, giving the following asymptotic expansion:

$$C_T(t) \sim \sum_n \langle 0|O|n\rangle \langle n|O^\dagger|0\rangle e^{-E_n t} + \langle 0|O^\dagger|\bar{n}\rangle \langle \bar{n}|O|0\rangle e^{-E_n(T-t)} \quad . \tag{1.31}$$

The terms $\sim e^{-E_n t}$ and $\sim e^{-E_n(T-t)}$ are called respectively *forward* and *backward* signals.
As an example, consider an operator annihilating the quantum numbers of the $\pi^+$: $\bar{d}\gamma_5 u$. $E_1$ will be the mass of the pion itself. The other $E_n$s are the energies of states with the same quantum numbers of $O$ (in common with the pion). They can be the masses of heavier particles or the energies of bound states.
Because of the statistical noise in the correlator, in many applications one is limited to considering the lightest state or the few lightest ones. For this reason, it's customary in literature to find correlators named according to the particle giving the leading (forward) exponential signal. For instance, in the example above, the interpolator $\bar{d}\gamma_5 u$ is said to generate the $\pi^+$ correlator, denoted as $C_{\pi^+\pi^-}$ (the subscript is the particle-antiparticle pair).

## 1.2 QCD on the lattice

### 1.2.1 Continuum QCD

The euclidean action of QCD is given by the sum of a fermionic and a gauge part:

$$S = S_F + S_G \quad , \tag{1.32}$$

where

$$S_F = \sum_f \int d^4x \overline{\psi}^{(f)}(x) \left(\gamma_\mu \left(\partial_\mu + iA_\mu(x)\right) + m^{(f)}\right) \psi^{(f)}(x) \quad , \tag{1.33}$$

and

$$S_G = \frac{1}{2g^2} \int d^4x Tr\left[F_{\mu\nu} F_{\mu\nu}\right] \quad . \tag{1.34}$$

$\psi^{(f)}$ is a shorthand for the $f$-flavor multi-index spinor of components $\psi_\alpha{}^{(f)}{}_c$. $\alpha$ is the Dirac index and $c$ is the color index.
Euclidean $\gamma$ matrices are twins of Dirac ones:

$$\gamma_i = -i\gamma_i^D \qquad \gamma_4 = \gamma_0^D \tag{1.35}$$

where the subscript $D$ stands for "Dirac". The gluon field is $A_\mu = A^a{}_\mu \hat{t}^a$, where the $\hat{t}^a$s are the generators of $SU(3)$ in their fundamental representation. $g$ is the bare coupling constant, and the *Field strength* tensor is $F_{\mu\nu} = -i\left[D_\mu, D_\nu\right]$, where $D_\mu = (\partial_\mu + iA_\mu)$ is the *covariant derivative*.

The trace is taken in the space of color and, since we can choose the elements of the algebra $su(3)$ so that they satisfy $Tr(\hat{t}^a\hat{t}^b) = \frac{1}{2}\delta^{ab}$, the gauge part of the actions is a sum over all gluons:

$$S_G = \frac{1}{4g^2}\sum_{a=1}^{8} F_{\mu\nu}^{(a)} F_{\mu\nu}^{(a)} \quad . \tag{1.36}$$

Let's show how we arrive at the above Lagrangian. given its immediate generalization, we consider the case of a single flavor of mass $m$. The starting point is the free fermionic Lagrangian:

$$\mathcal{L}_{\psi,\overline{\psi}} = \overline{\psi}\left(\gamma_\mu\partial_\mu + m\right)\psi \quad . \tag{1.37}$$

In the static quark model, we are motivated to introduce the color as an additional quantum number [19]. Hadrons are colorless combinations of valence quarks, and assuming the existence of 3 colors is sufficient to reproduce the symmetries of baryons wavefunctions. For this reason we are induced to think to an $SU(3)$ symmetry.
Inspired by QED, we build a Yang-Mills Lagrangian according to the principle of gauge symmetry under $SU(3)$ local trasformations $\hat{\Omega}(x) = e^{i\theta^a(x)\hat{t}^a}$:

$$\psi(x) \to \psi'(x) = \hat{\Omega}(x)\psi(x) \quad \text{and} \quad \overline{\psi}(x) \to \overline{\psi}'(x) = \overline{\psi}(x)\hat{\Omega}^\dagger(x) \quad , \tag{1.38}$$

We turn the ordinary derivatives into covariant ones,

$$\partial_\mu \to D_\mu = \partial_\mu + iA_\mu \quad ,$$

with $A_\mu$ trasforming as:

$$A_\mu(x) \to A_\mu'(x) = \hat{\Omega}(x)A_\mu(x)\hat{\Omega}^\dagger(x) + i\left(\partial_\mu\hat{\Omega}(x)\right)\hat{\Omega}^\dagger(x) \quad , \tag{1.39}$$

where is understood

$$\hat{\Omega}\psi = \sum_{b=1}^{3}\hat{\Omega}_{ab}\psi_b \quad .$$

The resulting Lagrangian,

$$\mathcal{L}_F = \overline{\psi}\left(\gamma_\mu D_\mu + m\right)\psi \quad , \tag{1.40}$$

is then invariant under any local $SU(3)$ transformation of the fields, and we interpret it as the fermionic part.
One can also show that

$$D_\mu \to D_\mu' = \hat{\Omega}(x)D_\mu\hat{\Omega}^\dagger(x) \quad . \tag{1.41}$$

Then, the only non-trivial contribution we can add to the Lagrangian, $SO(4)$ invariant[7], renormalizable and that doesn't require the introduction of other fields is [8] :

$$\mathcal{L}_G = \frac{1}{2g^2}Tr\left(F_{\mu\nu}F_{\mu\nu}\right) \quad . \tag{1.42}$$

This is the so called "gauge part" of the Lagrangian, and describes the behavior of free gluons and their self interactions (which are absent in the abelian case of QCD). The tree-level diagram of these interactions are shown in fig. (1.1).

[7]Note that in the euclidean the Lorentz group is replaced by the rotation group in 4 dimensions.

[8]To be precise, in principle also a term $\theta\frac{g^2}{32\pi^2}\epsilon_{\mu\nu\rho\sigma}Tr\left(F_{\mu\nu}F_{\rho\sigma}\right)$ could be included in the Lagrangian. However, experimentally the parameter $\theta$ is extremely small [20, 21], therefore this term can be ignored in our discussion.

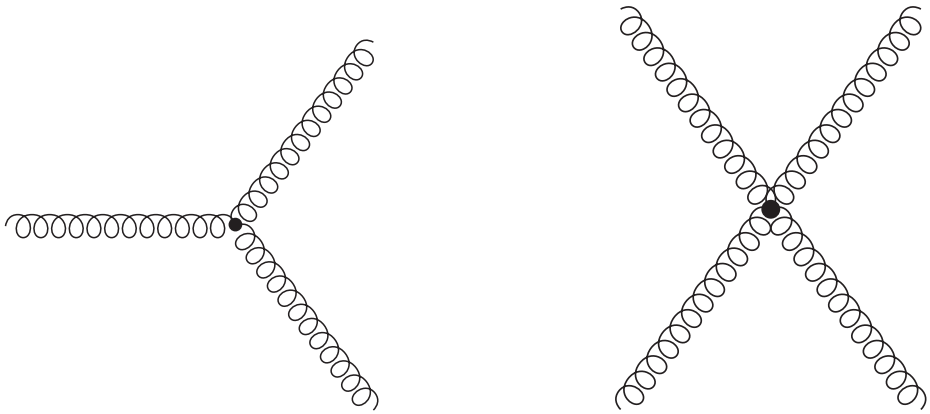

Figure 1.1: In QCD gauge bosons present tree-level self interactions because its gauge group is non-abelian. They are given by a 3 and a 4 gluons legs vertex.

From renormalization we know that the QCD running coupling decreases with energy [22]. This property leads to the interesting property of *color confinement*, namely no isolated quark can be observed in experiments. The coupling is so strong that separating two quarks in an hadron requires an energy so high that the production of $q\bar{q}$ pairs from the vacuum becomes favored instead of quark isolation. This is not a theoretically proven property of QCD. However it is consistent with the running coupling dependence on the exchanged impulse in a given process.

### 1.2.2 Lattice QCD Lagrangian

Despite of its simplicity in the continuum, QCD on the lattice is more complicated, since it requires a careful analysis for fermions. Let's now present a summary of the formulas and results, leaving a more detailed discussion to the following sections: (1.2.3) for gluons and (1.2.4) for fermions.
As usual, one starts from the free case for a fermion of mass $m$, whose action is:

$$S_F^{(0)} = a^4 \sum_{n\in\Lambda} \overline{\psi}(n) \left( \sum_\mu \gamma_\mu \frac{\psi(n+e_\mu) - \psi(n-e_\mu)}{2a} + m\psi(n) \right) \quad . \tag{1.43}$$

Now we want to introduce a symmetry with respect to the $SU(3)$ group. However, since we are dealing with derivatives on the lattice, that is

$$\partial_\mu \psi(x) \to \frac{\psi(x+e_\mu) - \psi(x-e_\mu)}{2a} \quad ,$$

we can immediately see that if we want to introduce a field $U_\mu(x)$ to get invariance under local transformations, a solution is

$$S_F[\psi, \overline{\psi}, U] = a^4 \sum_{n\in\Lambda} \overline{\psi}(n) \left( \sum_\mu \gamma_\mu \frac{U_\mu(n)\psi(n+e_\mu) - U_{-\mu}(n)\psi(n-e_\mu)}{2a} + m\psi(n) \right) \quad , \tag{1.44}$$

where the transformation under the group is defined by:

$$\psi(n) \to \psi'(n) = \hat{\Omega}(n)\psi(n) \quad \text{and} \quad \overline{\psi}(n) \to \overline{\psi}'(n) = \overline{\psi}(n)\hat{\Omega}^\dagger(n) \quad , \tag{1.45}$$

$$U_\mu(n) \to U'_\mu(n) = \hat{\Omega}(n) U_\mu(n) \hat{\Omega}^\dagger(n + e_\mu) \quad , \tag{1.46}$$

$$U_{-\mu}(n) := U_\mu(n - e_\mu)^\dagger \quad . \tag{1.47}$$

$U_\mu(x) = \exp(iaA_\mu(x))$ is called *link variable*. As discussed later, it can be interpreted as a field "connecting" the point $x$ to its nearest neighbour at $x + a\hat{\mu}$. In this sense it is said that, on the lattice, quark fields live on the lattice sites while gauge field on the links between them.
The above rules give $S_F[\psi', \overline{\psi}', U'] = S_F[\psi, \overline{\psi}, U]$, but it is not sufficient. For the reasons discussed in sec. (1.2.4), the fermionic part of the Lagrangian is instead given by the above expression plus an additional term:

$$\begin{aligned} S_F[\psi, \overline{\psi}, U] =& a^4 \sum_{n_1, n_2 \in \Lambda} \overline{\psi}(n_1) \left[ \sum_{\mu=1}^{4} \frac{1}{2} \gamma_\mu (\nabla_\mu + \nabla^*_\mu) - \frac{ar}{2} \nabla_\mu \nabla^*_\mu + m \right] \psi(n_2) \\ =& a^4 \sum_{n_1, n_2 \in \Lambda} \overline{\psi}(n_1) \left[ \sum_{\mu=1}^{4} (\gamma_\mu - r\mathbb{1}) \frac{U_\mu(n_1)\delta_{n_1 + e_\mu, n_2} - U_{-\mu}(n_1)\delta_{n - e_\mu, n_2}}{2a} + \right. \\ & \left. + \left( m + \frac{4}{a} r \right) \right] \psi(n_2) \quad , \end{aligned} \tag{1.48}$$

which of course must be summed over all different flavors. The parameter $r$ is called the *Wilson parameter*, and:

$$a \nabla_\mu \psi(x) = U^\dagger_\mu(x) \psi(x + a\hat{\mu}) - \psi(x) \tag{1.49}$$

$$\nabla^*_\mu \psi(x) = a U_\mu(x - a\hat{\mu}) \psi(x - a\hat{\mu}) - \psi(x) \quad . \tag{1.50}$$

This is the Wilson action for fermions. The additional mass term gives rise to 15 doublers (to be precise, 15 doublers for each flavor) which, in the limit $a \to 0$ become so heavy that they decouple from the theory.
The gauge part of the action is constructed from the so called *plaquette*. In virtue of its position in the Lagrangian (between $\psi(n)$ and $\psi(n + e_\mu)$, to the field $U(n)$ can be assigned a "direction", pointing from $n$ to $n + e_\mu$, as if the field is defined on the link between the two points. With this interpretation, the so called *plaquette*,

$$U_{\mu\nu}(n) = U_\mu(n) U_\nu(n + e_\mu) U_{-\mu}(n + e_\mu + e_\nu) U_{-\nu}(n + e_\nu) \quad , \tag{1.51}$$

can be imagined as a closed loop variable on the lattice. As shown in sec. (1.2.3) its trace is gauge invariant and can be used to build the gauge part of the action. As we'll see, the latter is:

$$S_G = \frac{2}{g^2} \sum_{n \in \Lambda} \sum_{\mu < \nu} Re \left[ Tr \left( \mathbb{1} - U_{\mu\nu}(n) \right) \right] \quad . \tag{1.52}$$

The partition function is then given by:

$$\mathcal{Z} = \int \mathcal{D}[\psi, \overline{\psi}] \mathcal{D}[U] e^{-S_F[\psi, \overline{\psi}, U] - S_G[U]} \quad , \tag{1.53}$$

where the measures are:

$$\mathcal{D}[\psi, \overline{\psi}] = \prod_f \prod_{n \in \Lambda} \prod_\alpha \prod_c d\psi_\alpha{}^{(f)}{}_c \, d\overline{\psi}_\alpha{}^{(f)}{}_c \quad , \tag{1.54}$$

integrated as *Grassmann numbers* (see section (1.2.4)), and

$$\mathcal{D}[U] = \prod_{n\in\Lambda}\prod_{\mu=1}^{4} dU_\mu(n) \quad , \tag{1.55}$$

with $dU_\mu$ being the *Haar measure* (see [7]).
In a lattice simulation, what we do is the following. Since the fermionic part of the path integral can be solved exactly (see sec. (1.2.4)), we find a set of configurations for the link variables at each point, called *gauge configurations*. These are finite in number, and *importance sampling* techniques are used in order to select those that contribute the most [7]. The final aim is to average over them, approximating the path integral and hance the desired functional.

### 1.2.3 Gauge fields on the lattice

Gauge fields on the lattice are defined differently from the continuum. They are link variables connecting two nearest neighbors points and lying in the gauge group itself, not of the corresponding Lie algebra. In this section we'll see how the continuum limit is recovered and build the gauge part (eq. (1.52)). For further details on the derivation see [7].
First we remark that the ordered product

$$P[U]_{n_1\to n_2} = U_{\mu_1}(n_1)U_{\mu_2}(n_1+\mu_1)\cdot\ldots\cdot U_{\mu_k}(n_2-\mu_k) \quad , \tag{1.56}$$

"connecting" the point $n_1$ to the point $n_2$ in a path of $k$ steps transforms as follows:

$$P[U]_{n_1\to n_2} \to P[U']_{n_1\to n_2} = \Omega(n_1)P[U]_{n_1\to n_2}\Omega(n_2)^\dagger \quad . \tag{1.57}$$

The *gauge transporter* connecting two points $x_1$ and $x_2$ in the continuum,

$$G(x,y) = \mathcal{P}\left(e^{i\int_\gamma A_\mu(x')dx'_\mu}\right) \quad , \tag{1.58}$$

where $\gamma$ is a curve connecting $x_1$ to $x_2$, transforms in the same way (see [1] for a proof). We then use its $O(a)$ approximation as an ansatz for $U_\mu(n)$:

$$U_\mu(n) = e^{iaA_\mu(n)} = \mathbb{1} + iaA_\mu(n) + O(a^2) \quad . \tag{1.59}$$

In the continuum limit we recover the interaction term:

$$S_F^{(int)} = ia^4\sum_{n\in\Lambda}\sum_{\mu=1}^{4}\left(\overline{\psi}(n)\gamma_\mu A_\mu(n)\psi(n) + O(a)\right) \quad . \tag{1.60}$$

If we now consider a closed path (from $n$ to $n$), the corresponding $P[U]$ goes to

$$\Omega(n)P[U]\Omega(n)^\dagger \quad .$$

From the cyclicity of the trace and the unitarity of the gauge group, the following term in invariant:

$$\mathbb{1} \quad \text{and} \quad Tr\,(U_{\mu\nu}U_{\mu\nu}) \quad .$$

At this point we observe that:

$$A_\nu(n+e_\mu) = A_\nu(n) + a\partial_\mu A_\nu + O(a^2)$$

and through the Baker-Campbell-Hausdorff expansion (see [23]),

$$e^{\hat{A}}e^{\hat{B}} = e^{\hat{A}+\hat{B}+\frac{1}{2}[\hat{A},\hat{B}]+\dots} \quad , \tag{1.61}$$

we can write the plaquette as a single exponential, whose $0^{\text{th}}$ term in its Taylor expansion cancels the $\mathbb{1}$. The first term contains the square of the field strength, and the gauge part of the action on the lattice is then recovered up to $O(a^2)$ terms:

$$S_G = \frac{1}{2g^2}a^4 \sum_{n\in\Lambda}\sum_{\mu\nu}\left(Tr\left(F_{\mu\nu}F_{\mu\nu}\right) + O(a^2)\right) \quad . \tag{1.62}$$

### 1.2.4 Fermions on the lattice

#### Grassmann variables and integration

In second quantization, fermionic fields anti-commute. They create states of identical particles with odd parity under exchange symmetry, in agreement with Fermi statistics.
In order to be consistent when we quantize with path integral, we can't use standard integration but need another tool called *Grassman integration* [7, 1]. Fermionic fields are Grassman variables $\{\psi_i\}$, satisfying the Grassmann algebra. Any two elements anti-commute:

$$\psi_i\psi_j = -\psi_j\psi_i \quad , \tag{1.63}$$

(from which $\psi_i\psi_i = 0$). It follows that any Taylor expansion of a function of these variables contains only a finite number of terms, each one containing not more than one variable of the family. For instance, if we are dealing with two Grassmann variables $\psi$ and $\bar{\psi}$ we would have:

$$f(\psi,\bar{\psi}) = a_0 + a_1\psi + a_2\bar{\psi} + a_{12}\psi\bar{\psi} \quad . \tag{1.64}$$

The derivatives satisfy:

$$\partial_{\psi_i}1 = 0, \quad \partial_{\psi_i}\psi_j = \delta_{ij}, \quad \partial_{\psi_i}\partial_{\psi_j} = -\partial_{\psi_j}\partial_{\psi_i}, \quad \partial_{\psi_i}\circ\psi_j = -\psi_j\circ\partial_{\psi_i} + \delta_{ij} \quad . \tag{1.65}$$

The integration is linear and satisfies:

$$\int d^N\psi\, \partial_{\psi_i}A = 0 \quad \forall i \quad , \tag{1.66}$$

from which follows that the only contribution comes from the term (in the Taylor expansion of A) containing all the members of the family once.
The measure over $N$ variables can be written as:

$$d^N\psi = d\psi_N d\psi_{N-1}...d\psi_1 \quad , \tag{1.67}$$

with

$$\int d\psi_i 1 = 0, \quad \int d\psi_i\psi_i = 1, \quad \int d\psi_i d\psi_j = -\int d\psi_j d\psi_i \quad . \tag{1.68}$$

Finally a linear change of variables through a matrix $M$, $\psi_i^{'} = \sum_j M_{ij}\psi_j$, the measure transforms like this:

$$d^N\psi = (\det M) d^N\psi^{'} \quad . \tag{1.69}$$

It can be shown that the gaussian integrals satisfy the following properties [1]. The first is

$$\int d\psi_N d\overline{\psi}_N d\psi_{N-1} d\overline{\psi}_{N-1} ... d\psi_1 d\overline{\psi}_1 e^{-\sum_{i,j}\overline{\psi}_i M_{ij}\psi_j} = \det M \quad , \tag{1.70}$$

telling us that:

$$Z_F = \int \mathcal{D}\psi\mathcal{D}\bar{\psi} e^{-S_F} = -\det(D[U]) \quad , \tag{1.71}$$

where $D[U]$ is the Dirac operator.
The second is Wick's theorem:

$$\langle\overline{\psi}(x_1)\psi(y_1)...\overline{\psi}(x_n)\psi(y_n)\rangle_F = (-1)^n \sum_{\sigma(P)} (-1)^{sgn(\sigma(P))} {D_\psi}^{-1}(x_1|y_{P_1})...{D_\psi}^{-1}(x_n|y_{P_n}) \quad . \tag{1.72}$$

This means that the expectation values over fermionic and gluonic fields of a generic observable can be rewritten as:

$$\begin{aligned} \langle O\rangle &= \langle \langle O\rangle_F \rangle_G \\ &= \frac{1}{Z[U]} \int \mathcal{D}U\, e^{-S_G[U]}\, Z_F[U]\, \langle O\rangle_F \quad , \end{aligned} \tag{1.73}$$

where

$$\langle O\rangle_F = \frac{1}{Z_F[U]} \int \mathcal{D}\psi\mathcal{D}\bar{\psi} e^{-S_F[\psi,\bar{\psi},U]} O[\psi,\bar{\psi},U] \quad . \tag{1.74}$$

The usefulness of the above representation lies in the fact that, at fixed gauge configuration, $\langle O\rangle_F$ is solved exactly by Wick's theorem.
In summary, LQCD simulation finds a set of gauge configurations, for each of them calculates the fermionic determinant, finds the fermionic propagator by numerical inversion of the Dirac operator, and combines the results in order to get the expectation value of the operator.

### Doubling problem

The naive quantization of fermions on the lattice is wrong, because it leads to the so called *doubling problem*. This consists in the emergence of more than one pole in the Dirac propagator. These poles correspond to the presence of additional (non-physical) fermions (the *doublers*). To solve this, one must introduce lattice artifacts such as the Wilson term, which gives an additional mass to the (unwanted) doublers so that in the limit $a \to 0$ they decouple from the theory.
This is easily seen in the massless case. Let's consider the $S_F$:

$$S_F[\psi,\overline{\psi},U] = \sum_{n_1,n_2\in\Lambda} \overline{\psi}(n_1) D(n_1|n_2)\psi(n_2) \quad , \tag{1.75}$$

where a sum over color and Dirac indices is understood. Pretending we don't know yet about the Wilson term, the Dirac operator would be given by:

$$D(n_1|n_2) = \sum_{\mu=1}^{4} \gamma_\mu \frac{U_\mu(n_1)\delta_{n_1+e_\mu,n_2} - U_{-\mu}(n_1)\delta_{n_1-e_\mu,n_2}}{2a} + m \quad . \tag{1.76}$$

If we calculate the Fourier transform of the lattice for the free case (i.e. $U_\mu(n) = \mathbb{1}$) we get:

$$\tilde{D}(p|q) = \delta(p-q)\tilde{D}(p) = \delta(p-q)\left(m + \frac{i}{a}\sum_{\mu=1}^{4}\gamma_\mu \sin(p_\mu a)\right) \quad . \tag{1.77}$$

The inverse is:

$$\tilde{D}(p)^{-1} = \frac{m - \frac{i}{a}\sum_{\mu=1}^{4}\gamma_\mu \sin(p_\mu a)}{m^2 + \frac{1}{a^2}\sum_{\mu=1}^{4}\sin(p_\mu a)^2} \quad . \tag{1.78}$$

Now consider the massless limit. $\tilde{D}(p)^{-1}$ becomes:

$$\frac{-\frac{i}{a}\sum_{\mu=1}^{4}\gamma_\mu \sin(p_\mu a)}{\frac{1}{a^2}\sum_{\mu=1}^{4}\sin(p_\mu a)^2} \quad . \tag{1.79}$$

which indeed recovers the continuum form in the limit $a \to 0$,

$$\frac{-i\not{p}}{p^2} \quad , \tag{1.80}$$

with the proper pole at p=(0,0,0,0).
On the lattice however, $(2^4 - 1)$ more unwanted poles emerge: they are the $p$s with components equal to 0 or $\pi/a$.
Since these poles are unphysical, we want to get rid of them. The solution suggested by Wilson [22] is to add an *ad hoc* piece to the Dirac operator in momentum space:

$$\tilde{D}(p) = \left(m + \frac{i}{a}\sum_{\mu=1}^{4}\gamma_\mu \sin(p_\mu a) + \frac{1}{a}\sum_{\mu=1}^{4}(1 - \cos(p_\mu a))\right) \quad . \tag{1.81}$$

With this artifact the 15 unwanted poles disappear. The doublers have a mass given by:

$$m + \frac{2\ell}{a} \quad , \tag{1.82}$$

where $\ell$ depends on the chosen doubler. The mass is given by the value of $p_\mu$ for which the "$\gamma$ term" in $\tilde{D}(p)$ vanishes, so that $\ell$ is the number of components of $p_\mu$ that are equal to $\pi/a$.
In the end, taking the inverse Fourier transform of the above expression one gets the Dirac operator (for a fermion flavor of mass $m$) in position space:

$$D(n_1|n_2) = \left(m + \frac{4}{a}\right) - \frac{1}{2a}\sum_{\mu=-4}^{4}(1-\gamma_\mu)U_\mu(n_1)\delta_{n_1+e_\mu,n_2} \quad , \tag{1.83}$$

where

$$\gamma_{-\mu} = -\gamma_\mu \quad \forall\mu \quad . \tag{1.84}$$

In compact notation, the we recover the action in position space of eq. (1.48):

$$S_F[\psi,\bar{\psi}] = a^4\sum_{n\in\Lambda}\overline{\psi}(n)\left[\sum_{\mu=1}^{4}\frac{1}{2}\gamma_\mu(\nabla_\mu + \nabla_\mu^*) - \frac{ar}{2}\nabla_\mu\nabla_\mu^* + m\right]\psi(n) \tag{1.85}$$

where in front of the Wilson terms (i.e. the ones proportional to the Laplacian operator $\nabla_\mu\nabla_\mu^*$) we've put the Wilson coefficient $r$. The $a$ factor in front of the Laplacian shows that this term vanishes in the naive continuum limit, making the sign of $r$ irrelevant.

**Fermionic expectation values**

As discussed before, euclidean correlators on the lattice can be expressed in the compact notation of the path integral. For an observable $O$:

$$\langle O[\psi,\bar{\psi},U]\rangle = \frac{\int \mathcal{D}\psi\mathcal{D}\bar{\psi}\mathcal{D}U e^{-S[\psi,\bar{\psi},U]}O[\psi,\bar{\psi},U]}{\int \mathcal{D}\psi\mathcal{D}\bar{\psi}\mathcal{D}U e^{-S[\psi,\bar{\psi},U]}} \quad . \tag{1.86}$$

The above equation is understood as follows. The integration over the fermionic degrees of freedom is not an integral in the common sense, but over Grassmann variables, hence must be done explicitly. This means applying Wick's theorem, so that what we really find is an average over gauge fields configurations.
In a Yang-Mills theory (as QCD) the action is written as:

$$S = S_F[\psi,\bar{\psi},U] + S_G[U] = \bar{\psi}D[U]\psi + S_G[U] \quad , \tag{1.87}$$

where $D$ is the Dirac operator at a given gauge configuration. The integration with respect to $\psi$ and $\bar{\psi}$ leads to a product of Dirac propagators and to the determinant of $D$. We can write:

$$\langle O\rangle = \langle \langle O\rangle_F\rangle_G \tag{1.88}$$

where:

$$\langle O\rangle_F = \frac{1}{Z_F}\int \mathcal{D}\psi\mathcal{D}\bar{\psi}e^{-S_F[\psi,\bar{\psi},U]} = \frac{\int \mathcal{D}\psi\mathcal{D}\bar{\psi}e^{-S_F[\psi,\bar{\psi},U]}O[\psi,\bar{\psi},U]}{\int \mathcal{D}\psi\mathcal{D}\bar{\psi}e^{-S_F[\psi,\bar{\psi},U]}} \quad . \tag{1.89}$$

The latter expectation value is done explicitly in terms of Wick contractions. What is left is a functional depending only on $U$, computable with Monte Carlo techniques as an average of a given number of configurations of the gluon fields.
The previous formulas correspond to the so called *dynamical* fermions. In general however, for numerical reasons is frequent to rely on approximations such as quenching and partial quenching.
The quenched approximation consists in fixing $Z_F = det(D[U]) = 1$. This means that we have only quark propagators source-to-source, source-to-sink and sink-to-sink, hence no quark loop is considered. In other words, sea quarks are quenched with respect to the gluons fields.
Partial quenching consists in considering two separate types of quarks in the Lagrangian, valence and sea, with different expressions for the Dirac operator. The fermionic determinant is the product of their determinants:

$$Z_F = \prod_{f_1\in \text{val.}} D_{f_1}[U] \prod_{f_2\in \text{sea}} D_{f_2}[U] \quad , \tag{1.90}$$

and in this approximation we set $\prod_{f_1\in \text{val.}} D_{f_1}[U] = 1$ . This theory is therefore not unitary, but gives the advantage that fermionic determinants are evaluated once and for all after the generation of gauge configurations, and the p.d.f. is:

$$e^{-S_G[U]} \prod_{f\in \text{sea}} D_f[U] \quad . \tag{1.91}$$

We also have more fine tuning on the physical point. We can find propagators for arbitrary values of the valence masses at the only cost of the inversion of the Dirac operator. We can simulate more than one value for them and interpolate such that we reproduce the physical point of hadronic observables.

### 1.2.5 Twisted mass QCD

The definition of the action on the lattice is not unique. Since a requirement is that in the limit $a \to 0$ discretization effects vanish, one can use equivalent actions which differ up to terms which disappear in the continuum limit. The latter property can be used to get *improvements* that can simplify the numerical computation. An example is the twisted mass formulation. Since the data used in the present work come from a simulation in a *twisted mass* setup, let's now briefly present how this lattice artifact plays a role in LQCD.
Twisted mass QCD (tmQCD) is a theory in which there are two degenerate quark forming a doublet of flavors $\chi$ under the $SU(2)$ isospin symmetry group. Furthermore it presents an additional mass term, purely imaginary and non trivial in the flavor indices. The twisted mass action is

$$S^{(tm)}[\chi, \overline{\chi}, U] = S_G[U] + S_F^{(tm)}[\chi, \overline{\chi}, U] \quad , \tag{1.92}$$

where:

$$S_F^{(tm)}[\chi, \overline{\chi}, U] = a^4 \sum_{n_1, n_2 \in \Lambda} \overline{\chi}(n_2) \left[ D(n_2|n_1) + i\mu\gamma_5\sigma^3\delta_{n_2,n_1} \right] \chi(n_1) \quad , \tag{1.93}$$

with $\sigma^i$ being the Pauli matrices and $D(n_2|n_1)$ the Dirac operator from eq. (1.83) in the massless case. Without getting lost in technicalities, we limit ourselves to observe the following. We define a polar mass $M$ and a twist angle $\theta$,

$$M = \sqrt{(m - m_c)^2 + \mu^2}, \quad \theta = \arctan\left(\frac{\mu}{m - m_c}\right) \quad , \tag{1.94}$$

where the parameter $m_c$ is just the value for which $\theta = \pi/2$. Passing from the so called *twisted* basis, $\{\chi, \overline{\chi}\}$, to the *physical* basis $\{\psi, \overline{\psi}\}$ via the change of variables

$$\psi = e^{i\theta\gamma_5 \frac{\sigma^3}{2}}\chi \quad \text{and} \quad \overline{\psi} = \overline{\chi} e^{i\theta\gamma_5 \frac{\sigma^3}{2}} \quad , \tag{1.95}$$

we get an action in the usual form:

$$S_F^{(tm)}[\chi, \overline{\chi}, U] \to S_F^{(tm)}[\psi, \overline{\psi}, U] = a^4 \sum_{n_1, n_2 \in \Lambda} \overline{\psi}(n_2) \left[ D^{\text{tw}}(n_2|n_1) + M\delta_{n_2,n_1} \right] \psi(n_1) \quad , \tag{1.96}$$

with:

$$D^{\text{tw}}(n_2|n_1) = \frac{4}{a} e^{-i\theta\gamma_5\sigma^3}\delta_{n_2,n_1} - \frac{1}{2a}\sum_{\mu=-4}^{4} (e^{-i\theta\gamma_5\sigma^3} - \gamma_\mu) U_\mu(n_2)\delta_{n_2+e_\mu,n_1} \quad . \tag{1.97}$$

Note that the *twist* is totally parametrized by the angle $\theta$. $\theta = 0$ corresponds to *zero* twist, while $\theta = \frac{\pi}{2}$ is the *maximal* (or *full*) twist. It can be shown [7] that the maximal twist leads to an $O(a)$ improvement, which is why the present technique is indeed useful.
The change of variables is non anomalous, i.e.

$$\mathcal{D}[\chi, \overline{\chi}] = \mathcal{D}[\psi, \overline{\psi}] \quad , \tag{1.98}$$

and we observe that only the Wilson part of the Dirac operator gets rotated by the twist. Then, naively, one can immediately convince himself that the twisting effects vanish in the continuum limit.

### 1.2.6 Renormalization on the lattice

#### Renormalization in QFTs

The usual formulation of QFTs is done in the continuum limit and infinite spacetime extension (see e.g. [1]). The action is obtained as $S = \int d^4x\, \mathcal{L}[\phi, \partial_\mu \phi]$, where $\mathcal{L}[\phi, \partial_\mu \phi]$ is the Lagrangian density. In euclidean spacetime the partition function is:

$$Z[\phi] = \int \mathcal{D}\phi\, e^{-S} \quad . \tag{1.99}$$

The $n$-points Green functions contain all the information about the theory, and are found by the means of functional derivatives of $Z[\phi]$. This formulation leads to compact formulas, allows to preserve Lorentz invariance, and the SM interactions manifest easily from gauge invariance.
However this is not strictly correct. In the above formula we jumped to the limit immediately, but according to the path integral formalism that is only the last step. This leads to the problems of UltraViolet (UV) and InfraRed (IR) divergences. The first typically arise when we compute probability amplitudes beyond the tree level approximation. Loops show divergent integral which have no physical significance. The second show up when we consider the region of vanishing momenta in the virtuality of initial and final states.
The solution to the above problem is to *regularize* the theory, i.e. defining an UV and IR cutoffs. Any prediction is done computing everything in presence of these cutoffs, and in the end sending the UV to $\infty$ and the IR to 0. When this procedure works, the theory is *renormalizable*.
Note that the formulation of a QFT on the lattice is itself a regularization, with the inverse of the lattice spacing $a^{-1}$ and the volume providing respectively an UV and IR regulators. In this sense LQCD is just a regularization of QCD.
The solution to UV divergences is done assuming the parameters in the Lagrangian to not coincide with the physical values. They are called *bare parameters* and depend on the UV cutoff. The physical (or *renormalized*) parameters are obtained by the means of Renormalization Constants (RCs) and their displacements from the bare ones (*counterterms*) compensates the UV divergences [1]. This procedure introduces a dependence on the *scale* (an unphysical parameter usually called $\mu$) in the renormalized parameters. The Renormalization Group (RG) equations guarantee that in the end physical observables don't depend on $\mu$. The solution to IR divergences comes from the remark that no experiment will ever have infinite resolution in energy. The presence of very low-energy (soft) particles in the initial or final state won't be detected. The correct calculation of any amplitude must include the presence of arbitrarily soft particles under the IR cutoff, which indeed cancel the divergences. This mechanism was understood by Block and Nordsieck [24] and further generalized by Kinoshita [25], Lee and Nauenberg [26] in what is called the KLN theorem.
On the lattice it's possible to use both perturbative and non-perturbative Renormalization Schemes (RSs). A popular perturbative choice is the *Modified minimal Subtraction* ($\overline{\text{MS}}$), often chosen at the scale $\mu = 2\,\text{GeV}$. The latter comes from continuum dimensional regularization, but in principle could be implemented also on the lattice. However, this is harder for technical reasons, and lattice calculations often rely on non-perturbative schemes.

### The RI'-MOM scheme

We now discuss the non-perturbative and mass-independent scheme called RI'-MOM (Regularization Independent and subtracted MOMentum) [27]. The RC for an operator $\mathcal{O}$ in the $\overline{\text{MS}}$ and RI'-MOM are connected by:

$$Z_{\mathcal{O}}^{\overline{\text{MS}}}(\mu) = R_{\mathcal{O}}(\mu)\, Z_{\mathcal{O}}^{\text{RI'-MOM}}(\mu) \quad , \tag{1.100}$$

where $R$ is a matching factor that can be found in perturbation theory (see e.g. [28, 29]). This scheme is realized as follows. One fixes a gauge for gluon fields (e.g. the Landau gauge [7]) and impose renormalization conditions directly on amputated Green functions in momentum space. The latter are calculated in the chiral limit, ensuring the mass-independence of the RCs. The method is supposed to work in the window:

$$\Lambda_{QCD} \ll \mu \ll a^{-1} \quad , \tag{1.101}$$

in order to match with other non-perturbative schemes ($\mu \gg \Lambda_{QCD}$) and keep under control discretization effects ($a^{-1} \gg \mu$).
We are interested in the renormalization of quark bilinears $J_\Gamma(x) = \bar{q}_1(x)\Gamma q_2(x)$, where 1 and 2 denote two different flavors and $\Gamma$ is a product of gamma matrices. The expectation value of the bare operator is:

$$J_\Gamma(x)(a, g(a)) = \langle J_\Gamma(x)\rangle_a = \langle \bar{q}_1(x)\Gamma q_2(x)\rangle_a \quad , \tag{1.102}$$

where $g$ is the strong coupling. The renormalized operator is defined as

$$J_\Gamma^R(\mu, g(\mu)) = Z_\Gamma(a\mu, g(a))\, J_\Gamma(a, g(a)) \quad , \tag{1.103}$$

where the RC $Z_\Gamma$ makes $J_\Gamma^R$ finite in the continuum limit $a \to 0$.
In the RI'-MOM we first consider the 2-point Green function in momentum space with off-shell quark states,

$$G_\Gamma(ap) = \frac{1}{V}\sum_{x,y} e^{-ip(x-y)} \left\langle q_1(x)\left(\bar{q}_1(0)\Gamma q_2(0)\right)\bar{q}_2(y)\right\rangle_a \quad , \tag{1.104}$$

and build the amputated one from the quark propagators:

$$G_\Gamma^{\text{amp.}}(ap) = D_1(ap)\, G_\Gamma(ap)\, D_2(ap) \tag{1.105}$$

where $D_f(ap)$ is the Dirac operator in momentum space for the flavor $f$. Finally we define:

$$\hat{\Gamma}_\Gamma(ap) = \frac{1}{12}\text{Tr}\left[P_\Gamma\, G_\Gamma^{\text{amp.}}(ap)\right] \quad . \tag{1.106}$$

The factor 1/12 is just an indices normalization factor (color×spin= $3 \times 4 = 12$). $P_\Gamma$ is a projector (e.g. $P_\Gamma = 1, \gamma_5, \gamma_\mu/4$ for $\Gamma = 1, \gamma_5, \gamma_\mu$) such that at tree-level $G^{\text{amp.}} = 1$.
The renormalization condition is given by:

$$1 = \hat{\Gamma}_\Gamma^R(ap, \mu, g(\mu))\Big|_{p^2=\mu^2} = Z_\Gamma(a\mu, g(a))\, Z_q(a\mu, g(a))^{-1}\, \hat{\Gamma}_\Gamma(ap, a, g(a))\Big|_{p^2=\mu^2} \quad , \tag{1.107}$$

where [9]:

$$Z_q(\mu a, g(a)) = -\frac{i}{12}\,\mathrm{Tr}\left[\frac{\not{p} D_f(ap)}{p^2}\right]\Bigg|_{p^2=\mu^2} \tag{1.108}$$

The implementation of mass-independent renormalization schemes such as the RI'-MOM requires dedicated lattice simulations. These are done calculating massive estimators for the RCs for progressively smaller and smaller values of quark masses, in order to control the extrapolation to the desired chiral limit ([30, 31]).

**Quark mass renormalization**

In tmLQCD we have 2 kinds of masses, twisted and untwisted. The first renormalizes multiplicatively while the second shows also an additive term because of the explicit breaking of chiral symmetry by the Wilson term [7]. Their renormalized values for a quark $q$ are respectively given by:

$$\mu_q^R(\mu) = Z_\mu(a\mu, \mu)\,\mu_q \tag{1.109}$$

$$m_q^R(\mu) = Z_m(a\mu, \mu)\,(m_q - m_c) \quad . \tag{1.110}$$

$m_c$ is the value of the bare parameter $m_q$ for which the renormalized mass vanishes. The calculation of these RCs is eased by the axial and vector Ward Identities (WIs) [32] [10] (for standard QCD see [34, 35]). In fact, LQCD with Ginsparg-Wilson (GW) fermions (which is chirally symmetric in the continuum limit) is renormalizable [36] . Adding mass terms does not break renormalizability, since the Lagrangian would differ only for super-renormalizable interactions. For the WIs in tmLQCD with GW fermions we find that the RCs of quark bilinears and quark masses are flavor-independent and satisfy:

$$Z_\mu Z_P = 1 \quad , \tag{1.111}$$

where the subscript corresponds to the bilinear $\bar{q}\Gamma q$. The notation is consistent with the one found in literature, where the RCs are denoted by the name the currents would have in the twisted basis:

$$S \;\to\; 1 \qquad \text{scalar} \tag{1.112}$$

$$P \;\to\; \gamma_5 \qquad \text{psudo-scalar} \tag{1.113}$$

$$V \;\to\; \gamma_\mu \qquad \text{vector} \tag{1.114}$$

$$A \;\to\; \gamma_\mu\gamma_5 \qquad \text{axial} \tag{1.115}$$

## 1.3 Hadron spectroscopy

In this section we give an overview of hadron spectroscopy from lattice data, namely how to construct hadronic correlators and extract hadrons masses from their time-behavior.

[9] We mention that in the RI-MOM scheme [7], the difference is that $Z_q^{-1}$ is found by a momentum derivative:

$$Z_q(\mu a, g(a)) = -\frac{i}{12}\,\mathrm{Tr}\left[\frac{\partial D_f(ap)}{\partial \not{p}}\right]\Bigg|_{p^2=\mu^2}$$

[10] For a proof of the non-renormalization theorem for conserved currents see [33].

### 1.3.1 Hadrons from quark fields

As discussed before, the construction of correlators is done in function of the quantum numbers we want to isolate. First of all color confinement restricts the eigenstates of the Hamiltonian to color singlets, so all hadronic interpolators are *gauge invariant* appropriate combination of fermionic and gauge fields.
Discrete symmetries as $C$, $P$ and $T$ are often used and even isospin when $u$ and $d$ are degenerate. The interpolator $\mathcal{O}$ corresponding to 2nd quantization annihilation operator $O$ is obtained replacing the latter with the respective fields of the path integral.
Finally, the creation interpolator is the hermitian conjugate $O^\dagger$ for bosons and or $\bar{O} = O^\dagger\gamma_4$ for fermions.
The strategy is to express the correlator in terms of Wick contractions, i.e. evaluationg explicitly the expectation value over the fermionic part of the action, and averaging over all gauge configurations. Quark propagators are replaced by their numerical solution found with the given lattice prescription (e.g. Wilson fermions), which contain all non the non-perturbative effects dependent on the gluon fields configuration.

#### Mesonic correlators

Let's consider for example the following interpolator:

$$O(x) = \overline{d}(x)\gamma_5 u(x) \quad . \tag{1.116}$$

This has the parity of a pion and under $C$ goes to $O^\dagger$. We interpret it as the field annihilating a $\pi^-$ and creating a $\pi^+$, i.e the pion interpolator.
In general, a mesonic interpolator has the form:

$$\overline{\psi}^{(f_1)}\Gamma\psi^{(f_2)} \quad , \tag{1.117}$$

where $\Gamma$ is a product of the $\gamma_\mu$s.
Quantum numbers are a consequence of the transformation properties of $\Gamma$ and the statistical properties of fermions as Grassman variables.
Using Wick's theorem [7], and the following identity

$$\overline{\psi}(...)\psi = \mathrm{Tr}(\psi\overline{\psi}(...)) \quad , \tag{1.118}$$

where the trace is taken with respect to the spinor indices, we can write the correlator of a meson in terms of quark propagators, finding:

$$\langle\overline{\psi}^{(f_1)}\Gamma\psi^{(f_2)}(n)\overline{\psi}^{(f_2)}\Gamma\psi^{(f_1)}(m)\rangle_F = -\mathrm{Tr}\left[D^{-1}_{\psi^{(f_1)}}(n|m)\Gamma D^{-1}_{\psi^{(f_2)}}(n|m)\Gamma\right] \quad . \tag{1.119}$$

The correlator built in this way does not distinguish between particle and anti-particle. This means that in the temporal dependence we have a backward signal with the same energy for each forward one. We'll see that this is not the case for baryons projected to a given spatial parity.
We conclude saying that if the flavors $f_1$ and $f_2$ above are equal, the coreraltors shows the so called *disconnected contributions*. These are terms containing a quark

propagator from one point to itself, $S(n|n)$. It is the case for instance of the $\pi^0$, for which $O_{\pi^0} = (1/\sqrt{2})(\bar{u}u - \bar{d}d)$. The correlator is [7]:

$$\begin{aligned}\langle O_{\pi^0}(n) O^\dagger_{\pi^0}(m)\rangle_F = &-\frac{1}{2}\mathrm{tr}\left[\Gamma S_u(n|m)\Gamma S_u(m|n)\right] \\ &+ \frac{1}{2}\,\mathrm{tr}\left[\Gamma S_u(n|n)\right]\mathrm{tr}\left[\Gamma S_u(m|m)\right] \\ &- \frac{1}{2}\,\mathrm{tr}\left[\Gamma S_u(n|n)\right]\mathrm{tr}\left[\Gamma S_d^{-1}(m|m)\right] + (u \leftrightarrow d) \quad .\end{aligned} \tag{1.120}$$

These are not the usual disconnected diagrams that cancel from the numerator and denominator in the expression of Green functions [1], and in general must be included. Recall that these propagators contain all possible non-perturbative effects coming from the interaction with gluons. These are computationally expensive, and in many applications, as in this work, they are neglected. This is justified by the OZI suppression rule [37], according to which diagrams that can be separated in two independent pieces cutting only gluonic lines are suppressed.

### Baryonic correlators

Baryons have the quantum numbers of color singlet bound states of 3 quarks. The isolation of these states requires interpolating operators of the following form [7]:

$$\mathcal{B}_\alpha(x) = \epsilon^{abc}\left(q_1^{T\,a}(x)\, C\Gamma\, q_2^b(x)\right)\, q_{3\,\alpha}^c(x) \quad , \tag{1.121}$$

where $\alpha$ is the free Dirac index (the spin is half-integer) and $\Gamma$ is a product of gamma matrices determining the quantum numbers of the baryon. The dirac singlet $q_1^{T\,a}(x)\, C\Gamma\, q_2^b(x)$ is called *diquark*.
Here we are interested in the $\Omega(3/2^+)$, the nucleons $N(1/2^+)$ and $\Delta(3/2^+)$ resonances, for which the interpolating operators are [38]:

$$\Omega^- \quad \epsilon_{abc} s_a \left[s_b^T C\gamma_\mu s_c\right] \tag{1.122}$$

$$p \quad \epsilon_{abc} u_a \left[u_b^T C\gamma_5 d_c\right] \tag{1.123}$$

$$n \quad \epsilon_{abc} d_a \left[d_b^T C\gamma_5 u_c\right] \tag{1.124}$$

$$\Delta^{++} \quad \epsilon_{abc} u_a \left[u_b^T C\gamma_\mu u_c\right] \tag{1.125}$$

$$\Delta^+ \quad \frac{1}{\sqrt{3}}\epsilon_{abc}\left\{d_a\left[u_b^T C\gamma_\mu u_c\right] + u_a\left[d_b^T C\gamma_\mu u_c\right] + u_a\left[u_b^T C\gamma_\mu d_c\right]\right\} \tag{1.126}$$

$$\Delta^0 \quad \frac{1}{\sqrt{3}}\epsilon_{abc}\left\{u_a\left[d_b^T C\gamma_\mu d_c\right] + d_a\left[u_b^T C\gamma_\mu d_c\right] + d_a\left[d_b^T C\gamma_\mu u_c\right]\right\} \tag{1.127}$$

$$\Delta^- \quad \epsilon_{abc} d_a \left[d_b^T C\gamma_\mu d_c\right] \quad . \tag{1.128}$$

where is understood the integration over spatial positions to set $\vec{p} = 0$.
In order to enforce $P = \pm 1$, the field has to be multiplied by the corresponding parity projector:

$$\mathcal{B}(x) \to P_\pm \mathcal{B}(x) = \frac{1}{2}(1 \pm \gamma_4)\mathcal{B}(x) \quad . \tag{1.129}$$

After some manipulation over the $\gamma$ matrices, the correlator is given by:

$$C_B(t) = \frac{1}{2}\mathrm{Tr}\left[(1 \pm \gamma_4)\sum_{\vec{x}} \langle \mathcal{B}^{(N)}(x)\bar{\mathcal{B}}^{(N)}(0)\rangle\right] \quad . \tag{1.130}$$

For interpolators containing $C\gamma_\mu$ in the diquark (e.g. $\Omega^-$ and $\Delta$s) we need to take care of the spin projection. In fact, the interpolating operator $B_\alpha \sim [q_1^T C\gamma_\mu q_2]q_{3\alpha}$ has both a Dirac index $\alpha$ and a Lorentz index $\mu$. Under the Lorentz group it transforms as $\psi_{\mu\,\alpha}$, i.e. (see page 232 of [14]):

$$\left(\frac{1}{2},\frac{1}{2}\right)\otimes\left[\left(\frac{1}{2},0\right)\oplus\left(0,\frac{1}{2}\right)\right] \tag{1.131}$$

The $\left(\frac{1}{2},\frac{1}{2}\right)$ is the diquark (which is unitarily equivalent to a Lorentz vector), and $\left(\frac{1}{2},0\right)\oplus\left(0,\frac{1}{2}\right)$ is the quark with a free Dirac index. Recalling that for $SU(2)\otimes SU(2)$

$$(j_1,\bar{j}_1)\otimes(j_2,\bar{j}_2)\;\sim\bigoplus_{\substack{|j_1-j_2|\le j\le j_1+j_2\\ |\bar{j}_1-\bar{j}_2|\le \bar{j}\le \bar{j}_1+\bar{j}_2}}(j,\bar{j})\quad , \tag{1.132}$$

the above interpolator transforms as:

$$\left[\left(\frac{1}{2},\frac{1}{2}\right)\otimes\left(\frac{1}{2},0\right)\right]\oplus\left[\left(\frac{1}{2},\frac{1}{2}\right)\otimes\left(0,\frac{1}{2}\right)\right]=\left(1,\frac{1}{2}\right)\oplus\left(0,\frac{1}{2}\right)\oplus\left(\frac{1}{2},1\right)\oplus\left(\frac{1}{2},0\right)\quad . \tag{1.133}$$

The $\left(\frac{1}{2},1\right)\oplus\left(1,\frac{1}{2}\right)$ part is the Rarita-Schwinger field, which under the group of spatial rotations transforms as the direct sum of a $j=3/2$ and two $j=1/2$. It follows that a field with both one Dirac and one Lorentz free index leads to a total of four $j=1/2$ and one $j=3/2$ excitation modes from the vacuum. In order to isolate the $j=3/2$ component in the correlator we make use of the spin projector $P^{3/2}_{\mu\nu}$ in momentum space [39]. In the rest frame and with euclidean metric the latter has the following components:

$$\begin{aligned} P^{3/2}_{00}&=P^{3/2}_{0i}=P^{3/2}_{i0}=0\\ P^{3/2}_{ij}&=\left(\delta_{ij}-\frac{1}{3}\gamma_i\gamma_j\right)\quad . \end{aligned} \tag{1.134}$$

As for the parity projector, $P^{3/2}$ can be brought to the left. If we define the following notation

$$C_{ij}=-\sum_{\vec{x}}\langle Tr\left[\gamma_i\gamma_j(1\pm\gamma_4)\mathcal{B}_i(x)\bar{\mathcal{B}}_j(0)\right]\rangle\quad , \tag{1.135}$$

the 2-point correlator of a spin $3/2^\pm$ particle is given by:

$$C(t)=\frac{1}{2}\sum_{\vec{x}}\langle Tr\left[P^{3/2}_{ij}(1\pm\gamma_4)\mathcal{B}_j(x)\bar{\mathcal{B}}_i(0)\right]\rangle=\frac{1}{3}\sum_i C_{ii}+\frac{1}{6}\sum_{i\neq j}C_{ij} \tag{1.136}$$

In terms of quark fields, the correlator of eq. (1.130) is given by the difference of only two connected contributions [7], the *direct* and *exchange* diagrams. If we denote with $\hat{P}_{\mu\nu}$ the product of needed projectors (parity and spin) and with $(fgh)$ the flavors in the interpolator $B=\epsilon_{abc}\hat{P}q_f^a[q_g^{b\,T}C\Gamma_\mu q_h^c]$ we get the following expressions.
For the a baryon with 3 quarks of the same flavor $f$ we have:

$$\begin{aligned} C^{(fff)}_{B\bar{B}}&=\epsilon_{a_1b_1c_1}\epsilon_{a_2b_2c_2}\,\{\\ &-2\mathrm{Tr}[S_f^{T\,a_1\,a_2}(x|0)C\Gamma_\mu S_f{}^{b_1\,b_2}(x|0)C\Gamma_\nu]\,\mathrm{Tr}[\hat{P}_{\mu\nu}S_f{}^{c_1\,c_2}(x|0)]\\ &+4\mathrm{Tr}[S_f{}^{a_1\,b_2}(x|0)\hat{P}_{\mu\nu}S_f{}^{b_1\,a_2}(x|0)C\Gamma_\mu S_f^{T\,c_1\,c_2}(x|0)C\Gamma_\nu]\,\}\quad . \end{aligned} \tag{1.137}$$

If 2 flavors are equal:

$$\begin{aligned} C^{(ffg)}_{B\bar{B}} &= \epsilon_{a_1b_1c_1}\epsilon_{a_2b_2c_2}\,\{ \\ &\quad \mathrm{Tr}[S_f^{T\,a_1\,a_2}(x|0)C\Gamma_\mu S_f{}^{b_1\,b_2}(x|0)C\Gamma_\nu]\,\mathrm{Tr}[\hat{P}_{\mu\nu}S_g{}^{c_1\,c_2}(x|0)] \\ &\quad -\mathrm{Tr}[S_f{}^{a_1\,b_2}(x|0)\hat{P}_{\mu\nu}S_f{}^{b_1\,a_2}(x|0)C\Gamma_\mu S_g^{T\,c_1\,c_2}(x|0)C\Gamma_\nu]\,\} \quad . \end{aligned} \tag{1.138}$$

Finally if all flavors are different:

$$C^{(fgh)}_{B\bar{B}} = \epsilon_{a_1b_1c_1}\epsilon_{a_2b_2c_2}\,\{\,\mathrm{Tr}[S_f^{T\,a_1\,a_2}(x|0)C\Gamma_\mu S_g{}^{b_1\,b_2}(x|0)C\Gamma_\nu]\,\mathrm{Tr}[\hat{P}_{\mu\nu}S_h{}^{c_1\,c_2}(x|0)]\,\} \quad . \tag{1.139}$$

### 1.3.2 Spectral decomposition

As seen in section (1.1), we can built a euclidean correlator from two operators $O_1$ and $O_2$, such that its time dependence has the form:

$$C(t) = \sum_n \langle 0|O_2|n\rangle\,\langle n|O_1|0\rangle\,e^{-E_nt} + \langle 0|O_1|\bar{n}\rangle\,\langle \bar{n}|O_2|0\rangle\,e^{-E_n(T-t)} \quad . \tag{1.140}$$

Here $O_2$ is some operator with the same quantum numbers chosen for $O_1^\dagger$. Let's now consider the case of bosonic interpolators [11]. Quark bilinears are either real or pure imaginary [40]. This applies to the correlator and, from linear independence, to all forward and backward signals. Since, for bosonic fields, charge conjugation coincides with hermitian conjugation up to a phase [41], we have:

$$C(t) = \sum_n \langle 0|O_2|n\rangle\,\langle n|O_1|0\rangle\,\left[e^{-E_nt} + (-)^p e^{-E_n(T-t)}\right] \quad . \tag{1.141}$$

The factor $(-)^p$ accounts for the phases coming from charge conjugation of $O_1$ and $O_2$, and the product of their signs under complex conjugation.
The same steps apply for operators projected to a definite spatial parity, where the conjugation will be under $CP$ (i.e. under time reversal $T$ from $CPT$ invariance [1]). In QCD hadrons are eigenstates of the time reversal operator $T$, giving $C(t) = (-)^pC(-t)$ for $p = 0, 1$. Moreover, from the fields boundary conditions, correlators are periodic or anti-periodic: $C(t) = \pm C(t + nT)$, with $n \in \mathbb{Z}$. Therefore, in order to improve the statistics in our simulations, for $t \leq T/2$ we evaluated $C(t)$, while for $t > T/2$ we calculated the correlator with the sink transformed under time reversal. Their combination generates a correlator, defined for $t \leq T/2$:

$$\begin{aligned} C_{\mathrm{lat.}}(t) &= \frac{1}{2}\left[C(t) + (-)^pC(-t)\right] = \frac{1}{2}\left[C(t) \pm (-)^pC(T-t)\right] \\ &= \sum_n A_n\left[e^{-E_nt} \pm (-)^p e^{-E_n(T-t)}\right] \quad , \end{aligned} \tag{1.142}$$

where "lat." means that this is the actual correlator considered in the analysis. Later this subscript will be dropped, being implied if not explicitly said. The "+" case is for mesonic sinks, while the "−" for baryons [12]. The latter simply shifts

[11] Later we'll discuss baryons and the issues connected to their backward signals.

[12] Recall that bosonic fields have periodic boundary conditions while for fermions they are anti-periodic.

$p \to p+1$, so that without loss of generality we can limit ourselves to study how to analyze a correlator of the form:

$$C(t) = \sum_n A_n \left[ e^{-E_n t} + (-)^p e^{-E_n (T-t)} \right] \quad . \tag{1.143}$$

One has from one hand the numerical results of the simulation at each time, and from the other a spectral decomposition. The equivalence of the two permits, at least in principle, to extract all the eigenvalues of the Hamiltonian with the quantum numbers of $O$.
This duality is traced back to the one between operators and functionals. In other words, given the operators $O^\dagger$ and $O$ (expressed in terms of the second-quantization fields), one must find the corresponding *interpolators* as functionals of the fields in the Lagrangian and evaluate the path integral.
In order to extract the mass of a particular hadron we look for an interpolating field with the quantum numbers of that particle. This operator will select only those eigenstates, the lightest of which is that hadron (at rest) with a mass corresponding to the $E_0$ in the equation (1.141).
It's worth mentioning this procedure works with certain restrictions. Given the impossibility of solving exactly the eigenvalue problem of the QCD Hamiltonian $\mathcal{H}$, the choice of the interpolators is made with the help of symmetries in the Hamiltonian itself. In fact, these symmetry operators have a (not-complete) set of eigenstates in common with $\mathcal{H}$, and the wave function created by $O^\dagger$ is indeed an approximation of that hadronic state. This leads for example to the presence, in the expansion of eq. (1.141), of excited and multi-particle states contribution.
The correlators considered in this thesis are, as they say, calculated *at rest*. This is needed in order to reproduce the correct extrapolation of observables [42].
Hadronic states contained inside have then vanishing spatial momentum. This is obtained evauating the correlator in momentum space by its Fourier transform and setting $\vec{p} = \vec{0}$:

$$C(t) = \sum_{\vec{x}} C(t, \vec{x}) = \sum_{\vec{x}} \langle O(t, \vec{x}) O^\dagger(0, \vec{0}) \rangle \, . \quad . \tag{1.144}$$

In fact we recall that $P_\mu |0\rangle = 0$, and that for any field $\phi(x)$ the dependence on position can be written as

$$\phi(x) = e^{i\hat{P}_\mu x^\mu} \phi(0) e^{-i\hat{P}_\mu x^\mu} \quad , \tag{1.145}$$

with $\hat{P}^\mu$ being the momentum "four-operator". Summing over $\vec{x}$ isolates the $\vec{p} = \vec{0}$ contribution.

### Baryonic correlators

For mesonic correlators we saw that for each forward propagating signal there is another with the same energy but propagating backwards.
The situation is different for baryons projected to a definite spatial parity because of their spin structure. This fact leads to a substantial difference in the spectral decomposition, which isn't symmetric under the exchange of a forward with its backward propagating signal. This means that given a state of energy $E_\lambda$ propagating forward in time, $e^{-E_\lambda t}$, the projection to a definite spatial parity kills the contribution coming from the corresponding backward exponential $e^{-E_\lambda (T-t)}$, and viceversa. For instance

in the correlator of the nucleon, $\frac{1}{2}^+$, the lightest state propagating backward is the heavier parity partner $N(1535)$, $\frac{1}{2}^-$.
The above property is seen noting that the replacement of the interpolating operator $\mathcal{B}$ with $\gamma_5\mathcal{B}$ doesn't change the states in the correlator [43]:

$$\langle \mathcal{B}(t,\vec{x})\,\bar{\mathcal{B}}(0,\vec{0})\rangle \quad \rightarrow \quad -\gamma_5\,\langle \mathcal{B}(t,\vec{x})\,\bar{\mathcal{B}}(0,\vec{0})\rangle\,\gamma_5 \quad . \tag{1.146}$$

This means that in the spectral decomposition are present the states with both parities [44]. According to the what found in sec. (1.1), for $T \to \infty$ the Fourier representations at spatial momentum $\vec{p}$ is:

$$\begin{aligned} C_T(t,\vec{p}) &= \langle \mathcal{B}(t,\vec{p})\,\bar{\mathcal{B}}(0,\vec{0})\rangle_T \\ &= \sum_{E_\pm} \frac{1}{2E_\pm}\left[\, |a_\pm|^2(\not{p} \pm M_\pm)e^{-E_\pm t} + |\bar{a}_\pm|^2(\not{p} \mp \bar{M}_\pm)e^{-\bar{E}_\pm(T-t)}\,\right] \quad , \end{aligned} \tag{1.147}$$

where we explicitly separated the positive and negative parity states. The "bars" indicate that the quantity is relative to the anti-particle annihilated by $\mathcal{B}$. The matrix elements follow from Lorentz invariance and are defined as:

$$\begin{aligned} \langle 0|\mathcal{B}|B_r^+\rangle &= a_+ u_r(p) & \langle \bar{B}_r^+|\mathcal{B}|0\rangle &= \bar{a}_+ v_r(p) \\ \langle 0|\mathcal{B}|B_r^-\rangle &= a_- \gamma_5 u_r(p) & \langle \bar{B}_r^-|\mathcal{B}|0\rangle &= \bar{a}_- \gamma_5 v_r(p) \end{aligned} \tag{1.148}$$

In the rest frame we get:

$$C_T(t,\vec{p}=\vec{0}) = \sum_{E_\pm} \frac{1}{2}\left[\, |a_\pm|^2(\gamma_4 \pm 1)e^{-E_\pm t} + |\bar{a}_\pm|^2(\gamma_4 \mp 1)e^{-E_\pm(T-t)}\,\right] \quad . \tag{1.149}$$

When $P_\pm$ selects spatial parity, some contribution are projected out. For instance if $P = P_+ = (1+\gamma_4)/2$ at finite $T$ we get:

$$C_T(t) = \sum_{\lambda_+} A_{\lambda_+} e^{-E_{\lambda_+} t} + \sum_{\lambda_-} A_{\lambda_-} e^{-E_{\lambda_-}(T-t)} \quad . \tag{1.150}$$

The sums are respectively over all positive ($\lambda_+$) and negative parity ($\lambda_-$) eigenstates, and shows the result claimed above. The derivation for $P = P_- = (1-\gamma_4)/2$ is analogous. Note that we used the fact that $E_\pm = \bar{E}_\pm$ by the $CPT$ theorem [18].
For the baryons studied in this work the lightest forward signal is much lighter than the lightest state with opposite parity. For this reason when we extract the mass of the lightest state from the correlator, we assume the asymptotic behavior $\sim A_+\exp(-E_+ t)$, with $|E_+\rangle$ being the lightest positive parity state. We restrict ourselves to large times, but far enough from $T$ so that the leading backward signal can be safely neglected.

### 1.3.3 Effective mass curve

In euclidean lattice correlators the effect of heavy states is important at small time, where their contributions are massed in a small temporal window. For this reason, in a many lattice analyses one is interested (and often restricted) in finding the lightest (ground) state of correlators, being the most feasible to isolate. In fact, in the time evolution the latter is the last signal that decays into the noise.

There are various feasible techniques that find the ground state. Here we used the fit to a constant of the effective mass curve, together with the leading exponential approximation and the ODE method [45] as consistency checks.
The first consists in finding the asymptotic limit of the *effective mass*, a time-dependent curve approaching a constant value equal to the mass of the lightest state in the correlator. In absence of a definite backward signal for each forward propagating state, the latter can be evaluated as:

$$M_{\text{eff}}(t) = \log \frac{C(t)}{C(t+1)} \quad . \tag{1.151}$$

Its asymptotic limit is found fitting to a constant in the *plateau* region, i.e. the range in which the data points are constant compatibly with the uncertainty.
This definition is valid in absence of a backward signal. In the latter case (mesons), if $(-)^p$ is the temporal parity of the correlator, the leading behavior of $C(t)$ is:

$$C(t) = A_0[e^{-E_0 t} + (-)^p e^{-E_0 t}] \quad , \tag{1.152}$$

and we can find $m_{\text{eff}}(t)$ by a numerically solution the implicit relation [7]:

$$\frac{C(t)}{C(t+a)} = \begin{cases} \frac{\cosh\left(m_{\text{eff}}(t)\cdot(t-T/2)\right)}{\cosh\left(m_{\text{eff}}(t)\cdot(t+1-T/2)\right)} & p=0 \\ \\ \frac{\sinh\left(m_{\text{eff}}(t)\cdot(t-T/2)\right)}{\sinh\left(m_{\text{eff}}(t)\cdot(t+1-T/2)\right)} & p=1 \end{cases} \quad . \tag{1.153}$$

The second method is similar. One assumes the following ansatz

$$C(t) = \begin{cases} A_0\left[e^{-E_0 t} + (-)^p\, e^{-E_0(T-t)}\right] & \text{mesons} \\ A_0\, e^{-E_0 t} & \text{baryons} \end{cases} \quad , \tag{1.154}$$

and makes a leading exponential fit in the plateau range found from $M_{\text{eff}}(t)$.
Finally the third one is independent of the range, and can then be used also as a consistency check for the previous choices of the plateau. It consists in finding the roots of a polynomial whose coefficients are the ones of a differential equation for the correlator and its lattice derivatives. In sec. (1.3.4) are discussed the details of its implementation.

### 1.3.4 ODE method

In this section is briefly discussed a technique for the extracion of masses and amplitudes from generic lattice correlators developed in [45].
The method relies on a discrete Ordinary Differential Equation through the inversion of appropriate mass and amplitude matrices. In the analysis it was used as a consistency check for the choice of the plateau regions used in the single exponential fits and constant fits of the effective mass curves.

#### The ODE method

Let's start by considering a correlator $C(t)$ composed by $N^{(+)}$ exponential signals in the forward time direction and $N^{(-)}$ exponentials in the backward one:

$$C(t) = \sum_{i=1}^{N^{(+)}} A_i^{(+)} e^{-M_i^{(+)} t} + \sum_{j=1}^{N^{(-)}} A_j^{(-)} e^{-M_j^{(-)}(T-t)}, \tag{1.155}$$

where $T$ is the temporal extension of the lattice. In Eq. (1.155) the *masses* $M_i^{(+)}$ and $M_j^{(-)}$ are nonnegative real numbers and the *amplitudes* $A_i^{(+)}$ and $A_j^{(-)}$ are real numbers.
The correlator $C(t)$ is supposed to be known at discretized values of the time distance $t$, namely $t \equiv na$ with $n = 1, ... N_T$, where $a$ is the lattice spacing and $N_T \equiv T/a$ is the number of lattice points in the temporal direction. In lattice QCD (or QCD+QED) simulations a correlator of the form (1.155) may correspond, e.g., to the case of a nucleonic correlator, where the backward signals correspond to negative parity partners of the nucleon and its excitations.
For sake of simplicity we will refer to the quantities $M_i^{(+)}$ and $M_j^{(-)}$ as masses. It is however clear that Eq. (1.155) may correspond also to the case of correlation functions for moving hadrons by simply replacing hadron masses with energies.
The correlator (1.155) can be rewritten as

$$C(t = na) \equiv C_n^{(0)} = \sum_{m=1}^{N} \widetilde{A}_m e^{-a\widetilde{M}_m n} \tag{1.156}$$

with $N \equiv N^{(+)} + N^{(-)}$ and

$$\widetilde{M}_m = M_i^{(+)} \ , \qquad \widetilde{A}_m = A_i^{(+)} \tag{1.157}$$

in the case of forward signals ($m = i = 1, ... N^{(+)}$) and

$$\widetilde{M}_m = -M_j^{(-)} \ , \qquad \widetilde{A}_m = A_j^{(-)} e^{-M_j^{(-)} T} \tag{1.158}$$

for backward signals ($m = N^{(+)} + j = N^{(+)} + 1, ... N^{(+)} + N^{(-)}$).
Let's now consider the discretized (symmetric) time derivative

$$C_n^{(1)} \equiv \frac{1}{2}\left[C_{n+1}^{(0)} - C_{n-1}^{(0)}\right] = \sum_{m=1}^{N} \widetilde{A}_m \, z_m \, e^{-a\widetilde{M}_m n} \ , \tag{1.159}$$

where

$$z_m \equiv -\sinh(a\widetilde{M}_m) \ . \tag{1.160}$$

By repeating the application of the differential operation (1.159) one gets

$$C_n^{(k)} = \frac{1}{2}\left[C_{n+1}^{(k-1)} - C_{n-1}^{(k-1)}\right] = \sum_{m=1}^{N} \widetilde{A}_m (z_m)^k e^{-a\widetilde{M}_m n} \ . \tag{1.161}$$

We also assume that the correlator $C_n^{(0)}$ is known, for each time distance, in terms of a number of jackknife or bootstrap events. Its statistical error $\sigma_n^{(0)}$ can be correspondingly evaluated. Starting from the correlator $C_n^{(0)}$, the sequence of the correlators $C_n^{(k)}$ with $k = 1, ... N$ can be evaluated for each jackknife or bootstrap event together with their statistical errors $\sigma_n^{(k)}$. It is understood that what follows applies for each single jackknife or bootstrap event.
The values of the correlator $C_n^{(0)}$ are provided in the range $n = [1, N_T]$, while the derivatives $C_n^{(k)}$ for $k = 1, .. N$ can be evaluated only in the range $n = [k+1, N_T - k]$. Outside this range we put $C_n^{(k)} = 0$.

Note that, because of the presence of the factor $(z_m)^k$ in Eq. (1.161), at a fixed value of $n$ the impact of the signals with higher masses increase as the order $k$ of the derivative $C_n^{(k)}$ increases.
The central step in our procedure consists in introducing $N+1$ real coefficients $x_k$ $(k = 0, 1, ... N)$ and considering the quantity

$$\sum_{k=0}^{N} x_k C_n^{(k)} = \sum_{m=1}^{N} \widetilde{A}_m \left[ \sum_{k=0}^{N} x_k z_m^k \right] e^{-a\widetilde{M}_m n} = \sum_{m=1}^{N} \widetilde{A}_m P_N(z_m) e^{-a\widetilde{M}_m n} \ , \qquad (1.162)$$

where the polynomial $P_N(z)$ of degree N is given by

$$P_N(z) \equiv \sum_{k=0}^{N} x_k z^k \ . \qquad (1.163)$$

The above polynomial has in general $N$ roots depending on the coefficients $x_k$. If the latter ones (which, we stress, are independent on $n$) are chosen so that the polynomial $P_N(z)$ has its roots at $z = z_m$ given by Eq. (1.160), then the condition

$$\sum_{k=0}^{N} x_k C_n^{(k)} = 0 \qquad (1.164)$$

holds for any value of $n$. Note that the roots $z_m$ of the polynomial $P_N(z)$ depend only on the masses $\widetilde{M}_m$ and are independent on the amplitudes $\widetilde{A}_m$. Moreover, from Eq. (1.160) it follows that the roots $z_m$ are real numbers, positive for backward signals and negative for forward ones.
Equation (1.164) is a typical ordinary (linear) differential equation (ODE). Usually the coefficients $x_k$ are given and, therefore, the solution of Eq. (1.164) corresponds to Eq. (1.156) with the masses $\widetilde{M}_m$ given by the roots (1.160) of the polynomial $P_N(z)$ and with the amplitudes $\widetilde{A}_m$ depending on a suitable number of initial conditions.
Here we are interested in the inverse problem: starting from the known values of the correlator $C_n^{(0)}$and its derivatives we want to determine the coefficients $x_k$ of the polynomial (1.163) having its roots at $z = z_m$. The procedure, which hereafter will be referred to as the ODE algorithm, is as follows.
Without any loss of generality we can put $x_N = 1$ so that

$$P_N(z) \equiv \sum_{k=0}^{N} x_k z^k = \sum_{k=0}^{N-1} x_k z^k + z^N = \prod_{m=1}^{N} (z - z_m) \qquad (1.165)$$

and Eq. (1.164) can be rewritten as

$$\sum_{k=0}^{N-1} x_k C_n^{(k)} = -C_n^{(N)} \ . \qquad (1.166)$$

The problem is to solve Eq. (1.166) for the $N$ unknowns $x_k$ $(k = 0, 1, ..., N-1)$.
Our aim is to extract the multiple exponential signals in the correlator (1.156) using as input the knowledge of the correlator in a given range of values of $n$, which eventually can span the full temporal extension $[1, N_T]$. Therefore, we multiply Eq. (1.166) by a set of $N$ functions $R_n^{(k')}$ with $k' = 0, 1, ... (N-1)$ and sum over $n$

in a given range from $n_{min}$ to $n_{max}$. Since the largest range in which the derivatives $C_n^{(k)}$ can be calculated is $n = [k+1,\, N_T - k]$, we put directly $n_{min} = N+1$ and $n_{max} = N_T - N$, so that all the values of the correlator (1.156) in the full range $[1,\, N_T]$ are taken into account. We get the following system of inhomogeneous linear equations

$$\sum_{k=0}^{N-1} M_{k'k} x_k = V_{k'} \ , \tag{1.167}$$

where the $N \times N$ *mass* matrix $M$ is given by

$$M_{k'k} \equiv \sum_{n=N+1}^{N_T-N} R_n^{(k')}\, C_n^{(k)} \ , \tag{1.168}$$

and the vector $V$ with dimension $N$ by

$$V_{k'} \equiv - \sum_{n=N+1}^{N_T-N} R_n^{(k')}\, C_n^{(N)} \ . \tag{1.169}$$

The choice of the functions $R_n^{(k')}$ is in principle arbitrary, provided it leads to a non-singular mass matrix $M$. We have explored different choices for $R_n^{(k')}$. Simple and natural choices are either

$$R_n^{(k')} = \frac{C_n^{(k')}}{[\sigma_n^{(0)}]^2} \ , \tag{1.170}$$

where $\sigma_n^{(0)}$ is the uncertainty of the correlator (1.156), or

$$R_n^{(k')} = \frac{C_n^{(k')}}{[\sigma_n^{(k')}]^2} \ , \tag{1.171}$$

where $\sigma_n^{(k')}$ is the uncertainty of the derivative (1.161). A more sophisticated choice is

$$R_n^{(k')} = D_{nn'}^{(0)} C_{n'}^{(k')} \ , \tag{1.172}$$

where $D_{nn'}^{(0)}$ is the inverse of the covariance matrix of the correlator (1.156). We have checked that the performance of the ODE algorithm is not changed by the three choices (1.170-1.172). In what follows we will use the definition (1.170). We point out that any autocorrelation between different values of $n$ is taken into account by the use of the jackknife (bootstrap) procedure.
Thus, we rewrite Eqs. (1.168) and (1.169) as

$$M_{k'k} \equiv \sum_{n=N+1}^{N_T-N} \frac{C_n^{(k')}\, C_n^{(k)}}{[\sigma_n^{(0)}]^2} \ , \tag{1.173}$$

and

$$V_{k'} \equiv - \sum_{n=N+1}^{N_T-N} \frac{C_n^{(k')}\, C_n^{(N)}}{[\sigma_n^{(0)}]^2} \ . \tag{1.174}$$

Equations (1.173) and (1.174) are evaluated starting from the correlator (1.156) and its derivatives (1.161) for each jackknife or bootstrap event. Note that using the definition (1.170) for $R_n^{(k')}$ the system of linear equations (1.167) corresponds to minimize the variable $\chi^2_M$ defined as

$$\chi^2_M \equiv \sum_{n=N+1}^{N_T-N} \frac{1}{[\sigma_n^{(0)}]^2} \left[ \sum_{k'=0}^{N} x_{k'} C_n^{(k')} \right]^2 , \tag{1.175}$$

i.e. to the constraints $\partial\chi^2_M/\partial x_k = 0$ for $k = 0, 1, ...(N-1)$ with $x_N = 1$.
For a non-singular matrix $M$ the coefficients $x_k$ can be determined by inverting the matrix $M$:

$$x_k = \sum_{k'=0}^{N-1} M^{-1}_{kk'} V_{k'} . \tag{1.176}$$

Once the coefficients $x_k$ are known, the roots of the polynomial $P_N(z)$ can be calculated, and thus the masses of the forward and backward exponential signals in lattice units, $aM_i^{(+)}$ and $aM_j^{(-)}$, can be determined from Eq. (1.160).
The last step is the determination of the amplitudes $\widetilde{A}_m$. To this end we introduce a $\chi^2$-variable defined as

$$\chi^2 \equiv \sum_{k=0}^{N} \chi^2_k , \tag{1.177}$$

$$\chi^2_k \equiv \sum_{n=k+1}^{N_T-k} \left( \frac{C_n^{(k)} - \sum_{m=1}^{N} \widetilde{A}_m z_m^k e^{-a\widetilde{M}_m n}}{\sigma_n^{(k)}} \right)^2 , \tag{1.178}$$

where $\sigma_n^{(k)}$ is the statistical error of the derivative $C_n^{(k)}$. Then, we impose the minimization condition $\partial\chi^2/\partial\widetilde{A}_m = 0$, which leads to the following linear system of equations

$$\sum_{m'=1}^{N} A_{mm'} \widetilde{A}_{m'} = W_m , \tag{1.179}$$

where

$$A_{mm'} \equiv \sum_{k=0}^{N} \sum_{n=k+1}^{N_T-k} (z_m z_{m'})^k \frac{e^{-a(\widetilde{M}_m + \widetilde{M}_{m'})n}}{[\sigma_n^{(k)}]^2} , \tag{1.180}$$

$$W_m \equiv \sum_{k=0}^{N} \sum_{n=k+1}^{N_T-k} (z_m)^k \frac{e^{-a\widetilde{M}_m n} C_n^{(k)}}{[\sigma_n^{(k)}]^2} . \tag{1.181}$$

The solution of the linear equation (1.179) is given by

$$\widetilde{A}_m = \sum_{m'=1}^{N} A^{-1}_{mm'} W_{m'} , \tag{1.182}$$

which allows to extract the forward and backward amplitudes, $A_i^{(+)}$ and $A_j^{(-)}$ using Eqs. (1.157-1.158).

We stress that the choice of the $\chi^2$-variable given by Eqs. (1.177-1.178) is not unique and, consequently, also the definitions of the amplitude matrix (1.180) and vector (1.181). For instance, one can limit the sum in Eq. (1.177) to the first term $k = 0$ without involving the derivatives $C_n^{(k)}$ with $k > 0$. Correspondingly also in Eqs. (1.180-1.181) the sum over $k$ should be limited to the first term $k = 0$ only.
The key feature of the ODE method is the inversion of the mass and amplitude matrices, given respectively by Eqs. (1.173) and (1.180). In the following subsections we want to illustrate how the ODE method can be applied to specific forms of the correlation functions typically encountered in QCD (or QCD+QED) simulations on the lattice.

## 1.4 Systematic effects

We have seen that lattice correlation functions are calculated as:

$$\langle \mathcal{O}(t)\overline{\mathcal{O}}(0)\rangle = \frac{1}{\mathcal{Z}_T}\int \mathcal{D}[\psi,\overline{\psi}]\mathcal{D}[U]e^{-S_E}\mathcal{O}(t)\overline{\mathcal{O}}(0) \quad . \tag{1.183}$$

In the actual calculation, the only parameters "seen" by the numerical simulation are $\beta = \frac{6}{g^2}$ (for the gauge part), the bare masses of particles multiplied by the lattice constant $a$ and of course the number of points of the lattice. In the simulation the set of configurations together with the set of parameters is called *ensemble*. However, any information about the "standard" bare parameters (in physical units) is hidden behind the lattice constant itself, which is not directly accessible.
In general, all the observables we get from lattice correlators are in *lattice units*, i.e. multiplied by some power of $a$ such that they are dimensionless. For instance, the energies found from the large time behavior of correlators only leads to the product $aE_n$ [13]. These observables can be thought to be given in units of an intrinsic scale of the system, independent of the other parameters in the Lagrangian but the bare strong coupling $g$. This quantity is not a parameter in the Lagrangian so that an observable must be "sacrified" to set the scale (loosing predictivity on it). The natural choice is to identify this scale indeed with $a$, the lattice spacing of our grid. Once we have fixed the scale, these quantities suffer from the following systematic effects:

- Finite Size Effects (FSEs), due to the finite temporal extent $T$ and volume $V$. In most cases one works with hypercubic lattices, $V = L \times L \times L$, so this means finite $L$. These vanish in the limit $T, L \to \infty$, and are corrected with asymptotic formulas found in effective models. In the analysis one often relies on ensembles which differ only for their size, as the case of our A40.XX ensembles. In our ensembles, $T = 2L$, so that we neglect FSEs coming from $T$. The condition $T \gg L$ is common to many lattice calculations, easing the convergence to the asymptotic spectral decomposition.

[13] To be precise, the number one finds is of course dimensionless and, since the convention is

$$1 = \hbar = c \quad ,$$

what we really handle with are the products $\frac{aE_n}{\hbar c}$.

- Discretization effects, coming from the finiteness of $a$ and vanishing in the limit $a \to 0$. The latter come both from the observable in question and the one used to set the scale of the system. The limit removes the doublers and recovers the continuity of spacetime (e.g., for periodic boudary conditions, the lattice $\Lambda$ becomes a dense torus $\mathbb{T}^4$). A typical simulation has $a \sim (10^{-1} - 10^{-2})$ fm.

  It's frequent to them into account with a polynomial dependence. In the case of tmQCD, one first reaches the condition of maximal twist. This guarantees the $O(a)$ improvement, allowing to start from $O(a^2)$.

- Distance from the physical values, because quarks masses are often not tuned to their physical values in order to reduce the cost of the simulation [46]. This means that the values of our observables are unphysical and must be extrapolated to the *physical point* (p.p.), namely the point in parameter space corresponding to the experimental values. In order to find it, we choose a set of observables which we compare with the experiment. The extrapolation of all the others to this point gives a prediction for their experimental values.

  In the literature this procedure is typically expressed in terms of mass eigenstates. For instance, the p.p.s of the light quark mass and the one of $M_\pi^2$ are used as synonyms, given the weak dependence of the latter from the other quark flavors. In many appolications the functional forms chosen to fit the data are inspired to the results of *Chiral Perturbation Theory* (ChPT), valid in the limit of small quark masses.

- It happens that, for some calculations, there exist contributions which are suppressed at the p.p. . These remain systematic effects, and are the hardest to correct since often based on estimates of negligibility. It is the case of "disconnected" diagrams suppressed according to the OZI rule [37].

  Examples in LQCD are the *quenching* and *partial quenching* approximations (see sec. (1.2.4)). They provide numerical advantage at the price of breaking the unitarity of the theory.

  The first neglects sea quark loops, and is justified or heavy quark masses. At the path integral level it is implemented neglecting the fermionic determinant.

  The second imposes different masses for the valence and sea quarks. The motivation behind it is that the p.p. of bare quark masses is determined necessarily with some uncertainty. In order propagate it correctly, it's useful to evaluate the fermionic determinant once and for all with some given masses, and over the resulting gauge configurations evaluate fermionic propagators for valence quark masses near those values. The interpolation among those points allows for a control of this systematic effect and reach the p.p. .

### 1.4.1 Physical point and ChPT

Many lattice calculations are done not at the physical point, that is to say with bare quark masses not coinciding with the values that reproduce the experimental measures. This choice is led by the cost of the simulation, which decreases with the pion mass. The latter is typically parametrized as [47] :

$$\text{cost} \propto M_\pi^{-z_\pi} \left(\frac{L}{a}\right)^{z_L} \frac{1}{a_a^z} \quad , \tag{1.184}$$

where $z_\pi$, $z_L$, $z_a$ and the overall constant are determined empirically. Typical values are $3 < z_\pi < 4$, $z_L = 4$, $z_a = 2$. Increasing the pion mass, i.e. the light quark masses, reduces the cost of the simulation.
In this case a proper lattice prediction needs more ensembles with different values of the pion mass, among which extrapolate to the physical point.
The extrapolation can be done using phenomenological models, which take into account the dependence on the light quark masses. The most popular choice is Chiral perturbation theory (ChPT), an effective field theory based on the approximate chiral symmetry of QCD. In the limit $m_u = m_d = m_\ell = 0$, the Lagrangian exhibits an $SU(2)_L \times SU(2)_R$ symmetry under left (L) and right (R) chiral rotations [48]. This symmetry is spontaneously broken to $SU(2)_I$, meaning that there exist 3 Nambu-Goldstone bosons [14] . Their fields have a non vanishing vacuum expectation value (VEV), so must have spin 0 in order to not break Lorentz invariance [15] Since the 3 pions are the lightest hadrons we interpret them as these bosons, which acquire a mass from $m_u$ and $m_d$.
This property of QCD can be used to build an effective field theory (EFT), simmetric under $SU(2)$, in which we expand over the chiral background with respect to the pion mass and powers of the momenta. This EFT is called Chiral Perturbation Theory (ChPT or $\chi$PT), and is expected to give an reasonably approximate description of hadron dynamics at low energies. In this regime quarks and gluons are confined inside hadrons, and pions behave as pseudo-Nambu-Goldstone bosons as indicated by their experimental masses which are much smaller than the other hadrons.
ChPT is non-renormalizable, and contains a set of low energy constants multiplying the operators in the Lagrangian. The latter are fixed from the experiment or even lattice calculations, in order to get predictions on other hadronic observables. In lattice extrapolations this may be used as follows (as done in the present work). One considers the ChPT prediction for the dependence on the pion mass, stopping at a given order accordingly to the precision and position of data points. Since the ChPT predistion is expected to be near the physical dependence, the low energy constants can be left free to vary as parameters of the fit, starting from values near the ChPT prediction.
In the analysis of this work we adopted the above technique, combining the formulas of ChPT with the dependence on the volume, discussed in the following section.

### 1.4.2 Finite Volume effects on hadronic observables

Here we discuss the rationale and basic results on Finite Size Effects in QCD. As we'll see, this is applied in our analysis in the extrapolation of physical observables. When we do a Lattice simulation of a system we build a grid of points in our space and fix their relative distancing. With a Lattice gauge theory these are the spacetime points in a 4-dimensional space.
These numbers have to be finite for a numerical simulation and the universe is limited in size. Boundary conditions must be imposed, causing the presence of the so called Finite Size Effects (FSE) in the observables.

[14] They are pseudo-Nambu-Goldstone bosons, since chiral symmetry is weakly broken by quark masses.

[15] If a field of spin $s > 0$ had a VEV $v \neq 0$, the latter would be a fixed value and trivially transform under the Lorentz group, while the field would not.

In most lattice simulations it is chosen an hyper-rectangular grid with fixed lattice spacing: the points are distributed along orthogonal directions with the same distance $a$ between any two nearest neighbors. In this case the extension is given by $T \times L_x \times L_y \times L_z$, where each dimension is given by the product of $a$ times the number of points in that direction.
In most cases a spatial hyper-cubic configuration is adopted, namely $L = L_x = L_y = L_z$, so that spatial isotropy is restored in the continuum limit. The total size is then $T \times V = T \times L^3$.
FSEs are then usually divided in two contributions, coming from the finiteness of $T$ and $V$. The first are often called *finite temperature effects*, in analogy with the statistical mechanics partition function. The $T \to \infty$ limit is called the *zero temperature limit*, since $T$ is inversely proportional to the temperature. The effects of a finite $V$ are called *finite volume effects* (FVE).
The total number of points of the lattice are often distributed so that $T$ is larger than $L$. This is done in order to improve the convergence of the spectral decomposition in the time variable.
In sec. (1.3.2) is shown how a finite $T$ leads to the presence of backward signals and to the modification of amplitudes. The latter differ from the $T \to \infty$ limit by corrections $\sim e^{-MT}$, where $M$ is the mass of the hadron.
In the present work we deal with ensembles for which $T = 2L$, so we neglect the latter effects with respect to the FVEs.
The treatment of FVEs is widely discussed in literature (see e.g. [49], [50], [51], [52], [53]), for mainly 2 reasons. The volume dependence of observables is useful not only to correct these systematic effects, but also to extract physical information. In short, in those formulas appear infinite-volume limits of other observables such as form factors, scattering amplitudes, etc. The analysis of volume dependence can then lead to the prediction of these quantities.
These concepts are more easily understood in the framework of finite volume ChPT, whose leading contributions will be briefly discussed in a moment. For the purpose of the present work, we are interested in understanding how the volume dependence arises in hadron masses in the so called *p-regime*, i.e. $ML \gg 1$ for all the eigenstates $M$ of the Hamiltonian.
In a finite volume with periodic boundary conditions, the pion propagator in the p-regime is given in terms of is infinite volume version [54, 55]:

$$\Delta_L(x) = \sum_{n_\mu} \int \frac{d^4k}{(2\pi)^4} G(k) e^{ik_\mu(x_\mu + n_\mu L_\mu)} = \sum_{n_\mu} \Delta(x + n_\mu L_\mu) \quad , \tag{1.185}$$

where $G$ is the pion propagator: $G(k)^{-1} = k^2 + m^2$. The derivation is analogous to the one of [56] for the thermal propagator already mentioned in sec. (1.3.2).
From the saddle point approximation of the so called *heat-kernel* form,

$$\Delta(x) = \int \frac{d^4k}{(2\pi)^4} \frac{e^{ikx}}{k^2 + m^2} = \frac{m^2}{16\pi^2} \int d\alpha \exp\left(-\frac{1}{\alpha} - \frac{\alpha m^2 x^2}{4}\right) \quad , \tag{1.186}$$

we get [54]:

$$\Delta(x) \approx \frac{m^2}{(4\pi)^2} \frac{\sqrt{8\pi}}{(mx)^{3/2}} e^{-mx} \quad . \tag{1.187}$$

In ChPT quantum fluctuations are dominated by pion loops. The behavior of a typical observable (such as a mass) $O$ is [54]:

$$O(L) = O_0 \left(1 + \frac{C_0}{f^2} I_1(L, m)\right) \quad . \tag{1.188}$$

$O_0$ and $C_0$ are constants and

$$I_1(L, m) = \sum_{n_\mu} \Delta_L(n_\mu L_\mu) \quad . \tag{1.189}$$

At Leading Order we get:

$$O(L) = O_0 \left(1 + \frac{C_0}{f^2} \sum_{n_\mu \neq 0} \Delta(n_\mu L_\mu)\right) \quad . \tag{1.190}$$

From eq. (1.187) we see that these FVEs are exponentially. It must be said that the above discussion applies to the eigenstates of the Hamiltonian. When when we deal with unstable particles (able to decay into $n$-particle states) also power-law FVEs enter in the energy shift. For more details see for instance [51, 57].
The above derivation shows how a particle loop induces FVEs. In general, all the particles in the theory take part. In practice however, given the exponential suppression, it is often sufficient to consider only the lightest states that contribute. For this reason, in QCD the main effect comes from $\pi$, $K$ and $D$ masses. When pion loops are allowed at LO, the latter two are subdominant.
Among the ensembles considered in this work, there are 5 which are equal in all respects but for the volume size. Later in the analysis we'll use them in order to check and control systematic FVEs according to the asymptotic expansion of ChPT results.

## 1.5 Numerical issues on the lattice

### 1.5.1 Signal-to-noise ratio in lattice correlators

In a lattice field theory with degrees of freedom $\Phi$, the vacuum expectation value of an operator is given by:

$$\langle O[\Phi] \rangle = \frac{\int D\Phi \, O[\Phi] \, e^{-S[\Phi]}}{\int D\Phi \, e^{-S[\Phi]}} \quad .$$

In QCD we integrate over the gauge link variables $U_\mu$.
The numerical evaluation of the correlator could be done, in principle, with multi-dimensional integration algorithms. However, for a tipical lattice simulation this is extremely costly, and the problem is better takled using Monte Carlo estimators [46]. This consists in generating a number $N_{cfg}$ of *configurations* for $\Phi$, which are randomly distributed according to the probability distribution $e^{-S[\Phi]}$. The correlator is then approximated by an average of the corresponding values of $O[\Phi]$:

$$\langle O[\Phi] \rangle \approx \bar{O}[\Phi] = \frac{1}{N_{cfg}} \sum_{i=1}^{N_{cfg}} O[\Phi_i] \tag{1.191}$$

The estimate would be exact in the limit $N_{cfg} \to \infty$. However, since we must work at finite values of it, it's important to know the behavior of the Signal-to-Noise (StN) ratio at fixed $N_{cfg}$.
From statistics we know that for large $N_{cfg}$ the Central Limit Theorem holds. The probability distribution of data tends to a Gaussian, and the standard deviation from the mean $\sigma_G$ can be estimated as:

$$\sigma_G^2 \approx \frac{1}{N_{cfg}} \left( \langle O^2 \rangle - \langle O \rangle^2 \right) \approx \frac{1}{N_{cfg}} \left( \frac{1}{N_{cfg}} \sum_i O[\Phi_i]^2 - \bar{O}[\Phi]^2 \right) \quad . \tag{1.192}$$

Now let's apply the above formula to mesons and baryons at rest for further reference see e.g. [58] and [59].
The pion correlator is

$$\langle G_\pi \rangle = \langle J_\pi(t) J_\pi^\dagger(0) \rangle \overset{t \gg 1}{\sim} e^{-M_\pi t} \quad ,$$

where $J_\pi$ can be for instance $\bar{\psi}\gamma_5\psi$. The operator $J_\pi^2$ is a 4-quark operator exciting the state with 2-pions at rest ($E_{\pi\pi} = 2M_\pi$):

$$\langle J_\pi^2(t) J_\pi^{2\dagger}(0) \rangle \overset{t \gg 1}{\sim} e^{-2M_\pi t} \quad .$$

This means that for large $t$:

$$\sigma(t) \sim \frac{1}{\sqrt{N_{cfg}}} \langle G_\pi(t) \rangle \quad ,$$

and the StN ratio tends to a constant:

$$\frac{\overline{G_\pi(t)}}{\sigma(t)} \sim \sqrt{N_{cfg}} \times \text{const.} \tag{1.193}$$

For other mesons $P$ such as Kaons the situation is similar, with the square of the current exciting $PP$ states as the lightest states.
For baryons the situations is different. Let's consider the proton correlator for instance. The interpolator is $J_p = (uC\gamma_5 d)u$. Its square contains 6 quarks, so that the lightest state excited is $\pi\pi\pi$ rather than $p\bar{p}$. The noise then goes like,

$$\sigma_p(t) \overset{t \gg 1}{\sim} e^{-(3M_\pi/2)t} \quad , \tag{1.194}$$

and the StN as:

$$\frac{\overline{G_p(t)}}{\sigma(t)} \overset{t \gg 1}{\sim} \sqrt{N_{cfg}} e^{-(M_p - 3M_\pi/2)t} \quad . \tag{1.195}$$

Since $M_\pi$ is much smaller than $M_p$, it follows that the mass of the proton is harder to measure with respect to the pion. In fact as soon as the ground state starts to dominate, one has to cope with the degradation of the signal.
The above argument is easily generalized to other baryons, for which the plateau region is then shorter than the mesonic case.

### 1.5.2 Gaussian smearing

When we build a correlator $C(t)$, we use a given interpolating operator $\mathcal{O}$ in order to study the hadronic state we are interested in. QCD is not solved analytically, so no hadronic state $|n_0\rangle$ (i.e. QCD Hamiltonian's eigenstate) is known explicitly in terms of the degrees of freedom of the theory. For this reason, the interpolator doesn't select only the state $|n_0\rangle$, namely

$$\langle 0|O|n\rangle \neq \text{const.} \times \delta_{n,n_0} \quad , \tag{1.196}$$

but the correlator will always contain a set of signals. Each of them corresponds to an eigenstate with quantum numbers in common with $\mathcal{O}$ (e.g. spin, parity). These can be different particles, bound states, excited states, etc.
Since one is often interested in the lightest of such states, the extraction of the corresponding signal is conditioned by its quality in the *plateau* region. As discussed in sec. (1.5.1), it's tipically better to have a plateau for early times. For this reason we are interested in improving the expression of the interpolator $\mathcal{O}$, so that the overlap with the desired state is higher and its signal starts to dominate soon in time $t$.
The improvement can be implemented using *smearing* techniques, which "de-localize" the operator $\mathcal{O}$. These are often inspired by Quantum Mechanics intuitions, according to which the smearing of an operator leads to a more realistic form of the hadron's wave function [7]. An example is given by the so called *Gaussian smearing* [60], in which a quark field $q$ is smeared as follows:

$$q^{(\text{smeared})} = (1 + \alpha_g H)^{n_g} \, q^{(\text{local})} \quad , \tag{1.197}$$

where $H$ is the *Hopping matrix*:

$$H(\vec{x}, \vec{y}) = \sum_{i=1}^{3} \left[ U_i(\vec{x}, t)\delta_{\vec{x},\vec{y}-a\hat{i}} + U_i^\dagger(\vec{x} - a\hat{i}, t)\delta_{\vec{x},\vec{y}+a\hat{i}} \right] \quad . \tag{1.198}$$

The parameter $\alpha_g$ represents the nearest neighbors "coupling strenght" in the spatial directions, while $n_g$ is the number of *Gaussian steps*. They are usually tuned manually over the specific gauge configurations and correlators (see sec. (A) for the details on this work).
Its must be pointed out that even if smearing provides a faster emergence of the plateau, on the other side it distorts the matrix elements and increases the noise in the correlator. Because of this, the optimal choice is empirical and depends on the given analysis. For instance, in addition to the tuning of $\alpha_g$ and $n_g$, one can decide to smear the the source, the sink, or both in the correlator.

### 1.5.3 Stochastic sources

The calculation of an hadronic correlator in QCD passes through the (numerical) inversion of the Dirac operator. The latter is a sparse matrix [61] (in position-spin-color space), whose size makes unfeasible the calculation of the analytic solution for the propagator $S$:

$$D \cdot S = \mathbb{1} \quad .$$

The inversion is then done numerically, usually with stochastic techniques [62]. Instead of solving the above equation, one considers:

$$D \cdot \Psi = \eta \quad , \tag{1.199}$$

where $\eta$ is a random vector with average $\vec{0}$.
This can be solved for the components of the vector $\Psi$ (e.g. with algorithms such as the `BiCGstab` [63]), giving:

$$\Psi = D^{-1} \cdot \eta \quad . \tag{1.200}$$

For example, if we are calculating the correlation function:

$$\langle O(x)\bar{O}(0)\rangle = \mathrm{Tr}[S(x|0)\,\gamma_5\,S(0|x)\gamma_5] = \quad , \tag{1.201}$$

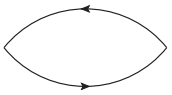


we can choose $\eta$ to vanish outside the origin with $\langle \eta(0)\eta^\dagger(0)\rangle = +1$. The correlator is approximated by:

$$\Psi(x)\Psi^\dagger(x) = \mathrm{Tr}[D^{-1}(x|z_1)\eta(z_1)\eta(z_2)^\dagger {D^{-1}}^\dagger(z_2|x)] \quad .$$

In fact, from $\gamma_5$-hermiticity [7] and averaging we get:

$$\langle \Psi(x)\Psi^\dagger(x)\rangle = \mathrm{Tr}[D^{-1}(x|0)\gamma_5 D^{-1}(0|x)\gamma_5] \quad ,$$

as desired.
The above expectation value is better reproduced if we average the $\Psi$ obtained through many separate inversions. The number of those is called *hits* or *stochastic sources*. The increase of that number, $N_s$, leads an higher cost of the simulation and to a better statistics, with a reduction in noise of a factor $\sim 1/\sqrt{N_s}$ in case of a Gaussian $\eta$. Henceforth, the number of hits is constrained by the available computational resources. See sec. (A) for details on stochastic sources used in this work).

### 1.5.4 Jackknife resampling

Expectation values of operators on the lattice are found numerically with Monte Carlo techniques. These use Markov chains to generate a set of fields configurations, which are made fall in the region where the p.d.f. in the functional integral is higher [7] (hence giving the leading contribution).
In LQCD the dependence on the fermionic fields is calculated explicitly in terms of Wick contractions, so the problem is reduced to the integration over the gauge links. For a functional $O[U]$ one approximates its value as:

$$\langle O[U]\rangle \approx \frac{1}{N_{\mathrm{cfg}}}\sum_{i=1}^{N_{\mathrm{cfg}}} O_i = \frac{1}{N_{\mathrm{cfg}}}\sum_{i=1}^{N_{\mathrm{cfg}}} O[U_i] \quad , \tag{1.202}$$

where $N_{\mathrm{cfg}}$ is the number of generated gauge configurations. This method is called *importance sampling* and is used in order to find the correlators from a finite number of field configurations.

The problem with the above definition is twofold. First, it makes hard or even impossible to estimate the statistical uncertainty on $O$. Second, the simulations are carried out using molecular dynamic algorithms, with each configuration keeping partly the memory of the previous one. Consequently these have progressively decreasing correlation, but are not completely independent of each other.
Moreover, the calculation of functions of these values requires some care. Eq. (1.201) provides an *unbiased* estimator, i.e. such that $\langle O[U]\rangle$ is restored for $N_{\rm cfg} \to \infty$). However this is not the case for the naive choice for a function $f(O)$:

$$f(\langle O\rangle) \not\approx \frac{1}{N_{\rm cfg}} \sum_{i=1}^{N_{\rm cfg}} f(O_i) \quad . \tag{1.202}$$

The latter is a *biased estimator*, namely its separation from $f(\langle O\rangle)$ doesn't vanish with increasing $N_{\rm cfg}$. For further details see [64].
In order to take these issues it into account, we used the Jackknife re-sampling technique [65], which is able to provide an unbiased estimator for any function of the random variable and its uncertainty. The latter works as follows. Let's consider a set of $N$ variables $x_i$, associated to the "real" variable $x$. They are divided into $N_{\rm jkf}$ groups $G_j = \{\bar{x}_1, ..., \bar{x}_{N-n}\}$ (of size $N-n$, where $n = N/N_{\rm jkf}$). Each of the $G_j$ consists of all the $x_i$ but the values $\{x_{(j-1)n+1}, ..., x_{jn}\}$. The jackknife values $X_j$ are obtained averaging the elements of each $G_j$:

$$X_j = \frac{1}{N-n} \sum_{k=1}^{N-n} \bar{x}_k \quad , j = 1, ..., N_{\rm jkf} \quad . \tag{1.203}$$

At this point any function $f(x)$ is evaluated as the mean over the $X_j$:

$$\bar{f} = \frac{1}{N_{\rm jkf}} \sum_{j=1}^{N_{\rm jkf}} f(X_j) \quad , \tag{1.204}$$

and the estimator for its uncertainty is:

$$\sigma_f = \sqrt{\frac{N_{\rm jkf}-1}{N_{\rm jkf}} \sum_{i=1}^{N_{\rm jkf}} \left[f(X_i) - \langle f\rangle\right]^2} \quad . \tag{1.205}$$

Other than providing a safe definition of the estimators for the reasons discussed above, jackknife re-sampling smooths the effect of self-correlation among gauge configurations. Each jackknife is obtained dividing the set in 2 blocks of weakly correlated of configurations, and averaging over the corresponding values. In this work, data were always grouped in blocks of 15 jackknifes.
The method can be used in the other direction too, generating random jackknife variables from the average and uncertainty of a given quantity.
In the following analysis this has been the case of renormalization constants, which were taken from previous ETMC works. The uncertainty $\sigma_0$ on a given quantity was propagated generating $N_{\rm jkf} = 15$ values, distributed according to a Gaussian with

$$\sigma = \frac{\sqrt{N_{\rm jkf}}}{N_{\rm jkf}-1}\sigma_0 \quad . \tag{1.206}$$

In fact, if one repeated the same analysis with $N_{\rm jkf}$, the estimate for $\sigma_0$ would be given by eq. (1.205). This matches the LHS of eq. (1.206) since the estimator of $\sigma$ for a Gaussian variable $f$ is:

$$\sqrt{\frac{1}{N_{\rm jkf}-1}\sum_{i=1}^{N_{\rm jkf}}(f_i-\bar{f})^2} \quad . \tag{1.207}$$

# Chapter 2

# Isospin Breaking Effects on the Lattice

Many lattice QCD calculation are done in the limit of isospin symmetry without including QED. In this theory the $u$ and $d$ quarks fields are degenerate degrees of freedom and some hadrons form degenerate isospin multiplets differing only for the 3rd component of isospin. This symmetry is broken in nature by the mass difference $\hat{m}_d - \hat{m}_u \, (\neq 0)$, causing the splitting of these states. In many lattice applications the level of precision of $O(1\%)$ has been reached, and these effects cannot be neglected anymore [66]. They can be taken into account simulating quarks with different masses, tuning their bare values to match some hadronic quantities and predict the others. This approach however has computational disadvantages, requiring to generate new gauge configurations. Another way to tackle the problem is to expand the action, and consequently the path integral, with respect to the breaking parameter. Any observable in the full theory will be the sum of its isosymmetric part and the Isospin Breaking (IB) effect. The perturbative expansion is justified by the fact that $\frac{\hat{m}_d - \hat{m}_u}{\Lambda_{QCD}} \sim O(1\%)$. This philosophy is the heart of the RM123 method ([67, 68, 12]) which is briefly outlined here. We now discuss the inclusion of the so called *strong IB* due to $\hat{m}_d - \hat{m}_u$ at leading order (LO), to show the main idea behind the method and set the notation. Aftwerwards we'll present how to include electromagnetism (QED), responsible effects of the same order of magnitude ($\alpha_{EM} \sim O(1\%)$).

## 2.1 Inclusion of up-down mass difference at LO

The $QCD$ Lagrangian $\mathcal{L}$ can be written as a kinetic term (K) plus a mass term:

$$\begin{aligned} \mathcal{L} &= \mathcal{L}_K + \mathcal{L}_{\text{mass.}} = \mathcal{L}_K - m_u \bar{u} u - m_d \bar{d} d \\ &= \mathcal{L}_K - m_{ud}(\bar{u}u + \bar{d}d) - \Delta m_{ud}(\bar{u}u - \bar{d}d) \\ &= \mathcal{L}_0 - \Delta m_{ud}\, \bar{q}\tau_3 q = \mathcal{L}_0 - \Delta m_{ud} \hat{\mathcal{L}} \quad . \end{aligned} \tag{2.1}$$

We write $m_u = m_{ud} - \Delta m_{ud}$, $m_d = m_{ud} + \Delta m_{ud}$. and denote the up-down doublet with $q = (u, d)^T$. $\tau_3$ is the third Pauli matrix.
From the expansion of the corresponding action $S = \int d^4x \, \mathcal{L} = S_0 - \Delta m_{ud} \int d^4x \hat{\mathcal{L}} = S_0 - \Delta m_{ud} \hat{S}$ in the path integral we get the expression of an observable $O$ at LO

[67]:

$$\langle O\rangle = \frac{\int \mathcal{D}\Phi\, O[\Phi]\, e^{-S}}{\int \mathcal{D}\Phi\, e^{-S}} \approx \frac{\int \mathcal{D}\Phi\, O[\Phi]\, e^{-S_0}[1+\Delta m_{ud}\hat{S}]}{\int \mathcal{D}\Phi\, e^{-S_0}} \quad , \tag{2.2}$$

where $\Phi$ is a shorthand notation for the degrees of freedom of the theory. Dividing numerator and denominator for the isoQCD partition function we get:

$$\langle O\rangle = \langle O\rangle_0 + \Delta m_{ud}\, \langle O\hat{S}\rangle_0 \quad . \tag{2.3}$$

The notation $\langle\cdot\rangle_0$ denotes the fully connected expectation value over the isoQCD background. In this theory the $u$ and $d$ quarks propagators are given by:

$$S_u(x|0) = \langle \mathrm{T}\,[u(x)\bar{u}(0)]\rangle = S_\ell(x|0) + \Delta m_{ud}\int d^4y S_\ell(x|y)S_\ell(y|0) + ... \quad , \tag{2.4}$$

$$S_d(x|0) = \langle \mathrm{T}\left[d(x)\bar{d}(0)\right]\rangle = S_\ell(x|0) - \Delta m_{ud}\int d^4y S_\ell(x|y)S_\ell(y|0) + ... \quad . \tag{2.5}$$

All correlation functions are expanded accordingly, neglecting higher orders than $\Delta m_{ud}$.

## 2.2 Inclusion of QED

In the continuum the introduction of QED is done including the $U(1)$ gauge part, $S[A]$, and modifying covariant derivatives including the photon field $A_\mu$. As a result, at 1st order any Green function is modified by the insertion of the photon propagator as:

$$\Delta[T\,\langle O(x_i)\rangle] \;=\; \int d^4x_1 d^4x_2 D_{\mu\nu}(x_1-x_2)\, T\,\langle O(x_i)J_\mu(x_1)J_\nu(x_2)\rangle \quad . \tag{2.6}$$

The resulting diagrams present both infrared (IR) and ultraviolet (UV) divergences [1]. The first can be coped with regulators such as a photon mass or the removal of divergent modes in the photon propagator (see sec, (2.5)). For the second, we must regularize our theory and introduce counterterms which compensate the UV divergences. Qualitatively, the difference in the electric charges of $u$ and $d$ gives them different electromagnetic self energies. QED makes the renormalized masses different even if their bare ones were equal, and its contribution is expected to be of the same order of magnitude of strong IB. As a consequence the separation between the effect of $m_u \neq m_d$ only (i.e. strong IB) and $q_u \neq q_d$ (QED) is unphysical [1] . In the following it is understood that, when talking about IB or the presence of QED, we are considering the two above effects simultaneously. Since we are at LO, we'll refer to them as LIBEs (Leading Isospin Breaking Effects). Our expansion will stop at $O(\hat{\alpha}_{EM}) \sim O(\frac{(m_d-m_u)}{\Lambda_{QCD}})$, neglecting mixed and higher order terms. We remark that the fine structure constant $\hat{\alpha}_{EM}$ renormalizes at higher orders with respect to our expansion, so that we can safely use the value $\alpha_{EM} = e^2/(4\pi) \approx 1/137...$ from [3] in the expansion.

[1] Nevertheless the latter contains some physical intuition and in sec. (2.6) we give our prescription.

### 2.2.1 Non compact QED on the lattice

We now discuss how to include QED on the lattice. This is done adding the gauge action for the electromagnetic field and modifying covariant derivatives in order to preserve gauge invariance. This is done promoting for each flavor the gluonic links through the substitution:

$$U_\mu(x) \rightarrow E_\mu^{(f)}(x) U_\mu(x) \quad , \tag{2.7}$$

where $E_\mu^{(f)}(x) = e^{iq_f A_\mu(x)}$ is the bosonic link variable associated to the photon field, and $q_f = e_f e$ is the electric charge of the particle. We'll refer to the action obtained with this procedure as *full theory* or *QCD+QED*. This formulation is called *compact* since the degrees of freedom $E_\mu^{(f)}$ live in a compact space, and is implemented on the lattice considering the QCD+QED action and integrating also over the electromagnetic gauge configurations. Here we formulate QED in a non-compact way, namely generating the photon field and not directly the gauge configurations for the electromagnetic link $E_\mu^{(f)}(x)$. This requires an infrared safe definition of the propagator since the $k = 0$ mode makes it diverge. The details about the numerical implementation are discussed in sec. (B).
With the notation of the previous section, the action is expanded with respect to $e = 0$, giving:

$$\begin{aligned} \Delta S_F &= \sum_f \sum_x \bar{\psi}_f(x) \left\{ D_f[U, A; \vec{g}] - D_f[U, 0, \vec{g}_0] \right\} \psi_f(x) \\ &= \sum_f \sum_{x,\mu} \bar{\psi}_f(x) \left\{ (e_f e) A_\mu(x) \Gamma_\mu^V(x) + \frac{1}{2} (e_f e)^2 A_\mu^2(x) \Gamma_\mu^T(x) \right\} \psi_f(x) + ... \quad . \end{aligned} \tag{2.8}$$

At the diagram level this theory is different from the continuum. The expansion of the lattice Dirac operator at $O(e^2)$ contains not only the $\sum_\mu A_\mu(x) V_\mu^{(f)}(x)$ term from the vector currents (which produces photon insertions at two different points) but also a *tadpole* interaction $\sum_\mu A_\mu(x) A_\mu(x) T_\mu^{(f)}(x)$ (which is not present in the continuum [69]). The latter is necessary to preserve gauge invariance on the lattice. The form of these two operators depend on the specific regularization chosen for fermions and are reported in sec. (C). Our choice corresponds to a mixed action theory, where the sea quarks action would be:

$$S_{\text{sea}} = \sum_x \bar{u}(x) D_u^+[U] u(x) + \bar{d}(x) D_d^+[U] d(x) \quad , \tag{2.9}$$

with:

$$\begin{aligned} D_f^\pm[U, A]\psi_f(x) =& m_f \psi_f(x) \pm i\gamma_5 (m_f^{cr} + 4) \\ &- \frac{1}{2} \sum_\mu (\pm i\gamma_5 - \gamma_\mu) U_\mu(x) E_\mu^{(f)}(x) \psi(x + \hat{\mu}) \\ &+ \frac{1}{2} \sum_\mu (\pm i\gamma_5 + \gamma_\mu) U_{-\mu}(x) E_{-\mu}^{(f)}(x) \psi(x - \hat{\mu}) \quad , \end{aligned} \tag{2.10}$$

and the $\pm$ corresponding to the sign of the Wilson term.

The action for valence quarks is:

$$= \sum_{x,f} \bar{\psi}_f(x) D_f[U,A] \psi_f(x) + \bar{\phi}(x) D_f[U,A] \phi(x) \quad , \tag{2.11}$$

where for each flavor $f$ we considered a doublet $\psi_f = (\psi_f^+, \psi_f^-)^T$ and:

$$D_f[U,A] = \frac{1+\tau_3}{2} D_f^+[U,A] + \frac{1-\tau_3}{2} D_f^-[U,A] \quad . \tag{2.12}$$

The projectors $(1 \pm \tau_3)/2$ have been isolated to show the two contributions coming from $\psi_f^+$ and $\psi_f^-$ separately. The doublet $\phi_f = (\phi_f^+, \phi_f^-)^T$ are additional bosonic degrees of freedom. The integration over them produces a fermionic determinant in the denominator of integrand of the path integral, which cancel out with the one of the valence quarks. This leads to an expression than reproduces our approximation in which the fermionic determinant are evaluated with the action of sea quarks, and quark propagators with the valence ones.
We conclude the discussion saying that for mesons we use interpolators of the form:

$$J_\Gamma = \bar{\psi}_{f_1}^+ \Gamma \psi_{f_2}^- \quad , \tag{2.13}$$

where $\Gamma$ is an appropriate combination of $\gamma$ matrices. This is done in order to reduce the statistical error and the cutoff effects [70, 71]. Moreover, for $f_1 = f_2$ it results implemented our approximation in which we neglect those (numerically noisy) diagrams with valence quark lines looping over the source or the sink.

## 2.3 Expansion of the path integral

We now discuss how to implement the LIBEs at the path integral level. This can be done including QED in the Lagrangian (see e.g. [72]), or expanding at the desired order in the breaking parameters. If we call $\vec{g}$ the set of bare parameters in the full theory, with our regularization for fermions the expectation value of an observable is:

$$O(\vec{g}) = \langle O \rangle^{(\vec{g})} = \frac{\int \mathcal{D}U \mathcal{D}A e^{-S_e[A] - \beta S_g[U]} \prod_f \det\left(D_f^\pm[U,A;\vec{g}]\right) O'[U,A;\vec{g}]}{\int \mathcal{D}U \mathcal{D}A e^{-S_e[A] - \beta S_g[U]} \prod_f \det\left(D_f^\pm[U,A;\vec{g}]\right)} \quad , \tag{2.14}$$

where $O'$ is the result of the Wick contractions resulting from the operator $O$. The action $S_e[A]$ is:

$$S_e[A] = \frac{1}{2} \sum_x \sum_{\mu,\nu} A_\mu(x) \left[-\nabla_\nu^- \nabla_\nu^+\right] A_\mu(x) = \frac{1}{2} \sum_k \sum_{\mu,\nu} \tilde{A}_\mu^\star(k) \left[2 \sin\left(k_\nu/2\right)\right]^2 \tilde{A}_\mu(k) \quad , \tag{2.15}$$

and $\beta S_g[U]$ is the gluonic action ($\beta = 6/g_s^2$). In our twisted mass regularization we have:

$$\vec{g} = (e^2, g_s^2, m_u, m_d, m_s, m_u^{cr}, m_d^{cr}, m_s^{cr}) \quad , \tag{2.16}$$

and at LO the observable is:

$$\begin{aligned} O(\vec{g}) &= O\left(\vec{g}_0\right) + \left\{ e^2 \frac{\partial}{\partial e^2} + \left[g_s^2 - \left(g_s^0\right)^2\right] \frac{\partial}{\partial g_s^2} + \left[m_f^{cr} - m_f^{cr\,0}\right] \frac{\partial}{\partial m_f^{cr}} + \left[m_f - m_f^0\right] \frac{\partial}{\partial m_f} \right\} O(\vec{g}) \Big|_{\vec{g}=\vec{g}_0} \\ &= \langle O \rangle^{\vec{g}_0} + \Delta O^{(EMC)} + \sum_f \left[m_f - m_f^0\right] \bar{\Delta} O^{(f)\,(MASS)} = \langle O \rangle^{\vec{g}_0} + \Delta O \quad , \end{aligned} \tag{2.17}$$

where we have already introduced a notation that will bel used later: $\Delta^{(EMC)}$ stands for the combination of the corrections coming from the coupling with the electromagnetic field and the variation in the critical mass counterterms, and $\bar{\Delta}^{MASS}$ is the slope induced by the physical mass counterterm.
With the following notation,

$$R[U,A;\vec{g}] = e^{-(\beta-\beta_0)S_g[U]} r[U,A;\vec{g}] \tag{2.18}$$

$$r[U,A;\vec{g}] = \prod_f r_f[U,A;\vec{g}] = \prod_f \frac{\det\left[D_f^{\pm}[U,A;\vec{g}]\right]}{\det\left[D_f^{\pm}[U,A,\vec{g}_0]\right]} \quad , \tag{2.19}$$

$$\langle O\rangle^A = \frac{\int \mathcal{D}A e^{-S_e[A]} O[A]}{\int \mathcal{D}e^{-S_e[A]}} \tag{2.20}$$

we can write the above expectation value as [68]:

$$O(\vec{g}) = \langle O\rangle^{\vec{g}} = \frac{\left\langle \langle R[U,A;\vec{g}] O'[U,A;\vec{g}]\rangle^A \right\rangle^{\vec{g}_0}}{\left\langle \langle R[U,A;\vec{g}]\rangle^A \right\rangle^{\vec{g}_0}} \quad , \tag{2.21}$$

where $\vec{g}_0$ is the set of coupling in isoQCD:

$$\vec{g_0} = (e^2, (g_s^{(0)})^2, m_{ud}^{(0)}, m_{ud}^{(0)}, m_s^{(0)}, {m_0}^{cr}, {m_0}^{cr}, {m_0}^{cr}) \quad . \tag{2.22}$$

In this work we used the values of $m_0^{cr}$ found from the PCAC Ward Identity in absence of IB [73]. Eq. (2.21) encodes the integration over the photon field and the link with the expectation value with respect to the isosymmetric background. The variation $\Delta O$ induced in a generic observable at LO is then given by:

$$\begin{aligned}\Delta O &= O(\vec{g}) - O(\vec{g}_0) \\ &= \left\langle \Delta O[U,A;\vec{g}]|_{\vec{g}=\vec{g}_0} \right\rangle^{A,\vec{g}_0} + \left\{ \left\langle \Delta(RO-O)[U,A;\vec{g}]|_{\vec{g}=\vec{g}_0} \right\rangle^{A,\vec{g}^0} - \left\langle \Delta R[U,A;\vec{g}]|_{\vec{g}=\vec{g}_0} \right\rangle^{A,\vec{g}_0} \langle O\,[U,\vec{g}_0]\rangle^{\vec{g}_0} \right\} \quad .\end{aligned} \tag{2.23}$$

The terms containing $R[U,A,\vec{g},\vec{g}_0]$ encode the modification in the quark determinants. As we'll see in a moment, this represents how sea quarks interact with $A_\mu$, giving rise to Feynman diagrams in which photons are exchanged with loop quark lines.

### 2.3.1 Diagrammatic notation for LIBEs

Here we set the notation for the diagrammatic expression of the contributions appearing in eq. (2.23). First, we note that

$$\left.\frac{\partial \langle O\rangle^A (e^2)}{\partial (e^2)}\right|_{e^2=0} = \left\langle \frac{1}{2} \left.\frac{\partial^2 O[A,e]}{\partial e^2}\right|_{e=0} \right\rangle^A \quad , \tag{2.24}$$

which comes trivially from the formula for a Taylor expansion. Moreover we recall that from $D_f S_f = \mathbb{1}$ it follows:

$$\frac{\partial D_f}{\partial \lambda} S_f + D_f \frac{\partial S_f}{\partial \lambda} = 0 \quad , \tag{2.25}$$

for any parameter $\lambda$. Therefore the quark propagator is modified as follows:

$$\frac{\partial S_f}{\partial m_f} = -S_f \frac{\partial D_f}{\partial m_f} S_f = -$$ 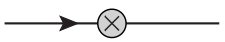 , (2.26)

$$\frac{\partial S_f^{\pm}}{\partial m_f^{cr}} = -S_f^{\pm} \frac{\partial D_f^{\pm}}{\partial m_f^{cr}} S_f^{\pm} = \mp$$  , (2.27)

and

$$\frac{\partial S_f}{\partial (e^2)} = \frac{1}{2}\frac{\partial^2 S_f}{\partial e^2} = S_f \frac{\partial D_f}{\partial e} S_f \frac{\partial D_f}{\partial e} S_f - \frac{1}{2} S_f \frac{\partial^2 D_f}{\partial e^2} S_f$$
$$= e_f^2$$ 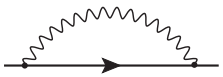 $+ e_f^2$ 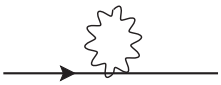 (2.28)

The variations induced in the $R$ factor are:

$$\frac{\partial R}{\partial g_s^2} = \frac{\beta^2}{6} S_g[U] = \boxed{G_{\mu\nu} G^{\mu\nu}} \quad , \tag{2.29}$$

and [2]

$$\frac{\partial r}{\partial (e^2)} = \frac{1}{2}\frac{\partial^2 r_f}{\partial e^2} = +\frac{1}{2}\,\mathrm{Tr}\left(S_f \frac{\partial D_f}{\partial e}\right)\mathrm{Tr}\left(S_f \frac{\partial D_f}{\partial e}\right) - \frac{1}{2}\,\mathrm{Tr}\left(S_f \frac{\partial D_f}{\partial e} S_f \frac{\partial D_f}{\partial e}\right) + \frac{1}{2}\,\mathrm{Tr}\left(S_f \frac{\partial^2 D_f}{\partial e^2}\right)$$
$$= -\sum_{f_1 \in \{\mathrm{sea}\}} e_{f_1} \left\{ \sum_{f_2 \in \{\mathrm{sea}\}} e_{f_2} \right.$$ 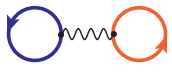 $- e_{f_1}$ 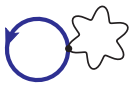 $- e_{f_1}$  $\Big\}$ . (2.32)

$$\frac{\partial r}{\partial m_f} = \mathrm{Tr}\left[S_f \frac{\partial D_f}{\partial m_f}\right] =$$  (2.33)

$$\frac{\partial r}{\partial m_f^{(cr)}} = \mathrm{Tr}\left[S_f \frac{\partial D_f}{\partial m_f^{(cr)}}\right] =$$  . (2.34)

We are now able to find the final expression for the quark propagator. We remark that we also need the following expressions (obtained at fixed QED background):

$$\frac{\partial S_f}{\partial e} = -S_f \frac{\partial D_f}{\partial e} S_f = e_f$$ 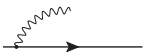 (2.35)

$$\frac{\partial r_f}{\partial e} = e_f\,\mathrm{Tr}\left(S_f \frac{\partial D_f}{\partial e}\right) =$$ 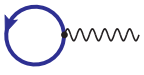 (2.36)

[2] These identities are easily derived recalling the Jacobi's formula [74] for the derivative of a matrix $A$ with respect to a parameter $\lambda$:

$$\frac{\partial \det A}{\partial \lambda} = (\det A)\,\mathrm{Tr}\left[A^{-1}\frac{\partial A}{\partial \lambda}\right] \tag{2.30}$$

$$\frac{\partial^2 \det A}{\partial \lambda^2} = (\det A)\,\mathrm{Tr}\left[A^{-1}\frac{\partial A}{\partial \lambda}\right]\mathrm{Tr}\left[A^{-1}\frac{\partial A}{\partial \lambda}\right] - (\det A)\,\mathrm{Tr}\left[A^{-1}\frac{\partial A}{\partial \lambda}A^{-1}\frac{\partial A}{\partial \lambda}\right] + (\det A)\,\mathrm{Tr}\left[A^{-1}\frac{\partial^2 A}{\partial \lambda^2}\right] \tag{2.31}$$

The variation $\Delta S_f^{\pm}$ is:

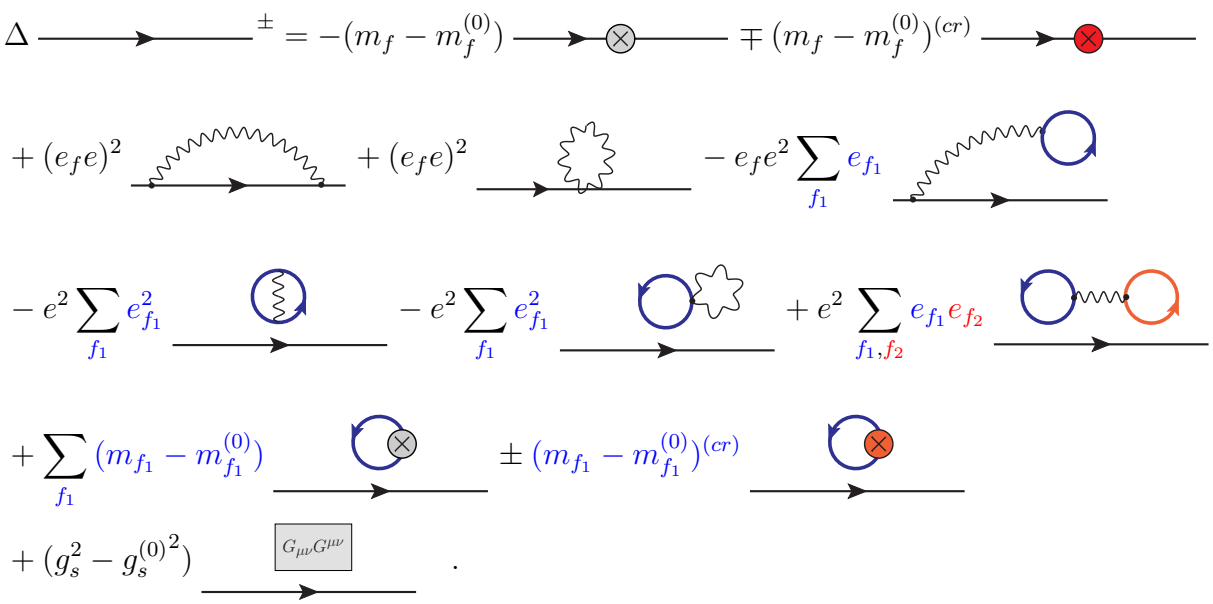


(2.37)

In order to find the LIBEs in a generic correlator, is then sufficient to write it in the full theory, consider all the possible variations of its quark propagators one by one, and summing all the resulting diagrams obtained using the above formula. We'll se the examples of IB slopes i sec. (C.1) and (C.2).

For the studies presented in this thesis we use the so called *electroquenched* approximation, in which sea quarks are neutral with respect to the electromagnetic field. Our theory is then equivalent to setting $e = 0$ in $S_{\text{sea}}$. Even if this theory is non unitary, with this approximation we gain the numerical advantage of not having to consider the variation in the sea quark determinants. At the path integral level, this consists in setting $r_f = 1$ for each flavor $f$, and the quark propagator reads:

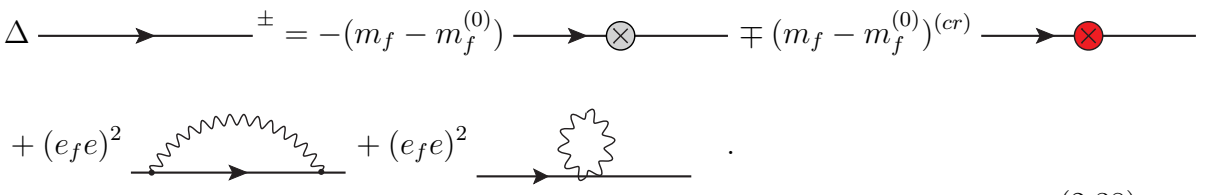


(2.38)

## 2.4 LIBEs from correlation functions

The IB slopes in the mass of an hadron $H$ can be found from the corresponding corrections in those correlators $C_H(t)$ whose isoQCD ground state has mass $M_H^{(0)}$. In fact, for large times $C_H(t) \approx Ae^{-Mt}$, and expanding at 1st order, i.e. $A = A_0(1 + \Delta A)$ and $M \to M + \Delta M$, shows that:

$$\frac{\Delta C_H(t)}{C_H^{(0)}(t)} = \Delta A - \Delta M\, t \quad , \tag{2.39}$$

where $C_H^{(0)}$ is the correlator in absence of the perturbation. The effective curves $\Delta M$ and $\Delta A$ are:

$$\begin{aligned} \Delta M_{\text{eff}}(t) =& -\partial_t \frac{\Delta C(t)}{C_0(t)} \\ \Delta A_{\text{eff}}(t) =& \frac{\Delta C(t)}{C_0(t)} + \Delta M_{\text{eff}}(t) \cdot t \quad , \end{aligned} \tag{2.40}$$

where $\partial_t$ is the lattice forward derivative. Equivalently, in the same range, one can do a linear fit of eq. (2.39) and find $\Delta M$ from the slope of the line. Note that for mesons, as before, the version of the above formula including the backward signal is more involved (see [12] for instance):

$$\Delta M_{\text{eff}}(t) = \frac{[\coth\left(E_0\left(T/2-t\right)\right)]^{(-)^p}}{(T/2-t)} \left( \frac{\Delta C(t)}{C_0(t)} - \frac{\Delta C(T/2)}{C_0(T/2)} \right) \quad , \tag{2.41}$$

where $p$ is the temporal parity of the correlator as in eq. (1.152) and $E_0$ has been obtained from the free correlator $C_0(t)$ [3] . The effective curve of the relative correction $\Delta A$ is given by:

$$\Delta A_{\text{eff}} = \frac{\Delta C(T/2)}{C_0(T/2)} + \Delta E_{\text{eff}}(t) T/2 \quad . \tag{2.42}$$

However we point out that the correction induced in the amplitude (i.e. in the matrix element) is unphysical, and depends on the chosen gauge [75]. In the following we'll always use the notation of (2.40), i.e. $-\partial_t$, as a shorthand to denote the mass slope of the lightest state of a correlator. In the present work, for consistency, we found the isoQCD masses and their slopes using in both cases the same technique, i.e. fitting to a constant the corresponding effective curves (eq. (1.151)) and eq. (2.40)) respectively) in their plateau intervals.

## 2.5 FVEs in presence of IB

The IB corrections suffer from FVE of 2 different origins. The first are the QCD effects, shown by the physical mass slopes. These are caused by the variation of the physical bare quark mass, and show the typical exponential suppression behavior [50]. This is seen applying the IB correction at 1st order to the asymptotic formulas $M(L) = M(\infty)(1 + f_L)$ of sec. (1.4.2) (here $f_L$ is the term exponentially suppressed in $L$). we see that the resulting mass correction $\Delta M$ goes approximately as $\sim e^{-M_P L}/(M_P L)^\alpha$ (for some $\alpha$), where $P$ is the pseudo-scalar meson appearing in the LO loop in ChPT. As discussed in a moment, QED FVEs are only power law suppressed, making the above QCD FVEs subleading with respect to the latter.
The second FVEs come from QED, due to the exchange of photons on the finite size lattice. QED is a long range interaction ($m_\gamma = 0$) [1], but when confined to a finite box with periodic boundary conditions it becomes rather different. For instance, Gauss's and Ampere's laws are not satisfied anymore [76, 77]. In fact, let's consider Gauss's law,

$$\nabla_i E^i(\vec{x}) = \rho(\vec{x}) \quad , \tag{2.43}$$

[3] Note that $E_0$ is supplied as a prior, and using the value of the effective mass a time $t$ for $E_0$ is not correct. In fact, the effective mass curve of $C_0(t)$ and the one of the corrections may have different plateau regions.

in the case of a point charge at the center of the lattice, $\rho(\vec{x}) = q\delta(\vec{x})$. Integrating the above equation and using the divergence theorem gives 0 on the LHS, while the RHS gives $q(\neq 0)$. This means that no single charge can live on the torus. The inconsistency of Ampere's law is proven similarly by explicit integration, finding that no electric current $\vec{J}$ can live on the torus.
The consequence of these properties is that the electromagnetic field cannot be taken as it is, simply imposing boundary conditions. Moreover, at the quantum level the photon propagator contains a divergence, caused by the zero-momentum mode. The regularization of the latter introduces prescription-dependent FVEs, which are polynomially suppressed in $1/L$ [77], where $L$ is the linear spatial extent of the lattice. In this work we adopted the $QED_L$ regularization, consisting in the removal of the $\vec{k} = 0$ momentum mode. This is equivalent to the introduction of a uniform background charge density which also restores Gauss's law [78, 77]. The asymptotic behavior of these FVE is widely discussed in literature (see e.g. [76, 77, 79, 72]), where it is found that the asymptotic volume dependence of an hadronic mass is:

$$M(T,L) \xrightarrow{T,L\to\infty} M(\infty)\left\{1 - Q^2\alpha_{EM}\left[\frac{\kappa}{2ML}\left(1+\frac{2}{ML}\right)\right]\right\} + O(\frac{\alpha_{EM}}{L^3}) \quad , \quad (2.44)$$

where $\kappa \approx 2.837297$ and $Q$ is the charge of the hadron in units of $e$. In the above expression we neglect terms which are exponentially suppressed or that fall faster than any power of $(MT)^{-1}$, and the $M$ in the denominators can be set equal to $M(L=\infty)$ at 1st order in $\alpha_{EM}$. The $\sim L^{-1}$ and $\sim L^{-2}$ terms are *universal*, in the sense that they don't depend on the spin or structure of the hadron, which appear only at higher orders.

## 2.6 Separation of strong IB and QED

Isospin Breaking is the effect coming from both the mass difference between $u$ and $d$, and the interaction with the photon field. In general this applies to any observable, meaning that the correction induced by IB is a combination of the modified quark masses and electromagnetic (self) energy. In the literature these two effects are respectively called *strong IB* (or *QCD*) and *QED* IB, and their separation is arbitrary. In fact, the distribution of finite terms in RCs is scheme dependent, hence unphysical. Anyhow, in some cases this separation is useful, since the two contributions have an intuitive interpretation. An example is indeed the mass difference between charged and neutral hadrons. Let's consider the nucleons. The neutron tends to be heavier because $m_d > m_u$. The $u$ however has a bigger electric charge, and hence the electromagnetic self energy of the proton is higher than the neutron. In nature it happens that these contributions are of the same order of magnitude, so that they cancel almost exactly leaving a small mass difference, $O(1\,\mathrm{MeV})$, compared to their masses, $O(1\,\mathrm{GeV})$.
We now discuss our prescription for the separation of these two effects and the renormalization of the mass difference $m_d - m_u$. In the analysis we find the bare counterterms $a\Delta m_f$ that reproduce the experimental values of given hadronic ratios. $\Delta m_u$ and $\Delta m_d$ contain a contribution from strong IB and one from QED, and we

write the difference $\Delta m_{ud} = (m_d - m_u)/2 = (\Delta m_d - \Delta m_u)/2$ as follows [12]:

$$\Delta m_{ud} = \Delta m_{ud}^{(QCD)} + \Delta m_{ud}^{(QED)} = Z_P^{(0)} \Delta \hat{m}_{ud} + \frac{(q_d^2 - q_u^2)}{32\pi^2} \left[6 \log (a\mu) - 22.595\right] m_\ell^{(0)} \quad . \tag{2.45}$$

This equation defines our separation and how to find the renormalized mass difference $\Delta \hat{m}_{ud}$. At LO, the $QED$ contribution to an observable is obtained combining the corrections from diagrams involving photons, critical mass counterterms, and $\Delta m_f^{(QED)}$ in place of the full physical mass counterterms. The strong IB effect is obtained considering only the latter diagrams, replacing the full $\Delta m_f$ with $\Delta m_f^{(QCD)}$. The values of $Z_P^{(0)}$ of the present work were taken from [13]. The expression for $\Delta m_{ud}^{(QED)}$ is obtained in the so called *factorization approximation*, which neglects the mixing of $QCD$ and $QED$ in renormalization, namely $Z_P^{(QCD+QED)} \approx Z_P^{(QCD)} Z_P^{(QED)}$. At 1st order Lattice $QCD$ and $QED$ are distinguished only by color factors, so we found $Z_P^{(QED)}$ (for each flavor) from the 1 loop calculation of [80] in the $\overline{\text{MS}}$ scheme.

## 2.7 IB corrections from Isospin structure

The IB corrections to a correlator are a direct consequence of Wick contractions, which contain all the information needed. These originate from the isospin structure of the interpolator, leading to defined patterns which may not be evident until one actually computes all the contractions. For this reason we now discuss how the infer *a priori* the form of LIBEs in the hadronic spectrum. This doesn't add information with respect to explicit Wick contractions, nevertheless serves a check for the results. We focus on the particular case of $\pi$, $N$ and $\Delta$, for which we find:

$$M_{\pi^+} = M_\pi + e^2 \left( B_0^{(\pi)} - \sqrt{\frac{3}{10}} B_2^{(\pi)} \right) \tag{2.46}$$

$$M_{\pi^0} = M_\pi + e^2 \left( B_0^{(\pi)} - \sqrt{\frac{2}{5}} B_2^{(\pi)} \right) \tag{2.47}$$

$$M_{\pi^-} = M_\pi + e^2 \left( B_0^{(\pi)} - \sqrt{\frac{3}{10}} B_2^{(\pi)} \right) \quad , \tag{2.48}$$

and

$$M_p = M_N - \Delta m_{ud} \sqrt{\frac{1}{3}} A^{(N)} + e^2 \left( B_0^{(N)} - \sqrt{\frac{1}{3}} B_1^{(N)} \right) \tag{2.49}$$

$$M_n = M_N + \Delta m_{ud} \sqrt{\frac{1}{3}} A^{(N)} + e^2 \left( B_0^{(N)} + \sqrt{\frac{1}{3}} B_1^{(N)} \right) \quad , \tag{2.50}$$

and

$$M_{\Delta^{++}} = M_\Delta + \Delta m_{ud}\sqrt{\frac{3}{5}}A_1^{(\Delta)} + e^2\left(B_0^{(\Delta)} + \sqrt{\frac{3}{5}}B_1^{(\Delta)} + \sqrt{\frac{1}{5}}B_2^{(\Delta)}\right) \tag{2.51}$$

$$M_{\Delta^{+}} = M_\Delta + \Delta m_{ud}\sqrt{\frac{1}{15}}A_1^{(\Delta)} + e^2\left(B_0^{(\Delta)} + \sqrt{\frac{1}{15}}B_1^{(\Delta)} - \sqrt{\frac{1}{5}}B_2^{(\Delta)}\right) \tag{2.52}$$

$$M_{\Delta^{0}} = M_\Delta - \Delta m_{ud}\sqrt{\frac{1}{5}}A_1^{(\Delta)} + e^2\left(B_0^{(\Delta)} - \sqrt{\frac{1}{15}}B_1^{(\Delta)} - \sqrt{\frac{1}{5}}B_2^{(\Delta)}\right) \tag{2.53}$$

$$M_{\Delta^{-}} = M_\Delta - \Delta m_{ud}\sqrt{\frac{3}{5}}A_1^{(\Delta)} + e^2\left(B_0^{(\Delta)} - \sqrt{\frac{3}{5}}B_1^{(\Delta)} + \sqrt{\frac{1}{5}}B_2^{(\Delta)}\right) \quad . \tag{2.54}$$

We denote with $H = \pi\,, N\,, \Delta$ the isoQCD limits of the members of each multiplet, with common coefficients $A_0^{(H)}$, $A_1^{(H)}$ and $B_0^{(H)}$, $B_1^{(H)}$, $B_2^{(H)}$.
The above relations imply the following properties.

$$M_{\pi^+} - M_{\pi^0} = e^2\left(\sqrt{\frac{2}{5}} - \sqrt{\frac{3}{10}}\right)B_2^{(\pi)} \quad , \tag{2.55}$$

from which we see that this is a purely electromagnetic effect.
For $\Delta$s we have:

$$M_{\Delta^{++}} - M_{\Delta^{-}} = 3(M_{\Delta^{+}} - M_{\Delta^{0}}) \quad , \tag{2.56}$$

$$(M_{\Delta^{++}} + M_{\Delta^{-}}) - (M_{\Delta^{+}} + M_{\Delta^{0}}) = 4e^2\sqrt{\frac{1}{5}}B_2^{(\Delta)} \quad . \tag{2.57}$$

Consequently there are only 2 independent mass splittings in the $\Delta$-multiplet. Eq. (2.57) expresses a pure QED effect.
We now prove eqs. (2.46), (2.49), (2.51), starting from the Lagrangian in QCD+QED:

$$\mathcal{L} = \mathcal{L}_K - m_u\bar{u}u - m_d\bar{d}d - eA_\mu\left(e_u\bar{u}\gamma_\mu u + e_d\bar{d}\gamma_\mu d\right) \tag{2.58}$$

$$= \mathcal{L}_K - m_{ud}\,\bar{q}q - \Delta m_{ud}\,\bar{q}\tau_3 q + eA_\mu\bar{q}\gamma_\mu\left(\frac{\tau_3}{2} + \frac{1}{6}\right)q \tag{2.59}$$

$$= \mathcal{L}_0 - \Delta m_{ud}\,\bar{q}\tau_3 q + eA_\mu\bar{q}\gamma_\mu\mathcal{Q}q \tag{2.60}$$

$$= \mathcal{L}_0 - \Delta m_{ud}\,\bar{q}\tau_3 q + eA_\mu J_\mu^{\mathcal{Q}} \quad . \tag{2.61}$$

The first term, $\mathcal{L}_0$, is symmetric under $SU(2)_I$ and chargeless (isoQCD theory) and the rest are isospin breaking terms. At LO in IB we expand in $\Delta m_{ud}$ and $e^2$, so for a (bare) correlator at LO we have:

$$\begin{aligned} C(t) = \langle T\left[O(t)O^\dagger(0)\right]\rangle &= \frac{\int \mathcal{D}A_\mu\mathcal{D}\Phi\, e^{-S}\, O(t)O^\dagger(0)}{\mathcal{D}A_\mu\mathcal{D}\Phi\, e^{-S}} \\ &= \frac{\int \mathcal{D}\Phi\, e^{-S_0}\left(1 + \Delta m_{ud}\hat{S}_1 + e^2\hat{S}_2\right)\, O(t)O^\dagger(0)}{\int \mathcal{D}\Phi\, e^{-S_0}\left(1 + \Delta m_{ud}\hat{S}_1 + e^2\hat{S}_2\right)} \quad . \end{aligned} \tag{2.62}$$

$T$ is the time-ordering operator, $A_\mu$ is the photon field and $\Phi$ is a shorthand for all the degrees of freedom of the isosymmetric theory. In the second step we have

stopped at LO, integrating over the spacetime points of application of the photon propagator. This means that $\hat{S}_2$ is:

$$\hat{S}_2 = \frac{1}{2}\int d^4x d^4y\, D_{\mu\nu}(x,y)\, J^{\mathcal{Q}}_{\mu}(x)\, J^{\mathcal{Q}}_{\nu}(y) \tag{2.63}$$

Note that we don't have $O(e)$ terms because of Furry's theorem [1]: vacuum expectation values with an odd number of photon fields vanish. The correlator is then:

$$C(t) = C_0(t) + \Delta m_{ud}\,\langle T\left[\hat{S}_1 O(t) O^{\dagger}(0)\right]\rangle_0 + e^2\,\langle T\left[\hat{S}_2 O(t) O^{\dagger}(0)\right]\rangle_0 \quad , \tag{2.64}$$

where the subscript 0 corresponds to the isoQCD limit of the connected diagrams (the disconnected contributions are canceled by the denominator [1]).
We now make a couple of remarks. The operator $\hat{S}_2$ has three contributions coming from the product of 2 currents, which determine its isospin quantum numbers. These behave as:

$$\hat{S}_{20} \sim \bar{q}(x)\gamma_\mu q(x)\,\bar{q}(y)\gamma_\nu q(y) \quad , \tag{2.65}$$

$$\hat{S}_{21} \sim \bar{q}(x)\gamma_\mu \tau_3 q(x)\,\bar{q}(y)\gamma_\nu q(y) \quad , \tag{2.66}$$

$$\hat{S}_{22} \sim \bar{q}(x)\gamma_\mu \tau_3 q(x)\,\bar{q}(y)\gamma_\nu \tau_3 q(y) \quad . \tag{2.67}$$

We observe that under $SU(2)_I$ the operator $\hat{S}_{2k}$ transform like the 0-th component of a $k$-rank spherical harmonic tensor $T^{(k)}_0$. $\hat{S}_1$ transforms like $T^{(1)}_0$.
The final result for $C(t)$ is the same as if we consider an effective Hamiltonian containing two 1st order perturbations:

$$H_{\text{eff.}} = H_0 + \Delta m_{ud}\hat{S}_1 + e^2\hat{S}_2 \quad . \tag{2.68}$$

The mass corrections at LO are then given by the Hellmann-Feynman theorem [81]:

$$\Delta M_H = \Delta m_{ud}\,\langle H|\hat{S}_1|H\rangle + e^2\,\langle H|\hat{S}_2|H\rangle \quad . \tag{2.69}$$

The degeneracy of the multiplets is not an issue because they happen to be eigenstates of $\hat{S}_1$ and $\hat{S}_2$.
From the above considerations, we can apply the Wigner-Eckart theorem:

$$\langle j_1, m_1|T^{(k)}_q|j_2, m_2\rangle = \langle j_2, m_2\,;\, k, q|j_1, m_1\rangle\,\langle j_1||T^{(k)}||j_2\rangle \quad , \tag{2.70}$$

and find the slope structure from Clebsh-Gordan coefficients. Recall that the reduced matrix element $\langle j_1||T^{(k)}||j_2\rangle$ is the same for a given multiplet.
These coefficients multiply the matrix elements in mass splittings. For $A^{(H)}_0$ and $B^{(H)}_0$ they're all 1 (the rank of the tensor is 0). On the other hand $A^{(H)}_1$ and $B^{(H)}_1$ multiply:

$$N \qquad \langle 1/2, I_z; 1, 0|1/2, I_z\rangle \qquad I_z = 1/2, -1/2 \tag{2.71}$$

$$\Delta \qquad \langle 3/2, I_z; 1, 0|3/2, I_z\rangle \qquad I_z = 3/2, 1/2, -1/2, -3/2 \quad . \tag{2.72}$$

Note that for $\pi$, the reduced matrix element $\langle\pi||(1,0)||\pi\rangle = 0$. In fact $|I = 1\rangle$ states (pions) are symmetric under the exchange $u \leftrightarrow d$, while any current $J_\Gamma = \bar{q}\Gamma\tau_3 q$ is anti-symmetric. Hence, its expectation value between them vanishes.

This can be understood also in terms of $G$-parity [67]. The latter is a combination of $C$ and $I_2$. Since both charge conjugation and Isospin are exact symmetries of the strong interaction (in the limit $m_u = m_d$), then $G$ is also conserved. Since $J_\Gamma$ is an eigenstate of $G$ with eigenvalue $-1$, it can have non-vanishing matrix elements only between eigenstates with eigenvalues opposite between each other. It follows that the reduced matrix element of $J_\Gamma$ between 2 pions is zero.
Finally $B_2^{(H)}$ multiplies:

$$\begin{aligned}
\pi \quad & \langle 1, I_z; 2, 0 | 1, I_z \rangle \quad && I_z = 1, 0, -1 && (2.73)\\
N \quad & \langle 1/2, I_z; 2, 0 | 1/2, I_z \rangle \quad && I_z = 1/2, -1/2 && (2.74)\\
\Delta \quad & \langle 3/2, I_z; 2, 0 | 3/2, I_z \rangle \quad && I_z = 3/2, 1/2, -1/2, -3/2 \quad . && (2.75)
\end{aligned}$$

## 2.8 Mesons in QCD+QED

In this work the mesons we deal with are pions ($\pi^+$, $\pi^0$) and kaons ($K^+$, $K^0$). In the full theory their correlators are:

$$\begin{aligned}
C_{\pi^+\pi^-}(x) &= -\langle [\bar{u}\gamma_5 d](x)\, [\bar{d}\gamma_5 u](0)\rangle && (2.76)\\
C_{\pi^0\pi^0}(x) &= -\frac{1}{2}\langle [\bar{u}\gamma_5 u - \bar{d}\gamma_5 d](x) [\bar{u}\gamma_5 u - \bar{d}\gamma_5 d](0)\rangle && (2.77)\\
C_{K^+K^-}(x) &= -\langle [\bar{s}\gamma_5 u](x)\, [\bar{u}\gamma_5 s](0)\rangle && (2.78)\\
C_{K^0\bar{K}^0}(x) &= -\langle [\bar{s}\gamma_5 d](x)\, [\bar{d}\gamma_5 s](0)\rangle && (2.79)
\end{aligned}$$

The corrections to their masses at LO are obtained from the considerations of the previous sections. We apply the variation $\Delta$ to the quark propagators in the correlators, divide by the free one and derive with respect to time. We now provide their diagrammatic expressions.

### 2.8.1 Pions

For pions we have:

$\Delta M_{\pi^+} = +2(m_{ud} - m_{ud}^{(0)})\partial_t$ 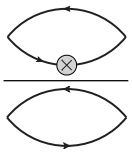 $- 2(m_{ud} - m_{ud}^{(0)})^{(crit)}\partial_t$ 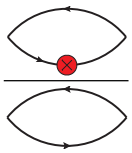

$- e_u e_d e^2 \partial_t$ 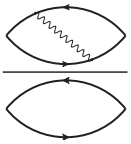 $- (e_u^2 + e_d^2) e^2 \partial_t$ 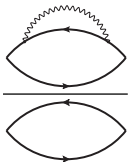 $- (e_u^2 + e_d^2) e^2 \partial_t$ 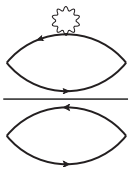

$- (e_u + e_d) e^2 \sum_{f \in \{\text{sea}\}} e_f \partial_t$ 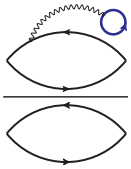 $+$ [isosymm. vac. pol. diag.] , (2.80)

$$\Delta M_{\pi^0} = +2(m_{ud} - m_{ud}^{(0)})\partial_t$$ 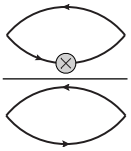 $$- (m_u + m_d - m_{ud}^{(0)})^{(crit)}\partial_t$$ 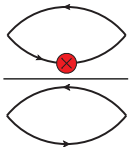

$$- \frac{(e_u^2 + e_d^2)}{2} e^2 \partial_t$$ 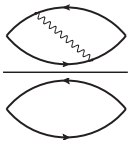 $$- (e_u^2 + e_d^2) e^2 \partial_t$$ 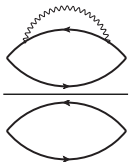 $$- (e_u^2 + e_d^2) e^2 \partial_t$$ 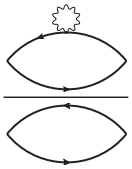

$$- (e_u + e_d) e^2 \sum_{f \in \{\text{sea}\}} e_f \partial_t$$ 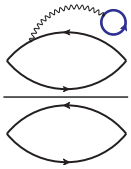 $$+ \frac{(e_u - e_d)^2}{2} e^2 \partial_t$$ 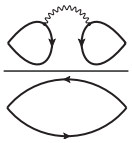

$$+ [\text{isosymm. vac. pol. diag.}] \quad , \tag{2.81}$$

and their mass difference is a purely electromagnetic effect:

$$M_{\pi^+} - M_{\pi^0} = \frac{(e_u - e_d)^2}{2} e^2 \left[ \partial_t \right.$$ 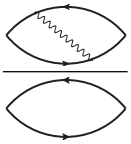 $$\left. - \partial_t \right.$$ 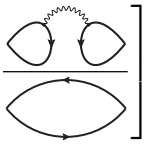 $$\left. \right] \quad . \tag{2.82}$$

In our study we neglect the disconnected term (usually called *handcuffs* diagram) which, being disconnected, represents a highly non-trivial numerical problem and demands a significative computational cost [82]. We approximate $M_{\pi^+} - M_{\pi^0}$ as:

$$M_{\pi^+} - M_{\pi^0} \approx \frac{(e_u - e_d)^2}{2} e^2 \partial_t$$ 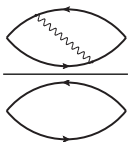 $$\quad . \tag{2.83}$$

This introduces a small systematic effect of $O(\hat{\alpha}_{EM}\hat{m}_\ell)$ [12], here neglected in virtue of the vicinity of the chiral point to the physical world. Our approximation then consists in putting $O(e^2\hat{m}_\ell)$ on the same level of $O(e^2[\hat{m}_d - \hat{m}_u])$, which is neglected at LO in IB. In fact, from Dashen's theorem in $SU(3)$ chiral symmetry ([83, 84]), we know that $M_{\pi^0} = 0$ (and thus $\Delta M_{\pi^0} = 0$) for arbitrary values of the electric charges $e_u$, $e_d$, $e_f$ and heavier quark masses $\hat{m}_f$. This applies directly to $SU(2)$. In particular, we can isolate the contributions to $\Delta M_{\pi^0}$ which respectively multiply $(e_u^2 + e_d^2)$, the $e_f$ from the sea and $(e_u - e_d)^2$. By linear independence, these have to vanish individually in that limit. Since the handcuffs diagram is the only one multiplying $(e_u - e_d)^2$, it is of $O(e^2\hat{m}_\ell)$.

### 2.8.2 Kaons

Kaons follow an analogous pattern:

$$\Delta M_{K^+} = + (m_u - m_{ud}^{(0)})\partial_t$$ 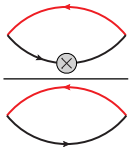 $$+ (m_s - m_s^{(0)})\partial_t$$ 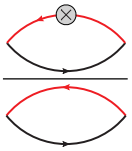

$$- (m_u - m_{ud}^{(0)})^{(crit)}\partial_t$$ 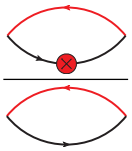 $$+ (m_s - m_s^{(0)})^{(crit)}\partial_t$$ 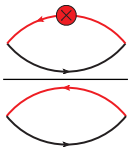

$$- (e_s e)^2\partial_t$$ 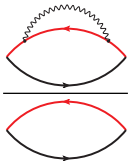 $$- (e_u e)^2\partial_t$$ 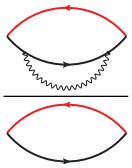 $$- (e_s e)^2\partial_t$$ 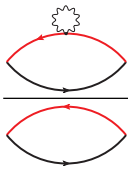 $$- (e_u e)^2\partial_t$$ 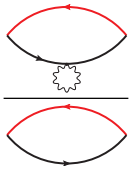

$$- e_u e_s e^2\partial_t$$ 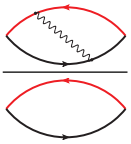 $$- e_s e^2 \sum_{f\in\{\text{sea}\}} e_f\partial_t$$ 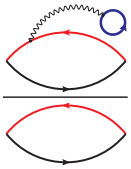 $$- e_u e^2 \sum_{f\in\{\text{sea}\}} e_f\partial_t$$ 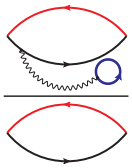

$$+ [\text{isosymm. vac. pol. diag.}] \qquad (2.84)$$

$$\Delta M_{K^0} = + (m_d - m_{ud}^{(0)})\partial_t$$ 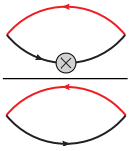 $$+ (m_s - m_s^{(0)})\partial_t$$ 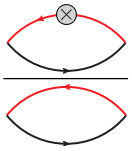

$$- (m_d - m_{ud}^{(0)})^{(crit)}\partial_t$$ 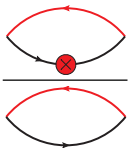 $$+ (m_s - m_s^{(0)})^{(crit)}\partial_t$$ 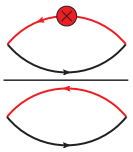

$$- (e_s e)^2\partial_t$$ 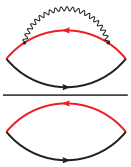 $$- (e_d e)^2\partial_t$$ 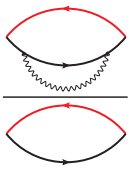 $$- (e_s e)^2\partial_t$$ 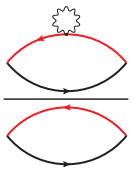 $$- (e_d e)^2\partial_t$$ 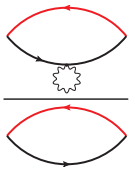

$$- e_d e_s e^2\partial_t$$ 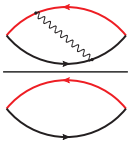 $$- e_s e^2 \sum_{f\in\{\text{sea}\}} e_f\partial_t$$ 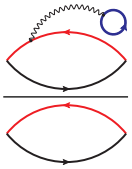 $$- e_d e^2 \sum_{f\in\{\text{sea}\}} e_f\partial_t$$ 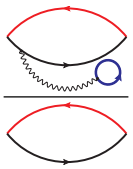

$$+ [\text{isosymm. vac. pol. diag.}] \qquad (2.85)$$

## 2.9 Baryons in QCD+QED

The IB corrections to the masses of baryons are built as for meson. We apply the variation to each quark propagator and consider the exchange of photons among all fermionic legs.

### 2.9.1 IB correction to $M_{\Omega^-}$

For the $\Omega^-$ we have:

$$\Delta M_{\Omega^-} = \Delta m_s \Bigg[ \partial_t \frac{\quad - 2 \quad}{\quad - 2 \quad} + \partial_t \frac{\quad - 2 \quad}{\quad - 2 \quad}$$

$$+ \partial_t \frac{\quad - 2 \quad}{\quad - 2 \quad} \Bigg]$$

$$- \Delta m_s^{(crit)} \Bigg[ \partial_t \frac{\quad - 2 \quad}{\quad - 2 \quad} + \partial_t \frac{\quad - 2 \quad}{\quad - 2 \quad}$$

$$+ \partial_t \frac{\quad - 2 \quad}{\quad - 2 \quad} \Bigg]$$

$$- q_s^2 \Bigg[ \partial_t \frac{\quad - 2 \quad}{\quad - 2 \quad} + \partial_t \frac{\quad - 2 \quad}{\quad - 2 \quad} \Bigg]$$

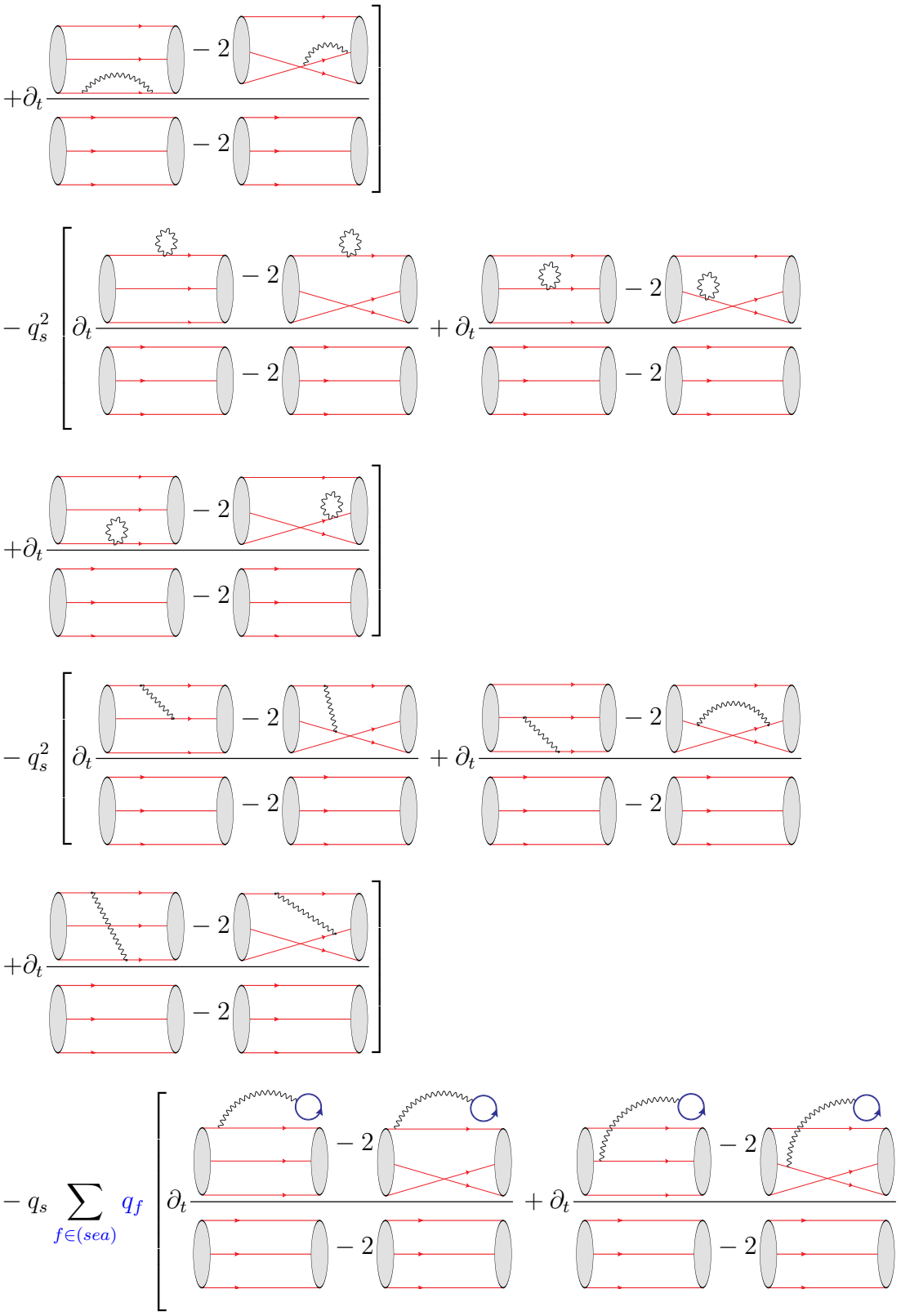
+∂t
− 2
− 2
− q_s^2
∂t
− 2
− 2
+ ∂t
− 2
− 2
+∂t
− 2
− 2
− q_s^2
∂t
− 2
− 2
+ ∂t
− 2
− 2
+∂t
− 2
− 2
− q_s
∑
f∈(sea)
q_f
∂t
− 2
− 2
+ ∂t
− 2
− 2

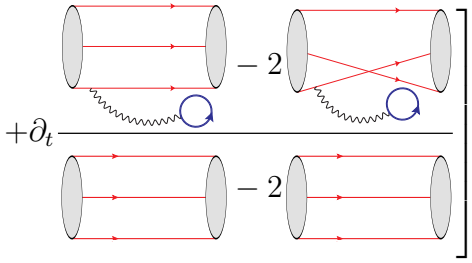

$$+\partial_t \frac{\quad - 2 \quad}{\quad - 2 \quad}\Bigg] + \text{[isosymm. vac. pol. diag.]} \quad . \quad (2.86)$$

### 2.9.2 IB correction to $M_N$

The nucleon eigenstate of QCD is split in $|p\rangle$ and $|n\rangle$ by IB, with mass corrections given by:

$$\Delta M_n = \Bigg[ \Delta m_u \, \partial_t \frac{\quad - \quad}{\quad - \quad} + \Delta m_d \, \partial_t \frac{\quad - \quad}{\quad - \quad}$$

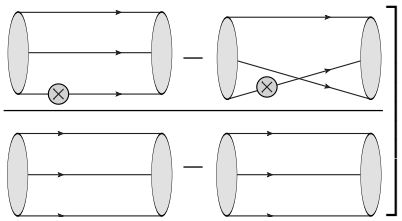

$$+\Delta m_d \, \partial_t \frac{\quad - \quad}{\quad - \quad}\Bigg]$$

$$- \Bigg[ \Delta m_u^{(crit)} \, \partial_t \frac{\quad - \quad}{\quad - \quad} + \Delta m_d^{(crit)} \, \partial_t \frac{\quad - \quad}{\quad - \quad}$$

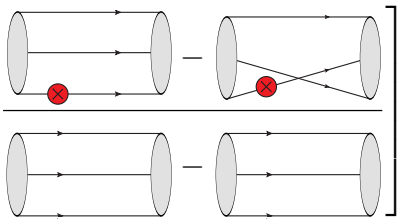

$$+\Delta m_d^{(crit)} \, \partial_t \frac{\quad - \quad}{\quad - \quad}\Bigg]$$

$$- \Bigg[ q_u^2 \, \partial_t \frac{\quad - \quad}{\quad - \quad} + q_d^2 \, \partial_t \frac{\quad - \quad}{\quad - \quad}$$

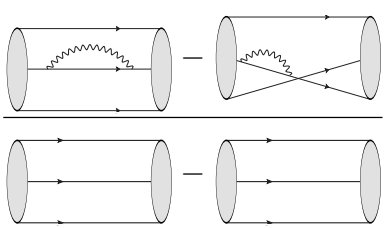

$$\Bigg]$$

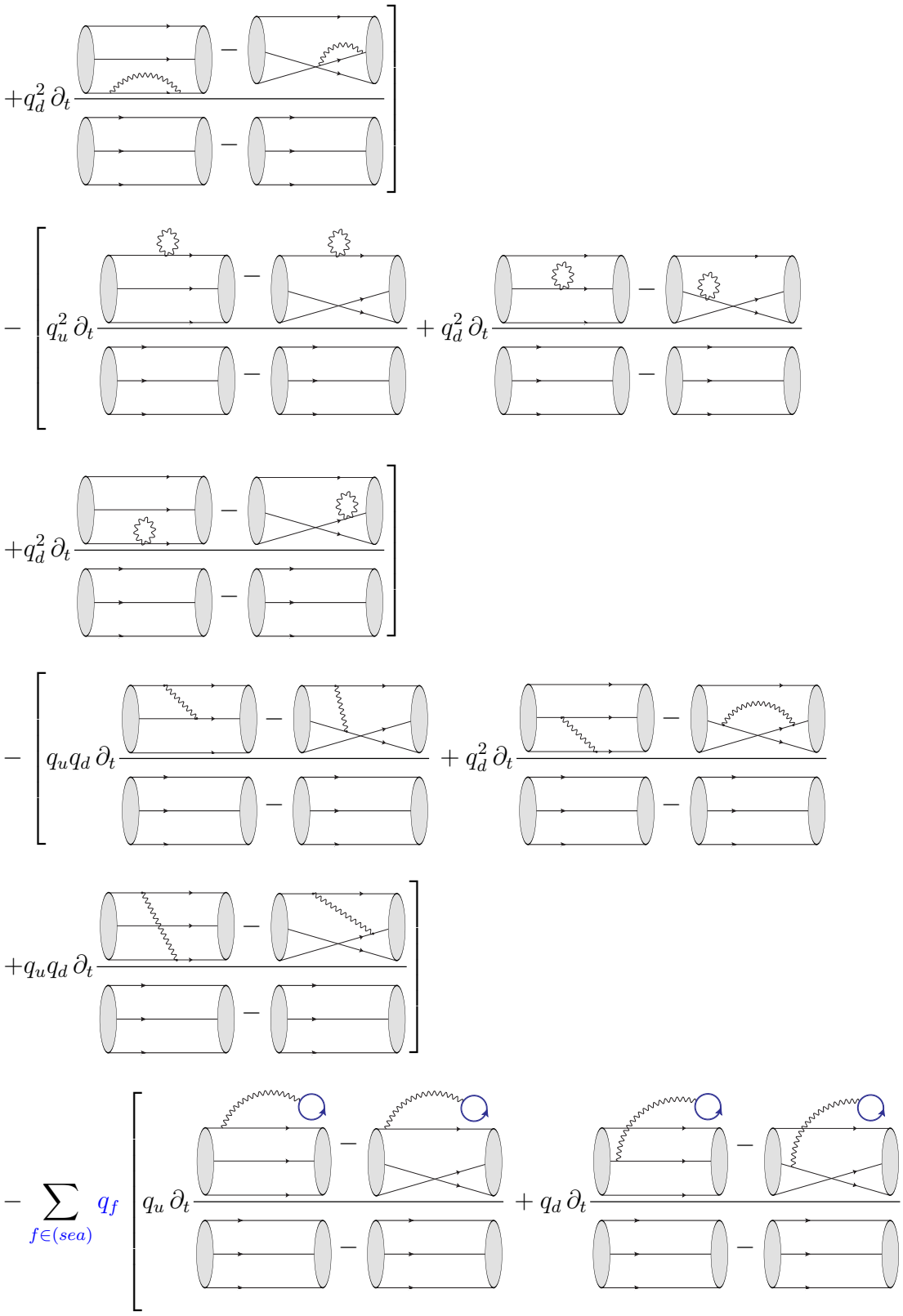
$+q_d^2\,\partial_t$
$-\Big[\,q_u^2\,\partial_t$
$+\,q_d^2\,\partial_t$
$+q_d^2\,\partial_t$
$-\Big[\,q_u q_d\,\partial_t$
$+\,q_d^2\,\partial_t$
$+q_u q_d\,\partial_t$
$-\sum_{f\in(sea)} q_f \Big[\, q_u\,\partial_t$
$+\,q_d\,\partial_t$

$+q_d\,\partial_t$ 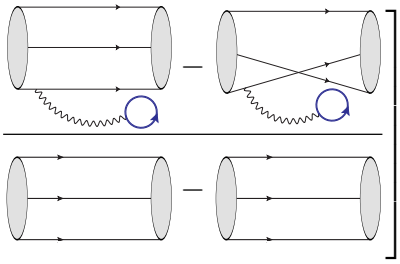 $+$ [isosymm. vac. pol. diag.] . (2.87)

and

$\Delta M_p =$ 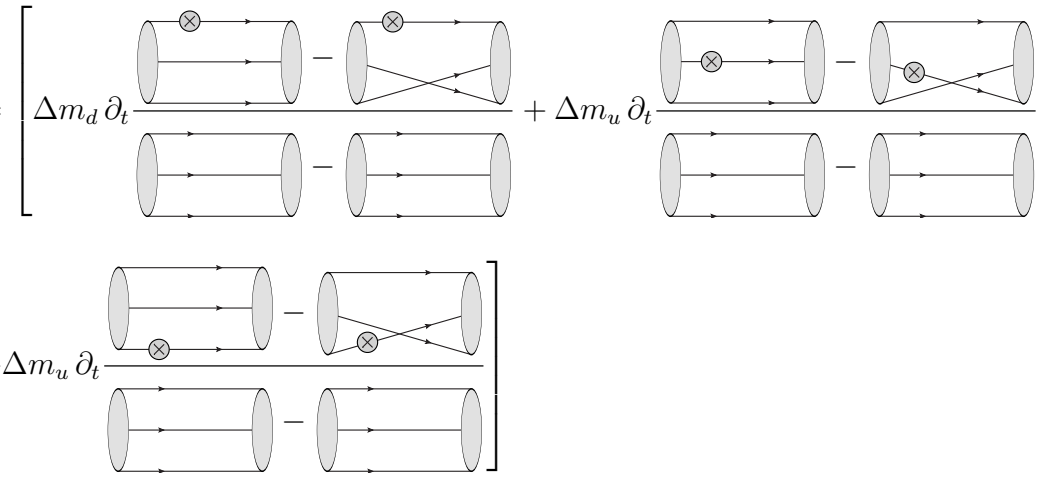

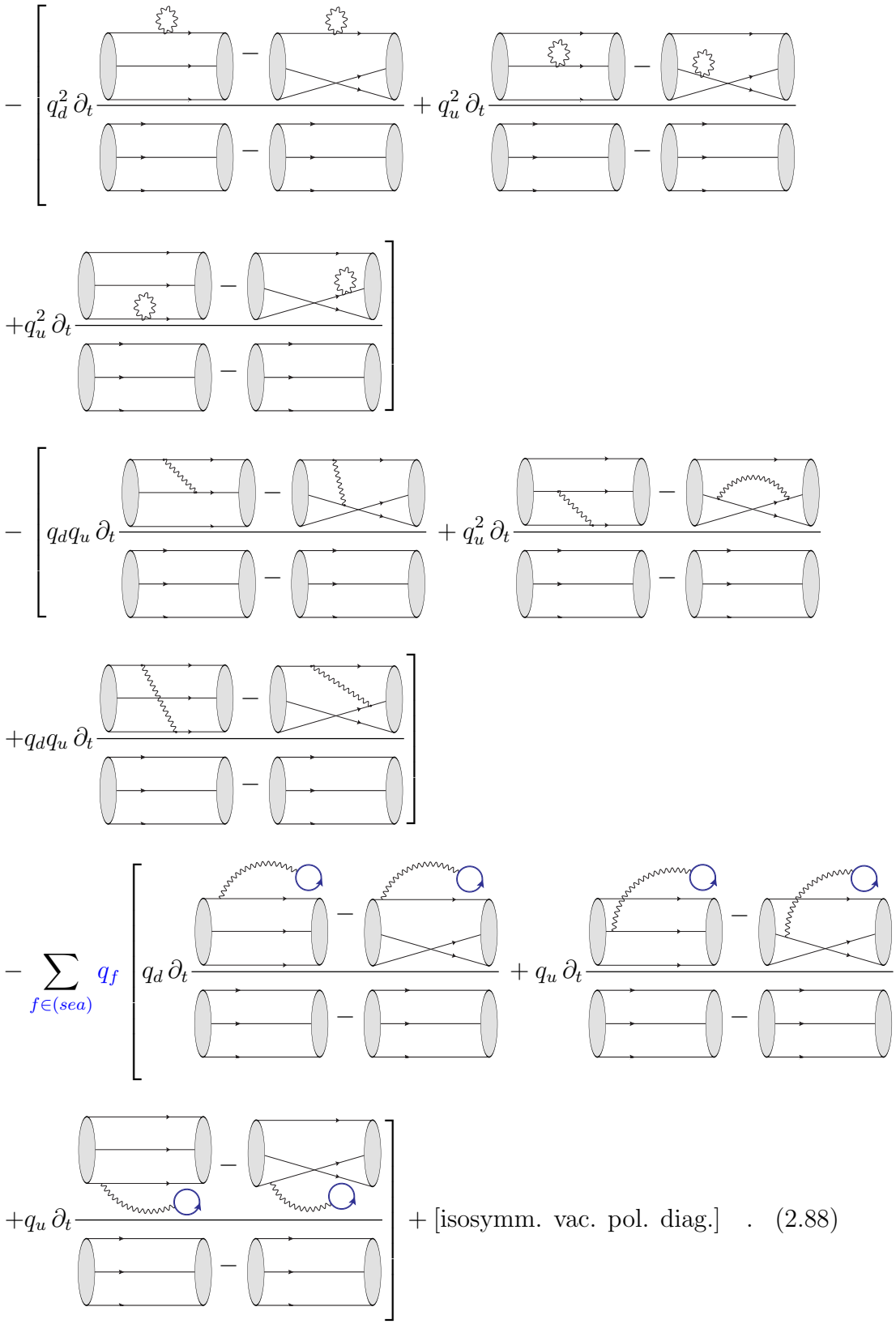

$$+ \text{[isosymm. vac. pol. diag.]} \quad . \quad (2.88)$$

### 2.9.3 $M_n - M_p$

The mass difference $M_n - M_p$ is readily obtained. Neutron and proton differ for the exchange $u \leftrightarrow d$, therefore:

$$M_n - M_p = (m_d - m_u)\Bigg[ -\partial_t$$

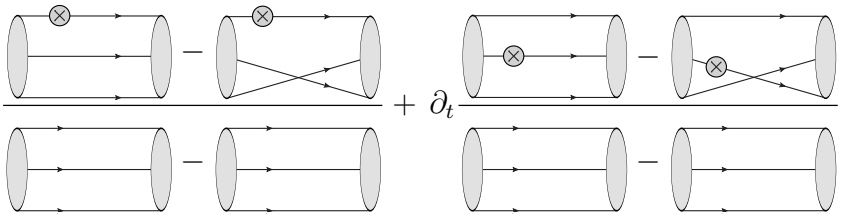

$$+\partial_t$$

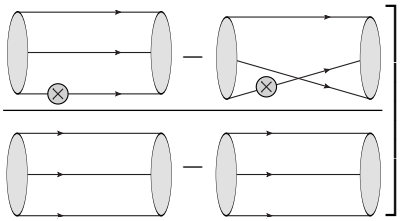

$$- (m_d - m_u)^{(crit)}\Bigg[ -\partial_t$$

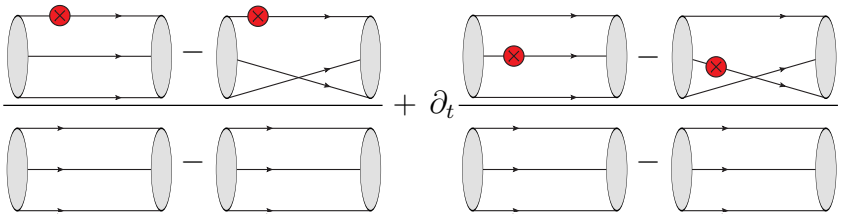

$$\partial_t$$

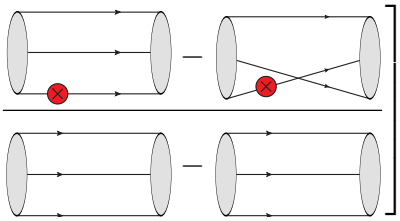

$$- (q_d^2 - q_u^2)\Bigg[ \partial_t$$

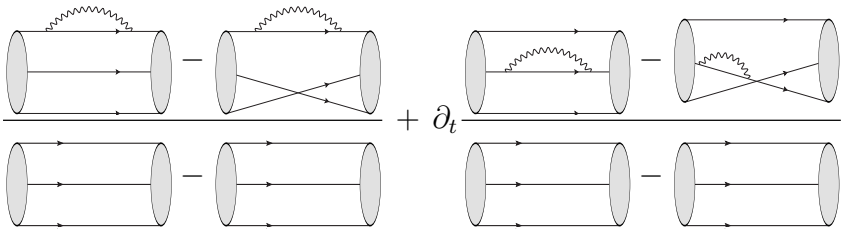

$$+\partial_t$$

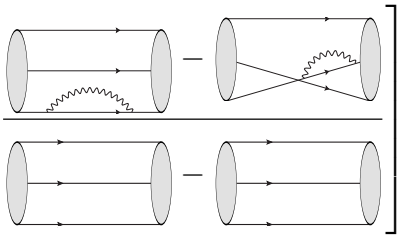

$$- (q_d^2 - q_u^2)\Bigg[ \partial_t$$

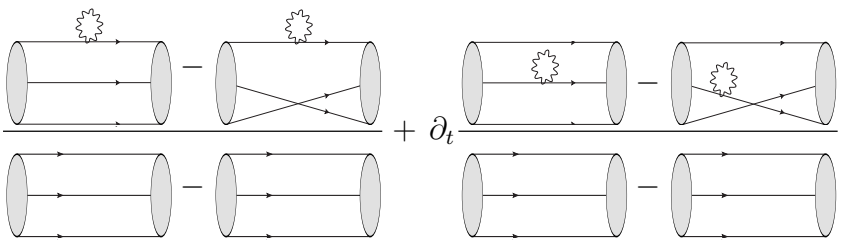

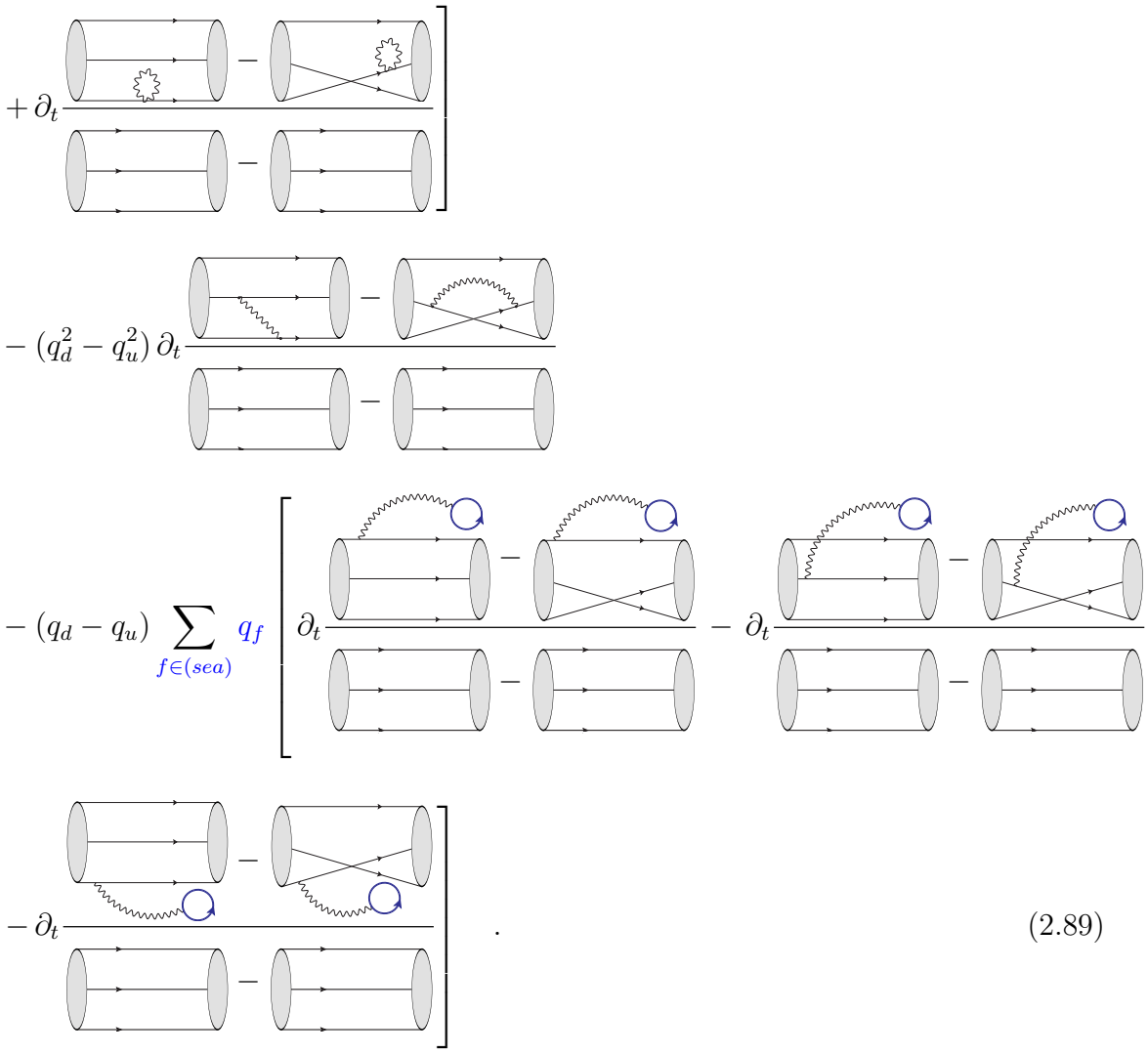

(2.89)

The strong IB contribution to this quantity is expected to be positive, as a result of $m_d > m_u$, while the electromagnetic one is negative due to higher electromagnetic self energy of the proton ($|Q_p| > |Q_n|$). According to the separation described in sec. (2.6), in terms of Feynman diagrams we have:

$(M_n - M_p)^{(QCD)} =$

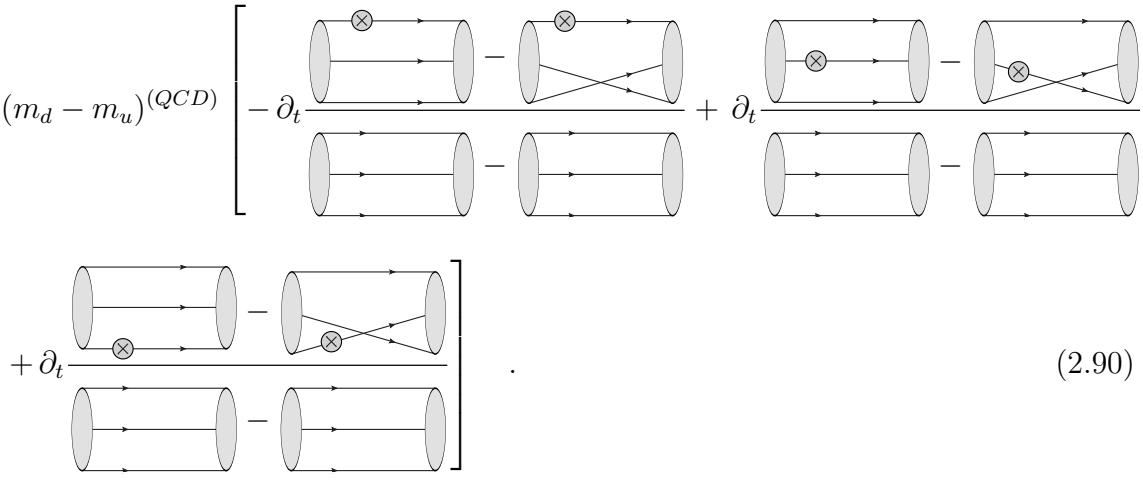

(2.90)

and

$(M_n - M_p)^{(QED)} =$

$(m_d - m_u)^{(QED)}$

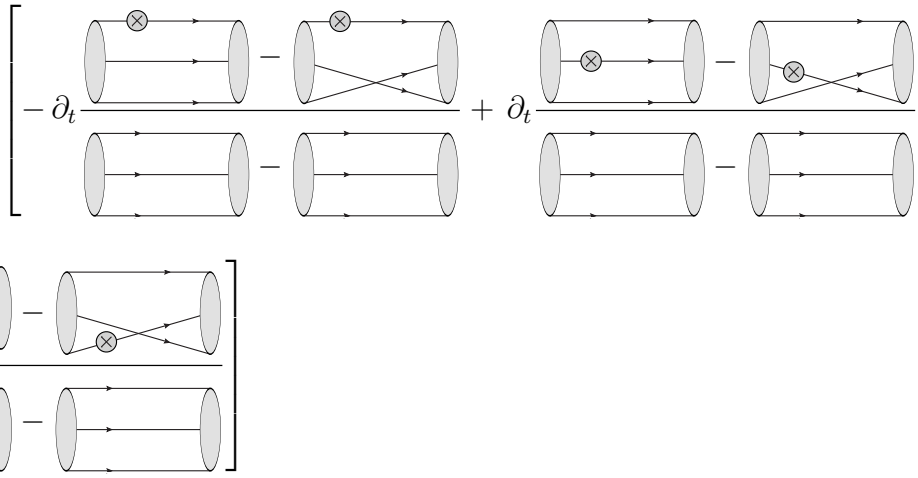

$- (m_d - m_u)^{(crit)}$

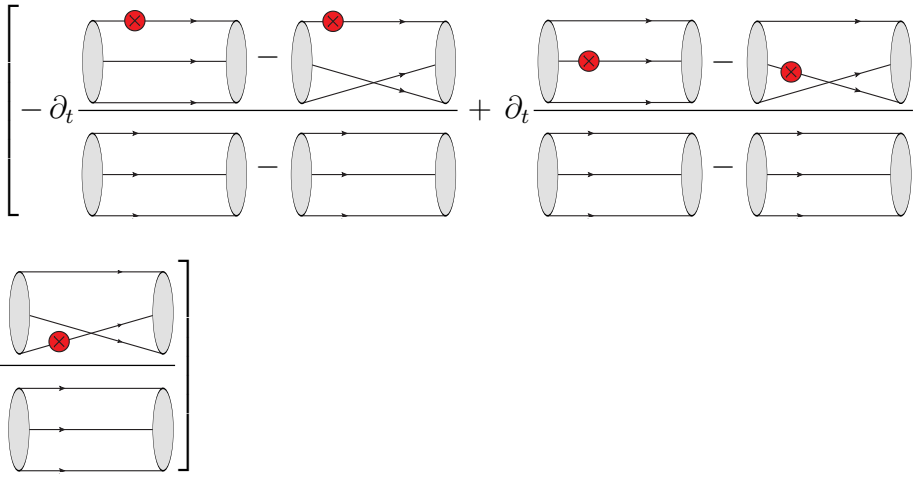

$- (q_d^2 - q_u^2)$

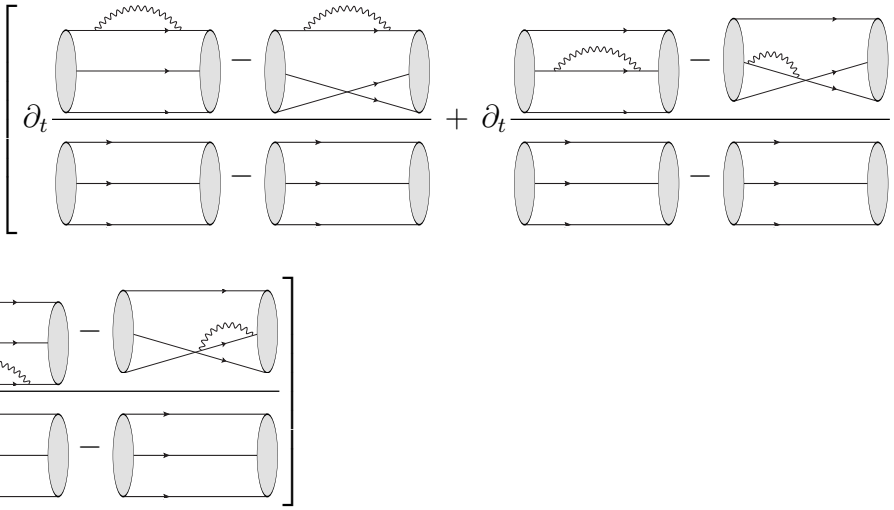

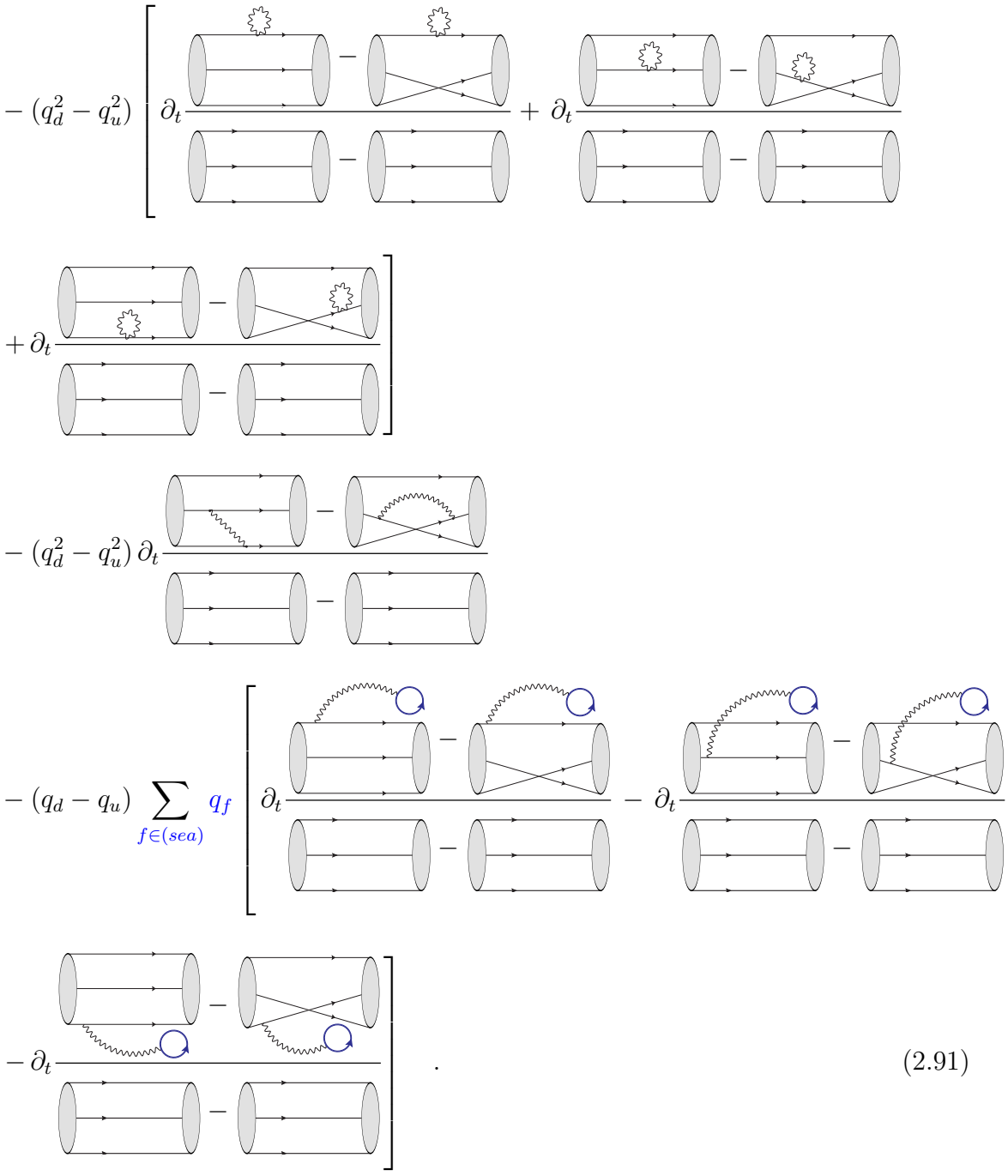

(2.91)

## 2.9.4 IB in Δ masses

In the $SU(3)$ decuplet of baryons we find a quadruplet of particles with $I(J^{PC}) = 3/2(3/2^+)$ and valence quarks in the light sector. Experimentally this corresponds to the isoQCD state $\Delta(1232)$, split into 4 resonances by $IB$: $\Delta^{++}$, $\Delta^{+}$, $\Delta^{0}$, $\Delta^{-}$. Their quark content is:

$$\Delta^- = |ddd\rangle \ , \Delta^0 = |udd\rangle \ , \Delta^+ = |duu\rangle \ , \Delta^{++} = |uuu\rangle \ . \tag{2.92}$$

These have masses between 1230 MeV and 1234 MeV and in experiments are found as the lowest lying resonant states in artificial processes of $N\gamma$ photoproduction and $\pi N$ electroproduction [3].

The $\Delta$ is the most important baryon resonance [85]. It has a mass close to $M_N$ and is strongly coupled to nucleons, pions and photons. Studying the properties

of the $\Delta$ has a role in the construction of effective models for $\pi N$ interactions (see e.g. [86, 87]). The latter are often applied in astrophysics, in the description of processes such as active galactic nuclei, Gamma Ray Bursts and Neutron Stars (see eg. [88, 89]). The masses of the $\Delta^0$, $\Delta^+$ and $\Delta^{++}$ have been measured explicitly, as it's relatively easy to generate $p\gamma$ or $\pi^{+/-}p$ scattering events. On the other hand, the artificial production of a $\Delta^-$ would require a $\pi^- n$ scattering, which is not easily achievable with the present technology.
In this work we focused on the calculation of the masses and mass splittings among these particles at LO in Isospin Breaking. The method applied with nucleons can be immediately extended here, so that the mass differences are found from mass slopes calculated in *isoQCD* and appropriately tuned counterterms.
In terms of Feynman diagrams we have:

$\Delta M_{\Delta^{++}} = \Delta m_u$

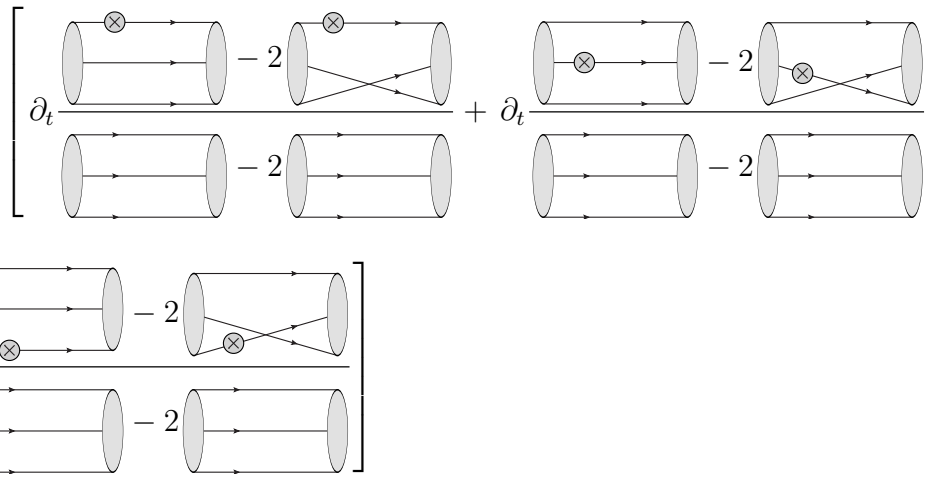


$- \Delta m_u^{(crit)}$

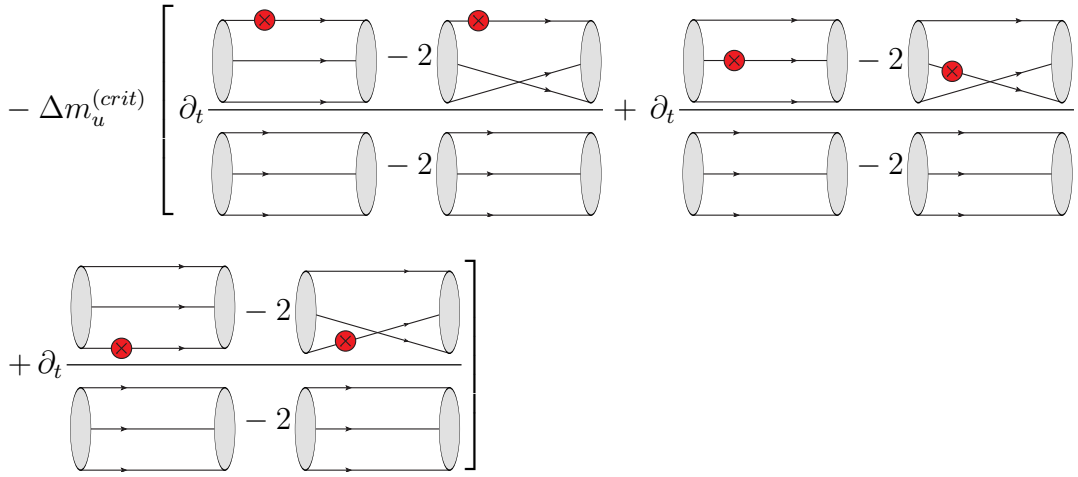


$- q_u^2$

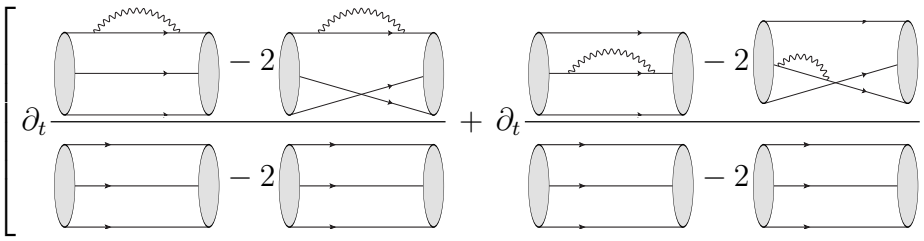

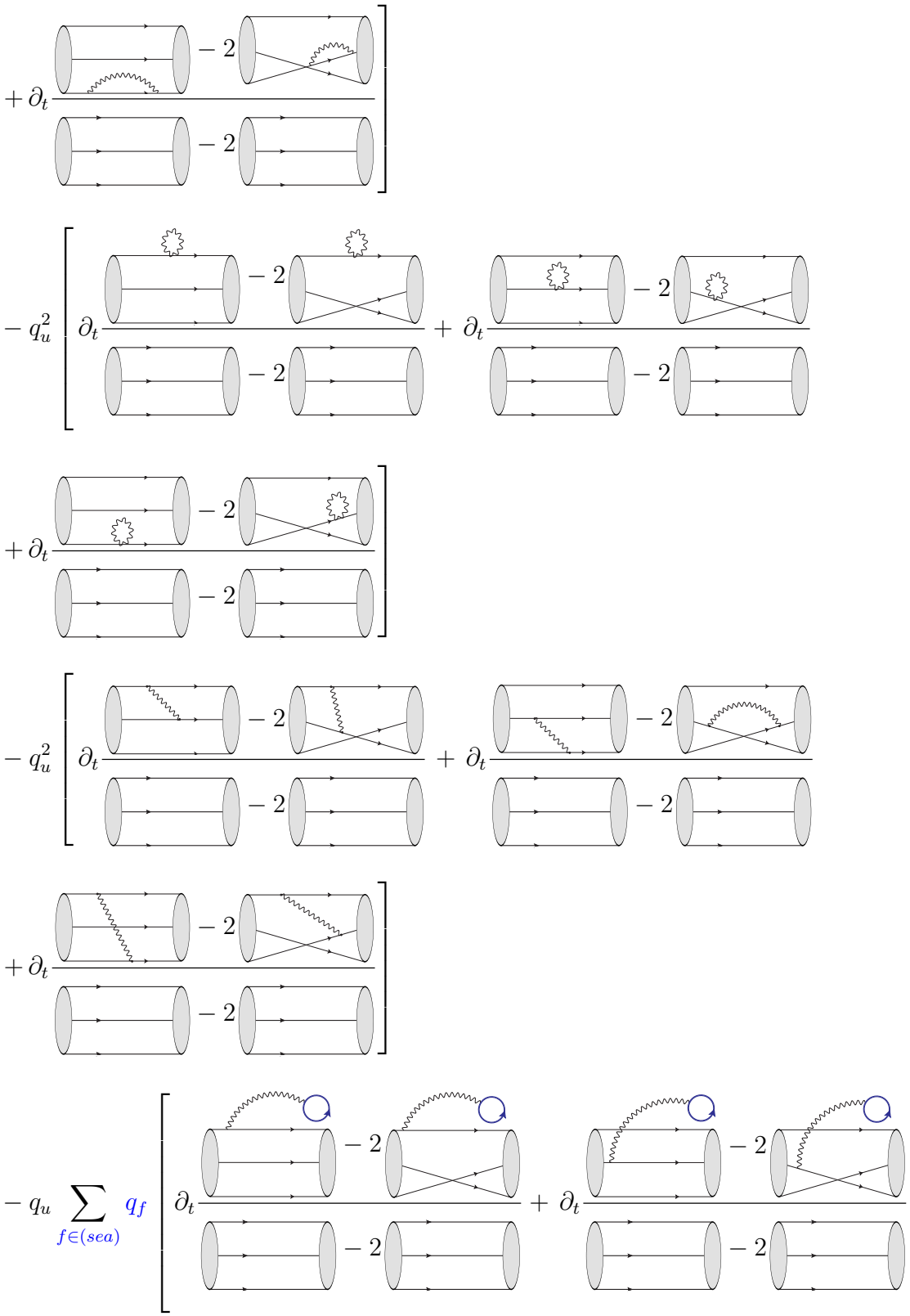

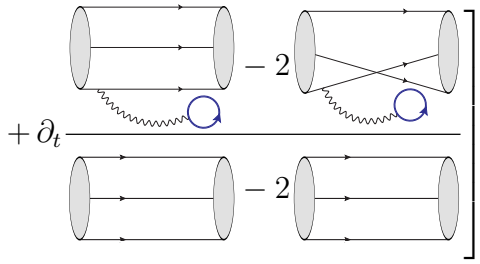

+ [isosymm. vac. pol. diag.] .

(2.93)

and

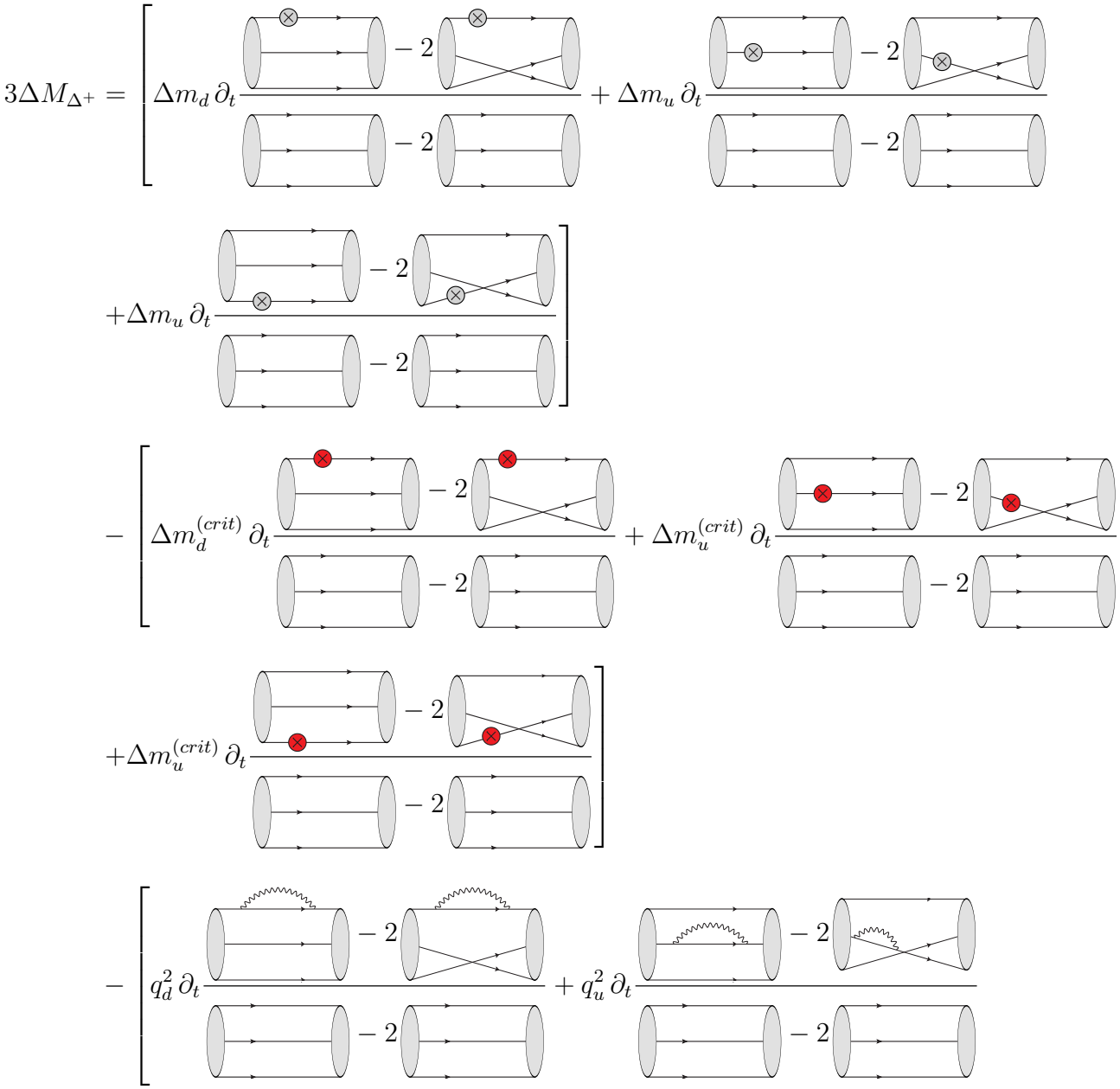

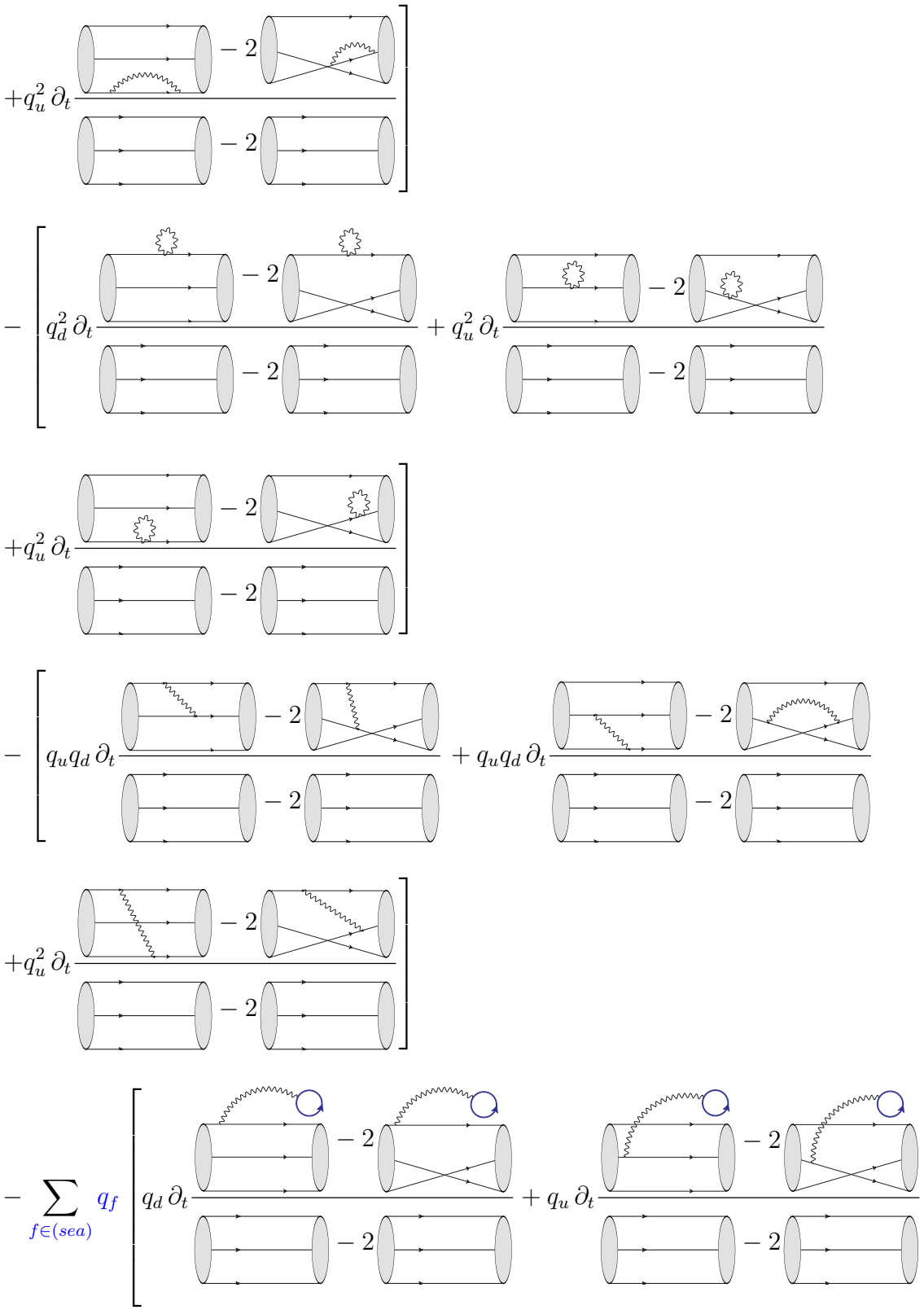

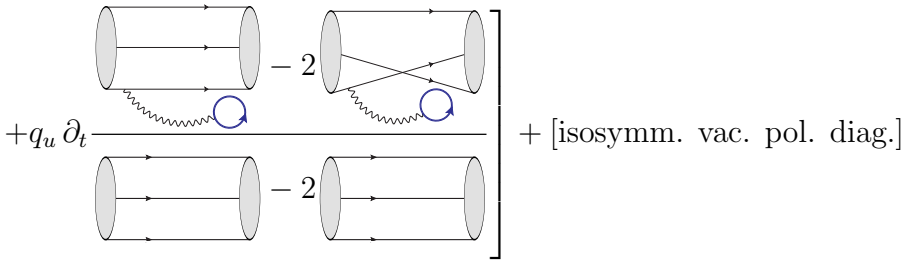

$$+\left\{\begin{matrix} d & \to & u \\ u & \to & d \\ u & \to & u \end{matrix}\right\} + \left\{\begin{matrix} d & \to & u \\ u & \to & u \\ u & \to & d \end{matrix}\right\} \quad , \tag{2.94}$$

where the last two terms correspond to the explicit expression, with the 3 legs permuted as specified by the arrows.
The other mass corrections are obtained by trivial tranformations. In fact, if we consider them as functions of 3 flavor indices, namely

$$\Delta M_{\Delta^{++}} = F_1(u,u,u) \tag{2.95}$$
$$\Delta M_{\Delta^{+}} = F_2(d,u,u) \quad , \tag{2.96}$$

we have:

$$\Delta M_{\Delta^{-}} = F_1(d,d,d) \tag{2.97}$$
$$\Delta M_{\Delta^{0}} = F_2(u,d,d) \quad . \tag{2.98}$$

From eqs. (2.93) - (2.98) we can verify that:

$$M_{\Delta^{++}} - M_{\Delta^{-}} = 3(M_{\Delta^{+}} - M_{\Delta^{0}}) \quad , \tag{2.99}$$

so that there are only 2 independent mass splittings. In this work we concentrate on the following IB effects:

$3(M_{\Delta^{++}} - M_{\Delta^{0}}) =$

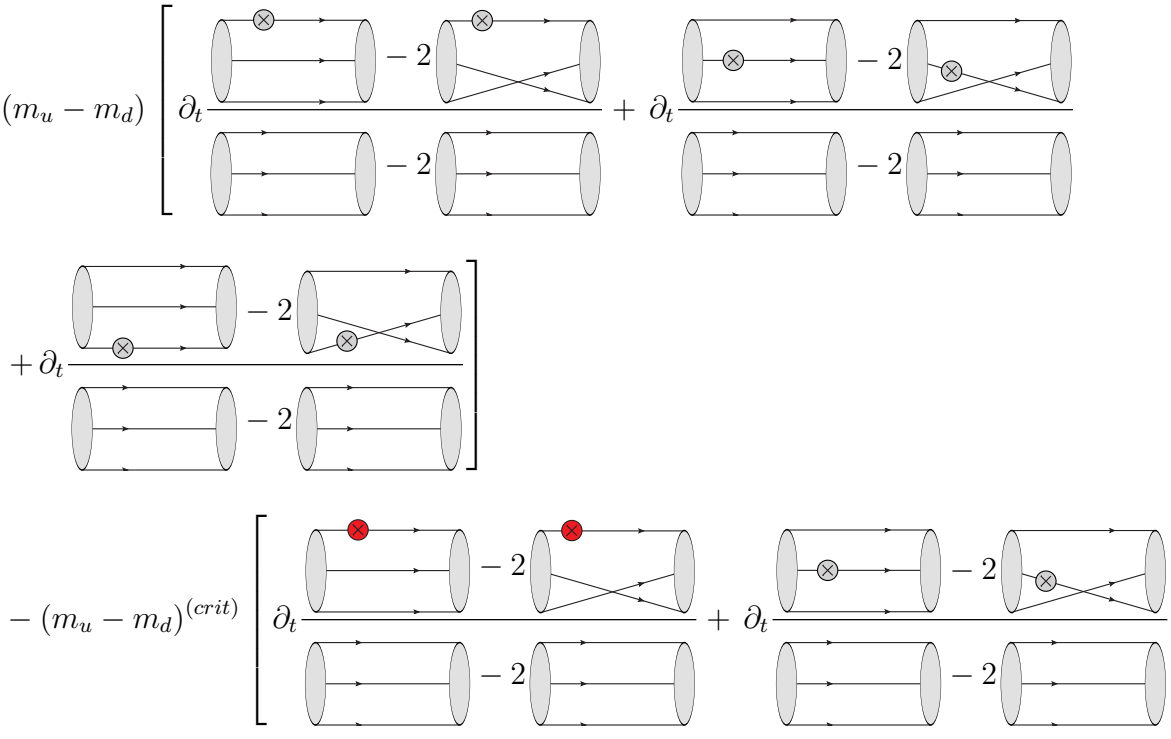

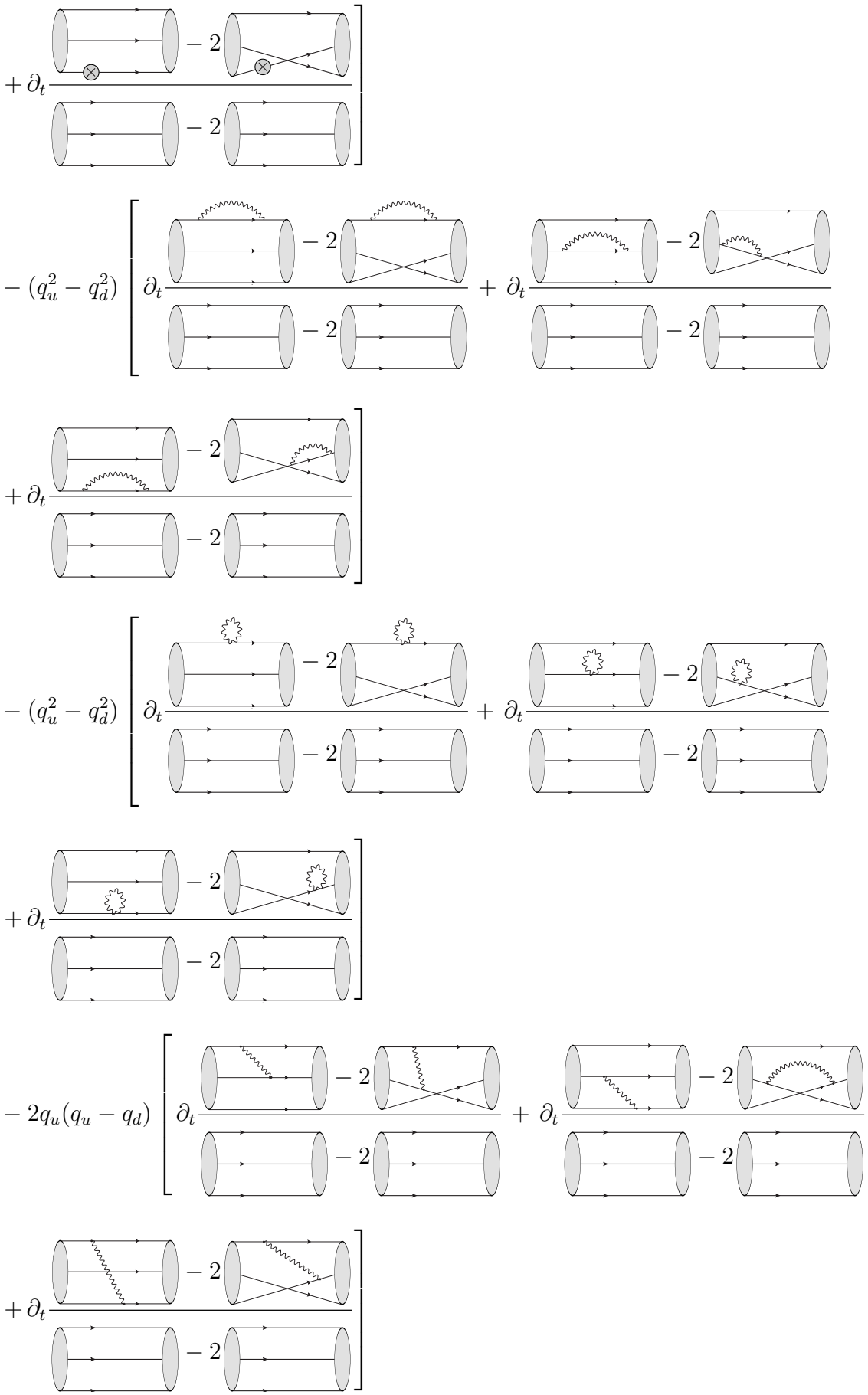

$$-(q_u-q_d)\sum_{f\in(sea)} q_f \Bigg[ \partial_t \frac{\quad - 2 \quad}{\quad - 2 \quad} + \partial_t \frac{\quad - 2 \quad}{\quad - 2 \quad}$$

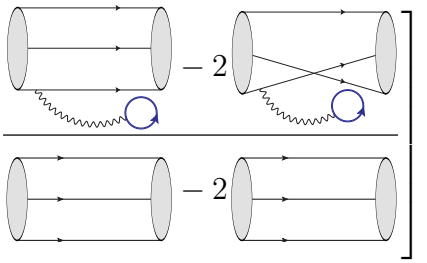

$$+\partial_t \frac{\quad - 2 \quad}{\quad - 2 \quad} \Bigg] \quad . \qquad (2.100)$$

and

$$(M_{\Delta^{++}} + M_{\Delta^-}) - (M_{\Delta^+} + M_{\Delta^0}) =$$

$$-\frac{2}{3}(q_u-q_d)^2 \Bigg[ \partial_t \frac{\quad - 2 \quad}{\quad - 2 \quad}$$

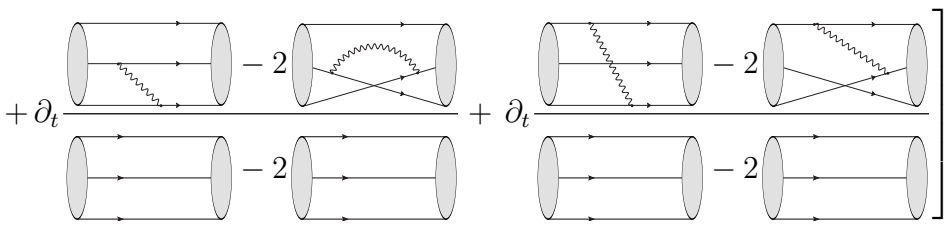

$$+\partial_t \frac{\quad - 2 \quad}{\quad - 2 \quad} + \partial_t \frac{\quad - 2 \quad}{\quad - 2 \quad} \Bigg] \quad . \qquad (2.101)$$

The latter quantity can be considered a particulary clean theoretical prediction, being a purely electromagnetic effect independent of the tuning scheme.

# Chapter 3

# Analysis of the isoQCD background

The correlation functions analyzed in this work were computed using the ETMC $N_f = 2 + 1 + 1$ gauge configurations, generated with the action ([13, 73]):

$$S[U, \psi, \bar{\psi}] = S_g[U] + S^{\ell}_{tm}[U, \psi] + S^{h}_{tm}[U, \psi] \quad . \tag{3.1}$$

$S_g$ is the IM11 version of the Iwasaky action ([90, 91]), $S^{\ell}_{tm}$ and $S^{h}_{tm}$ are twisted mass mixed fermionic actions (at maximal twist) respectively for light and heavy quarks. The choice of this formulation has the intent of minimizing the cutoff effects. In the following we'll refer to this theory as *isosymmetric background* or simply *isoQCD*, in the sense that it's an action which contains only QCD in the limit of isospin symmetry (i.e. $m_u = m_d = m_\ell$).
The evaluation of IBEs is done with the RM123 method described in sec. (2), so that all the euclidean correlators are found in the isosymmetric theory. Before considering the inclusion these corrections, we carried on an analysis of the isoQCD background. This served both as a test bench for our choice of the renormalization scheme and also to find the isosymmetric contributions to the quantities evaluated in the full theory.
In this theory the simulated, for each ensemble, 3 values of the bare valence strange quark mass. This partially quenched setup was chosen in order to control the uncertainty in the physical point of $am_s$. For this reason, in our extrapolations we consider the dependence on the strange quark mass together with the dependence on the lattice spacing $a$, $am_\ell$ and the volume size $L$ [1] . As discussed in sec. (3.2), the extrapolation to the physical $am_s$ can be done in separate steps, i.e. interpolating the observables depending on it at fixed ensemble to its physical point (dependent on the given ensemble). This (local) point has a dependence on the given ensemble which is removed in the final extrapolation.
We adopt a purely hadronic scheme, in which the physical point is expressed in

[1] In our ensembles the time extent $T$ is always the double of $L$. This justifies our approximation in which we neglect finite temperature effect, namely the dependence on $T$.

terms of (dimensionless) hadronic ratios, compared with their experimental values:

$$r_s = \frac{2M_K^2 - M_\pi^2}{M_\Omega^2} \quad , \tag{3.2}$$

$$r_\ell = \frac{M_\pi^2}{M_\Omega^2} \quad . \tag{3.3}$$

In other words, we evaluate these ratios from the masses found from the hadronic correlators and extrapolate the other observables to the experimental value of $r_s$ and $r_\ell$ [2] . This is equivalent to the extrapolation in terms of renormalized quark masses $\hat{m}_s$ and $\hat{m}_\ell$, however in this way we don't suffer from the uncertainty in the quark mass renormalization constants.
The choice of these ratios is led by ChPT, which at LO predicts for the mass of a pseudo-scalar meson with valence quarks of flavors $f_1$ and $f_2$:

$$M_P(f_1, f_1) \propto (\hat{m}_{f_1} + \hat{m}_{f_2}) \quad . \tag{3.4}$$

For the $\Omega$ we expect a small dependence from the quark mass, since in nature its mass is much larger than its valence constituents. This means that $r_s$ is a good choice to play the role of $\hat{m}_s$ and $r_\ell$ it is for $\hat{m}_\ell$.
The rest of the chapter is organized as follows. In sec. (3.3) we discuss the treatment of FVEs, which are checked against the A40.XX ensembles. In sec. (3.4) we show how we set the scale, and finally in sec. (3.5) are discussed the extrapolations over all the ensembles of $M_N$ and $M_\Delta$.

## 3.1 Identification of ground states

The hadronic masses involved in the present analysis are extracted as ground states from the large time behavior of appropriate euclidean correlators at rest (i.e. projected at $\vec{p} = \vec{0}$):

$$C(t) = \sum_{\vec{x}} \langle O_{\text{sink}}(t, \vec{x}) O_{\text{source}}(0, \vec{0}) \rangle \quad . \tag{3.5}$$

For pseudoscalar mesons (P), at the sink we place a quark bilinear of the form:

$$O_P(x) = \bar{\psi}^+_{f_1}(x) \Gamma \psi^-_{f_2}(x) \quad , \tag{3.6}$$

where $f_1$ and $f_2$ are the valence quarks flavors of $|P\rangle$ and the $+$ and $-$ are the signs of the Wilson parameter $r$. We choose opposite values for it in order to make the discretization effects on $M_P^2$ start at $O(a^2 m)$ [70, 92]. At the source we place the hermitian conjugate $O_P^\dagger(0)$.
For baryons we use the correlators of the form

$$C_B(t) = \text{Tr}\big[\mathcal{P} \sum_{\vec{x}} \langle \mathcal{B}(t, \vec{x}) \bar{\mathcal{B}}(0) \rangle\big] \tag{3.7}$$

[2] Note that isoQCD is not a real theory comparable with the experiment, thus we have some freedom in the definition of the physical point. Here the experimental values for pions and kaons masses can be any combination from $\pi^+$, $\pi^0$, $\pi^-$, $K^+$, $K^0$, $K^-$ sharing the same isoQCD limit. The difference arises at $O(\alpha)$, which is an IB effect. We'll come back to this point in sec. (4.4), discussing the tuning of mass counterterms.

were $\mathcal{P}$ projects to definite parity, and spin 3/2 for the $\Omega$ and $\Delta$ resonance. In sec. (1.3.1) the explicit expression for baryonic interpolators is given. The extraction of the masses $M_\pi$, $M_K$ $M_\Omega$, $M_N$ and $M_\Delta$ was done using the leading exponential approximation for large times. As previously anticipated in sec. (1.3.3) , we found the masses in lattice units using a fit to a constant of the effective mass curve $aM_{\text{eff}}(t)$. The mesons are built from positive time parity correlators, so that the effective mass is defined implicitly from the following expression:

$$\frac{C(t)}{C(t+a)} = \frac{\cosh\left(M_{\text{eff}}(t)\cdot(t-T/2)\right)}{\cosh\left(M_{\text{eff}}(t)\cdot(t+1-T/2)\right)} \quad . \tag{3.8}$$

For baryons the backward signal is absent, and the curve is found simply as:

$$M_{\text{eff}}(t) = \log\frac{C(t)}{C(t+1)} \quad . \tag{3.9}$$

The choice of the plateau region $[t_{\min}, t_{\max}]$ is done upon requiring the compatibility with a constant curve and an approximate scaling behavior with the lattice spacing. We require that the starting point of the plateau (in physical units) depends mainly on $\beta$, with a smaller dependence on the volume and pion mass. In tab. (3.1) we list the intervals for $t/a$ chosen to fit the effective masse curves to a constant. The bounds are not strict, in the sense that we allow for fluctuations of 1 or 2 lattice spacings in $t$ due to the effects given by the pion mass and volume.

| $\beta$ | $M_\pi$ | $M_N$ | $M_\Delta$ | $M_K$ | $M_\Omega$ |
|---|---|---|---|---|---|
| 1.90 | $[10, 23]$ | $[10, 15]$ | $[10, 14]$ | $[13, 20]$ | $[12, 20]$ |
| 1.95 | $[11, 23]$ | $[11, 17]$ | $[11, 15]$ | $[14, 21]$ | $[13, 21]$ |
| 2.10 | $[14, 30]$ | $[14, 18]$ | $[14, 22]$ | $[18, 24]$ | $[17, 24]$ |

Table 3.1: Approximate plateau intervals for $[t_{\min}/a, t_{\max}/a]$, chosen to fit the effective mass curves to a constant and extract the mass of the ground states. For $M_K$ and $M_\Omega$ we use the same plateau for each value of the simulated strange quark mass.

In fig. (3.1) are shown some plots of some effective mass curves, which give an idea of the quality of the plateaus. In order to give an order of magnitude for the masses involved in the analysis, these are summarized in tab. (3.2).

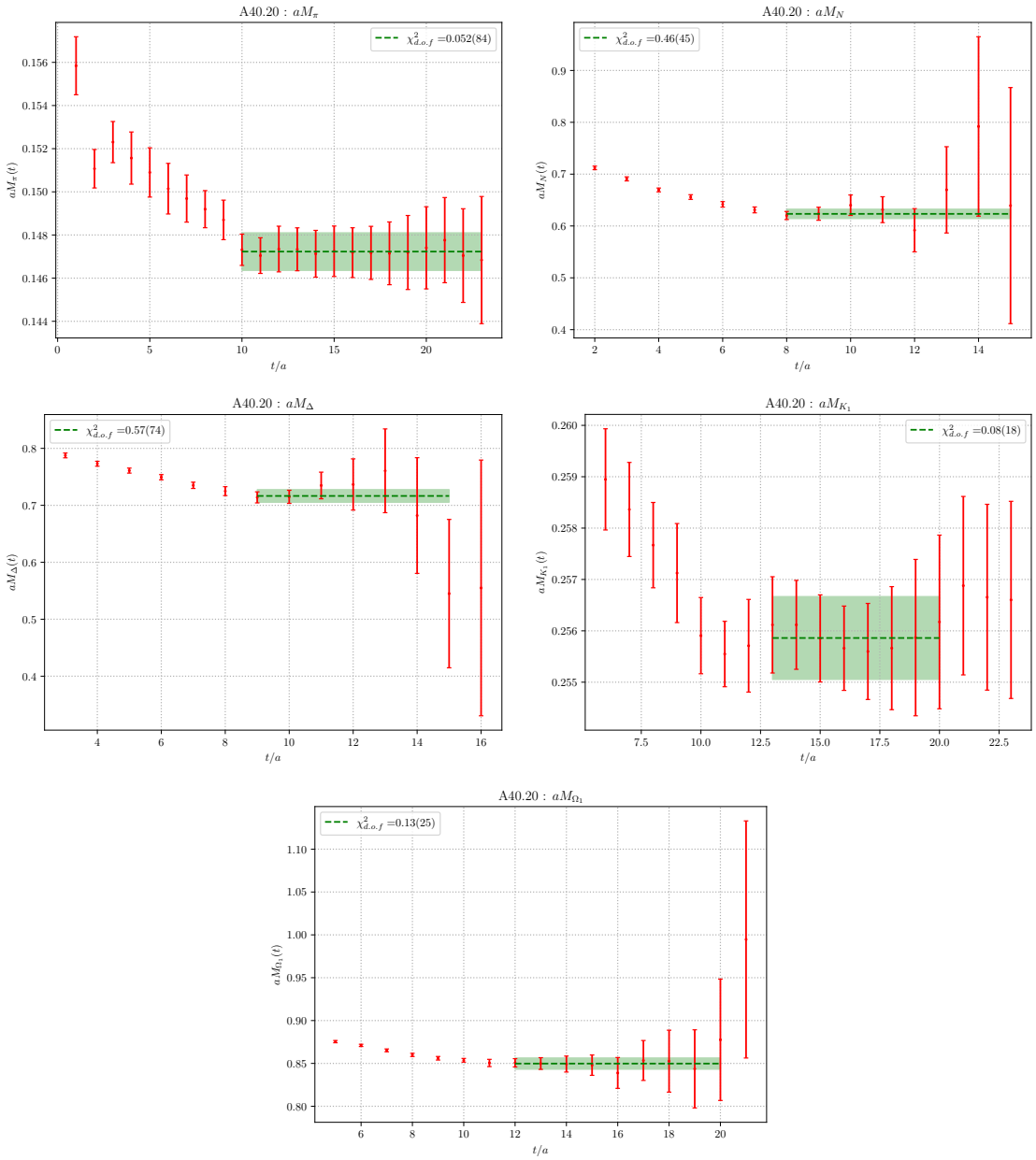


Figure 3.1: Fit to a constant of the effective mass curves for the ensemble $A40.20$.

| Ensemble | $M_\pi$ (MeV) | $M_N$ (GeV) | $M_\Delta$ (GeV) | $M_{K_1}$ (MeV) | $M_{\Omega_1}$ (GeV) |
|---|---|---|---|---|---|
| A100.24 | 434.2(4.3) | 1.304(13) | 1.482(12) | 547.3(5.5) | 1.673(15) |
| A30.32 | 242.5(2.6) | 1.114(19) | 1.309(21) | 484.4(5.2) | 1.623(15) |
| A40.20 | 288.1(3.8) | 1.220(21) | 1.402(25) | 500.7(5.7) | 1.663(25) |
| A40.24 | 283.4(3.7) | 1.170(23) | 1.319(32) | 496.9(5.4) | 1.647(21) |
| A40.32 | 277.0(3.0) | 1.147(12) | 1.333(17) | 491.5(5.0) | 1.628(17) |
| A40.40 | 278.1(3.0) | 1.122(13) | 1.333(18) | 490.4(5.1) | 1.635(16) |
| A40.48 | 276.7(3.0) | 1.150(12) | 1.313(16) | 491.2(5.2) | 1.638(19) |
| A50.32 | 307.7(2.9) | 1.166(17) | 1.353(14) | 500.3(5.0) | 1.635(17) |
| A60.24 | 339.7(3.7) | 1.201(20) | 1.396(29) | 512.3(5.5) | 1.639(24) |
| A80.24 | 388.8(4.2) | 1.255(17) | 1.429(20) | 528.1(5.6) | 1.647(19) |
| B25.32 | 235.0(2.5) | 1.117(20) | 1.330(24) | 473.9(4.8) | 1.616(15) |
| B35.32 | 273.5(2.9) | 1.131(16) | 1.358(22) | 483.0(4.9) | 1.624(18) |
| B55.32 | 339.0(3.5) | 1.200(14) | 1.409(17) | 502.3(5.0) | 1.637(17) |
| B75.32 | 394.7(3.8) | 1.239(15) | 1.440(15) | 523.1(5.1) | 1.642(17) |
| B85.24 | 423.2(4.5) | 1.274(13) | 1.456(20) | 535.9(5.6) | 1.651(14) |
| D15.48 | 204.4(2.0) | 1.048(16) | 1.312(31) | 442.9(4.6) | 1.580(16) |
| D20.48 | 231.8(2.3) | 1.092(15) | 1.346(32) | 449.8(4.9) | 1.588(13) |
| D30.48 | 282.5(3.1) | 1.094(14) | 1.316(24) | 464.0(5.0) | 1.582(17) |

Table 3.2: For each ensemble, the masses of $M_\pi$, $M_N$, $M_\Delta$, $M_K$, $M_\Omega$, found from the fit to a constant of the effective mass curves. Their values are in physical units, obtained using the values of the lattice spacings found later in the analysis (see sec. (3.4)). For $K$ and $\Omega$ we report the masses for the 1st value of $am_s$.

## 3.2 Physical point of $m_s$

For each $\beta$ we have 3 values of the valence quark mass $am_s$ (see tab. (3.3)).

| $\beta$ | $am_{s_1}$ | $am_{s_2}$ | $am_{s_3}$ |
|---|---|---|---|
| 1.90 | 0.0220 | 0.0260 | 0.0300 |
| 1.95 | 0.0190 | 0.0220 | 0.0250 |
| 2.10 | 0.0136 | 0.0161 | 0.0186 |

Table 3.3: Values of $am_s$ for each $\beta$ of the first run within the isoQCD theory.

These values are near the physical point. This justifies an interpolation at fixed ensemble, done for each observable dependent of the strange quark mass in the valence. The physical point found in such a way contains an induced dependence on the light quark mass and volume (and lattice spacing), removed in the final extrapolation.
In this analysis we interpolate using the ratio:

$$r_s = \frac{2M_K^2 - M_\pi^2}{M_\Omega^2} \quad . \tag{3.10}$$

We express these oservables in terms of it, and find their values corresponding to the experimental value of $r_s$. Since the extrapolation with respect to $\hat{m}_\ell$ is done with the ratio $r_\ell$ of eq. (3.3), this means that the physical point for each ensemble will have a dependence on $r_\ell$, volume and lattice spacing. Given the vicinity to the physical point a polynomial ansatz is used, namely we fit these observables as:

$$O = O_0[1 + c_1 r_s + c_2 r_s^2] \quad , \tag{3.11}$$

where $O_0$, $c_1$ and $c_2$ are free parameters of the fit. In fig. (3.2) are shown the extrapolations of $M_K$ and $M_\Omega$ for 3 ensembles (one for each $\beta$), and in fig. (3.3) the ones for $am_s$.

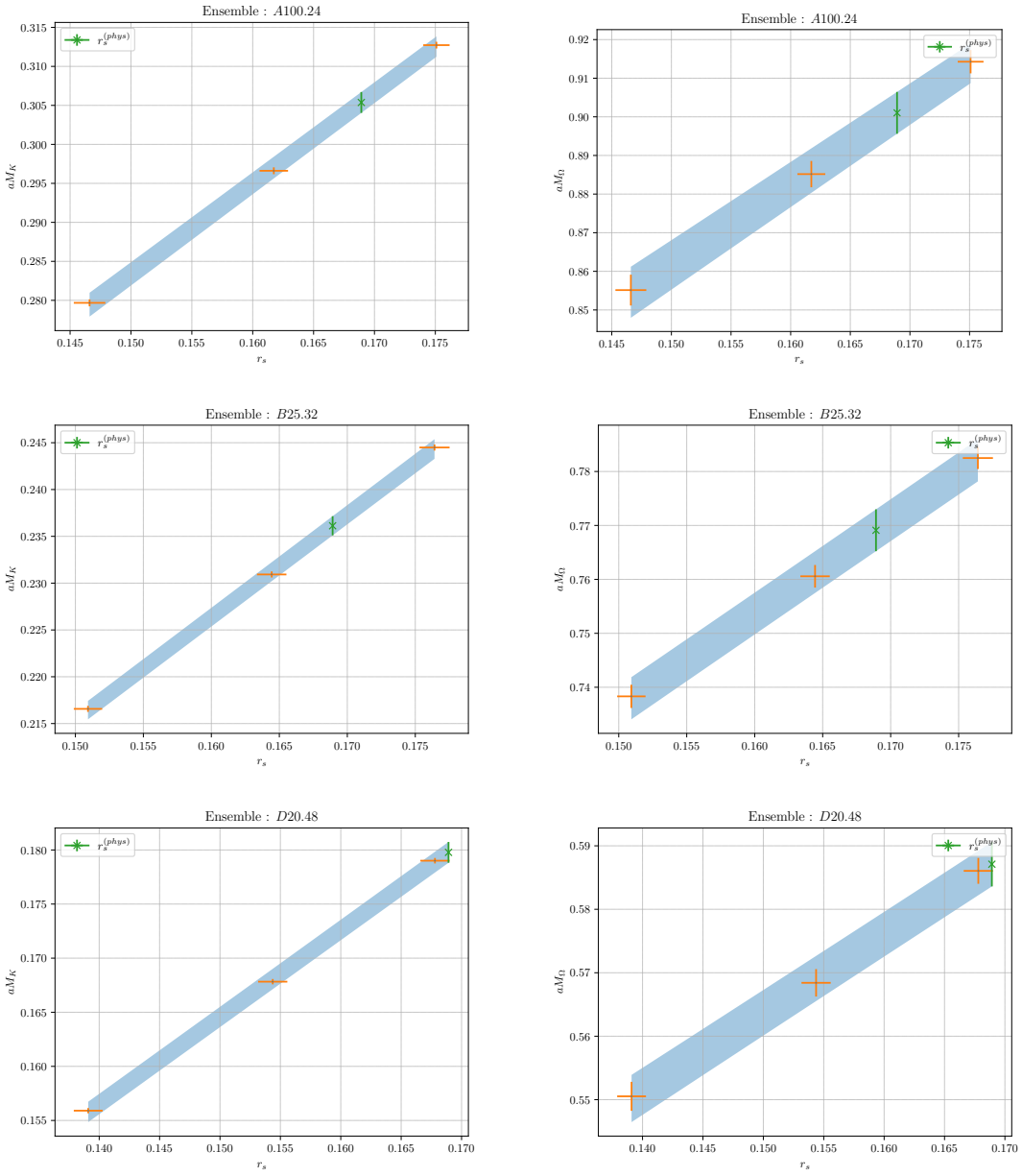


Figure 3.2: Extrapolations of $M_K$ and $M_\Omega$ for the ensembles $A100.24$, $B25.32$, $D20.48$.

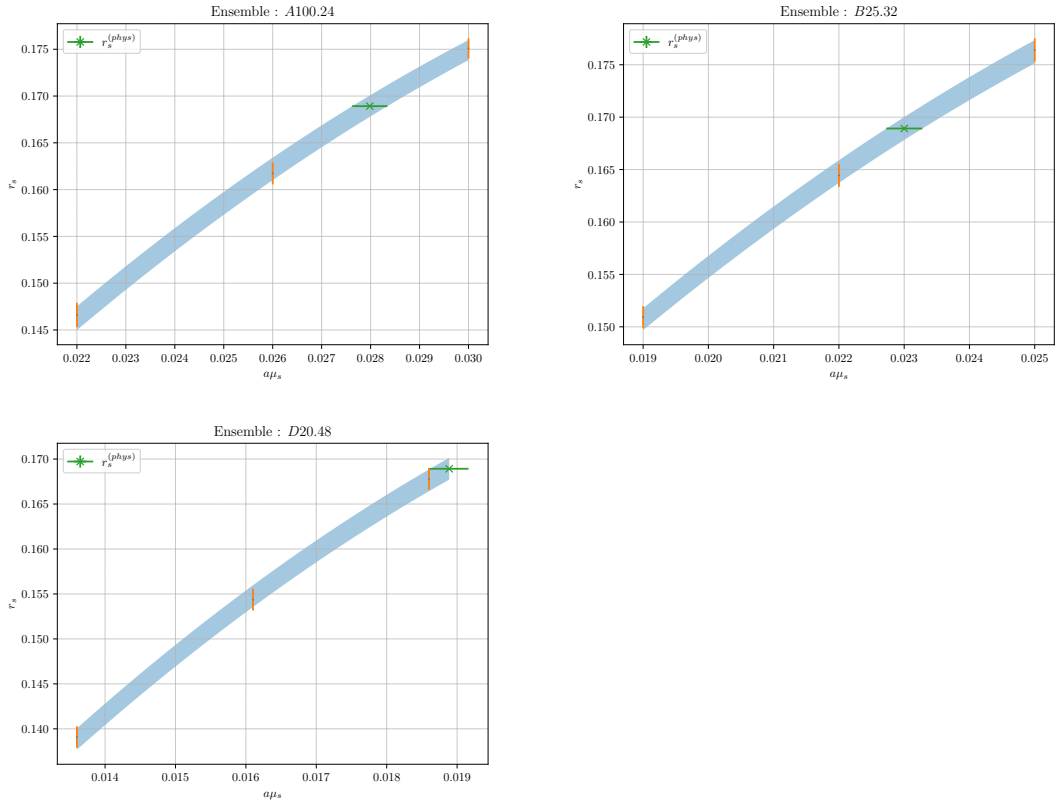


Figure 3.3: Extrapolations of $am_s$ with respect to $r_s$ for the ensembles $A100.24$, $B25.32$, $D20.48$.

## 3.3 FVE from the $A40.XX$ ensembles

The FVEs shown by our data are found to be moderate. However these are visible looking at the A40.XX, which differer from each other only for the volume. In order to correct them, we use the asymptotic ChPT results found in the p-regime and restricted to the leading contributions coming from the lightest state. This is implemented leaving the $L \to \infty$ limit of the mass and the coefficient in front of the $L$-dependent factor as a free parameters of the fit. In other words we use the following ansätze. From [55] and [93] we have for $\pi$ and $K$:

$$M_\pi(L) = M_\pi(\infty)\left[1 + C_\pi M_\pi^2 \frac{e^{-M_\pi L}}{(M_\pi L)^{3/2}}\right] \quad , \tag{3.12}$$

$$M_K(L) = M_K(\infty)\left[1 + C_K M_\pi^2 \frac{e^{-M_\pi L}}{(M_\pi L)^{3/2}}\right] \quad . \tag{3.13}$$

The plots of $M_\pi(L)$ and $M_K(L)$ from the A40.XX ensembles are reported in fig. (3.4).

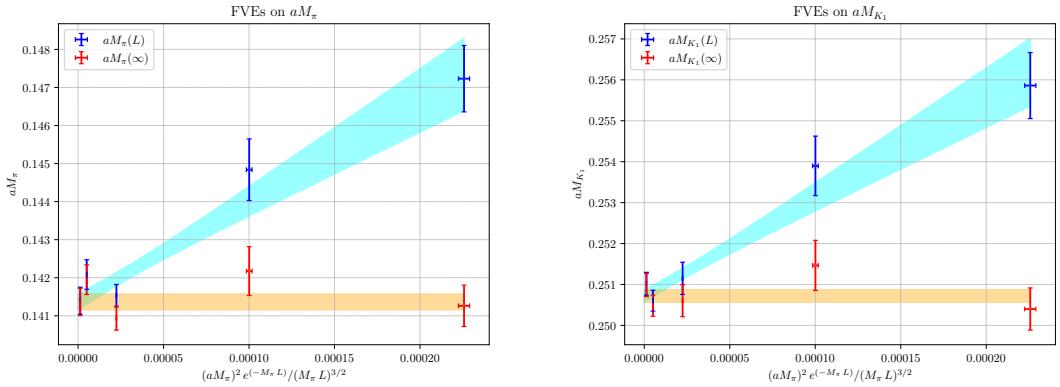


Figure 3.4: Volume dependence of $M_\pi$ and $M_K$ (1st simulated value of $m_s$). The data were fitted according to the equations (3.12). Blue and red points respectively are evaluated at finite and infinite volume, with bands representing the fit curve and infinite volume mass.

From the resummed formula for $N$ we have [94]:

$$M_N(L) = M_N(\infty)\left[1 + C_N M_\pi^3 \frac{e^{-M_\pi L}}{(M_\pi L)}\right] \quad . \tag{3.14}$$

The plot of $M_N(L)$ is given in fig. (3.5).

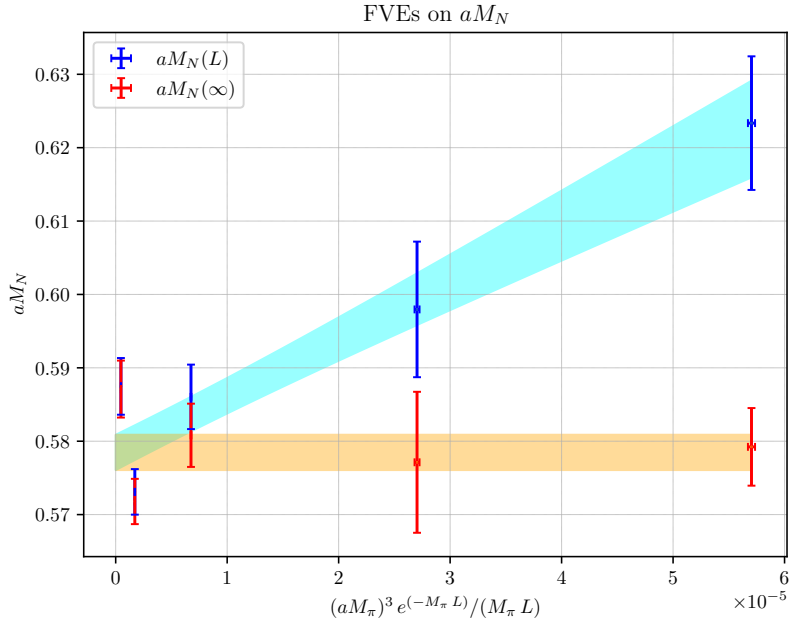


Figure 3.5: Volume dependence of $M_N$ fitted according to eq. (3.14). Blue and red points respectively are evaluated at finite and infinite volume, with bands representing the fit curve and infinite volume mass.

In our ensembles $\Omega$ and $\Delta$ are stable, with FVEs found to be small and consistent with the asymptotic formulas for stable particles. Numerically, this is also reassured

by the fact that the ODE method doesn't find more than 1 state in their correlators. For the $\Delta$ we checked the stability explicitly looking at the masses of $\pi$ and $N$ for each ensemble, recalling that the decay at threshold is forbidden in a finite volume [95]. The volume dependence of their masses is then written as ([96, 97] and [98]):

$$M_\Omega(L) = M_\Omega(\infty)\left[1 + C_\Omega M_K^2 \frac{e^{-M_K L}}{(M_K L)^{3/2}}\right] \quad , \tag{3.15}$$

$$M_\Delta(L) = M_\Delta(\infty)\left[1 + C_\Delta M_\pi^2 \frac{e^{-M_\pi L}}{(M_\pi L)^{3/2}}\right] \quad . \tag{3.16}$$

Note that for the $\Omega$ we don't have an exponential in $M_\pi$, which is further suppressed by $M_\pi^2$ in the chiral expansion and hence neglected in our approximation. In fact, in ChPT, FVEs are due to chiral loops (see sec. (1.4.2)) and the kaon is the lightest particle that can produce a loop in the $\Omega$ propagator, obtained taking only one light quark from the sea. Moreover, the presence of $M_K$ instead of $M_\pi$ is implied by isospin. Since $I_\Omega = 0$ while $I_\pi = 1$, in order to have the total isospin conserved the $\Omega$ should do a transition to a $I = 1$ state made of 3 $s$ quarks, which doesn't exist. The plots of the volume dependence for $M_\Omega$ and $M_\Delta$ is shown in fig. (3.6).

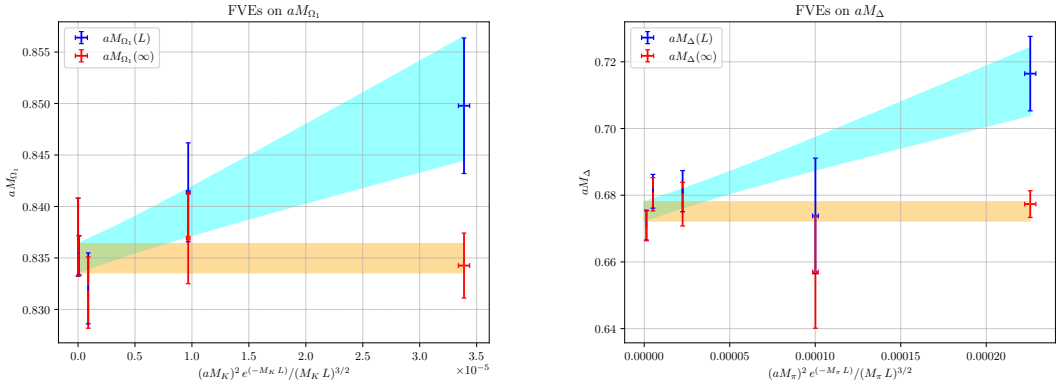


Figure 3.6: Volume dependence of $M_\Delta$ and $M_\Omega$ (1st simulated value of $m_s$) fitted according to the equations (3.15). Blue and red points respectively are evaluated at finite and infinite volume, with bands representing the fit curve and infinite volume mass.

## 3.4 Scale setting

In this work the lattice spacings are found from the mass of the $\Omega$ baryon, through its experimental value [3]:

$$M_\Omega^{(exp)} = 1672.45(29)\,\text{MeV} \quad . \tag{3.17}$$

This is done extrapolating the values of $aM_\Omega$ to the infinite volume limit and physical point of the quark masses, and then setting:

$$a = \frac{(aM_\Omega)|_{phys}}{M_\Omega^{(exp)}} \quad . \tag{3.18}$$

As explained in [99], the quality of the values in physical units depend on the precision of the observable used to set the scale. In our analysis we don't have to worry about this because the experimental uncertainty on $M_\Omega^{(exp)}$ is negligible with respect to our lattice results.
It must be said that one can choose a parameter different from $a$, such as the Sommer parameter $r_0$ or $w_0$. The advantage may be to compare different works, assuming a common physical value of that parameter as found from one of them [99]. However, in a self contained analysis (as this one) we can't add information simply using a different parameter. This makes no difference, and in general only increases the noise.
The extrapolation to the physical point of $m_\ell$ and $m_s$ was done for each $\beta$, reaching the $L \to \infty$ limit and the physical point of the aforementioned ratios $r_s$ and $r_\ell$ of eq. (3.2) and (3.2).
As discussed before, from ChPT results we know that the continuum and physical point limits are not interchangeable. For this reason the extrapolation of $aM_\Omega$ was done simultaneously over the 3 $\beta$s. In the following are reported the discussions on the following simultaneous extrapolations:

$$\begin{aligned} (L,s,\ell) &\to aM_\Omega = aM_\Omega(L,r_s,r_\ell) &&, \\ (s,\ell) &\to aM_\Omega = aM_\Omega(r_s,r_\ell) &&, \\ (\ell) &\to aM_\Omega = aM_\Omega(r_\ell) &&. \end{aligned}$$

The letters in the parentheses are a shorthand for the parameter dependence of $aM_\Omega$. The extrapolation $(L,s,\ell)$ takes simply the values obtained from the analysis of the correlators. In $(s,\ell)$ the values of $aM_\Omega$ are the ones corrected from FVEs using the information on the A40.XX ensembles (see sec. (3.3)). In $(\ell)$ the values are the ones corrected from FVEs and, for each ensemble, interpolated among the values of $r_s$ (see sec. (3.2)).
In tab. (3.4) are summarized the lattice spacings found with the above procedures. The compatibility of the results is reassuring about the validity of the procedure in separate steps.

| $\beta$ | 1.90 | 1.95 | 2.10 |
|---|---|---|---|
| $(L,s,\ell)$ | 0.1008(10) | 0.09017(92) | 0.06840(73) |
| $(s,\ell)$ | 0.1008(10) | 0.09017(92) | 0.06840(73) |
| $(\ell)$ | 0.1008(10) | 0.09017(92) | 0.06840(73) |

Table 3.4: Lattice spacings $a$(fm) obtained from $aM_\Omega$ with the extrapolations $(L,s,\ell)$, $(s,\ell)$, $(\ell)$.

### 3.4.1 Extrapolation $(L,s,\ell)$

Here the values of $aM_\Omega$ are the ones found from the leading exponential behavior of the correlator $C_\Omega(t)$ in the plateau region. In isoQCD the latter suffer from FVEs and depend on the strange and light quark mass. According to the asymptotic expansion of FVEs discussed in sec. (1.4.2), the $\Omega$ at finite volume contains a

leading contribution that goes like

$$M_K^2 \frac{e^{-M_K L}}{(M_K L)^{3/2}} \quad ,$$

while from $M_\pi$ and $M_K$ in $r_s$ and $r_\ell$ we get also the term

$$M_\pi^2 \frac{e^{-M_\pi L}}{(M_\pi L)^{3/2}} \quad .$$

The former is subleading with respect to the latter, given that $M_K$ is higher that $M_\pi$.
By the above considerations, the following phenomenological ansatz is adopted:

$$\begin{aligned}(aM_\Omega)_i \; = & a_{\beta(i)}\, M_\Omega^{(exp)} \left[ 1 + \; c_L \left( \frac{M_\pi}{\Lambda_{QCD}} \right)^2 \frac{e^{-M_\pi L}}{(M_\pi L)^{3/2}} + \; c_s\, \Delta r_s \; + \; c_\ell\, \Delta r_\ell + \right. \\ & \left. c_{s\ell}\, \Delta r_s \Delta r_\ell + \; c_s^{(2)}\, \Delta r_s^2 + \; c_\ell^{(2)}\, \Delta r_\ell^2 \right] \quad .\end{aligned} \tag{3.19}$$

The index $i$ corresponds to a generic ensemble, and $\beta(i)$ is one of the 3 $\beta$s to which that ensemble corresponds to. $\Delta r_s$ and $\Delta r_\ell$ are the displacements of $r_s$ and $r_\ell$ from the isoQCD value. For the latter we use the quadratic average of the charged and neutral mesons, viz:

$$\Delta r_s = \frac{2M_K^2 - M_\pi^2}{M_\Omega^2} - \left( \frac{2(M_{K^+}^2 + M_{K^0}^2) - (M_{\pi^+}^2 + M_{\pi^0}^2)}{2M_{\Omega^-}^2} \right)^{(exp.)} \quad , \tag{3.20}$$

$$\Delta r_\ell = \frac{M_\pi^2}{M_{\Omega^-}^2} - \left( \frac{M_{\pi^+}^2 + M_{\pi^0}^2}{2M_{\Omega^-}^2} \right)^{(exp.)} \quad . \tag{3.21}$$

The lattice spacings are free parameters of the fit, as $c_L, c_s, c_\ell, c_{s\ell}, c_s^{(2)}, c_\ell^{(2)}$. The latter are all dimensionless and $\Lambda_{QCD} = 300\,\mathrm{MeV}$ is a reference scale used to make $c_L$ so.
In table (3.5) are reported the values of the lattice spacings obtained in isoQCD with the above fit. In fig. (3.7) are given the plots of the simultaneous extrapolation among the 3 $\beta$s.

| $\beta$ | $a$(fm) | $a(\mathrm{GeV}^{-1})$ |
|---|---|---|
| 1.90 | 0.1008(10) | 0.5110(53) |
| 1.95 | 0.09017(92) | 0.4570(46) |
| 2.10 | 0.06840(73) | 0.3466(37) |

Table 3.5: Lattice spacings obtained from $aM_\Omega$ with the simultaneous fit over $L$, $r_s$, $r_\ell$.

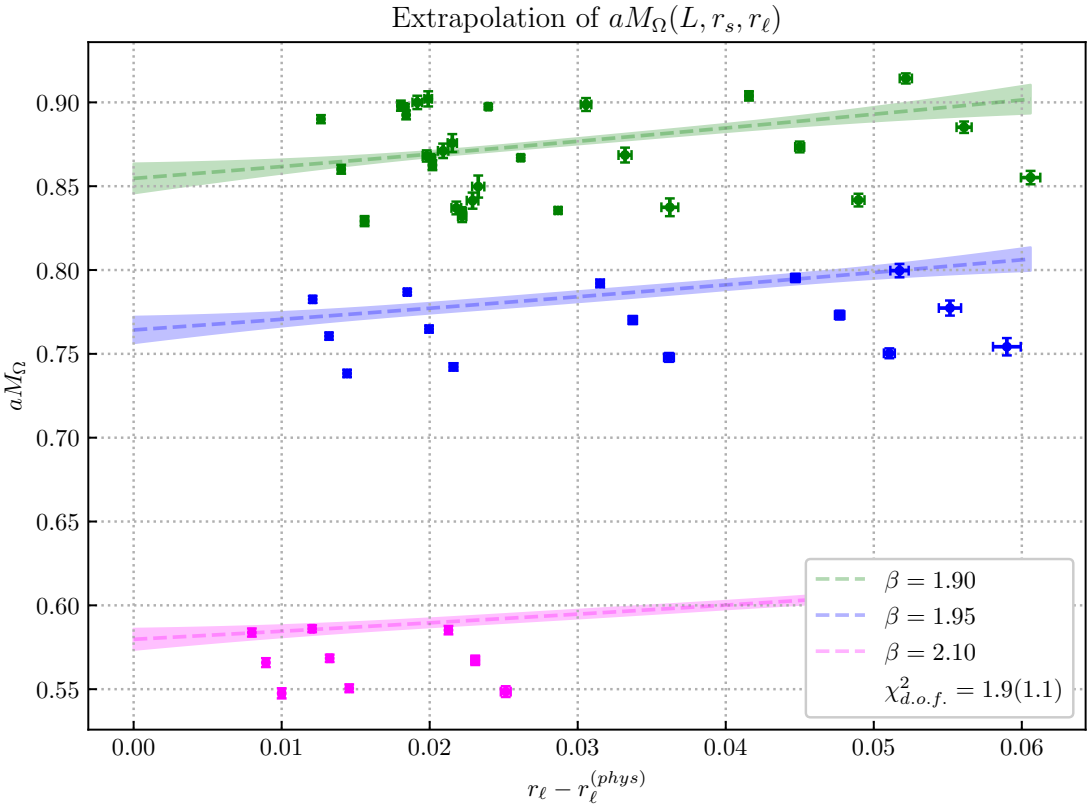


Figure 3.7: Extrapolation of $aM_\Omega$ in isoQCD over all the ensembles according to the ansatz given in eq. (3.19). For each ensemble we have a triplet of points corresponding to the 3 values of $am_s$ used in the isoQCD simulation. The colored dashed lines (with error bands) are the curves extrapolated to $L \to \infty$ and $r_s^{(phys)}$.

Note that if we knew the lattice spacings, the correct functional form would include an $a^2$ term, in order to account for discretization effects. This is equivalent to considering the ansatz:

$$(aM_\Omega)_i = a_{\beta(i)}\, M_\Omega^{(exp)} \left[ 1 + c_L \left( \frac{M_\pi}{\Lambda_{QCD}} \right)^2 \frac{e^{-M_\pi L}}{(M_\pi L)^{3/2}} + c_s\, \Delta r_s + c_\ell\, \Delta r_\ell + c_{s\ell}\, \Delta r_s \Delta r_\ell + c_s^{(2)}\, \Delta r_s^2 + c_\ell^{(2)}\, \Delta r_\ell^2 + c_a (\Lambda_{QCD}\, a_{\beta(i)})^2 \right] \quad . \tag{3.22}$$

Note that $c_a$ is dimensionless too.
At this stage however we haven't set the scale yet, and the result for $c_a$ would be ambiguous. This is easily seen in the approximation in which mixed terms in $a^2$ and higher are neglected. In this case the parameter $c_a$ could be "reabsorbed" in the definition of the parameters $a_i$:

$$a_{\beta(i)}\, (1 + c_a (\Lambda_{QCD}\, a_{\beta(i)})^2) \;\to\; a'_{\beta(i)}$$

The equation (3.22) would then lead to the removal of some discretization effects under some arbitrary prescription.
Moreover the minimization of the $\chi^2$ function would not have in principle a well definite minimum, but an hyper-surface of "minima" in the parameter space.

In practice however, some testing over the data has shown that there are indeed some local minima, to which the minimization falls naturally starting from a meaningful (but still boundless) guess for $c_a$. As is it manifest from the data shown in fig. (3.7), $c_a > 0$ as $\frac{\partial M_\Omega}{\partial a} > 0$.
It's interesting to focus on one of those minima, found at $c_a \approx 0.7$. The corresponding lattice spacings are reported in tab. (3.6) .

| $\beta$ | $a$(fm) | $a$(GeV$^{-1}$) |
|---|---|---|
| 1.90 | 0.08795(50) | 0.4457(25) |
| 1.95 | 0.08034(49) | 0.4071(25) |
| 2.10 | 0.06356(50) | 0.3221(25) |

Table 3.6: Lattice spacings obtained from $aM_\Omega$ with the simultaneous fit over $L$, $r_s$, $r_\ell$. The ansatz is given in eq. (3.22) with $c_a \approx 0.7$.

If we compare the results of tab. (3.5) with a previous determination of the lattice spacings over the same gauge configurations (see [13]), we see that our lattice spacings are $\sim 10\%$ bigger. This means that the discretization effects on $M_\Omega$ are or this order of magnitude. The discrepancy is solved if we include a $c_a a^2$ term in the ansatz, with $c_a \approx 0.7$. In this case, we find $1\sigma$-compatible values with [13], which found $a = 0.0885(36), 0.0815(30), 0.0619(18)$ fm at $\beta = 1.90, 1.95, 2.10$.
The above finding reassures us about the fact that, even if bigger, the lattice spacings of tab. (3.5) have the correct $a^2$ scaling behavior. Even if they contain the discretizaton effects of $M_\Omega$, the latter are expected to vanish in the continuum limit. This is also found to be so in practice from the extrapolated values of hadronic quantities in the analysis.

### 3.4.2 Extrapolation $(s, \ell)$

Finite volume effects can be corrected from the A40.XX ensembles, which are equal in all respects but for the volume size. The present approximation consist in using the information on this ensembles to correct the FVEs on all the others. According to what said in sec. (3.3), the free parameter extracted from the fit is assumed to be the same for all the ensembles, neglecting a mixed dependence on both the volume and the other parameters in the Lagrangian. This allows to correct the FVEs for all the ensembles, obtaining values at $L \to \infty$ of $r_s$, $r_\ell$ and $aM_\Omega$.
The functional form for $aM_\Omega$ is then the following:

$$\begin{aligned}(aM_\Omega)_i = a_{\beta(i)}\, M_\Omega^{(exp)} [1 + c_s\, \Delta r_s + c_\ell\, \Delta r_\ell + \\ c_{s\ell}\, \Delta r_s \Delta r_\ell + c_s^{(2)}\, \Delta r_s^2 + c_\ell^{(2)}\, \Delta r_\ell^2 \Big] \quad .\end{aligned} \tag{3.23}$$

The labelling is analogous to the one in eq. (3.19), but now the $aM_\Omega$ are calculated at $L \to \infty$. In table (3.7) are reported the values of the lattice spacings, and in fig. (3.8) is given the plot of the extrapolation.

| $\beta$ | $a$(fm) | $a$(GeV$^{-1}$) | $a$(MeV$^{-1}$) |
|---|---|---|---|
| 1.90 | 0.10059(98) | 0.5098(49) | 0.0005098(49) |
| 1.95 | 0.09005(76) | 0.4563(38) | 0.0004563(38) |
| 2.10 | 0.06825(59) | 0.3459(30) | 0.0003459(30) |

Table 3.7: Lattice spacings obtained from $aM_\Omega$ with the simultaneous fit over $r_s$, $r_\ell$.

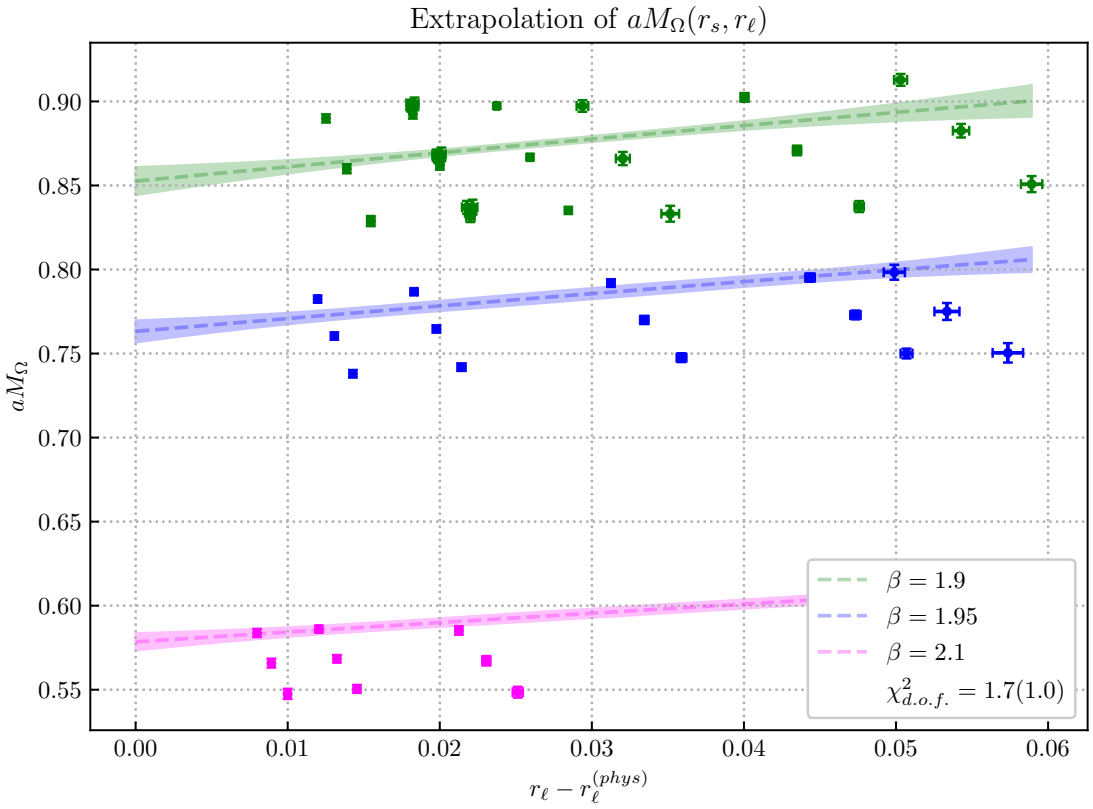


Figure 3.8: Extrapolation of $aM_\Omega$ in isoQCD over all the ensembles according to the ansatz given in eq. (3.23). Note that the removal of FVEs leads to the clustering of the points corresponding to the A40.XX ensembles. The colored dashed lines (with error bands) are the curves extrapolated to $r_s^{(phys)}$.

### 3.4.3 Extrapolation ($\ell$)

The dependence on the strange quark mass on a given observable can be removed, for each ensemble, interpolating among the 3 values of $am_s$. As discussed in sec. (3.2), this is obtained interpolating with respect to the corresponding 3 values of $r_s$. After this further step, we are left with the values of $aM_\Omega$ and $r_\ell$ at $L \to \infty$ and $r_s = r_s^{(phys)}$.
The dependence of $aM_\Omega$ on $r_\ell$ is then written as follows:

$$(aM_\Omega)_i = a_{\beta(i)}\, M_\Omega^{(exp)} \left[1 + c_\ell\, \Delta r_\ell + c_\ell^{(2)}\, \Delta r_\ell^2\right] \quad , \tag{3.24}$$

with the obvious labelling.

In table (3.8) are reported the values of the lattice spacings. and in fig (3.9) the plot of the extrapolation.

| $\beta$ | $a$(fm) | $a(\text{GeV}^{-1})$ | $a(\text{MeV}^{-1})$ |
|---|---|---|---|
| 1.90 | 0.1012(10) | 0.5126(52) | 0.0005126(52) |
| 1.95 | 0.09030(76) | 0.4576(39) | 0.0004576(39) |
| 2.10 | 0.06834(62) | 0.3463(31) | 0.0003463(31) |

Table 3.8: Lattice spacings obtained from $aM_\Omega$ with the simultaneous fit over $r_s$, $r_\ell$.

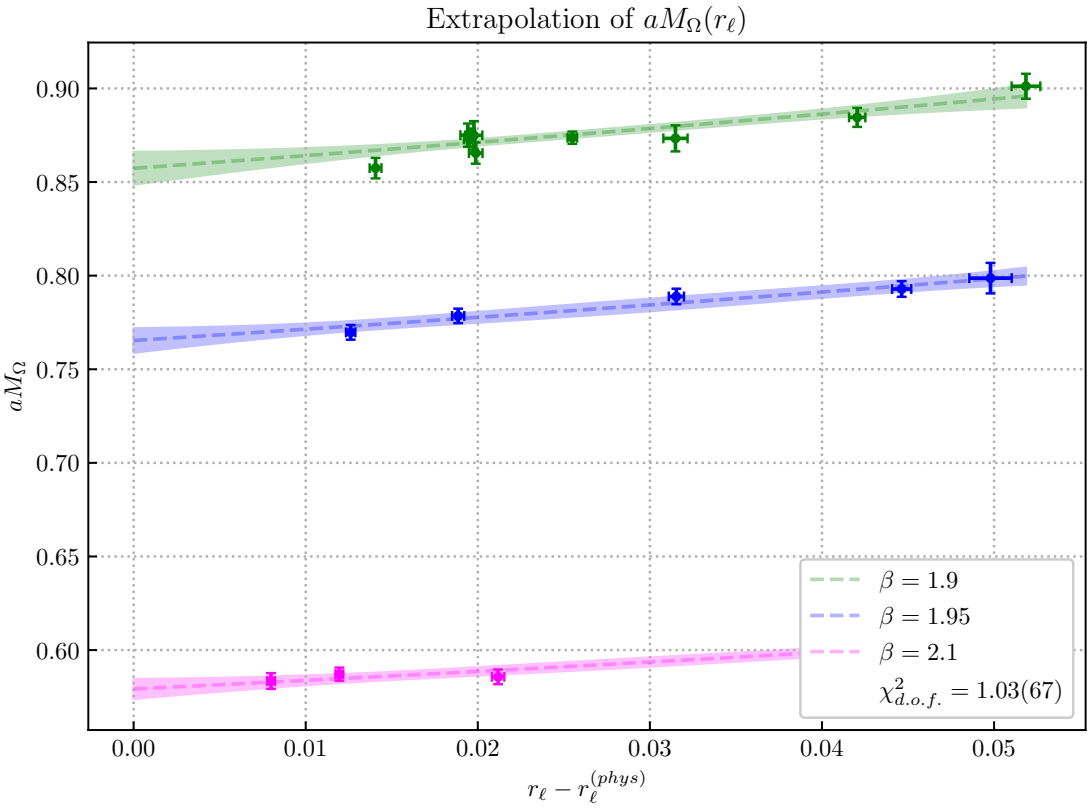


Figure 3.9: Extrapolation of $aM_\Omega$ in isoQCD over all the ensembles according to the ansatz given in eq. (3.24). Note that now the triplets of each ensemble are reduced to a single point, representing the physical point of $r_s$ for that ensemble. The colored dashed lines (with error bands) are the fitting curves.

## 3.5 Extrapolation of hadronic masses

### 3.5.1 Nucleon mass

In the full theory the interpolating operators for $p$ and $n$ are [100]:

$$\begin{aligned} p \qquad & \epsilon_{abc}(u_a^T(C\gamma_5)d_b)\, u_c \\ n \qquad & \epsilon_{abc}(d_a^T(C\gamma_5)u_b)\, d_c \end{aligned}$$

Their isosymmetric limit is the nucleon $N$, interpolated by:

$$N \quad \epsilon_{abc}(\ell_a^T(C\gamma_5)\ell_b)\,\ell_c \quad , \tag{3.25}$$

where $\ell$ is the isoQCD limit of $u$ and $d$ quarks. In terms of fermionic propagators we have:

$C_N =$ 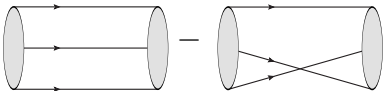 , (3.26)

with the notation discussed in sec. (C).
The mass was extracted fitting the effective mass curve to a constant at large times. These values have a dependence on the volume, lattice spacing and light quark mass. The leading FVEs is proportional to [94]:

$$M_\pi^3 \frac{e^{-M_\pi L}}{(M_\pi L)}$$

We approximate the dependence on $m_\ell$ with by the ChPT result ([101, 102]), whose leading contributions go as:

$$\sim M_\pi^2, \quad \sim M_\pi^3 \quad .$$

Discretization effects are included with an $a^2$ term since we are at maximal twist. For the above reasons we use the following ansatz to extrapolate the data:

$$M_N = M_0 \left[ 1 + c_L \left( \frac{M_\pi}{\Lambda_{QCD}} \right)^3 \frac{e^{-M_\pi L}}{(M_\pi L)} + c_2\, r_\ell + c_3\, r_\ell^{3/2} + c_a\, (\Lambda_{QCD} a)^2 \right] \quad , \tag{3.27}$$

where the arbitrary scale $\Lambda_{QCD} = 300\,\mathrm{MeV}$ is needed only to make the coefficients dimensionless. The values of $r_\ell$ are the ones extrapolated at fixed ensemble to the physical point of $r_s$ (see sec. (3.2)).
The value obtained from the extrapolation is:

$$M_N = 0.9549(97)\,\mathrm{GeV} \tag{3.28}$$

Moreover, assuming the ChPT expression, we also get a prediction for the $\pi N$ sigma term consistent with other findings in the literature (e.g. [103, 104]):

$$\sigma_{\pi N} = m_\ell \frac{\partial M_N}{m_\ell} \approx M_\pi^2 \frac{\partial M_N}{M_\pi^2} = 43.2(1.4) \quad . \tag{3.29}$$

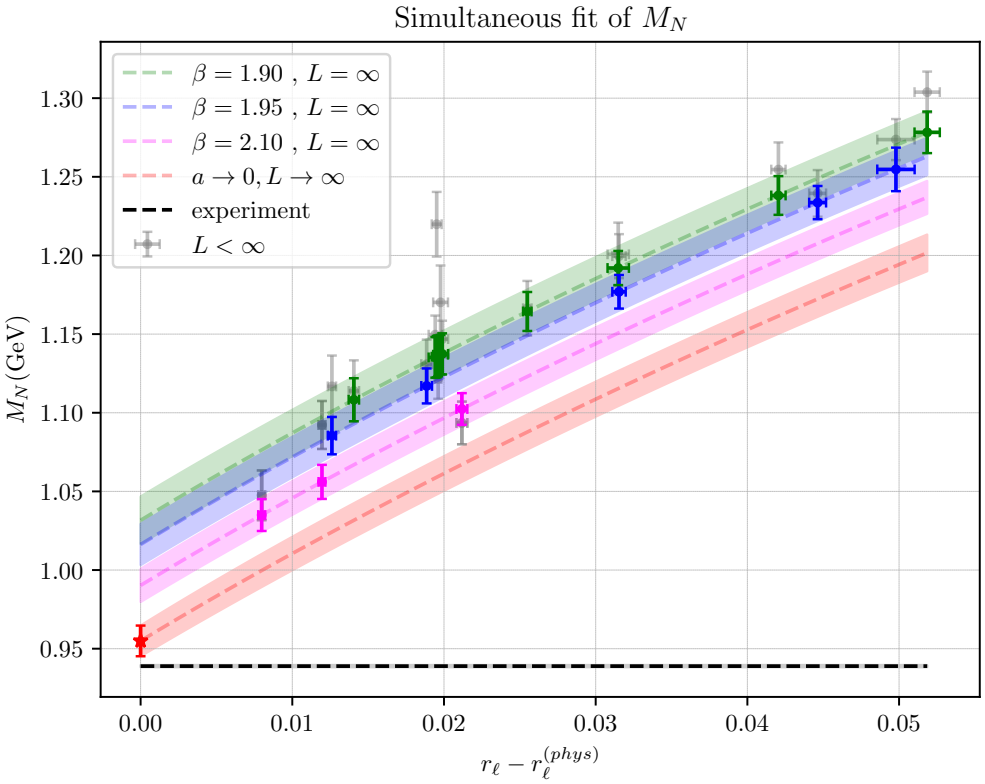


Figure 3.10: Extrapolation in isoQCD of $M_N$ according to the eq. (3.27). The faint grey points are the values at finite $L$. The colored points and dashed lines (with error bands) are the curves extrapolated to $L \to \infty$, $r_s^{(phys)}$ and fixed lattice spacing. The "experimental" value is a (narrow) band ranging from $M_p$ to $M_n$.

### 3.5.2 Delta resonance

In the full theory the interpolating operators for the $\Delta$ resonances are [100]:

$$\begin{aligned}
\Delta^{++} &\qquad \epsilon_{abc}(u_a^T(C\gamma_\mu)u_b)\, u_c \\
\Delta^{+} &\qquad \tfrac{1}{\sqrt{3}}\epsilon_{abc}\left(2(u_a^T(C\gamma_\mu)d_b)\, u_c + (u_a^T(C\gamma_\mu)u_b)\, d_c\right) \\
\Delta^{0} &\qquad \tfrac{1}{\sqrt{3}}\epsilon_{abc}\left(2(d_a^T(C\gamma_\mu)u_b)\, d_c + (d_a^T(C\gamma_\mu)d_b)\, u_c\right) \\
\Delta^{-} &\qquad \epsilon_{abc}(d_a^T(C\gamma_\mu)d_b)\, d_c
\end{aligned}$$

These generate correlators with the correct quantum numbers ($J^{PC}$, $I$) after the projection to positive parity and spin-3/2.
In the isosymmetric limit the $\Delta$ is a degenerate state, which is splitted into 4 levels by IB. This is reflected in the fact that the correlators are all equivalent in this limit (i.e. they show the same Wick contractions). For this reason, in isoQCD is sufficient to study the $\vec{p} = \vec{0}$ correlator:

$$C_{3\ell}(t) = \sum_{\vec{x}} \langle P^+_{\mu\nu} \mathcal{O}^{(\ell)}_\mu(x) \bar{\mathcal{O}}^{(\ell)}_\mu(0) \rangle \quad , \tag{3.30}$$

where:

$$\mathcal{O}_\mu{}^{(\ell)} = \epsilon_{abc}\,(\ell_a^T C\gamma_\mu \ell_b)\,\ell_c \tag{3.31}$$

$\ell$ is the light quark field, namely the limit of $u$ and $d$, and:

$$P^+_{\mu\nu} = P^{3/2}_{\mu\nu}\frac{1+\gamma_4}{2} \quad . \tag{3.32}$$

The explicit expression in terms of fermionic propagators has the same form for the $\Omega$:

$C_\Delta =$ 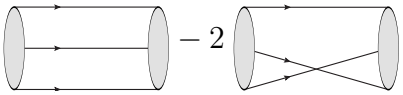 , (3.33)

where is understood the projection to positive parity and spin-3/2.
The mass was extracted from the large time behavior of the correlator, fitting the effective mass curve to a constant. The extracted values suffer from FVEs, dependence on the light quark mass and lattice spacing.
As seen in sec. (1.4.2), we know the leading contribution is proportional to the factor:

$$M_\pi^2\frac{e^{-M_\pi L}}{(M_\pi L)^{3/2}}$$

The dependence on $m_\ell$ is approximated by the ChPT result [102] predicting two leading contributions:

$$\sim M_\pi^2, \quad \sim M_\pi^3 \quad .$$

Discretization effects are taken into account with an $a^2$ term since we are at maximal twist.
As a result, we use the following ansatz to extrapolate the data:

$$M_\Delta = M_0\left[1 + c_L\left(\frac{M_\pi}{\Lambda_{QCD}}\right)^2\frac{e^{-M_\pi L}}{(M_\pi L)^{3/2}} + c_2\, r_\ell + c_3\, r_\ell^{3/2} + c_a\,(\Lambda_{QCD}a)^2\right] \quad , \tag{3.34}$$

where $\Lambda_{QCD} = 300\,\text{MeV}$ is an arbitrary scale chosen to make the coefficients dimensionless.
Here the values of $r_\ell$ are the ones extrapolated at fixed ensemble to the physical point of $r_s$ (see sec. (3.2)).
The value obtained from the extrapolation is:

$$M_\Delta = 1.261(30)\,\text{GeV} \quad , \tag{3.35}$$

consistently with the experimental range $1.230 - 1.234$ GeV from the peak of the $\Delta(1232)$ resonance [3]. We also find the $\pi\Delta$ sigma term consistent with the findings of [105].

$$\sigma_{\pi\Delta} = m_\ell\frac{\partial M_\Delta}{m_\ell} \approx M_\pi^2\frac{\partial M_\Delta}{M_\pi^2} = 24.55(77) \quad . \tag{3.36}$$

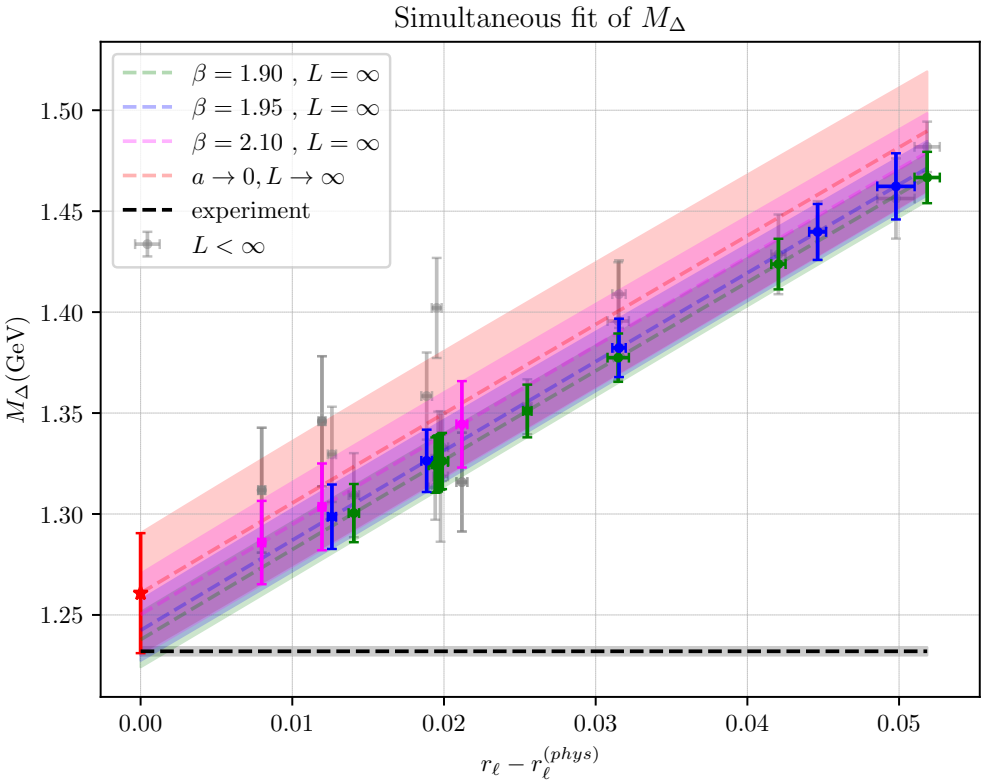


Figure 3.11: Extrapolation in isoQCD of $M_\Delta$ according to the eq. (3.34). colored dashed lines (with error bands) are the curves extrapolated to $L \to \infty$, $r_s^{(phys)}$ and fixed lattice spacing.

## 3.6 Renormalized quark masses

As discussed in sec. (1.2.6), renormalized quark masses can be found from the renormalization constants $Z_P$. Their calculation is not object of this work but they are taken from [13], which found them on dedicated ensembles with $N_f = 4$. In tab. (3.9) are reported their values in the $\overline{\text{MS}}$ scheme at the scale of 2 GeV, for the two methods M1 and M2 developed in [13].

| | method M1 | method M2 |
|---|---|---|
| $\beta = 1.90$ | 0.529(7) | 0.574(4) |
| $\beta = 1.95$ | 0.509(4) | 0.546(2) |
| $\beta = 2.10$ | 0.516(2) | 0.545(2) |

Table 3.9: Values of the RC $Z_P$ in the $\overline{\text{MS}}$ scheme from [13] at the scale $\mu = 2$ GeV.

The renormalized quark masses $\hat{m}_\ell$ and $\hat{m}_s$ are then found as:

$$\hat{m}_\ell = Z_P^{-1}\, m_\ell \tag{3.37}$$
$$\hat{m}_s = Z_P^{-1}\, m_s \quad . \tag{3.38}$$

We compute their values for each ensemble, which can be extrapolated to the physical point as discussed in the following sections.

### 3.6.1 Extrapolation of $\hat{m}_\ell$

The extrapolation of $\hat{m}_\ell$ was done using the pion mass. In our setup the latter depends only on the light quark mass, the lattice spacing and volume of our grid. We followed an approach analogous to the analysis B of [13], fitting the values of $M_\pi^2$ with a polynomial ansatz:

$$M_\pi^2 = P_0 \Lambda_{QCD} \hat{m}_\ell \left[ 1 + c_L \left( \frac{M_\pi}{\Lambda_{QCD}} \right)^2 \frac{e^{-M_\pi L}}{(M_\pi L)^{3/2}} + c_a (a\Lambda_{QCD})^2 + c_\ell^{'} \left( \frac{\hat{m}_\ell}{\Lambda_{QCD}} \right) + c_\ell^{''} \left( \frac{\hat{m}_\ell}{\Lambda_{QCD}} \right)^2 \right] \quad , \tag{3.39}$$

where FVEs are implicitly defined. $\Lambda_{QCD}$ is an arbitrary scale to make coefficients dimensionless and fixed to 300 MeV. $P_0$, $c_L$, ..., are free parameters in the fit over the ensembles. In fig. (3.12) is shown the extrapolation of $M_\pi^2$ over the ensembles as a function of $\hat{m}_\ell$. Our prediction is obtained setting $L \to \infty$, $a = 0$ and $M_\pi$ at the physical point in the above expression and inverting numerically for $\hat{m}_\ell$. Using eq. (28) of [13], we combine the results obtained with the $Z_P$ found with the methods M1 and M2. We find:

$$\hat{m}_\ell(\mu = 2\,\text{GeV}) = 3.781(76)\,\text{MeV} \quad , \tag{3.40}$$

compatibly within $1\sigma$ with [13], which found $\hat{m}_\ell = 3.70(17)\,\text{MeV}$.

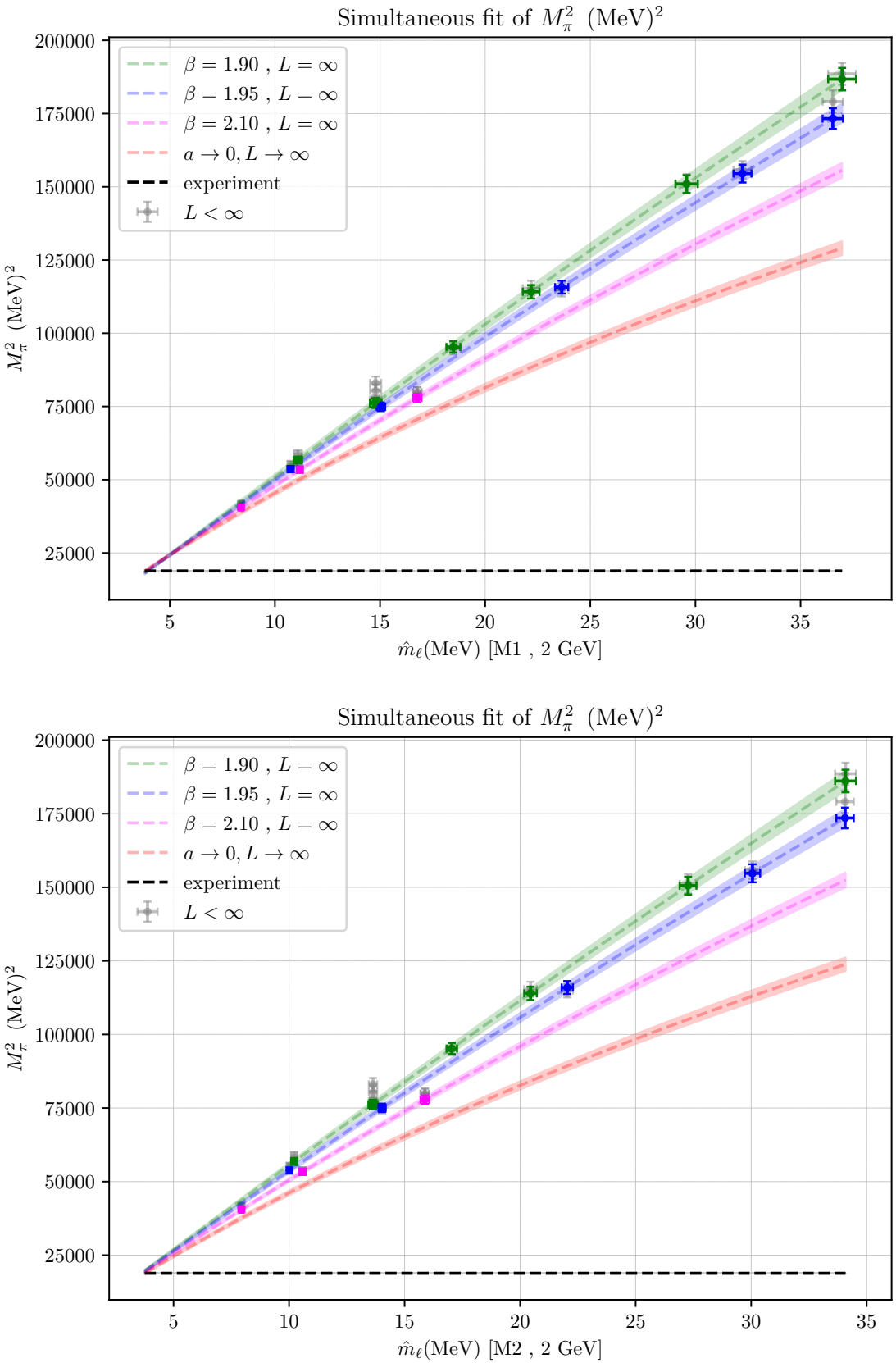


Figure 3.12: Extrapolation of $M_\pi^2$ according to the eq. (3.39) as a funcion of $\hat{m}_\ell(\mu = 2\,\text{GeV})$ found using the $Z_P$ of the methods M1 and M2. The faint grey points are the values at finite $L$. The colored points and dashed lines (with error bands) are the curves extrapolated to $L \to \infty$ and fixed lattice spacing. The "experimental" value is a (narrow) band ranging from $M_{\pi^0}$ to $M_{\pi^+}$.

### 3.6.2 Extrapolation of $\hat{m}_s$

The extrapolation of $\hat{m}_s$ was done using the Kaon mass. The latter has a dependence on both the light and strange quark masses, the lattice spacing and the volume. As for the light quark mass, we followed an approach analogous to the analysis B of [13] The values of $M_K^2$ were fitted according to the following polynomial ansatz:

$$M_K^2 = P_0 \Lambda_{QCD}(\hat{m}_\ell + \hat{m}_s) \left[ 1 + c_L \left( \frac{M_\pi}{\Lambda_{QCD}} \right)^2 \frac{e^{-M_\pi L}}{(M_\pi L)^{3/2}} + c_a (a\Lambda_{QCD})^2 + c_1 \left( \frac{\hat{m}_\ell}{\Lambda_{QCD}} \right) + c_2 \left( \frac{\hat{m}_\ell}{\Lambda_{QCD}} \right)^2 \right] \quad . \tag{3.41}$$

$\Lambda_{QCD}$ is an arbitrary scale to make coefficients dimensionless and fixed to 300 MeV. $P_0$, $c_L$, ... , are free parameters of the fit over all the ensembles. In fig. (3.13) is shown the extrapolation of $M_K^2$ over the ensembles and 3 values of $\hat{m}_s$ as a function of $\hat{m}_\ell$. Our prediction is obtained setting $L \to \infty$, $a = 0$, $M_K$ at the physical point and $\hat{m}_\ell$ at the physical value found in (3.6.1) in the above expression, and inverting numerically for $\hat{m}_s$. Using eq. (28) of [13], we combine the results obtained with the $Z_P$ found with the methods M1 and M2. We find:

$$\hat{m}_s(\mu = 2\,\text{GeV}) = 103.2(2.0)\,\text{MeV} \quad . \tag{3.42}$$

compatibly within $1\sigma$ with [13], which found $\hat{m}_s = 99.6(4.3)\,\text{MeV}$.

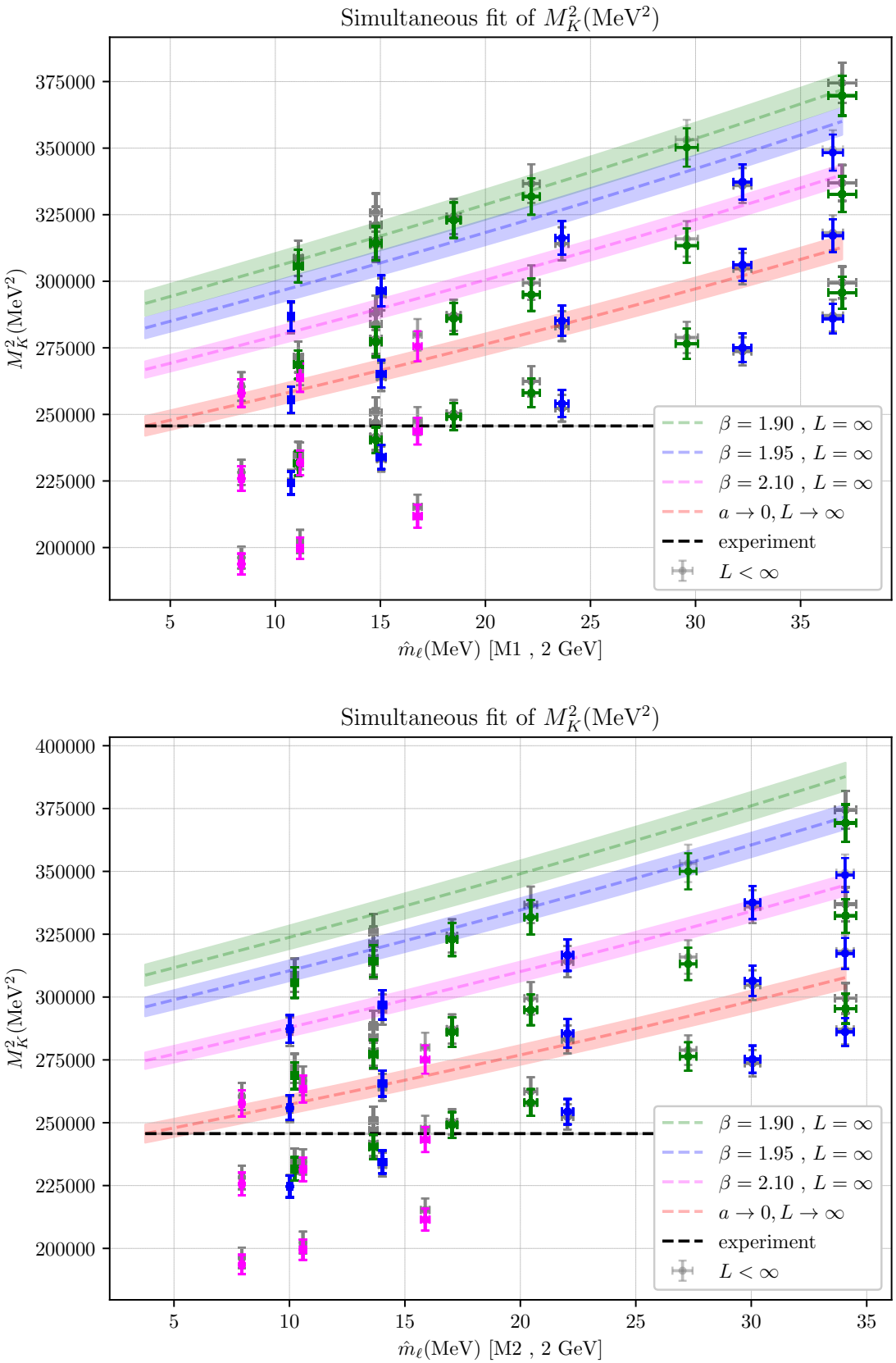


Figure 3.13: Extrapolation of $M_K^2$ according to the eq. (3.41) as a funcion of $\hat{m}_\ell(\mu = 2\,\text{GeV})$ found using the $Z_P$ of the methods M1 and M2. The faint grey points are the values at finite $L$. The vertical triplets of points correspond to the 3 values of $m_s$ simulated for each ensemble. The colored points and dashed lines (with error bands) are the curves extrapolated to $L \to \infty$ and fixed lattice spacing. The "experimental" value is a (narrow) band ranging from $M_{K^+}$ to $M_{K^0}$.

# Chapter 4

# Analysis in QCD+QED

In this section are discussed the details of the analysis in presence of IB effects. At LO the latter are evaluated from the combination of slopes found in the isosymmetric theory, multiplied by the appropriate counterterms and charge factors. This requires the tuning of counterterms, in our case the critical and physical mass ones.
The first ($\Delta m_f^{(crit)}$ , $f = u, d, s$) are found for each ensemble from the PCAC Ward Identity, requiring to preserve the maximal twist condition at $O(\alpha_{EM})$ and hence the $O(a)$ improvement on discretization effects (see sec. (4.1)). The second are found in an hadronic scheme, in which we find the 3 bare mass counterterms in lattice units ($a\Delta m_u$, $a\Delta m_d$, $a\Delta m_s$) such that they match the experimental values of the 3 hadronic ratios $r_s$ $r_\ell$ and $r_p$ (see sec. (4.4)). The latter depend on ($M^2_{\pi^+} + M^2_{\pi^0}$), $M^2_{K^+}$, $M^2_{K^0}$, $M^2_{\Omega^-}$, which we use as inputs to tune $m_u$, $m_d$, $m_s$ and the lattice spacing $a$. We are then able to predict the spectrum of nucleons (sec. (4.7)) and $\Delta(1232)$ resonances (sec. (4.8)).
The modification in the lattice spacing induced by IB is fixed by $M_{\Omega^-}$, whose value (in the full theory) determines the scale of the system analogously as we did in isoQCD (see sec. (4.5)).
In $QCD + QED$ we simulated 2 values of the valence strange quark mass, between which we interpolate at fixed ensembles the observables depending on it (see sec. (4.3)). Here these are the masses and mass slopes of kaons and $\Omega$.
After that, we combine the electromagnetic ($EM$) slopes with the ones coming multiplying the critical mass counterterms ($C$). The first originate from diagrams involving photons and the second from the ones with the insertion of the pseudoscalar current. The combination of the two is denoted with $EMC$ ($= EM + C$).
We then correct the universal $QED_L$ FVEs on these slopes, in order to avoid their presence in the physical mass counterterms.
At this point we tune the $a\Delta m_f$ for each ensemble, and get the observables in physical units. These are extrapolated among all the ensembles, taking simultaneously into account FVEs, discretization effects and dependence on $r_\ell$.

## 4.1 Critical mass counterterms

The bare critical mass (and its counter-term in the presence of QED) is tuned using the PCAC Ward-Takahashi identity (WTi) [106]. The latter reads:

$$\partial_\mu \langle A^a_\mu(t,\vec{x})\, P^a(0,\vec{0})\rangle = 2\, m_f^{PCAC}\, \langle P^a(t,\vec{x})\, P^a(0,\vec{0})\rangle \quad a = 1,2 \quad , \qquad (4.1)$$

where $m^{PCAC}$ is the renormalized twisted mass (see [7] for the notation), and $P^a = \bar{\chi}_f \gamma^5 \frac{\tau^a}{2} \chi_f$ and $A^a_\mu = \bar{\chi}_f \gamma_\mu \gamma^5 \frac{\tau^a}{2} \chi_f$ in the twisted basis $\{\bar{\chi}_f, \chi_f\}$. The $\frac{\tau^a}{2}$ are the Pauli matrices.
When we integrate over the spatial positions the $\partial_i$ term gives a surface contribution, which vanishes in the limit $L \to \infty$. The above equation then becomes

$$\partial_t \int d\vec{x} \, \langle A^a_4(t, \vec{x}) \, P^a(0, \vec{0}) \rangle = 2m^{PCAC} \int d\vec{x} \, \langle P^a(t, \vec{x}) \, P^a(0, \vec{0}) \rangle \quad . \tag{4.2}$$

The maximal twist condition, $m^{PCAC} = 0$, can be set from here, requiring the LHS of (4.2) to vanish. This was done in advance before the isoQCD simulations, which then already started at maximal twist. When adding the QED interaction to the Lagrangian, we are interested in preserving the maximal twist so as to get the $O(a)$ improvement [107]. In other words we require:

$$0 = \Delta m^{PCAC} = \Delta \left( \frac{\partial_t \langle A^a_4(t) \, P^a(0) \rangle}{\langle P^a(t) \, P^a(0) \rangle} \right) \quad , \tag{4.3}$$

where $\Delta$ represents the variation caused by the counter-term $\Delta m_{crit}$ and the diagrams with photons. The condition $m^{PCAC} = 0$ does not depend on the twisted mass $m_f$, and hence on the counter-term $\Delta m_f$ when IB is introduced. The above equation fixes $\Delta m^{(cr)}$ and is equivalent to:

$$\partial_t \, \Delta \langle A^a_4(t) \, P^a(0) \rangle - 2m^{PCAC}_0 \, \Delta \langle P^a(t) \, P^a(0) \rangle = 0 \quad . \tag{4.4}$$

Note that we kept the dependence on the isoQCD value $m^{PCAC}_0$ with the purpose of correcting any inaccuracy in the isosymmetric maximal twist. Fig. (4.1) contains the fits to a constant of the effective mass curves for $a\Delta m^{(cr)}_f$. We show the case of one ensemble for each $\beta$ for $a\Delta m^{(cr)}_u$ [1] and $a\Delta m^{(cr)}_s$.

## 4.2 $QED$ finite size effects

As discussed in sec. (2.5), QED on a torus induces FVEs in the hadronic spectrum suppressed by powers of $1/L$. The $\sim 1/L$ and $\sim 1/L^2$ terms are universal, i.e. don't depend on the spin or structure of the hadron which enter at $O(\frac{\alpha_{EM}}{L^3})$ in the volume dependence. The asymptotic behavior in a mass correction $\Delta M$ induced by QED is then:

$$\Delta M(L) \to \Delta M(\infty) - Q^2 \alpha_{EM} \left[ \frac{\kappa}{2L} \left( 1 + \frac{2}{ML} \right) \right] + O\left( \frac{\alpha_{EM}}{L^3} \right) \quad . \tag{4.5}$$

Using the above formula we remove these universal FVEs from the mass corrections generated by diagrams with photons. In the analysis this is done at fixed ensemble and fixed value of strange quark mass. As discussed later, we use these mass corrections to tune physical mass counterterms. Having corrected them from these $1/L$ and $1/L^2$ effects means that the $a\Delta m_f$ we'll find will contain only residual structure dependent FVEs of $O(1/L^3)$. These are taken into account afterwards in the global extrapolations among all the ensembles at the end of the tuning.

[1] Note that $a\Delta m^{(cr)}_d = (e_d/e_u)^2 \cdot a\Delta m^{(cr)}_u$

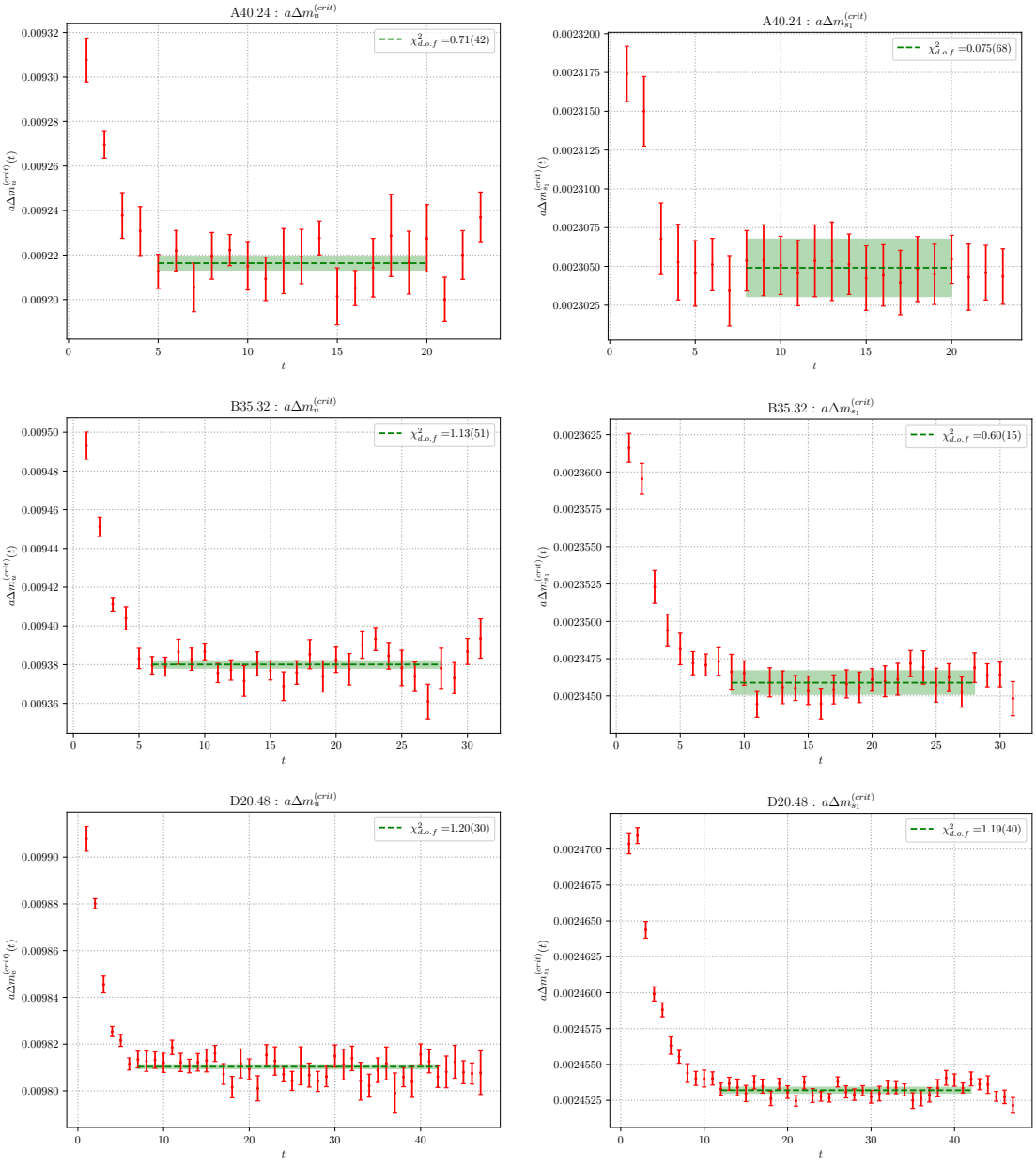


Figure 4.1: Effective curves of $\Delta m_u^{(cr)}$ and $\Delta m_s^{(cr)}$ (1st value of $m_s$) as a functions of time, for the ensembles $A40.24$, $B35.32$, $D20.48$ (one for each $\beta$). The starting point $t_0$ of the plateau is chosen such that approximately $t_0/a$ is constant over the 3 values of $\beta$.

We remark that, in principle, if we had enough $A40.XX$ ensembles we could have fit the finite volume effects on them, finding (and subtracting) the higher order terms. In practice however, we found that this often results in a less stable fit and final extrapolation result, due to the uncertainties and small number of points. The following plots show the QED FVEs for the A40.XX ensembles for some of the EM mass corrections involved in the analysis. As expected, the displacement from the "universal" curve, namely the structure-dependence, is more severe for small volumes.

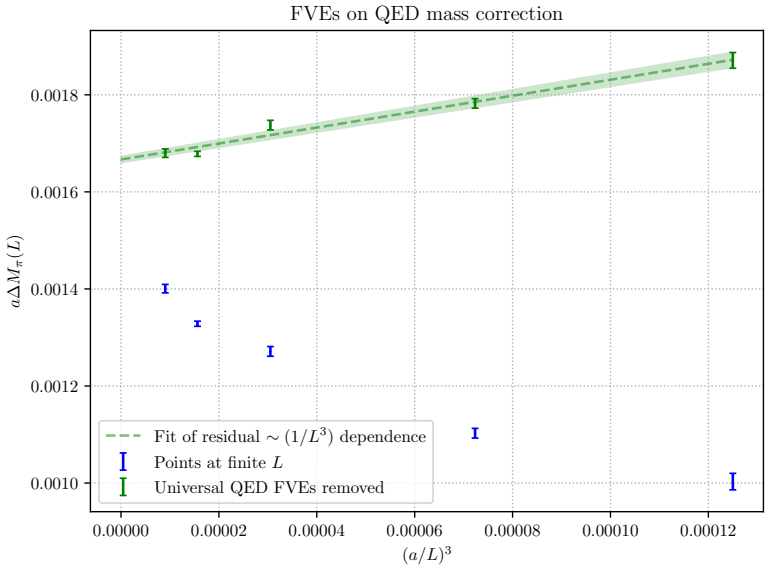


Figure 4.2: The blue points are the $EMC$ corrections in lattice units at finite volume. The green points are the values after the correction of the universal QED FVEs. The green band is a fit of the latter with an ansatz of the form $A + B\left(\frac{a}{L}\right)^3$, with $A$ and $B$ free parameters of the fit.

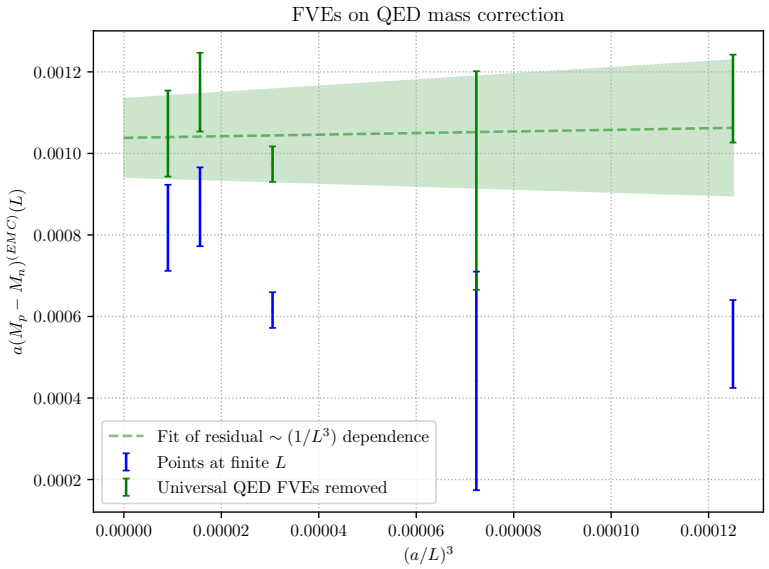


Figure 4.3: Same as fig. (4.2) but for the mass difference $(M_p - M_n)^{(EMC)}$.

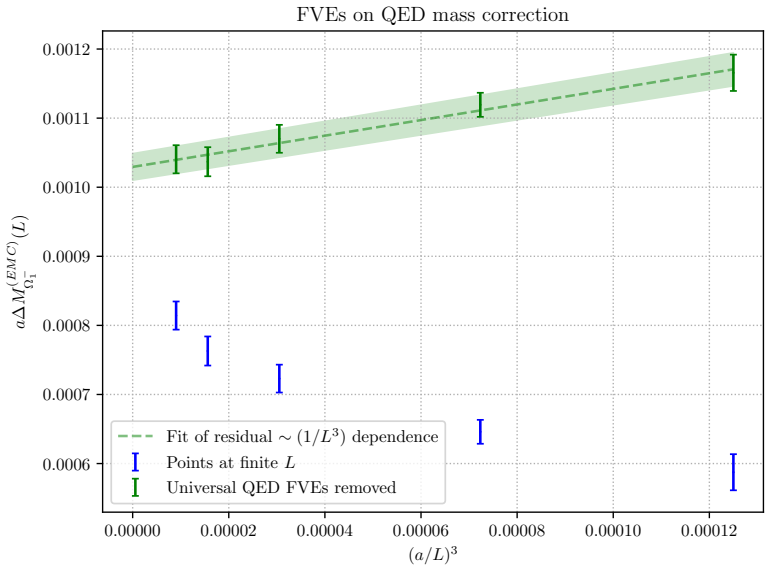


Figure 4.4: Same as fig. (4.2) but for the $\Omega^-$ corresponding to the 1st value of the strange quark mass.

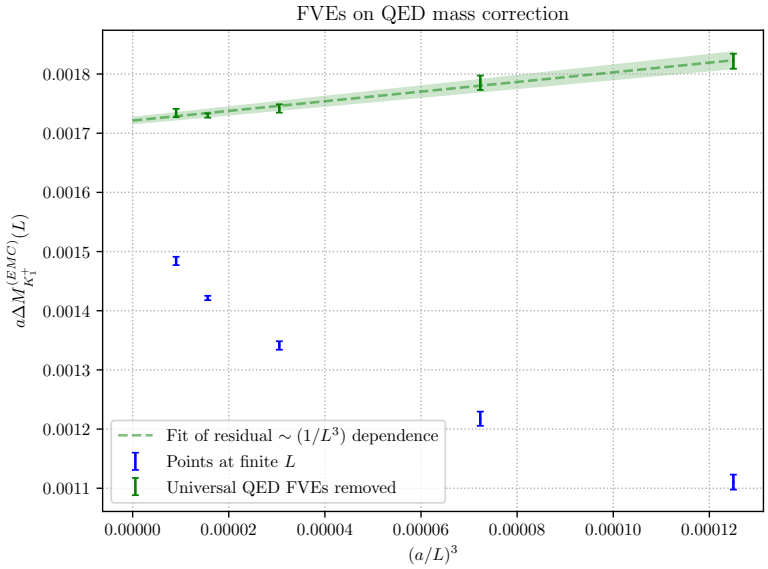


Figure 4.5: Same as fig. (4.4) but for the $K^+$.

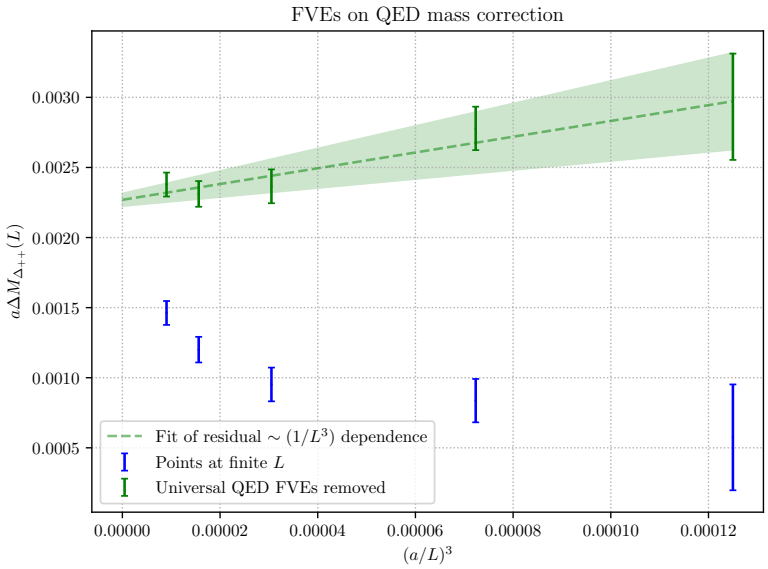


Figure 4.6: Same as fig. (4.2) but for the $\Delta^{++}$ resonance.

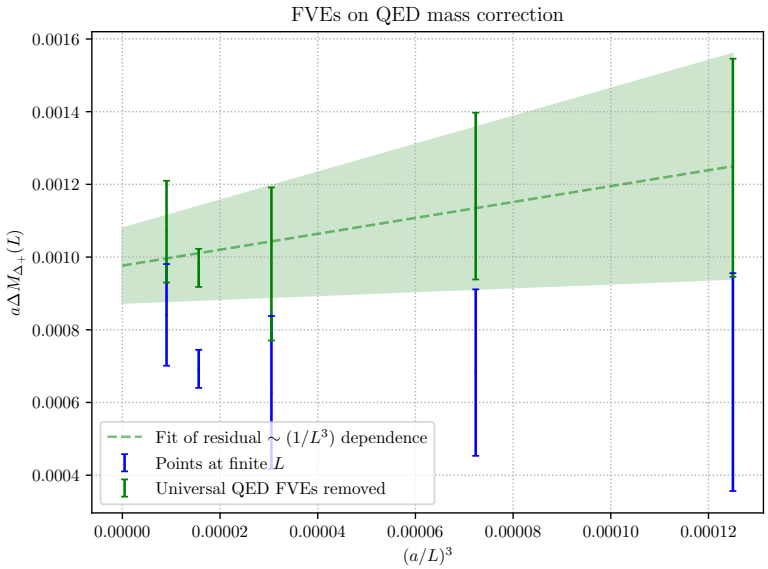


Figure 4.7: Same as fig. (4.6) but for the $\Delta^{+}$.

## 4.3 Interpolation to the physical point of $m_s$

In the extrapolation of the observables, together with $L \to \infty$ and $a \to 0$, we reach the physical point of quark masses. Here we do this in separate steps, interpolating the slopes to the physical point of $am_s$ at fixed ensemble, using these slopes to find counterterms for each $am_\ell$ (see sec. (4.4)), and leaving the extrapolation in this parameter as the last step.
In $QCD + QED$ we simulated 2 values of $am_s^{(0)}$ in the Lagrangian, near to the physical point found in isoQCD (see tab. (4.1)).

| $\beta$ | $am_{s_1}^{(0)}$ | $am_{s_2}^{(0)}$ |
|---|---|---|
| 1.90 | 0.0242 | 0.0261 |
| 1.95 | 0.0216 | 0.0230 |
| 2.10 | 0.0176 | 0.0186 |

Table 4.1: Values of $am_s^{(0)}$ for each $\beta$ of the 2nd run for QCD+QED.

As in the analysis in the isoQCD background we interpolate in terms of an hadronic ratio, which here is:

$$r_s = \frac{2(M_{K^+}^2 + M_{K^0}^2) - (M_{\pi^+}^2 + M_{\pi^0}^2)}{2M_{\Omega^-}^2} \quad . \tag{4.6}$$

The interpolation is done using a straight line:

$$O(am_s) = O_0 \left[1 + C_s(r_s - r_s^{(phys)})\right] \quad , \tag{4.7}$$

where $O$ is a generic observable and $O_0$, $C_s$ are free parameters of the fit. This is justified by the closeness to the physical point. Examples of the extrapolations for $M_K$ and $M_\Omega$ slopes are reported below in the following figures. We show the case of the ensembles $A100.24$, $B25.32$, $D15.48$ (one for each $\beta$).

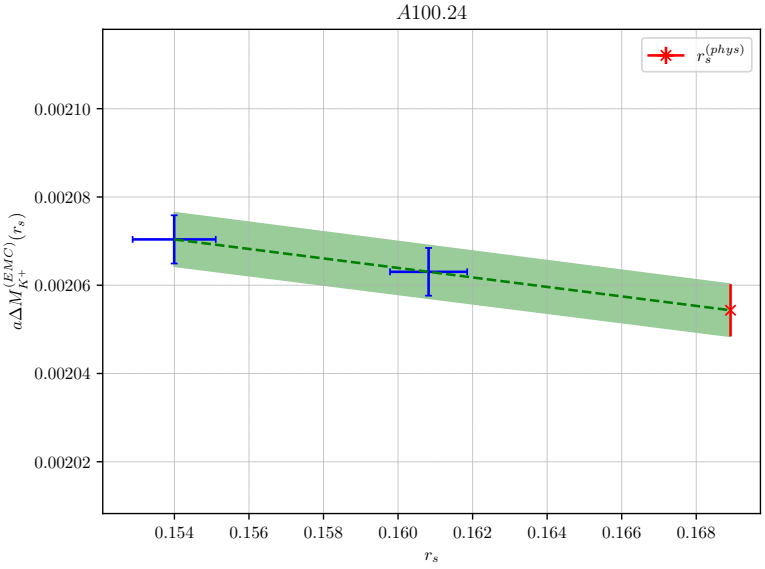


Figure 4.8: Extrapolations to the physical point of $r_s$ of the electromagnetic correction $\Delta M_{K^+}^{(EMC)}$ for the ensemble $A100.24$. The blue points (with errorbars) are the points for the 2 values of the strange quark mass, with the green band being the fitting curve (with error). In red, the extrapolation to the physical point of $r_s$.

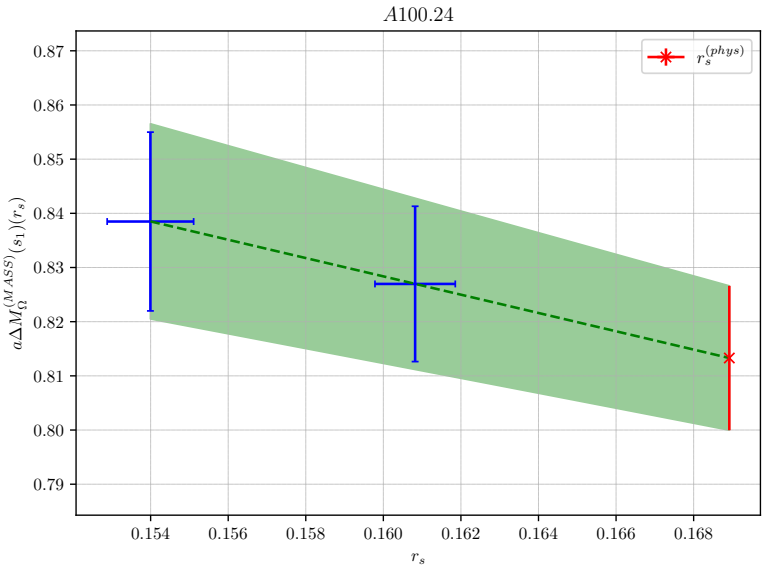


Figure 4.9: Same as fig. (4.8) but for the mass slopes $\Delta M_\Omega^{(MASS)}(s_1)$ coming from the insertion of the scalar current on the 1st leg.

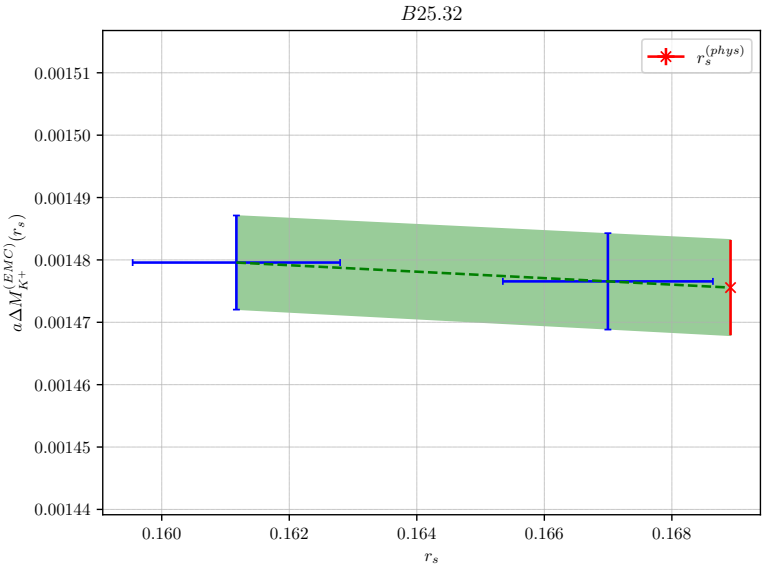


Figure 4.10: Same as fig. (4.8) but for the ensemble $B25.32$.

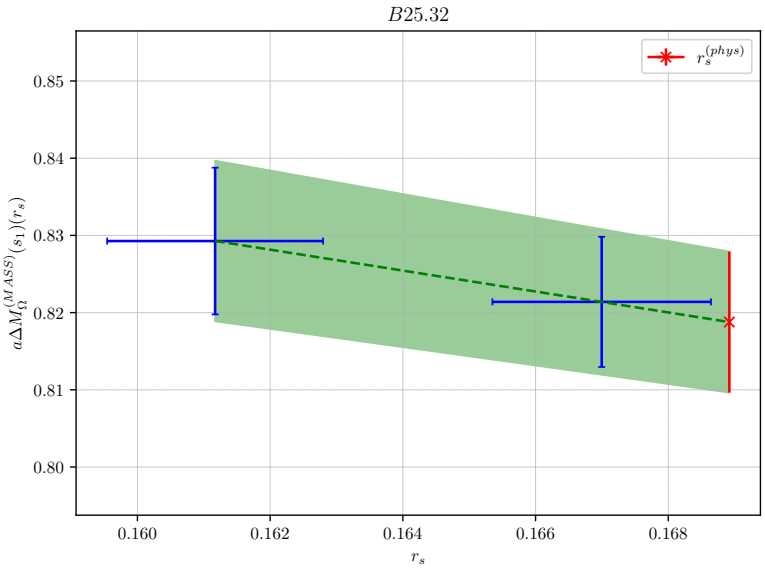


Figure 4.11: Same as fig. (4.9) but for the ensemble $B25.32$.

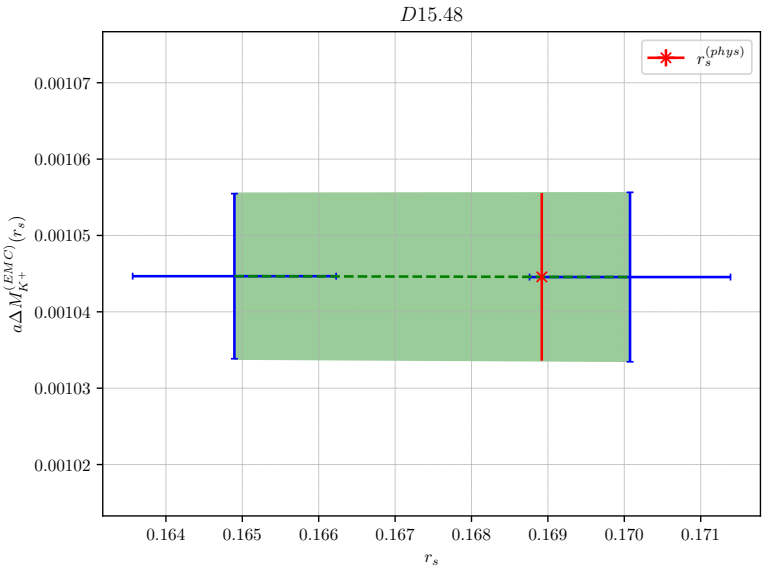


Figure 4.12: Same as fig. (4.8) but for the ensemble $D15.48$.

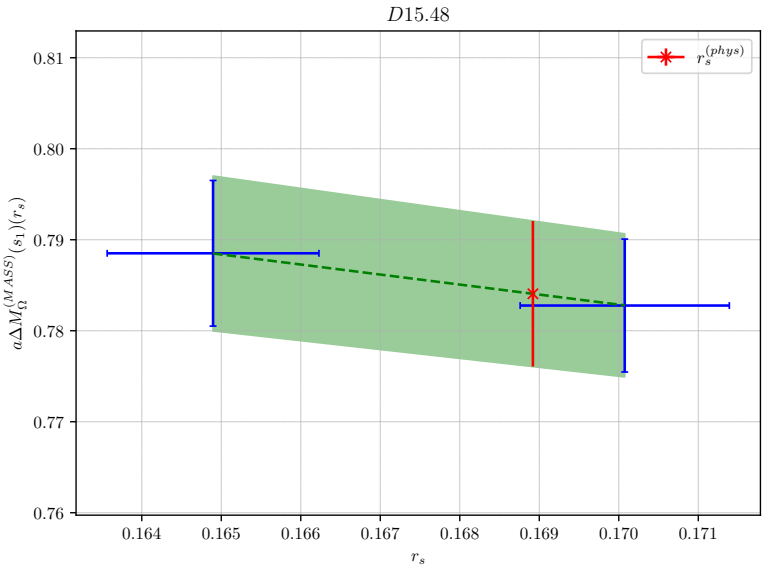


Figure 4.13: Same as fig. (4.9) but for the ensemble $D15.48$.

## 4.4 Tuning of mass counterterms

The physical point of a theory is defined by the values of its $n$ renormalized couplings at some scale. On the lattice we can equivalently provide their bare values in lattice units, requiring to match the experimental values of $n$ physical observables. Here we define the physical point of isoQCD and QCD+QED from the following ratios:

$$r_s = \frac{2(M_{K^+}^2 + M_{K^0}^2) - (M_{\pi^+}^2 + M_{\pi^0}^2)}{2M_{\Omega^-}^2} \quad , \tag{4.8}$$

$$r_\ell = \frac{M_{\pi^+}^2 + M_{\pi^0}^2}{2M_{\Omega^-}^2} \quad , \tag{4.9}$$

$$r_p = \frac{M_{K^+}^2}{M_{\Omega^-}^2} \quad , \tag{4.10}$$

imposing $r_s = r_s^{(exp)}$, $r_\ell = r_\ell^{(exp)}$ and $r_p = r_p^{(exp)}$. This also implies, by definition, that their total IB corrections vanishes.
At LO we have:

$$r_s = r_s^{(0)} + \sum_{f\in(u,d,s)} a\Delta m_f \bar{\Delta} r_s{}^{(f)} + \Delta r_s^{(EMC)} \tag{4.11}$$

$$r_\ell = r_\ell^{(0)} + \sum_{f\in(u,d,s)} a\Delta m_f \bar{\Delta} r_\ell{}^{(f)} + \Delta r_\ell^{(EMC)} \tag{4.12}$$

$$r_p = r_p^{(0)} + \sum_{f\in(u,d,s)} a\Delta m_f \bar{\Delta} r_p{}^{(f)} + \Delta r_p^{(EMC)} \quad , \tag{4.13}$$

where $\bar{\Delta} r_i^{(f)}$ $(i = s, \ell, p)$ is the slope caused by the insertion of the scalar current multiplied by the counterterm $a\Delta m_f$, and $(EMC)$ denotes the combination of QED and critical mass counterterms corrections. Note that the latter are already known for each ensemble because their tuning was done using the PCAC Ward Identity.

The solution to the above system gives us the tuning condition for physical mass counterterms:

$$\begin{bmatrix} a\Delta m_u \\ a\Delta m_d \\ a\Delta m_s \end{bmatrix} = - \begin{bmatrix} \bar{\Delta} r_s^{(u)} & \bar{\Delta} r_s^{(d)} & \bar{\Delta} r_s^{(s)} \\ \bar{\Delta} r_\ell^{(u)} & \bar{\Delta} r_\ell^{(d)} & \bar{\Delta} r_\ell^{(s)} \\ \bar{\Delta} r_p^{(u)} & \bar{\Delta} r_p^{(d)} & \bar{\Delta} r_p^{(s)} \end{bmatrix}^{-1} \begin{bmatrix} \Delta r_s^{(EMC)} \\ \Delta r_\ell^{(EMC)} \\ \Delta r_p^{(EMC)} \end{bmatrix} \quad . \tag{4.14}$$

These equations give the counterterms at the isoQCD physical point of $am_s$ and $am_\ell$. In the analysis the $a\Delta m_f$ are found at fixed ensemble, after the interpolation of the slopes among the 2 values of $am_s$ to the physical point of $r_s$ . These $a\Delta m_f$ are used to evaluate the other observables , which are then extrapolated to $L \to \infty$, $a \to 0$ and $r_\ell = r_\ell^{(exp)}$ over all the ensembles. For each observable $O$ this is just an extrapolation in separate steps, done on the slice $r_s = r_s^{(exp)}$ of the hyper-surface $O(r_s, r_\ell, L, a)$.

## 4.5 Scale setting in QCD+QED

The scale of the system is modified by the inclusion of IB effects. This is caused by the modification of the observable(s) used to set the scale. In our case this is $aM_{\Omega^-}$. In isoQCD we evaluated an approximation of the mass ($M_\Omega$) neglecting IBEs, but in the full theory these values are subject to corrections. The lattice spacings in the full theory are defined as:

$$a_{\beta(i)} = \frac{aM_{\Omega^-}}{M_{\Omega^-}^{\text{exp.}}} = \frac{a_0 M_\Omega + \Delta(aM_{\Omega^-})}{M_{\Omega^-}^{\text{exp.}}} = a_{\beta(i)}^{(0)}(1 + \delta a_{\beta(i)}) \quad , \tag{4.15}$$

where $a_{\beta(i)}^{(0)}$ are the values found from the isosymmetric limit $M_\Omega$. The values of $aM_{\Omega^-}$ are found after the tuning of physical mass counterterms:

$$aM_{\Omega^-} = a\left[M_\Omega + \Delta m_s \bar{\Delta} M_\Omega + (\Delta M_{\Omega^-})^{(EMC)}\right] \quad , \tag{4.16}$$

and fitted with the same technique used in isoQCD among all the ensembles, keeping into account a dependence on the parameters $(L, r_\ell)$:

$$(aM_\Omega)_i(L, r_\ell) \;=\; a_{\beta(i)}\, M_\Omega^{(exp)} \left[1 +\; c_L \frac{\alpha_{EM}}{L^3} +\; c_\ell\, \Delta r_\ell \;+\; c_\ell^{(2)}\, \Delta r_\ell^2\right] \quad . \tag{4.17}$$

$c_L$, $c_\ell$, $c_\ell^{(2)}$ and $a_{\beta(i)}$ $(i = 1, 2, 3)$ are free parameters of the fit. The difference with isoQCD is that here the leading FVE comes from QED, and is taken into account with the $\sim 1/L^3$ term. This comes from the residual volume dependence in $a\Delta m_s$ and $\Delta M_{\Omega^-}^{EMC}$, to which universal $1/L$ and $\sim 1/L^2$ terms have already been subtracted (see sec. (4.2)). The $a_{\beta(i)}$ are the 3 lattice spacing in the full theory, whose values are reported in tab. (4.2). In fig. (4.14) is shown the plot of the simultaneous extrapolation.

| $\beta$ | $a$(fm) | $a$(GeV$^{-1}$) |
|---|---|---|
| A | 0.1011(10) | 0.5126(52) |
| B | 0.09029(77) | 0.4576(39) |
| D | 0.06834(63) | 0.3463(32) |

Table 4.2: Lattice spacings obtained from $aM_{\Omega^-}$ with the simultaneous fit over $L$ and $r_\ell$.

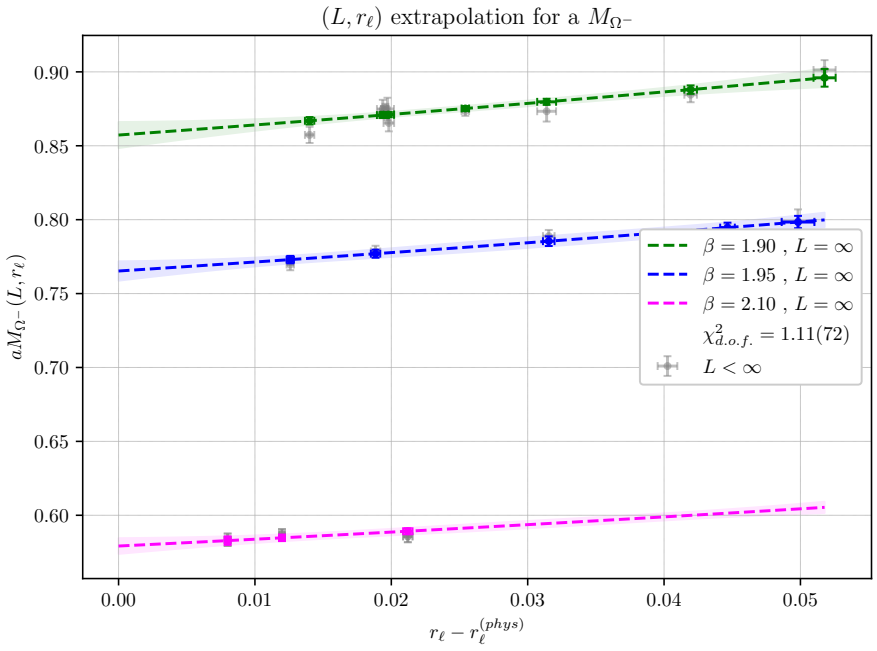


Figure 4.14: Extrapolation of $aM_{\Omega^-}$ in QCD+QED over all the ensembles according to the ansatz given in eq. (4.17). In faint grey are shown the points at finite volume, and the colored dashed lines (with error bands) are the curves extrapolated to $L \to \infty$.

## 4.6 Pions mass difference

The pion mass difference $M_{\pi^+} - M_{\pi^0}$ is a purely electromagnetic effect independent of counterterms. In our calculation we neglected the computation of the so called *handcuffs* diagram $\partial_t$ 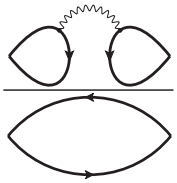 , extrapolating among the ensembles the quantity:

$$M^2_{\pi^+} - M^2_{\pi^0} = 2M_\pi(M_{\pi^+} - M_{\pi^0}) = 2M_\pi \frac{(e_u - e_d)^2}{2} e^2 \partial_t \quad . \tag{4.18}$$

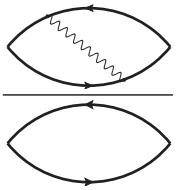

The latter is fitted according to the following simple polynomial ansatz:

$$M^2_{\pi^+} - M^2_{\pi^0} = A_0 \Lambda^2_{QCD} \left\{ 1 + \alpha_{EM} \left( \frac{M_\pi}{\Lambda_{QCD}} \right) \frac{c_L^{(3)}}{(\Lambda_{QCD} L)^3} + c_\ell r_\ell + c_\ell^{(2)} r_\ell^2 + c_a (a\Lambda_{QCD})^2 \right\} \tag{4.19}$$

where $\Lambda_{QCD} = 300\,\text{MeV}$ is just an arbitrary scale, and the coefficients $A_0$, ... , are free parameters of the fit. The $\sim 1/L^3$ term is the leading volume effect [77], with

$\sim 1/L^4$ (from QED) and exponential (from QCD) effects found to be numerically negligible in this fit. In fig. (4.15) is reported the plot of the extrapolation.

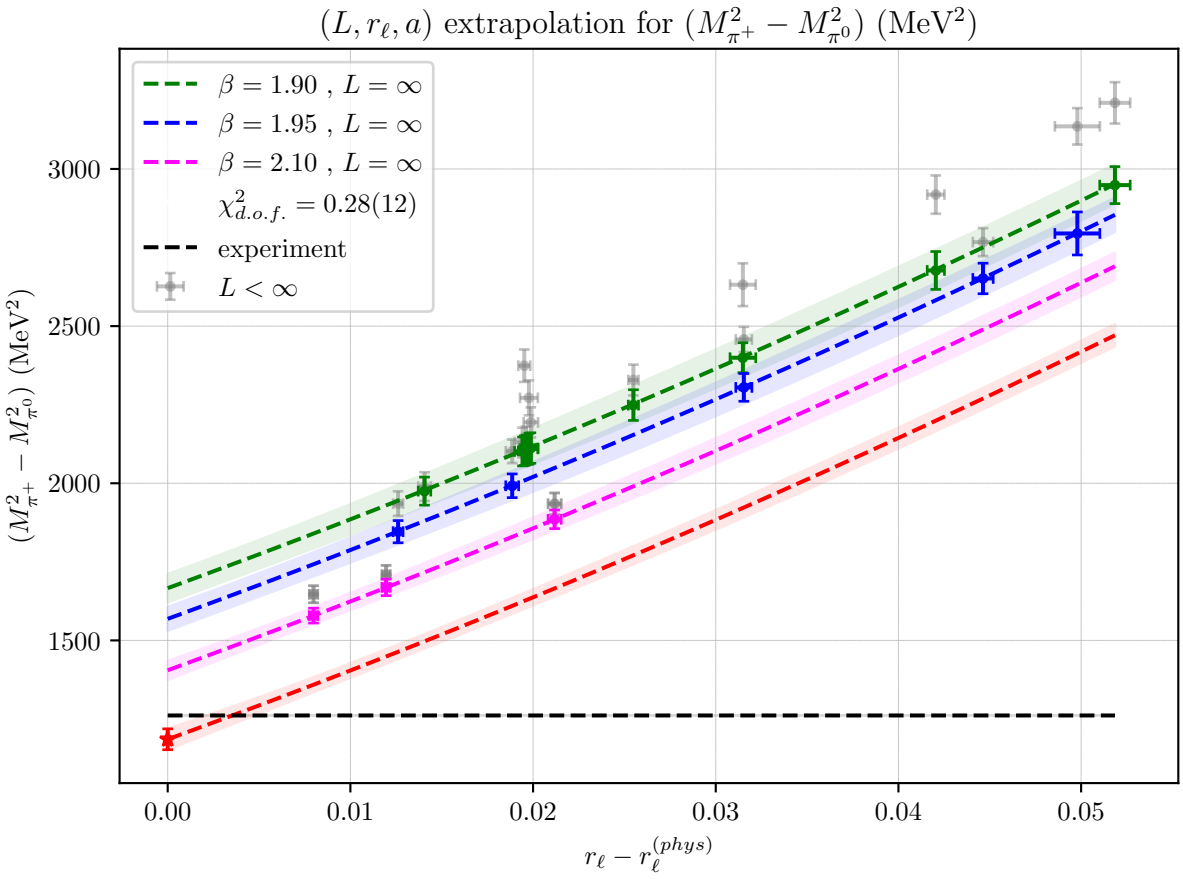


Figure 4.15: Extrapolation of $M^2_{\pi^+} - M^2_{\pi^0}$ over the ensembles. In grey are plotted the points at finite volume (already corrected from universal QED FVEs). The colored points and the corresponding theoretical curves are evaluated at $L \to \infty$. The red curve is the $L \to \infty$ and $a \to 0$ limit, with the final prediction at $r_\ell = r_\ell^{(\mathrm{phys})}$. The horizontal black line is the experimental value.

Our prediction is:

$$M^2_{\pi^+} - M^2_{\pi^0} = 1185(33)\,\mathrm{MeV}^2 \quad [1261.2(1)\,\mathrm{MeV}^2]_{\mathrm{exp}} \quad , \tag{4.20}$$

where the discrepancy with the experiments is also due to the missing handcuffs diagram.

## 4.7 Nucleons spectrum

### 4.7.1 $M_n$ and $M_p$

At this point we are able to find the neutron and proton masses in the full theory. The masses $M_n$ and $M_p$ are found adding respectively $\Delta M_n$ and $\Delta M_p$ of sec. (2.9) to the isosymmetric value $M_N$ for the nucleon mass. As for $M_N$ in isoQCD, we inspire our ansatz on ChPT, including structure dependent term $\sim \frac{1}{L^3}$ from $QED$

FVEs. The latter are a result of both the nucleons themselves as well the mass counterterms, which contain residual structure dependent FVEs from the tuning (see sec. (4.4)). We verified that at out level of precision we're not sensitive to $\sim 1/L^4$ terms or to the exponentially suppressed FVEs from QCD.

$$M_n(L, r_\ell, a) = A_n \left[ 1 + \alpha_{EM} \frac{c_3^{(n)}}{(\Lambda_{QCD} L)^3} + c_a^{(n)} (a\Lambda_{QCD})^2 + c_\ell^{(n)} r_\ell + c_{3/2}^{(n)} r_\ell^{3/2} \right] \tag{4.21}$$

$$M_p(L, r_\ell, a) = A_p \left[ 1 + \alpha_{EM} \frac{c_3^{(p)}}{(\Lambda_{QCD} L)^3} + c_a^{(p)} (a\Lambda_{QCD})^2 + c_\ell^{(p)} r_\ell + c_{3/2}^{(p)} r_\ell^{3/2} \right] \quad , \tag{4.22}$$

where the coefficients $A_{n/p}$, ..., are free parameters of the fit and $\Lambda_{QCD}$ is just an arbitrary scale fixed to 300 MeV. In fig. (4.16) and (4.17) we show the plots of the extrapolation for $M_n$ and $M_p$ respectively.

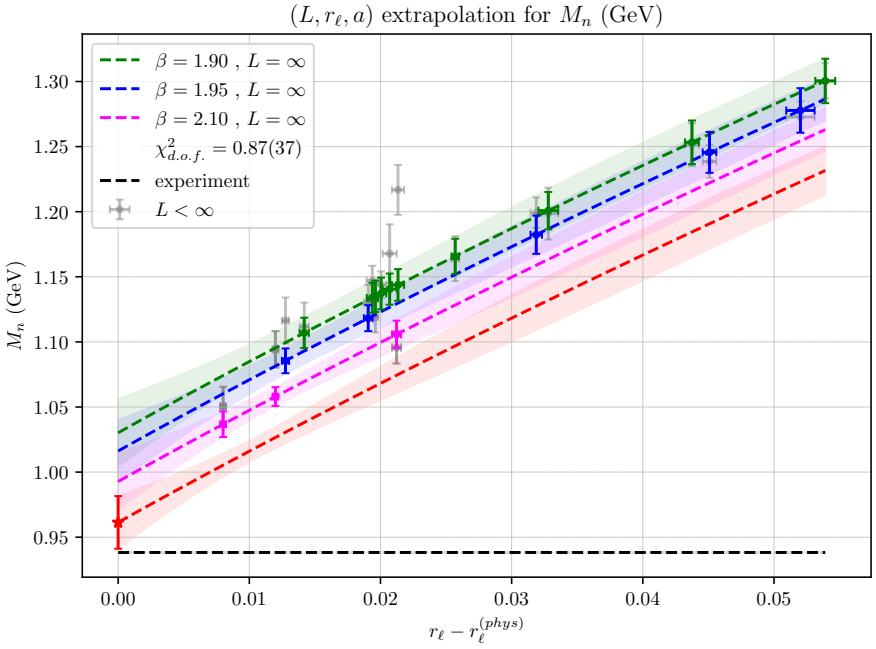


Figure 4.16: Extrapolation of $M_n$ in QCD+QED at LO. Grey points are the values at finite volume. The colored points and lines correspond to the limit $L \to \infty$. The red curve is the continuum and infinite volume limit. The final prediction at $r_\ell = r_\ell^{(\text{phys})}$ is marked on the left. The horizontal black line is the experimental value.

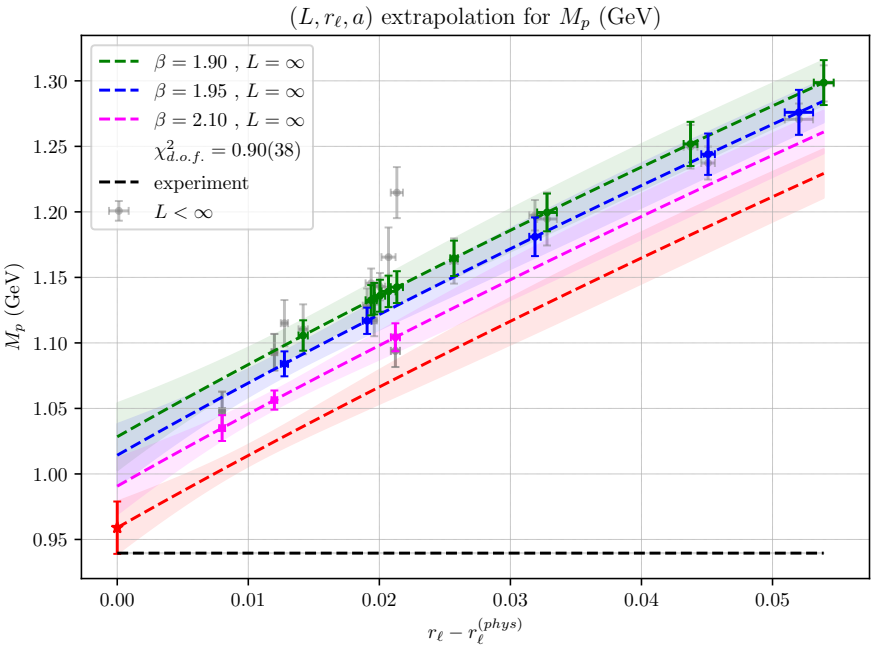


Figure 4.17: The same as fig. (4.16) but for $M_p$.

Our prediction are then:

$$M_n = 0.961(20)\,\text{GeV} \tag{4.23}$$
$$M_p = 0.959(20)\,\text{GeV} \tag{4.24}$$

which are compatible within $1.5\sigma$ with the experimental values:

$$M_n = 0.939565413(6)\,\text{GeV} \tag{4.25}$$
$$M_p = 0.9382720813(58)\,\text{GeV} \tag{4.26}$$

### 4.7.2 $M_n - M_p$

The neutron-proton mass difference is fitted according to a polynomial ansatz. The same functional form, with different coefficients, is used for the full quantity as well as its 2 contributions from strong IB and QED:

$$(M_n - M_p)(L, r_\ell, a) = A_{np}\left[1 + \alpha_{EM}\frac{c_3}{(\Lambda_{QCD}L)^3} + c_a(a\Lambda_{QCD})^2 + c_\ell r_\ell\right] \quad , \tag{4.27}$$

where the coefficients $A_{np}$, ..., are free parameters of the fit and $\Lambda_{QCD} = 300$ MeV is just an arbitrary scale. QCD FVEs and $1/L^4$ from QED are found to be negligible with respect to the term $\sim 1/L^3$. In fig. (4.18), (4.19) and (4.20) we show the plots of the extrapolation for $M_n - M_p$ and its 2 contributions coming from strong IB and QED.

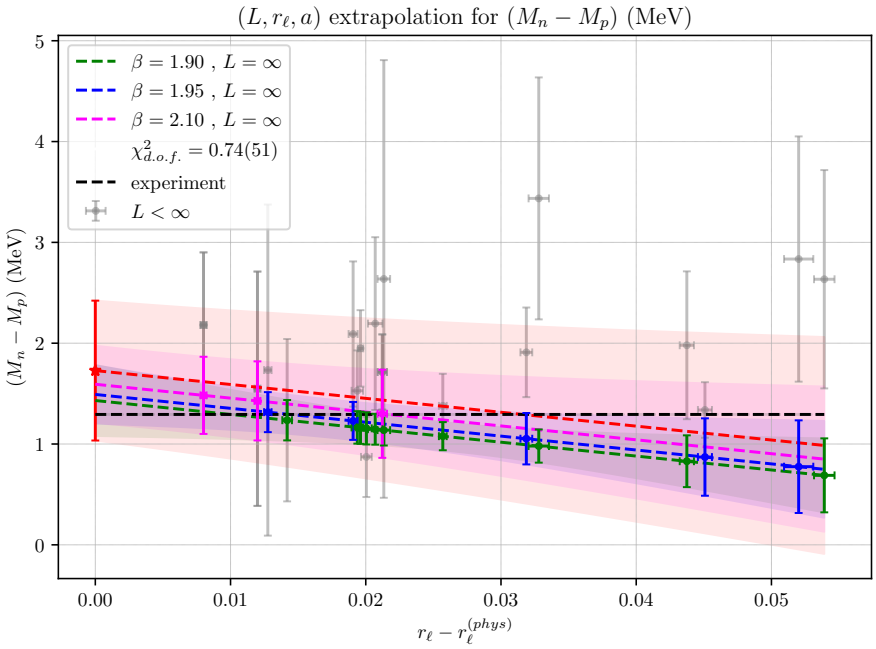


Figure 4.18: Extrapolation of $M_n - M_p$. Grey points are the values at finite volume. The colored points and lines correspond to the limit $L \to \infty$. The red curve is the continuum and infinite volume limit. The final prediction at $r_\ell = r_\ell^{(\text{phys})}$ is marked on the left. The horizontal black line is the experimental value.

Our prediction is:

$$M_n - M_p = 1.73(69)\,\text{MeV} \tag{4.28}$$

which is compatible within $1\sigma$ with the experiment:

$$M_n - M_p = 1.29333205(51)\text{MeV} \tag{4.29}$$

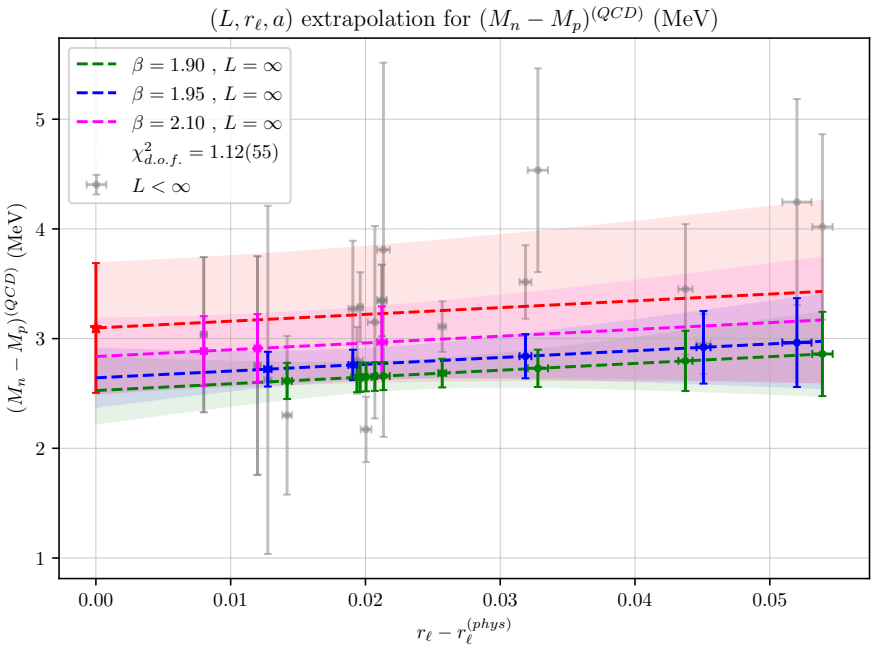


Figure 4.19: The same as fig. (4.18) but for $(M_n - M_p)^{(QCD)}$.

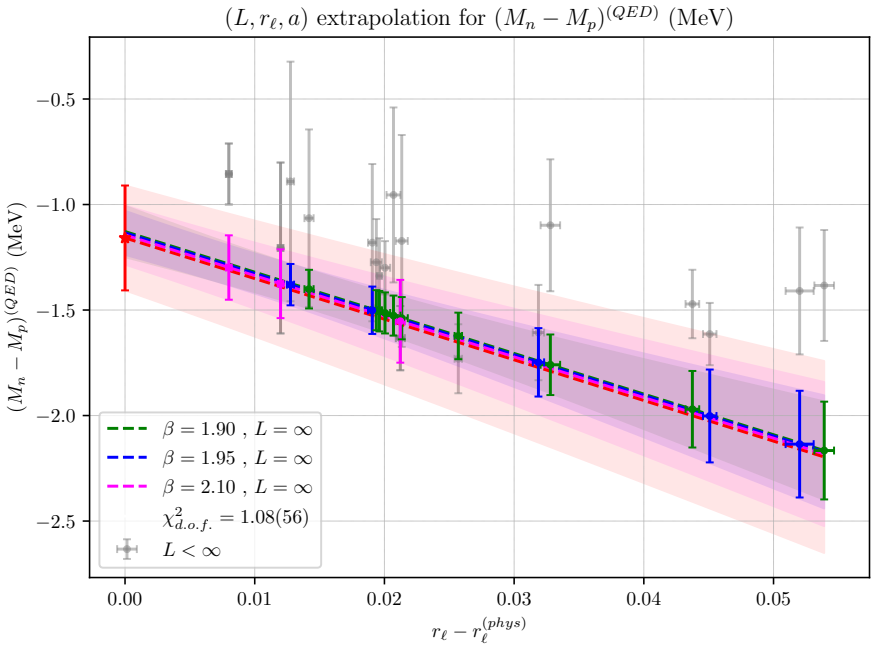


Figure 4.20: The same as fig. (4.19) but for $(M_n - M_p)^{(QED)}$.

The final extrapolation gives:

$$(M_n - M_p)^{(QCD)} = 3.10(59)\,\text{MeV} \tag{4.30}$$

$$(M_n - M_p)^{(QED)} = -1.16(25)\,\text{MeV} \tag{4.31}$$

The separation of these two effects is scheme dependent, and no experiment can discern between the two. Nevertheless we obtain what we expect, i.e. a positive

QCD contribution partially compensated by QED, consistently with our physical intuition. We also note that our prediction is $1\sigma$ compatible with the separation of [72].

## 4.8 Spectrum of the $\Delta$ resonances

### 4.8.1 IB effects on $M_\Delta$

The masses of the $\Delta$ resonances don't coincide because of Leading IBEs. As for the $(n,\, p)$ doublet, the $(\Delta^{++},\, \Delta^{-})$ and $(\Delta^{+},\, \Delta^{0})$ have masses differing in virtue of a combination strong IB and QED effects. The $\Delta^{++}$ tends to be lighter than $\Delta^{-}$ because $m_d > m_u$, but its electric charge is higher in modulus, leading to a bigger electromagnetic self-energy. With the $(\Delta^{+},\, \Delta^{0})$ is the same, with a stronger analogy with the $(n,\, p)$ doublet since they differ only for spin (and isospin). For this reason, the mass splitting among these particles can be studied with the same technique used for nucleons.
After the tuning of $\Delta m_u$ and $\Delta m_d$ (see sec. (4.4)), from the lattice spacings in QCD+QED (see sec. (4.5)) we can find, at fixed ensemble, the masses in the full theory: $M_{\Delta^{++}}$, $M_{\Delta^{+}}$, $M_{\Delta^{0}}$, $M_{\Delta^{-}}$ obtained from the variations of sec. (2.9). The latter have been extrapolated according to the equation:

$$M_{\Delta_i} = M_0^{(i)} \left[ 1 + + \alpha_{EM} \frac{\lambda_3^{(i)}}{(\Lambda_{QCD} L)^3} + c_2^{(i)}\, r_\ell + c_3^{(i)}\, r_\ell^{3/2} + c_a^{(i)}\, (\Lambda_{QCD} a)^2 \right] \qquad i = ++, +, 0, - \quad . \tag{4.32}$$

The inclusion of a $\sim \alpha_{EM}/L^3$ term take into account the residual $QED_L$ effects, dependent on the internal structure of the hadrons and coming from the counterterms (see sec. (4.4)). In principle also higher orders of $1/L$ are present, together with the exponentially suppressed terms from QCD FVEs, h however we found them to be negligible with respect to $O(1/L^3)$ in the fit. The terms $M_0$, $c_L^{(i)}$, $\lambda_3^{(i)}$, $c_2^{(i)}$, $c_3^{(i)}$ and $c_a^{(i)}$ are free parameters of the fit and $\Lambda_{QCD} = 300\,\mathrm{MeV}$ is just an arbitrary scale to make the coefficients dimensionless. In fig. (4.21), (4.22), (4.23), (4.24) are shown the extrapolations of the 4 masses among the ensembles, and in tab. (4.3) the extrapolated values.

| | $M$(GeV) |
|---|---|
| $\Delta^{-}$ | 1.251(40) |
| $\Delta^{0}$ | 1.247(39) |
| $\Delta^{+}$ | 1.245(39) |
| $\Delta^{++}$ | 1.244(39) |

Table 4.3: Values of the $\Delta(1232)$ masses obtained after the extrapolation over all the ensembles.

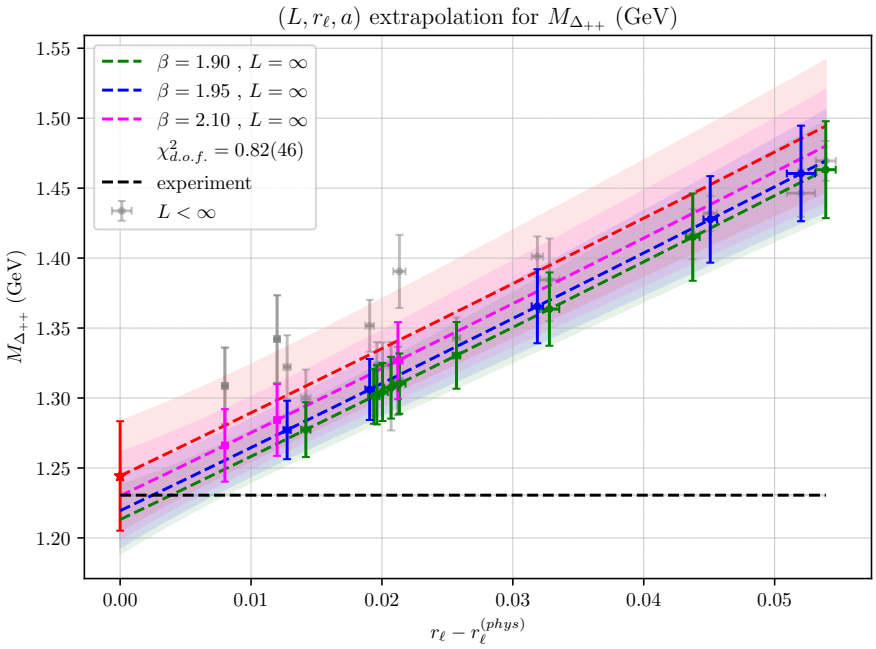


Figure 4.21: Extrapolation in QCD+QED of $M_{\Delta^{++}}$ according to eq. (4.32). Grey points are the data at finite volume, while colored dashed lines (with error bands) are the curves extrapolated to $L \to \infty$ and fixed lattice spacing. The red line is evaluated at infinite volume and continuum limit. The final extrapolation is marked on the left, and the horizontal black lines are the experimental values (when available) from [108] and [109].

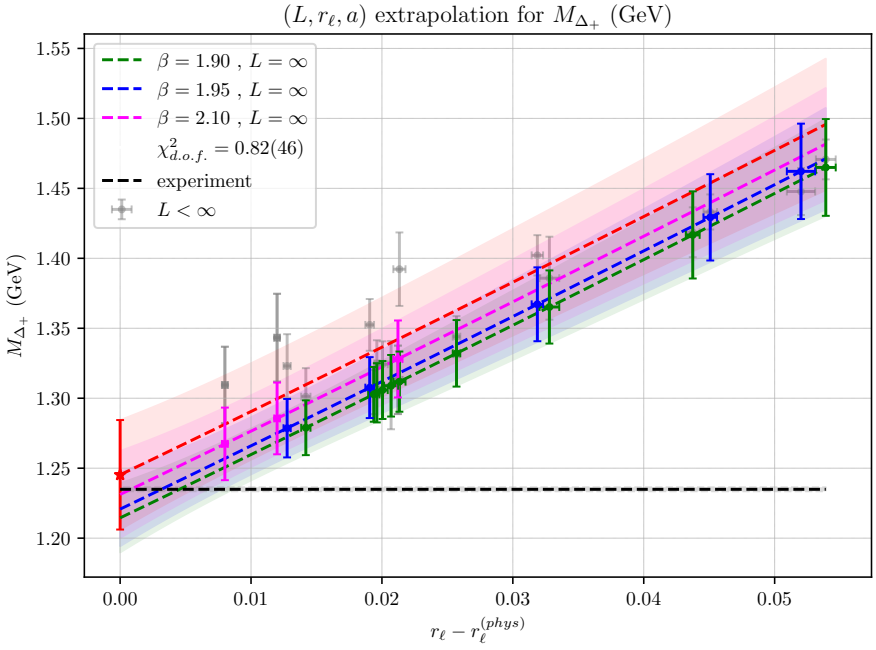


Figure 4.22: Same as fig. (4.21) but for the $\Delta_+$.

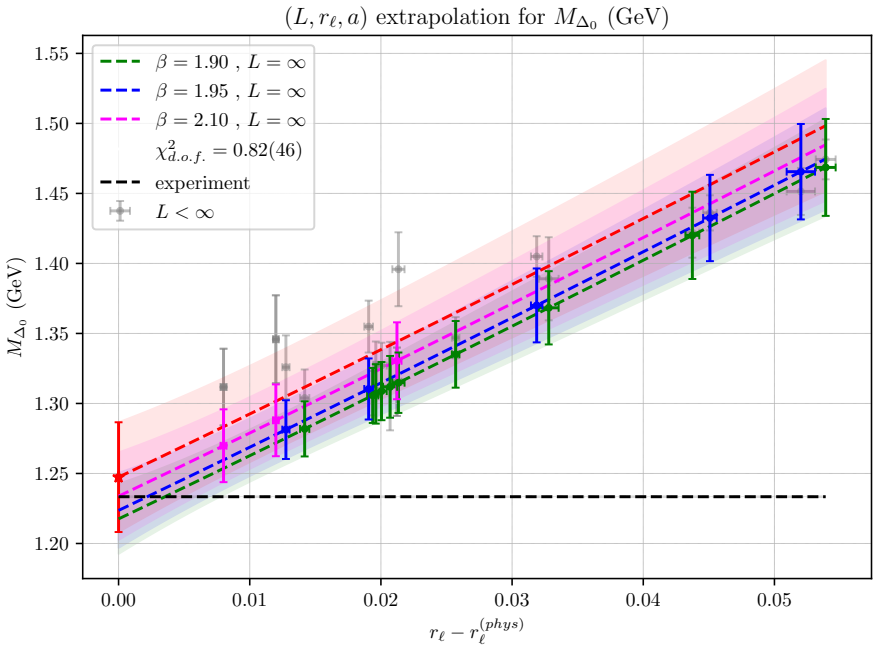


Figure 4.23: Same as fig. (4.21) but for the $\Delta_0$.

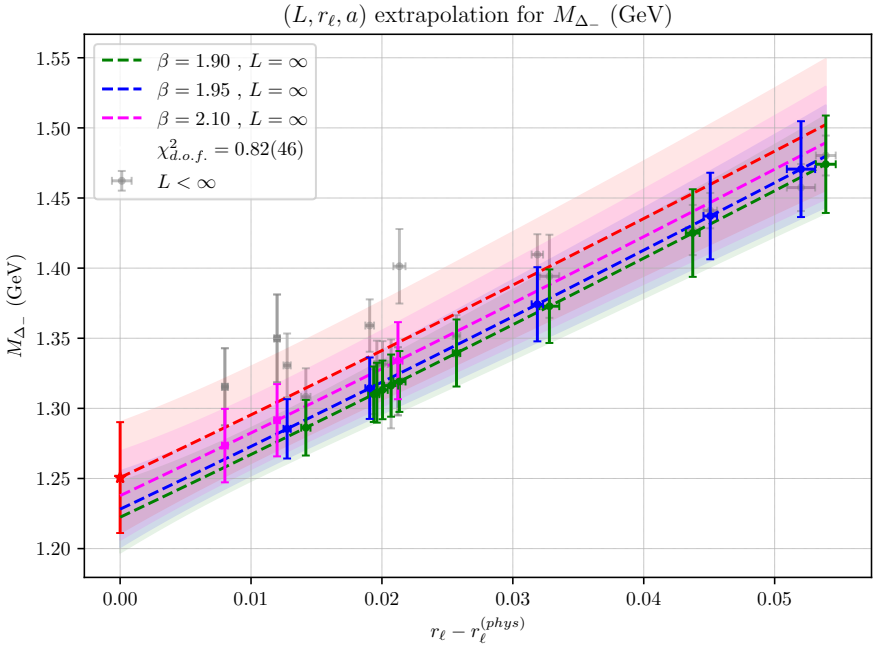


Figure 4.24: Same as fig. (4.21) but for the $\Delta_-$.

### 4.8.2 Combinations of Δ masses

The mass splittings are then easily obtained [2]. The extrapolation is done according to a simple polynomial ansatz:

[2] We've used the lattice spacings found in QCD+QED, but the isoQCD values are valid as well because we're at LO.

$$\Delta M = D_0 \left[ 1 + + \alpha_{EM} \frac{\lambda_3}{(\Lambda_{QCD} L)^3} + c_2\, r_\ell + c_a\, (\Lambda_{QCD} a)^2 \right] \quad . \tag{4.33}$$

The coefficients $D_0$, $\lambda_3$, $c_2$, $c_3$ and $c_a$ are free parameters of the fit, and $\Lambda_{QCD} = 300$ MeV is just an arbitrary scale. As for the masses, the QED structure-dependent effects are taken into account by the $\sim 1/L^3$ term. This is the FVE numerically leading with respect to the higher orders if $1/L$ and the exponentially suppressed terms from QCD.
Our predictions for the splittings are reported in the following table:

| | $\Delta M$(MeV) |
|---|---|
| $\Delta^{++} - \Delta^{+}$ | -0.48(26) |
| $\Delta^{++} - \Delta^{0}$ | -2.06(38) |
| $\Delta^{++} - \Delta^{-}$ | -4.76(55) |
| $\Delta^{+} - \Delta^{0}$ | -1.59(18) |
| $\Delta^{+} - \Delta^{-}$ | -4.41(50) |
| $\Delta^{-} - \Delta^{0}$ | 2.85(35) |
| $(\Delta^{++} + \Delta^{-}) - (\Delta^{+} + \Delta^{0})$ | 2.41(51) |

Table 4.4: Our results for the mass splittings among the 4 lightest Δ resonances. The splitting $(M_{++} + M_{-}) - (M_{+} + M_0)$ is the only combination that is purely electromagnetic, i.e. doesn't depend of physical mass counterterms at LO (see sec. (2.9)).

As we saw in sec. (4.8), at LO there are only 2 independent mass splittings. In fig. (4.25) and (4.26) are shown the plots for the extrapolations over all the ensembles of $[M_{++} - M_0]$ and the purely electromagnetic splitting $[(M_{++} + M_{-}) - (M_{+} + M_0)]$ (see sec. (2.9)).

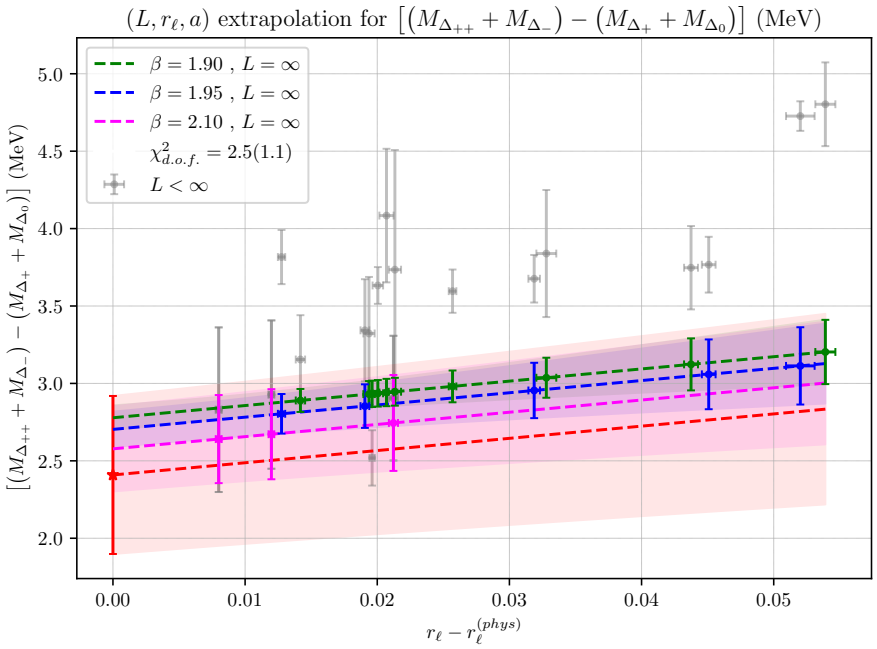


Figure 4.25: Extrapolation in QCD+QED of the mass splitting $[(M_{++} + M_-) - (M_+ + M_0)]$ according to eq. (4.33). Colored dashed lines (with error bands) are the curves extrapolated to $L \to \infty$ and fixed lattice spacing.

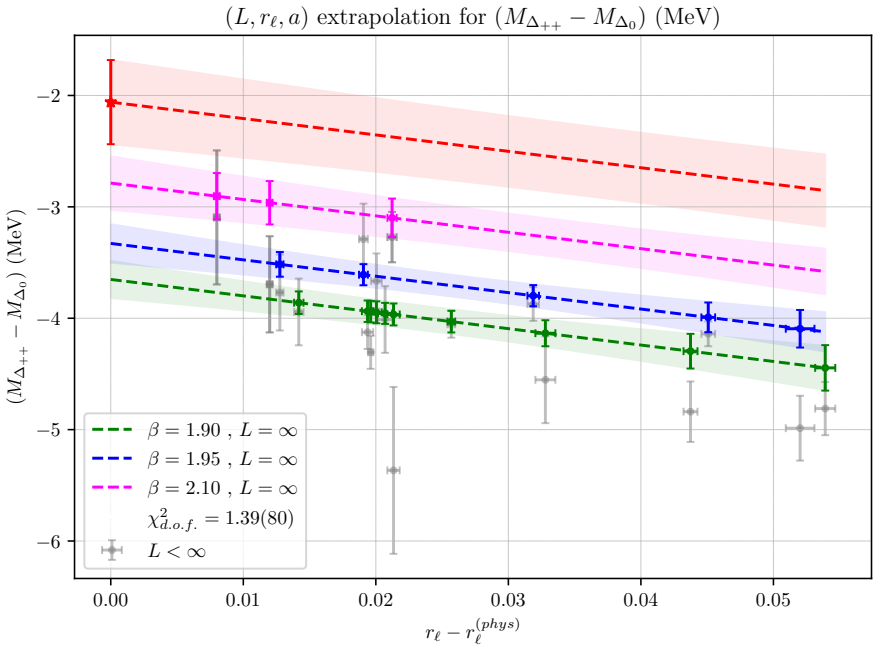


Figure 4.26: Same as fig. (4.25) but for $M_{++} - M_0$.

## 4.9 $\hat{m}_d - \hat{m}_u$

After the tuning of counterterms (see sec. (4.4)), we have the bare counterterms $a\Delta m_u$ and $a\Delta m_d$ for each ensemble. Using the RCs of [13] and adopting the pre-

scription described in sec. (2.6), from their difference we get the renormalized value $\Delta\hat{m}_{ud} = (\hat{m}_d - \hat{m}_u)/2$, which is fitted among the ensembles with a simple polynomial ansatz:

$$\Delta\hat{m}_{ud} = \frac{\hat{m}_d - \hat{m}_u}{2} = D_0 \left[ 1 + \alpha_{EM} \frac{\lambda_3}{(\Lambda_{QCD} L)^3} + c_2\, r_\ell + c_a\, (\Lambda_{QCD} a)^2 \right] \quad . \tag{4.34}$$

The coefficients $D_0$, $\lambda_3$, $c_2$ and $c_a$ are free parameters of the fit. The $\sim 1/L^3$ term accounts for the residual QED FVEs in the slopes used to tune the bare counterterms. This effect is dominant with respect to both the higher order terms of $O(1/L^4)$ and the exponentially suppressed terms from QCD, which are found to be numerically negligible. Our prediction for this quantity is:

$$\Delta\hat{m}_{ud}(\mu = 2\,\text{GeV}) = 1.208(43)\,\text{MeV} \quad , \tag{4.35}$$

where we have combined the results found with the $Z_P$ from methods M1 and M2 using eq. (28) of [13]. We note that the result is in agreement with [12]. The following figures show the extrapolation over the ensembles.

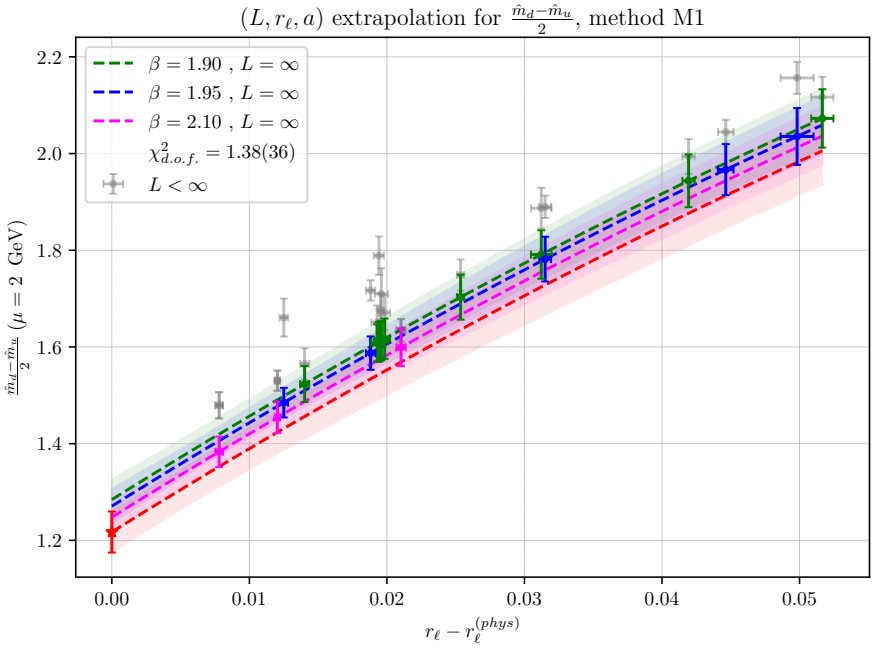


Figure 4.27: Extrapolation in QCD+QED of $(\hat{m}_d - \hat{m}_u)/2$ according to eq. (4.34) with $Z_P$ found with the method M1. Colored dashed lines (with error bands) are the curves extrapolated to $L \to \infty$ and fixed lattice spacing.

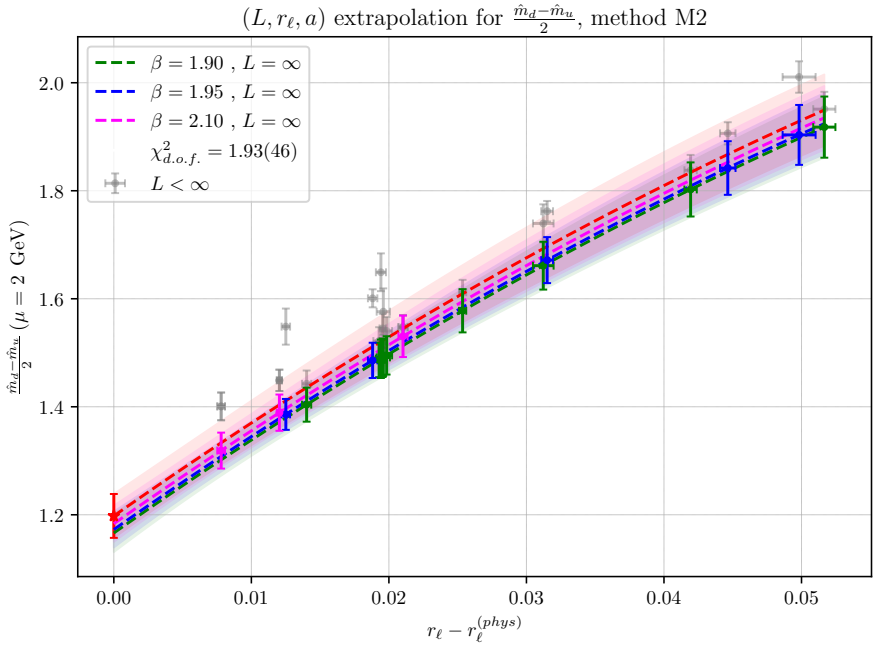


Figure 4.28: The same as fig. (4.27) but with the $Z_P$ found with the method M2.

# Conclusions

In this thesis I discussed the evaluation of Isospin Breaking effects in the hadronic spectrum. The calculation was carried out using the RM123 method [12] in the framework of Lattice QCD+QED, up to the Leading Order in the electromagnetic fine structure constant $\hat{\alpha}_{EM}$ and the mass difference between $u$ and $d$ quarks $\frac{\hat{m}_d - \hat{m}_u}{\Lambda_{QCD}}$. The quantities in the full theory are evaluated as the sum of their isosymmetric part (i.e. coming from QCD with isospin symmetry) plus the IB correction at 1st order. The main prediction of this thesis is the neutron-proton mass difference,

$$M_n - M_p = 1.73(69)\,\text{MeV} \quad , \tag{4.36}$$

together with the mass splittings of the $\Delta(1232)$ resonance quadrupet:

| | $\Delta M$(MeV) |
|---|---|
| $\Delta^{++} - \Delta^{+}$ | -0.48(26) |
| $\Delta^{++} - \Delta^{0}$ | -2.06(38) |
| $\Delta^{++} - \Delta^{-}$ | -4.76(55) |
| $\Delta^{+} - \Delta^{0}$ | -1.59(18) |
| $\Delta^{+} - \Delta^{-}$ | -4.41(50) |
| $\Delta^{-} - \Delta^{0}$ | 2.85(35) |
| $(\Delta^{++} + \Delta^{-}) - (\Delta^{+} + \Delta^{0})$ | 2.41(51) |

We also find the masses of nucleons and $\Delta$,

$$M_N = 0.9549(97)\,\text{GeV} \quad , \tag{4.37}$$

$$M_\Delta = 1.261(30)\,\text{GeV} \quad , \tag{4.38}$$

the sigma terms $\sigma_{\pi N}$ and $\sigma_{\pi\Delta}$,

$$\sigma_{\pi N} = 43.2(1.4)\,\text{MeV} \quad , \tag{4.39}$$

$$\sigma_{\pi\Delta} = 24.55(77)\,\text{MeV} \quad . \tag{4.40}$$

The simulation was performed using the tmLQCD regularization, adopting a mixed action approach and evaluating correlators over the $N_f = 2 + 1 + 1$ ETMC gauge configurations [13]. We extrapolate among 3 values of the lattice spacing and pion masses in the range $M_\pi \simeq 200 - 450$ MeV We implemented an hadronic renormalization scheme, setting the scale using the mass of the $\Omega$ baryon and reach the physical point in phase space using dimensionless hadronic ratios. The inclusion of IB was implemented considering the interactions with photons and including counterterms in the critical and physical masses. The former were tuned from the

PCAC Ward Identity in order to preserve the maximal twist at $O(\alpha_{EM})$, and the latter requiring to match the experimental values of 3 hadronic ratios.
We took the values of the quark masses renormalization constants in the $\overline{\text{MS}}$ scheme from [13], finding:

$$\hat{m}_\ell(\mu = 2\,\text{GeV}) = \frac{\hat{m}_u + \hat{m}_d}{2} = 3.781(76)\,\text{MeV} \tag{4.41}$$

$$\hat{m}_s(\mu = 2\,\text{GeV}) = 103.2(2.0)\,\text{MeV} \quad . \tag{4.42}$$

We also considered a separation between electromagnetic (QED) and strong IB (QCD) effects in order to provide physical intuition about the two contributions. We find:

$$(M_n - M_p)^{(QCD)} = 3.10(59)\,\text{MeV} \quad , \tag{4.43}$$

$$(M_n - M_p)^{(QED)} = -1.16(25)\,\text{MeV} \quad . \tag{4.44}$$

Moreover we evaluate the mass difference between the up and down quarks, finding:

$$\Delta\hat{m}_{ud}(\mu = 2\,\text{GeV}) = \frac{\hat{m}_d - \hat{m}_u}{2} = 1.208(43)\,\text{MeV} \tag{4.45}$$

Our predictions for the hadronic spectrum are find to be compatible within $1 - 1.5\sigma$ with the experiments. Nevertheless, we introduced some approximations in our analysis which leave space for improvements in the future:

- We neglected the interaction of sea quarks with the photon field, working in the electroquenched approximation. Here the quark loops never exchange a photon with other quarks and only a direct computation can estimate correctly the systematic error induced by neglecting the resulting diagrams. The extension of tmQCD+QED beyond this approximation has been formulated [110], with numerical simulations in progress.

- The same can be said for QCD disconnected diagrams, namely those in which source-to-source and sink-to-sink propagators appear. An example is the handcuffs diagram appearing in the mass difference $M_{\pi^+} - M_{\pi^0}$, recently included in [111]. Without the the handcuffs diagram we get $M^2_{\pi^+} - M^2_{\pi^0} = 1185(33)\,\text{MeV}^2\,[1261.2(1)\,\text{MeV}^2]_{\text{exp}}$ .

- Together with that, we also suffer from the uncertainty induced by the extrapolations to the physical point, needed because we simulated pion masses significantly larger than 140 MeV. Lattice calculations with quark masses at their physical point have already been done by our group [112] using the new ETMC gauge ensembles, and this is likely to be a source of improvement.

Apart from approximations, an increase in statistics and signal quality is desirable for sure. For instance, the quantum numbers of nucleonic interpolators require to have an earlier dominance of the ground state in the correlator, and the uncertainty in the quark propagator decreases with the number of stochastic sources used for the inversion of the Dirac Operator. The latter represent the two main factors which can be improved immediately dedicating an higher number of core hours to apply more smearing steps and use an higher number of stochastical sources.
In conclusion, this work has shown that we are able to include the LIBEs in the spectrum of baryons using the ETMC gauge configurations. Within the present level

of precision, this can be done in the approximations listed above, giving compatible results with the experiments. At this point, for the future we can consider working on the radiative corrections in neutron beta decay, as well as further investigate the spectrum of the whole baryonic octet and decupet.

# Appendix A

# Details of the simulation

The correlators generated by our simulation are calculated in the *partial-quenching* approximation. We use different masses for the sea and valence strange quark, while for the light they are kept equal.
The statistical uncertainty was propagated using the jackknife re-sampling technique with 15 jackknifes for each ensemble. In tab. (A.1) are reported the informations about the ensembles used in the the simulation.

| Ensemble | $\beta$ | $V/a^4$ | $am_{sea} = am_\ell$ | $am_\sigma$ | $am_\delta$ | $\kappa$ | $N_{cfg}$ |
|---|---|---|---|---|---|---|---|
| $A30.32$ | 1.90 | $32^3 \times 64$ | 0.0030 | 0.15 | 0.19 | 0.163272 | 150 |
| $A40.32$ | | | 0.0040 | | | 0.163270 | 150 |
| $A50.32$ | | | 0.0050 | | | 0.163267 | 150 |
| $A40.20$ | 1.90 | $20^3 \times 48$ | 0.0040 | 0.15 | 0.19 | 0.163270 | 150 |
| $A40.24$ | 1.90 | $24^3 \times 48$ | 0.0040 | 0.15 | 0.19 | 0.163270 | 150 |
| $A60.24$ | | | 0.0060 | | | 0.163265 | 150 |
| $A80.24$ | | | 0.0080 | | | 0.163255 | 150 |
| $A100.24$ | | | 0.0100 | | | 0.163260 | 150 |
| $A40.48$ | 1.90 | $48^3 \times 96$ | 0.0040 | 0.15 | 0.19 | 0.163270 | 90 |
| $A40.40$ | 1.90 | $40^3 \times 80$ | 0.0040 | 0.15 | 0.19 | 0.163270 | 150 |
| $B25.32$ | 1.95 | $32^3 \times 64$ | 0.0025 | 0.135 | 0.170 | 0.1612420 | 150 |
| $B35.32$ | | | 0.0035 | | | 0.1612400 | 150 |
| $B55.32$ | | | 0.0055 | | | 0.1612360 | 150 |
| $B75.32$ | | | 0.0075 | | | 0.1612320 | 75 |
| $B85.24$ | 1.95 | $24^3 \times 48$ | 0.0085 | 0.135 | 0.170 | 0.1612312 | 150 |
| $D15.48$ | 2.10 | $48^3 \times 96$ | 0.0015 | 0.12 | 0.1385 | 0.156361 | 90 |
| $D20.48$ | | | 0.0020 | | | 0.156357 | 90 |
| $D30.48$ | | | 0.0030 | | | 0.156355 | 90 |

Table A.1: Parameters of the ensembles used in this work. The space-time volume is reported in the format $L^3 \times T$. The bare values for $\beta$, sea and valence quark masses and hopping parameter $\kappa$ are reported. $am_\sigma$ and $am_\delta$ are the parameters which determine the renormalized strange and charm sea quark masses according to eq. (9) of [13]. In the rightmost column there are the number of analyzed gauge configurations.

Gaussian smearing was applied to our quark fields according to [67], with the pa-

rameter $\alpha_g$ optimized as in [101]. Some testing over the ensembles lead us to the choice of $n_g = 50$ steps on the source of our correlators, as an appropriate middle ground for a soon plateau and moderate noise in the signal.
In order to reduce the noise in our correlator, we used 16 stochastic sources [62] for the numerical inversion of the Dirac operator. This was compatible with our computational resources and gave us fine results, given which is also desirable in the future to try improving the analysis with and higher number of stochastic sources.

# Appendix B

# Sequential propagators

We now discuss the numerical issues involved in the calculation of correlator slopes in QCD+QED.
The interaction with photons leads to the insertion of EM currents on fermionic legs, accompained by the photon propagator $D_{\mu\nu}(y|z)$ summed over all the points of application. In a numerical computation on the lattice this produces terms in the correlator of the form:

$$\sum_{y,z} D_{\mu\nu}(y|z) \times (\dots) \quad , \tag{B.1}$$

where $(\dots)$ represent a generic product of Wick contractions with EM currents inserted at $y$ and $z$ somewhere.
The latter is numerically expensive, scaling as $N^2$ (total number of lattice points). In order to reduce the computational cost, we used *sequential propagators* as in [113]. These are modified versions of the quark propagators containing randomly generated fields. As discussed later in this section, the expectation value of appropriate products of them gives back the correlators with photon insertions.
The sequential propagators needed in the analysis are defined as:

$$S^{\Gamma^V A} = S(x|y) \left[\Gamma^V_\mu A_\mu(y)\right] S(y|0) \tag{B.2}$$

$$S^{\Gamma^V A \Gamma^V A} = S(x|y) \left[\Gamma^V_\mu A_\mu(y)\right] S^{\Gamma^V A}(y|0) \tag{B.3}$$

$$S^{\Gamma^T} = S(x|y) \left[\Gamma^T_\mu A_\mu(y) A_\mu(y)\right] S(y|0) \tag{B.4}$$

$$S^{P} = S(x|y)(i\gamma_5) S(y|0) \tag{B.5}$$

$$S^{S} = S(x|y) S(y|0) \quad , \tag{B.6}$$

with the repeated Lorentz ($\mu$) and spacetime ($y$, $z$) indices being summed over. The photon field $A_\mu$ is be generated with probability:

$$P(A)dA \propto \exp\left[-A_\mu(y_1) G^{-1}_{\mu\nu}(y_1, y_2) A_\nu(y_2)\right] \quad , \tag{B.7}$$

where $G_{\mu\nu}$ is the photon propagator:

$$G_{\mu\nu}(y_1, y_2) = \langle A_\mu(y_1) A_\nu(y_2)\rangle = \lim_{n\to\infty} \sum_{i=1}^{n} A^i_\mu(y_1) A^i_\nu(y_2) \quad . \tag{B.8}$$

Numerically, this is implemented in the following way. First we note that the p.d.f. of $A_\mu$ is local in momentum space [8]:

$$P(\widetilde{A})d\widetilde{A} \propto \exp\left[-\widetilde{A}_\mu(k) \widetilde{G}^{-1}_{\mu\nu}(k) \widetilde{A}_\nu(k)\right] \quad , \tag{B.9}$$

and through the change of variable $\tilde{A}_\mu(k) = \sqrt{\widetilde{G}_{\mu\nu}(k)}\tilde{B}_\nu(k)$ we see that $\widetilde{B}$ is distributed according to:

$$P(\widetilde{B})d\widetilde{B} \propto \exp\left[-\widetilde{B}^2_\mu(k)\right] \quad . \tag{B.10}$$

For the Wilson action in the Feynman gauge, the matrix $\sqrt{\widetilde{G}}$ is:

$$\sqrt{\tilde{G}_{\mu\nu}(k)} = \delta_{\mu\nu}\sqrt{\frac{1}{\hat{k}^2}} \tag{B.11}$$

Therefore we generate $\widetilde{B}_\mu$ according to the latter p.d.f., apply the change of variable with $\widetilde{A}_\mu$, and recover it in position space by the Fast Fourier Transform.
In mesonic and baryonic correlators they appear expressions of the type:

$$\sum_{y,z} D_{\mu\nu}(y|z)\, S_1(x|y)\Gamma^V_\mu S_1(y|0)\Gamma S_2(x|y)\Gamma^V_\nu S_2(y|0) \qquad \text{(photon exchange)} \tag{B.12}$$

$$\sum_{y,z} D_{\mu\nu}(y|z)\, S_1(x|y)\Gamma^V_\mu S_1(y|0)\Gamma S_2(x|y)\Gamma^V_\nu S_2(y|0) \qquad \text{(self energy)} \tag{B.13}$$

$$\sum_{y} D_{\mu\mu}(y|y)\, S_1(x|y)\Gamma^T{}_\mu(y) S_1(y|0)\Gamma S_2(x|0) \qquad \text{(tadpole insertion)} \tag{B.14}$$

$$\sum_{y,z} S_1(x|y)(i\gamma_5) S_1(y|0)\Gamma S_2(x|0) \qquad \text{(critical mass counterterm)} \tag{B.15}$$

$$\sum_{y} S_1(x|y) S_1(y|0)\Gamma S_2(x|0) \qquad \text{(physical mass counterterm)} \tag{B.16}$$

$$\ldots \tag{B.17}$$

where 1 and 2 are two generic flavors and $\Gamma$ is a product of $\gamma$ matrices. The expressions for $\Gamma^V_\mu$ and $\Gamma^T_\mu$ for our regularization can be found in sec. (C).
From the definition of the photon field given above as random variable, these expressions are approximated by the means of the following replacements:

$$S(x|y)\Gamma^V_\mu S(y|0) \quad \to \quad S^{\Gamma^V A^i} \tag{B.18}$$

$$S(x|y)\Gamma^V_\mu S(y|0)\Gamma S_2(x|y)\Gamma^V_\nu S_2(y|0) \quad \to \quad S^{\Gamma^V A^i \Gamma^V A^i} \tag{B.19}$$

$$S(x|y)\Gamma^T_\mu S(y|0) \quad \to \quad S^{\Gamma^T A^i A^i} \tag{B.20}$$

$$S(x|y)(i\gamma_5) S(y|0) \quad \to \quad S^P \tag{B.21}$$

$$S(x|y) S(y|0) \quad \to \quad S^S \tag{B.22}$$

and averaging over $i = 1, ..., n$ sources. In the treatment of LIBES this leads to the need for 6 inversions per gauge configuration. In this analysis we generated a different $A^i$ for each stochastic source of the quark propagator.
We remark that in the resulting products there are terms going as ($\mu$ and $\nu$ are not summed over here):

$$\langle S(x|y)\Gamma^V_\mu S(y|0)\Gamma S(x|z)\Gamma^V_\nu S(z|0) A_\mu(y) A_\nu(z)\rangle \quad \mu \neq \nu \tag{B.23}$$

which however vanish in the Feynman gauge.
Note also that in isoQCD we don't need 2 separate inversions for the choice of the Wilson parameter $r = \pm 1$. In fact in the twisted-mass regularization, the $d$-quark propagator ($r = -1$) is found from the $u$ ($r = +1$) by employing the $r$-$\gamma_5$ hermiticity:

$$S_r = \gamma_5 S^\dagger_{-r} \gamma_5 \quad . \tag{B.24}$$

The numerical inversions are done as in [12]. Let's consider e.g. the case of the product $S^{\Gamma^V A}\,\Gamma\,S^{\Gamma^V A}$. We solve numerically (for each $i$), the following equation for the components of the complex vector $\Psi$:

$$D(x|y)\Psi(y) = A_\mu(y)\Gamma^V_\mu S(y|0) \quad , \tag{B.25}$$

so that the estimator of the aforementioned product is:

$$\mathrm{Tr}\left[\Psi^T(x)\Gamma\Psi(x)\right] \quad . \tag{B.26}$$

# Appendix C

# Feynman diagrams of Wick contractions

Here are given the representations of Wick contractions in terms of Feynman diagrams. These serve as a reference for the explicit expressions found in the rest of the thesis. We use the notation of [12] and [113].
The fermionic propagator for a given flavor $f$ is:

$$\langle 0|\mathrm{T}\left\{\psi_f(x)\,\bar{\psi}_f(0)\right\}|0\rangle = \quad . \tag{C.1}$$

The corrections induced by scalar and pseudo-scalar currents are:

$$\int d^4y\ \langle 0|\mathrm{T}\left\{\psi_f(x)\ \left[\bar{\psi}_f(y)\psi_f(y)\right]\bar{\psi}_f(0)\right\}|0\rangle_{\text{conn.}} = \tag{C.2}$$

$$\int d^4y\ \langle 0|\mathrm{T}\left\{\psi_f(x)\ \left[\bar{\psi}_f(y)\psi_f(y)\right]\bar{\psi}_f(0)\right\}|0\rangle_{\text{disc.}} = \tag{C.3}$$

$$\int d^4y\ \langle 0|\mathrm{T}\left\{\psi_f(x)\ \left[i\bar{\psi}_f(y)\gamma_5\psi_f(y)\right]\ \bar{\psi}_f(0)\right\}|0\rangle_{\text{conn.}} = \tag{C.4}$$

$$\int d^4y\ \langle 0|\mathrm{T}\left\{\psi_f(x)\ \left[i\bar{\psi}_f(y)\gamma_5\psi_f(y)\right]\ \bar{\psi}_f(0)\right\}|0\rangle_{\text{disc.}} = \quad , \tag{C.5}$$

where the subscripts "conn." and "disc." denote if all the pieces of the diagram are connected to valence fermionic legs by other fermionic legs or photons.
With the same notation, the insertion of photon leads to the following diagrams:

$$\int d^4y\,d^4z\ \langle 0|\mathrm{T}\left\{\psi_f(x)\,J_\mu(y)J_\nu(z)\,\bar{\psi}_f(0)D_{\mu\nu}(y,z)\right\}|0\rangle_{\text{conn.}} = \tag{C.6}$$
$$q_f^2 \quad + q_f^2 \quad ,$$

$$\int d^4y\,d^4z\ \langle 0|\mathrm{T}\left\{\psi_f(x)\,J_\mu(y)J_\nu(z)\,\bar{\psi}_f(0)D_{\mu\nu}(y,z)\right\}|0\rangle_{\text{disc.}} = \tag{C.7}$$
$$q_f \sum_{f_1=\{u,d,s,c\}} q_{f_1} \quad + \sum_{f_1=\{u,d,s,c\}} q_{f_1}^2 \quad +$$
$$\sum_{(f_1,f_2)=\{u,d,s,c\}} q_{f_1}q_{f_2} \quad ,$$

where $J_\mu$ is the conserved EM current on the lattice:

$$\begin{aligned} J_\mu(y) &= \sum_f q_f \bar{\psi}_f(y) \Gamma^V_\mu \psi_f(y) \\ &= \frac{1}{2} \sum_f q_f \left[ \bar{\psi}_f(y) \left(\gamma_\mu - i\tau^3\gamma_5\right) U_\mu(y) \psi_f(y+a\hat{\mu}) + \bar{\psi}_f(y+a\hat{\mu}) \left(\gamma_\mu + i\tau^3\gamma_5\right) U^\dagger_\mu(y) \psi_f(y) \right] \quad . \end{aligned} \tag{C.8}$$

We also have the diagrams:

$$\int d^4y \, \langle 0|\mathrm{T}\left\{\psi_f(x)\, T_\mu(y)\, \bar{\psi}_f(0) D_{\mu\mu}(y,y)\right\}|0\rangle_{\text{conn.}} = \tag{C.9}$$

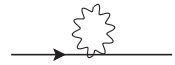

$$\int d^4y \, \langle 0|\mathrm{T}\left\{\psi_f(x)\, T_\mu(y)\, \bar{\psi}_f(0) D_{\mu\mu}(y,y)\right\}|0\rangle_{\text{disc.}} = \quad , \tag{C.10}$$

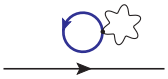

coming from the insertion of the tadpole operator $T_\mu$:

$$\begin{aligned} T_\mu(y) &= \sum_f q_f^2 \bar{\psi}_f(y) \Gamma^T_\mu \psi_f(y) \\ &= \frac{1}{2} \sum_f q_f^2 \left[ \bar{\psi}_f(y) \left(\gamma_\mu - i\tau^3\gamma_5\right) U_\mu(y) \psi_f(y+a\hat{\mu}) - \bar{\psi}_f(y+a\hat{\mu}) \left(\gamma_\mu + i\tau^3\gamma_5\right) U^\dagger_\mu(y) \psi_f(y) \right] \quad . \end{aligned} \tag{C.11}$$

The corrections to a correlator are given by:

$$\begin{aligned} \Delta C^J(t) &= \int d^3x\, d^4y\, d^4z \, \left\langle 0 \left| \mathrm{T}\left\{ O^\dagger(t,\vec{x}) J_\mu(y)\, J_\nu(z)\, O(0) D_{\mu\nu}(y,z) \right\} \right| 0 \right\rangle \quad , \\ \Delta C^T(t) &= \int d^3x\, d^4y \, \left\langle 0 \left| \mathrm{T}\left\{ O^\dagger(t,\vec{x}) T_\mu(y) O(0) D_{\mu\mu}(y,y) \right\} \right| 0 \right\rangle \quad , \\ \Delta C^{P_f}(t) &= \int d^3x\, d^4y \, \left\langle 0 \left| \mathrm{T}\left\{ O^\dagger(t,\vec{x}) \left[ i\bar{\psi}_f(y)\gamma_5\psi_f(y) \right] O(0) \right\} \right| 0 \right\rangle \quad , \\ \Delta C^{S_f}(t) &= -\int d^3x\, d^4y \, \left\langle 0 \left| T\left\{ O^\dagger(t,\vec{x}) \left[ \bar{\psi}_f(y)\psi_f(y) \right] O(0) \right\} \right| 0 \right\rangle \quad , \end{aligned} \tag{C.12}$$

where $J$ and $T$ correspond to the insertion of the electromagnetic currents and tadpole operator respectively. $S_f$ and $P_f$ correspond to the insertion of a pseudoscalar or scalar current of flavor $f$.

## C.1 Mesons from quark fields

We now write the explicit expression of mesonic correlators in terms of Wick contractions, finding their isoQCD limits and the slopes with respect to the IB parameters. The combination of the latter with the appropriate charge factors and counterterms gives the correlation functions at LO in QCD+QED.
In order to do that we compute the form of the correlator in QCD+QED without and with the insertions of the operators appearing in the LO expansion, setting $u = d$ in the end. For the details on the notation see sec. (C).
In the following it is understood that correlators will be put at rest projecting to $\vec{p} = \vec{0}$ by a Fourier transform with respect to $\vec{x}$.

### Correlators in QCD+QED

For pions we have [7]:

$$\begin{aligned} C_{\pi^+\pi^-}(x) &= -\langle[\bar{u}\gamma_5 d](x)\,[\bar{d}\gamma_5 u](0)\rangle \\ &= \mathrm{Tr}\left[\gamma_5 S_u(x|0)\gamma_5 S_d(0|x)\right] = \end{aligned} \quad , \tag{C.13}$$

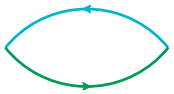

and

$$\begin{aligned} C_{\pi^0\pi^0}(x) &= -\frac{1}{2}\langle[\bar{u}\gamma_5 u - \bar{d}\gamma_5 d](x)[\bar{u}\gamma_5 u - \bar{d}\gamma_5 d](0)\rangle \\ &= \frac{1}{2}\{\mathrm{Tr}\left[\gamma_5 S_u(x|0)\gamma_5 S_u(0|x)\right] - \mathrm{Tr}\left[\gamma_5 S_u(x|x)\right]\mathrm{Tr}\left[\gamma_5 S_u(0|0)\right] \\ &+\mathrm{Tr}\left[\gamma_5 S_u(x|x)\right]\mathrm{Tr}\left[\gamma_5 S_d(0|0)\right]\} + (u \leftrightarrow d) \quad . \end{aligned} \tag{C.14}$$

In our approximation we neglect the "disconnected" contributions, i.e. those diagrams whose pieces are not connected by fermionic valence legs. Hence we have:

$$\begin{aligned} C_{\pi^0\pi^0}(x) &= \frac{1}{2}\mathrm{Tr}\left[\gamma_5 S_u(x|0)\gamma_5 S_u(0|x)\right] + \frac{1}{2}\mathrm{Tr}\left[\gamma_5 S_d(x|0)\gamma_5 S_d(0|x)\right] \\ &= \frac{1}{2}\left[ \quad + \quad \right] \end{aligned} \tag{C.15}$$

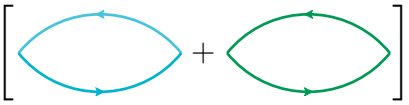

For the kaons we have:

$$\begin{aligned} C_{K^+K^-}(x) &= -\langle[\bar{s}\gamma_5 u](x)\,[\bar{u}\gamma_5 s](0)\rangle \\ &= \mathrm{Tr}\left[\gamma_5 S_s(x|0)\gamma_5 S_u(0|x)\right] = \end{aligned} \quad , \tag{C.16}$$

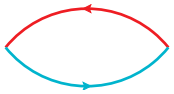

and

$$\begin{aligned} C_{K^0\bar{K}^0}(x) &= -\langle[\bar{s}\gamma_5 d](x)\,[\bar{d}\gamma_5 s](0)\rangle \\ &= \mathrm{Tr}\left[\gamma_5 S_s(x|0)\gamma_5 S_d(0|x)\right] = \end{aligned} \quad . \tag{C.17}$$

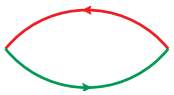

The isoQCD limits are obtained setting $u = d = \ell$:

$$C_{\pi^+\pi^-}(x) = C_{\pi^0\pi^0}(x) = \tag{C.18}$$

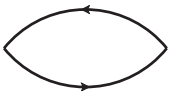

$$C_{K^+K^-}(x) = C_{K^0\bar{K}^0}(x) = \tag{C.19}$$

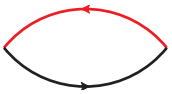

### Slopes from IB

The connected corrections induced by IB are found inserting the corresponding currents on the fermionic legs. For convenience we jump directly to the form of the isosymmetric slopes, so the equations below are understood in that limit.

$$\Delta C^{J^{(u)}_\mu J^{(u)}_\nu}_{\pi^+\pi^-}(x) = \sum_{y,z} D_{\mu\nu}(y,z)\mathrm{Tr}\left[\gamma_5 S_\ell(x|y)\Gamma^V_\mu S_\ell(y|z)\Gamma^V_\nu S_\ell(z|0)\gamma_5 S_\ell(0|x)\right] = \tag{C.20}$$

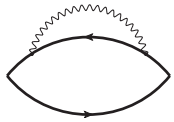

$$\Delta C^{J^{(d)}_\mu J^{(d)}_\nu}_{\pi^+\pi^-}(x) = \sum_{y,z} D_{\mu\nu}(y,z)\mathrm{Tr}\left[\gamma_5 S_\ell(x|0)\gamma_5 S_\ell(0|y)\Gamma^V_\mu S_\ell(y|z)\Gamma^V_\nu S_\ell(z|x)\right] = \tag{C.21}$$

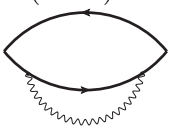

$$\Delta C^{J^{(u)}_\mu J^{(d)}_\nu}_{\pi^+\pi^-}(x) = \sum_{y,z} D_{\mu\nu}(y,z)\mathrm{Tr}\left[\gamma_5 S_\ell(x|y)\Gamma^V_\mu S_\ell(y|0)\gamma_5 S_\ell(0|y)\Gamma^V_\nu S_\ell(y|x)\right] = \tag{C.22}$$

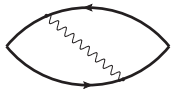

$$\Delta C^{T^{(u)}}_{\pi^+\pi^-}(x) = \sum_{y} D_{\mu\mu}(y|y)\mathrm{Tr}\left[\gamma_5 S_\ell(x|y)T^{(\ell)}_\mu(y)S_\ell(y|0)\gamma_5 S_\ell(0|x)\right] = \tag{C.23}$$

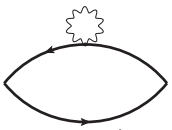

$$\Delta C^{T^{(d)}}_{\pi^+\pi^-}(x) = \sum_{y} D_{\mu\mu}(y|y)\mathrm{Tr}\left[\gamma_5 S_\ell(x|y)\gamma_5 S_\ell(0|y)T^{(\ell)}_\mu(y)S_\ell(y|x)\right] = \tag{C.24}$$

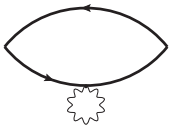

$$\Delta C^{J^{(u)}_P}_{\pi^+\pi^-}(x) = \sum_{y} \mathrm{Tr}\left[\gamma_5 S_\ell(x|y)(i\gamma_5)S_\ell(y|0)\gamma_5 S_\ell(0|x)\right] = \tag{C.25}$$

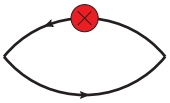

$$\Delta C^{J^{(d)}_P}_{\pi^+\pi^-}(x) = \sum_{y} \mathrm{Tr}\left[\gamma_5 S_\ell(x|0)\gamma_5 S_\ell(0|y)(i\gamma_5)S_\ell(y|x)\right] = \tag{C.26}$$

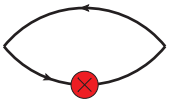

$$\Delta C^{J^{(u)}_S}_{\pi^+\pi^-}(x) = \sum_{y} \mathrm{Tr}\left[\gamma_5 S_\ell(x|y)S_\ell(y|0)\gamma_5 S_\ell(0|x)\right] = \tag{C.27}$$

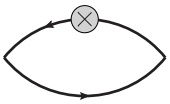

$$\Delta C^{J^{(d)}_S}_{\pi^+\pi^-}(x) = \sum_{y} \mathrm{Tr}\left[\gamma_5 S_\ell(x|0)\gamma_5 S_\ell(0|y)S_\ell(y|x)\right] = \tag{C.28}$$

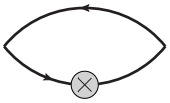

For the $\pi^0$ these slopes are the same, divided by a factor 2.
Kaons follow the same pattern:

$$\Delta C^{J^{(s)}_\mu J^{(s)}_\nu}_{K^+K^-}(x) = \sum_{y,z} D_{\mu\nu}(y,z)\mathrm{Tr}\left[\gamma_5 S_s(x|y)\Gamma^V_\mu S_s(y|z)\Gamma^V_\nu S_s(z|0)\gamma_5 S_\ell(0|x)\right] = \tag{C.29}$$

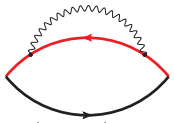

$$\Delta C^{J^{(s)}_\mu J^{(u)}_\nu}_{K^+K^-}(x) = \sum_{y,z} D_{\mu\nu}(y,z)\mathrm{Tr}\left[\gamma_5 S_s(x|0)\gamma_5 S_\ell(0|y)\Gamma^V_\mu S_\ell(y|z)\Gamma^V_\nu S_\ell(z|x)\right] = \tag{C.30}$$

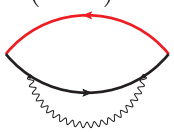

$$\Delta C^{J^{(s)}_\mu J^{(u)}_\nu}_{K^+K^-}(x) = \sum_{y,z} D_{\mu\nu}(y,z)\mathrm{Tr}\left[\gamma_5 S_s(x|y)\Gamma^V_\mu S_s(y|0)\gamma_5 S_\ell(0|y)\Gamma^V_\nu S_\ell(y|x)\right] = \quad \text{(C.31)}$$

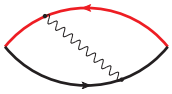

$$\Delta C^{T^{(s)}}_{K^+K^-}(x) = \sum_{y} D_{\mu\mu}(y|y)\mathrm{Tr}\left[\gamma_5 S_s(x|y)T^{(s)}_\mu(y)S_s(y|0)\gamma_5 S_\ell(0|x)\right] = \quad \text{(C.32)}$$

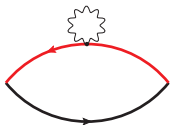

$$\Delta C^{T^{(u)}}_{K^+K^-}(x) = \sum_{y} D_{\mu\mu}(y|y)\mathrm{Tr}\left[\gamma_5 S_s(x|y)\gamma_5 S_\ell(0|y)T^{(\ell)}_\mu(y)S_\ell(y|x)\right] = \quad \text{(C.33)}$$

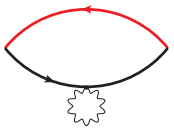

$$\Delta C^{J^{(s)}_P}_{K^+K^-}(x) = \sum_{y} \mathrm{Tr}\left[\gamma_5 S_s(x|y)(i\gamma_5)S_s(y|0)\gamma_5 S_\ell(0|x)\right] = \quad \text{(C.34)}$$

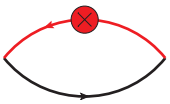

$$\Delta C^{J^{(u)}_P}_{K^+K^-}(x) = \sum_{y} \mathrm{Tr}\left[\gamma_5 S_s(x|0)\gamma_5 S_\ell(0|y)(i\gamma_5)S_\ell(y|x)\right] = \quad \text{(C.35)}$$

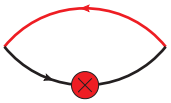

$$\Delta C^{J^{(s)}_S}_{K^+K^-}(x) = \sum_{y} \mathrm{Tr}\left[\gamma_5 S_s(x|y)S_s(y|0)\gamma_5 S_\ell(0|x)\right] = \quad \text{(C.36)}$$

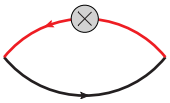

$$\Delta C^{J^{(u)}_S}_{K^+K^-}(x) = \sum_{y} \mathrm{Tr}\left[\gamma_5 S_s(x|0)\gamma_5 S_\ell(0|y)S_\ell(y|x)\right] = \quad \text{(C.37)}$$

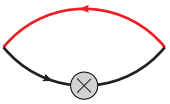

For the $K^0$ they are the same (obtained replacing $u$ with $d$).
The above relations can be found from explicit Wick contractions. However their structure arise as a consequence of the properties of the quark propagator, which in the full theory satisfies:

$$\frac{\partial S(x|y)}{\partial\lambda} = -\sum_{z_1,z_2} S(x|z_1)\frac{\partial D(z_1|z_2)}{\partial\lambda}S(z_2|y) \quad , \quad \text{(C.38)}$$

for any parameter $\lambda$. This means that for a term $\lambda\bar{\psi}\Gamma\psi$ in the Lagrangian we have:

$$\frac{\partial S(x|y)}{\partial\lambda} = -\sum_{z} S(x|z)\Gamma S(z|y) \quad , \quad \text{(C.39)}$$

with $\Gamma$ being an arbitrary product of $\gamma$ matrices.
In sec. (2) we saw that in the electroquenched approximation, the variation of an observable is encoded in its derivative with respect to counterterms and $e^2$. Any hadronic correlator is a product quark propagators $S$, so by derivation we find that the insertion of a current leads to a sum of diagrams with the insertion in all possible legs with that flavor. In the case of photon insertions, this is easily seen deriving twice with respect to $e$ according to eq. (2.24).

## C.2 Baryons from quark fields

The baryons involved in the analysis are the $\Omega^-$, the nucleons $p$ and $n$, and the $\Delta(1232)$ resonances $\Delta^{++}$, $\Delta^+$, $\Delta^0$, $\Delta^-$. We recall here the interpolating fields used for them:

$$O_\mu^{(\Omega^-)} = \epsilon_{abc}\left[s_a^T C\gamma_\nu s_b\right] P_{\mu\nu}^{3/2}\, P_+\, s_c \quad , \tag{C.40}$$

$$O^{(p)} = \epsilon_{abc}\left[u_a^T C\gamma_5 d_b\right] P_+ u_c \quad , \tag{C.41}$$

$$O^{(n)} = \epsilon_{abc}\left[d_a^T C\gamma_5 u_b\right] P_+ d_c \quad , \tag{C.42}$$

(C.43)

$$O_\mu^{(\Delta^{++})} = \epsilon_{abc}\left[u_a^T C\gamma_\mu u_b\right] P_{\mu\nu}^{3/2}\, P_+\, u_c \quad , \tag{C.44}$$

$$\begin{aligned} O_\mu^{(\Delta^+)} = \epsilon_{abc}\frac{1}{\sqrt{3}}\{ & \left[d_a^T C\gamma_\mu u_b\right] P_{\mu\nu}^{3/2}\, P_+\, u_c \\ & + \left[u_a^T C\gamma_\mu d_b\right] P_{\mu\nu}^{3/2}\, P_+\, u_c \\ & + \left[u_a^T C\gamma_\mu u_b\right] P_{\mu\nu}^{3/2}\, P_+\, d_c \,\} \quad , \end{aligned} \tag{C.45}$$

$$\begin{aligned} O_\mu^{(\Delta^0)} = \epsilon_{abc}\frac{1}{\sqrt{3}}\{ & \left[u_a^T C\gamma_\mu d_b\right] P_{\mu\nu}^{3/2}\, P_+\, d_c \\ & + \left[d_a^T C\gamma_\mu u_b\right] P_{\mu\nu}^{3/2}\, P_+\, d_c \\ & + \left[d_a^T C\gamma_\mu d_b\right] P_{\mu\nu}^{3/2}\, P_+\, u_c \,\} \quad , \end{aligned} \tag{C.46}$$

$$O_\mu^{(\Delta^-)} = \epsilon_{abc}\left[d_a^T C\gamma_\mu d_b\right] P_{\mu\nu}^{3/2}\, P_+\, d_c \quad , \tag{C.47}$$

where $P_+ = \frac{1+\gamma_4}{2}$ and $P_{\mu\nu}^{3/2}$ in the spin projector (see sec. (1.3.1)).
Their correlators in terms of Wick contractions are given below. In the analysis the type of baryon considered is always specified and we never mix different baryonic correlators. Therefore there's no ambiguity in using the same diagrammatic expression for spin 1/2 and 3/2 (which is implied from the context) and distinguishing them only by flavor.

$$\begin{aligned} C_{\Omega^-\bar{\Omega}^-} = & -2\epsilon_{a_1b_1c_1}\epsilon_{a_2b_2c_2}\mathrm{Tr}[S_s^{T\,a_1\,a_2}(x|0)C\gamma_i S_s^{\ b_1\,b_2}(x|0)C\gamma_j]\,\mathrm{Tr}[P_+ P_{ij}^{3/2} S_s^{\ c_1\,c_2}(x|0)] \\ & + 4\epsilon_{a_1b_1c_1}\epsilon_{a_2b_2c_2}\mathrm{Tr}[S_s^{\ a_1\,b_2}(x|0)P_+ P_{ij}^{3/2} S_s^{\ b_1\,a_2}(x|0)C\gamma_i S_s^{T\,c_1\,c_2}(x|0)C\gamma_j] \\ & = -2\Big[ \quad - 2 \quad \Big] \quad , \end{aligned} \tag{C.48}$$

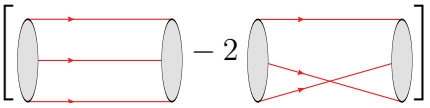

with the isoQCD limit having the same form, but with $s$ not corrected by QED effects.

$$\begin{aligned} C_{p\bar{p}} = & +\epsilon_{a_1b_1c_1}\epsilon_{a_2b_2c_2}\mathrm{Tr}[S_u^{T\,a_1\,a_2}(x|0)C\gamma_5 S_u^{\ b_1\,b_2}(x|0)C\gamma_5]\,\mathrm{Tr}[P_+ S_d^{\ c_1\,c_2}(x|0)] \\ & -\epsilon_{a_1b_1c_1}\epsilon_{a_2b_2c_2}\mathrm{Tr}[S_u^{\ a_1\,b_2}(x|0)P_+ S_u^{\ b_1\,a_2}(x|0)C\gamma_5 S_d^{T\,c_1\,c_2}(x|0)C\gamma_5] \\ & \Big[ \quad - \quad \Big] \quad , \end{aligned} \tag{C.49}$$

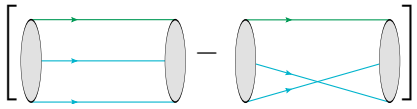

and

$$C_{n\bar{n}} = + \epsilon_{a_1b_1c_1}\epsilon_{a_2b_2c_2}\mathrm{Tr}[S_d^{T\,a_1\,a_2}(x|0)C\gamma_5 S_d{}^{b_1\,b_2}(x|0)C\gamma_5]\,\mathrm{Tr}[P_+ S_u{}^{c_1\,c_2}(x|0)] - \epsilon_{a_1b_1c_1}\epsilon_{a_2b_2c_2}\mathrm{Tr}[S_d{}^{a_1\,b_2}(x|0)P_+ S_d{}^{b_1\,a_2}(x|0)C\gamma_5 S_u^{T\,c_1\,c_2}(x|0)C\gamma_5]$$

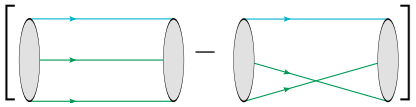

, (C.50)

which coincide when $u = d$:

$$C_{N\bar{N}} = + \epsilon_{a_1b_1c_1}\epsilon_{a_2b_2c_2}\mathrm{Tr}[S_\ell^{T\,a_1\,a_2}(x|0)C\gamma_5 S_\ell{}^{b_1\,b_2}(x|0)C\gamma_5]\,\mathrm{Tr}[P_+ S_\ell{}^{c_1\,c_2}(x|0)] - \epsilon_{a_1b_1c_1}\epsilon_{a_2b_2c_2}\mathrm{Tr}[S_\ell{}^{a_1\,b_2}(x|0)P_+ S_\ell{}^{b_1\,a_2}(x|0)C\gamma_5 S_\ell^{T\,c_1\,c_2}(x|0)C\gamma_5]$$

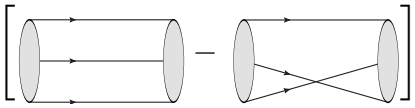

. (C.51)

The $\Delta$ correlators are:

$$C_{\Delta^{++}\bar{\Delta}^{++}} = - 2\epsilon_{a_1b_1c_1}\epsilon_{a_2b_2c_2}\mathrm{Tr}[S_u^{T\,a_1\,a_2}(x|0)C\gamma_i S_u{}^{b_1\,b_2}(x|0)C\gamma_j]\,\mathrm{Tr}[P_+ P_{ij}^{3/2} S_u{}^{c_1\,c_2}(x|0)] + 4\epsilon_{a_1b_1c_1}\epsilon_{a_2b_2c_2}\mathrm{Tr}[S_u{}^{a_1\,b_2}(x|0)P_+ P_{ij}^{3/2} S_u{}^{b_1\,a_2}(x|0)C\gamma_i S_u^{T\,c_1\,c_2}(x|0)C\gamma_j]$$

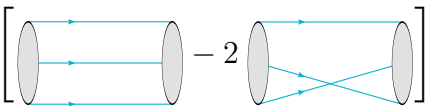

, (C.52)

$$\begin{aligned} C_{\Delta^+\bar{\Delta}^+} = & -\frac{2}{3}\epsilon_{a_1b_1c_1}\epsilon_{a_2b_2c_2}\{ \\ & + \mathrm{Tr}[S_d^{T\,a_1\,a_2}(x|0)C\gamma_5 S_d{}^{b_1\,b_2}(x|0)C\gamma_5]\,\mathrm{Tr}[P_+ P_{ij}^{3/2} S_u{}^{c_1\,c_2}(x|0)] \\ & + \mathrm{Tr}[S_d^{T\,a_1\,a_2}(x|0)C\gamma_5 S_u{}^{b_1\,b_2}(x|0)C\gamma_5]\,\mathrm{Tr}[P_+ P_{ij}^{3/2} S_d{}^{c_1\,c_2}(x|0)] \\ & + \mathrm{Tr}[S_u^{T\,a_1\,a_2}(x|0)C\gamma_5 S_d{}^{b_1\,b_2}(x|0)C\gamma_5]\,\mathrm{Tr}[P_+ P_{ij}^{3/2} S_d{}^{c_1\,c_2}(x|0)] \\ & - 2\,\mathrm{Tr}[S_d{}^{a_1\,b_2}(x|0)P_+ P_{ij}^{3/2} S_d{}^{b_1\,a_2}(x|0)C\gamma_5 S_u^{T\,c_1\,c_2}(x|0)C\gamma_5] \\ & - 2\,\mathrm{Tr}[S_d{}^{a_1\,b_2}(x|0)P_+ P_{ij}^{3/2} S_u{}^{b_1\,a_2}(x|0)C\gamma_5 S_d^{T\,c_1\,c_2}(x|0)C\gamma_5] \\ & - 2\,\mathrm{Tr}[S_d{}^{a_1\,b_2}(x|0)P_+ P_{ij}^{3/2} S_u{}^{b_1\,a_2}(x|0)C\gamma_5 S_d^{T\,c_1\,c_2}(x|0)C\gamma_5]\ \} \end{aligned} \tag{C.53}$$

$$= -\frac{2}{3}\Bigg[ + \quad + \quad + \quad - 2 \quad - 2 \quad - 2 \quad \Bigg]$$

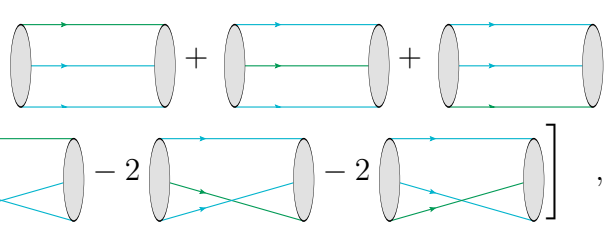

,

$$
\begin{aligned}
C_{\Delta^0\bar{\Delta}^0} = &-\frac{2}{3}\epsilon_{a_1b_1c_1}\epsilon_{a_2b_2c_2}\,\{ \\
&+\mathrm{Tr}[S_u^{T\,a_1\,a_2}(x|0)C\gamma_5 S_u{}^{b_1\,b_2}(x|0)C\gamma_5]\,\mathrm{Tr}[P_+P_{ij}^{3/2}S_d{}^{c_1\,c_2}(x|0)] \\
&+\mathrm{Tr}[S_u^{T\,a_1\,a_2}(x|0)C\gamma_5 S_d{}^{b_1\,b_2}(x|0)C\gamma_5]\,\mathrm{Tr}[P_+P_{ij}^{3/2}S_u{}^{c_1\,c_2}(x|0)] \\
&+\mathrm{Tr}[S_d^{T\,a_1\,a_2}(x|0)C\gamma_5 S_u{}^{b_1\,b_2}(x|0)C\gamma_5]\,\mathrm{Tr}[P_+P_{ij}^{3/2}S_u{}^{c_1\,c_2}(x|0)] \\
&-2\,\mathrm{Tr}[S_u{}^{a_1\,b_2}(x|0)P_+P_{ij}^{3/2}S_u{}^{b_1\,a_2}(x|0)C\gamma_5 S_d^{T\,c_1\,c_2}(x|0)C\gamma_5] \\
&-2\,\mathrm{Tr}[S_u{}^{a_1\,b_2}(x|0)P_+P_{ij}^{3/2}S_d{}^{b_1\,a_2}(x|0)C\gamma_5 S_u^{T\,c_1\,c_2}(x|0)C\gamma_5] \\
&-2\,\mathrm{Tr}[S_u{}^{a_1\,b_2}(x|0)P_+P_{ij}^{3/2}S_d{}^{b_1\,a_2}(x|0)C\gamma_5 S_u^{T\,c_1\,c_2}(x|0)C\gamma_5]\,\}
\end{aligned}
\tag{C.54}
$$

$$
= -\frac{2}{3}\Bigg[ +
$$

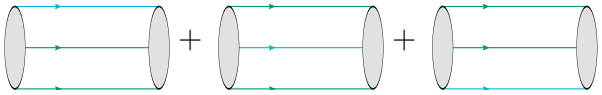

$$
+
$$



$$
+
$$



$$
-2
$$

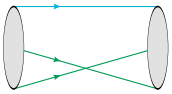

$$
-2
$$

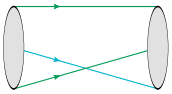

$$
-2
$$

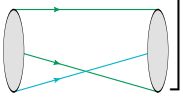

$$
\Bigg] \quad ,
$$

and

$$
\begin{aligned}
C_{\Delta^-\bar{\Delta}^-} = &-2\epsilon_{a_1b_1c_1}\epsilon_{a_2b_2c_2}\mathrm{Tr}[S_d^{T\,a_1\,a_2}(x|0)C\gamma_i S_d{}^{b_1\,b_2}(x|0)C\gamma_j]\,\mathrm{Tr}[P_+P_{ij}^{3/2}S_d{}^{c_1\,c_2}(x|0)] \\
&+4\epsilon_{a_1b_1c_1}\epsilon_{a_2b_2c_2}\mathrm{Tr}[S_d{}^{a_1\,b_2}(x|0)P_+P_{ij}^{3/2}S_d{}^{b_1\,a_2}(x|0)C\gamma_i S_d^{T\,c_1\,c_2}(x|0)C\gamma_j] \\
= &-2\Bigg[
\end{aligned}
$$

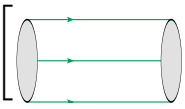

$$
-2
$$

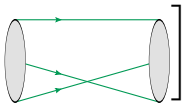

$$
\Bigg] \quad ,
\tag{C.55}
$$

which share the same isoQCD limit:

$$
\begin{aligned}
C_{\Delta\bar{\Delta}} = &-2\epsilon_{a_1b_1c_1}\epsilon_{a_2b_2c_2}\mathrm{Tr}[S_\ell^{T\,a_1\,a_2}(x|0)C\gamma_i S_\ell{}^{b_1\,b_2}(x|0)C\gamma_j]\,\mathrm{Tr}[P_+P_{ij}^{3/2}S_\ell{}^{c_1\,c_2}(x|0)] \\
&+4\epsilon_{a_1b_1c_1}\epsilon_{a_2b_2c_2}\mathrm{Tr}[S_\ell{}^{a_1\,b_2}(x|0)P_+P_{ij}^{3/2}S_\ell{}^{b_1\,a_2}(x|0)C\gamma_i S_\ell^{T\,c_1\,c_2}(x|0)C\gamma_j] \\
= &-2\Bigg[
\end{aligned}
$$

$$
-2
$$

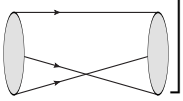

$$
\Bigg] \quad .
\tag{C.56}
$$

The slopes are build via explicit Wick contractions or as for the meson case, inserting the currents consistently with eq. (C.39). Baryonic correlation functions of flavors $f_1$, $f_2$, $f_3$ have the form:

$$
C_{B\bar{B}} \sim S_{f_1}\,S_{f_2}\,S_{f_3} \quad , \tag{C.57}
$$

and the slope with respect to a parameter $\lambda$ goes as:

$$
\frac{\partial C_{B\bar{B}}}{\partial\lambda} \sim \frac{\partial}{\partial\lambda}\left(S_{f_1}\,S_{f_2}\,S_{f_3}\right) = \frac{\partial S_{f_1}}{\partial\lambda}\,S_{f_2}\,S_{f_3} + S_{f_1}\,\frac{\partial S_{f_2}}{\partial\lambda}\,S_{f_3} + S_{f_1}\,S_{f_2}\frac{\partial S_{f_3}}{\partial\lambda} \quad . \tag{C.58}
$$

For the $\Omega^-$ we have:

$$
\begin{aligned}
\Delta C^{J_P^{(s)}}_{\Omega^-\bar{\Omega}^-}(x) = \epsilon_{a_1b_1c_1}\epsilon_{a_2b_2c_2}\sum_y \{ \\
&- 2\mathrm{Tr}[S_s^{T\,a_1\,a_2}(x|0)C\gamma_i S_s{}^{b_1\,b_2}(x|0)C\gamma_j]\,\mathrm{Tr}[P_+P_{ij}^{3/2}S_s{}^{c_1\,c'}(x|y)(i\gamma_5)S_s{}^{c'\,c_2}(y|0)] \\
&- 2\mathrm{Tr}[S_s^{T\,a_1\,a_2}(x|0)C\gamma_i S_s{}^{b_1\,b'}(x|y)(i\gamma_5)S_s{}^{b'\,b_2}(y|0)C\gamma_j]\,\mathrm{Tr}[P_+P_{ij}^{3/2}S_s{}^{c_1\,c_2}(x|0)] \\
&- 2\mathrm{Tr}[S_s^{T\,a_1\,a'}(x|y)(i\gamma_5)^T S_s^{T\,a'\,a_2}(y|0)C\gamma_i S_s{}^{b_1\,b_2}(x|0)C\gamma_j]\,\mathrm{Tr}[P_+P_{ij}^{3/2}S_s{}^{c_1\,c_2}(x|0)] \\
&+ 4\mathrm{Tr}[S_s{}^{a_1\,b'}(x|0)P_+P_{ij}^{3/2}S_s{}^{b_1\,a_2}(x|0)C\gamma_i S_s^{T\,c_1\,c'}(x|y)(i\gamma_5)^T S_s^{T\,c'\,c_2}(y|0)C\gamma_j] \\
&+ 4\mathrm{Tr}[S_s{}^{a_1\,b_2}(x|0)P_+P_{ij}^{3/2}S_s{}^{b_1\,a'}(x|y)(i\gamma_5)S_s{}^{a'\,a_2}(y|0)C\gamma_i S_s^{T\,c_1\,c_2}(x|0)C\gamma_j] \\
&+ 4\mathrm{Tr}[S_s{}^{a_1\,b'}(x|y)(i\gamma_5)S_s{}^{b'\,b_2}(y|0)P_+P_{ij}^{3/2}S_s{}^{b_1\,a_2}(x|0)C\gamma_i S_s^{T\,c_1\,c_2}(x|0)C\gamma_j] \}\,.
\end{aligned}
\tag{C.59}
$$

$= -2\Big[$ 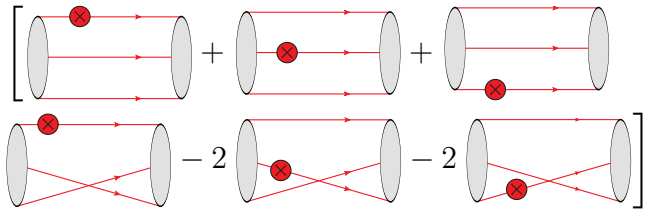 $\Big]$ ,

$$
\begin{aligned}
\Delta C^{J_S^{(s)}}_{\Omega^-\bar{\Omega}^-}(x) = \epsilon_{a_1b_1c_1}\epsilon_{a_2b_2c_2}\sum_y \{ \\
&- 2\mathrm{Tr}[S_s^{T\,a_1\,a_2}(x|0)C\gamma_i S_s{}^{b_1\,b_2}(x|0)C\gamma_j]\,\mathrm{Tr}[P_+P_{ij}^{3/2}S_s{}^{c_1\,c'}(x|y)S_s{}^{c'\,c_2}(y|0)] \\
&- 2\mathrm{Tr}[S_s^{T\,a_1\,a_2}(x|0)C\gamma_i S_s{}^{b_1\,b'}(x|y)S_s{}^{b'\,b_2}(y|0)C\gamma_j]\,\mathrm{Tr}[P_+P_{ij}^{3/2}S_s{}^{c_1\,c_2}(x|0)] \\
&- 2\mathrm{Tr}[S_s^{T\,a_1\,a'}(x|y)S_s^{T\,a'\,a_2}(y|0)C\gamma_i S_s{}^{b_1\,b_2}(x|0)C\gamma_j]\,\mathrm{Tr}[P_+P_{ij}^{3/2}S_s{}^{c_1\,c_2}(x|0)] \\
&+ 4\mathrm{Tr}[S_s{}^{a_1\,b'}(x|0)P_+P_{ij}^{3/2}S_s{}^{b_1\,a_2}(x|0)C\gamma_i S_s^{T\,c_1\,c'}(x|y)S_s^{T\,c'\,c_2}(y|0)C\gamma_j] \\
&+ 4\mathrm{Tr}[S_s{}^{a_1\,b_2}(x|0)P_+P_{ij}^{3/2}S_s{}^{b_1\,a'}(x|y)S_s{}^{a'\,a_2}(y|0)C\gamma_i S_s^{T\,c_1\,c_2}(x|0)C\gamma_j] \\
&+ 4\mathrm{Tr}[S_s{}^{a_1\,b'}(x|y)S_s{}^{b'\,b_2}(y|0)P_+P_{ij}^{3/2}S_s{}^{b_1\,a_2}(x|0)C\gamma_i S_s^{T\,c_1\,c_2}(x|0)C\gamma_j] \}\,.
\end{aligned}
\tag{C.60}
$$

$= -2\Big[$ 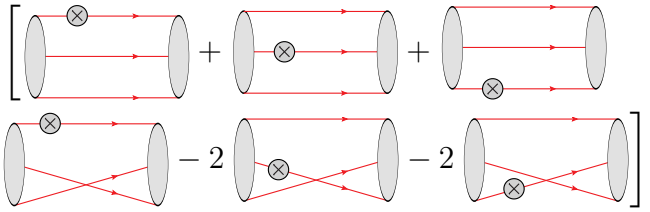 $\Big]$ ,

and

$$\Delta C^{T_\mu^{(s)}}_{\Omega^-\bar\Omega^-}(x) = \epsilon_{a_1b_1c_1}\epsilon_{a_2b_2c_2}\sum_y \{$$

$$\begin{aligned}
&- 2\mathrm{Tr}[S_s^{T\,a_1\,a_2}(x|0)C\gamma_i S_s^{\,b_1\,b_2}(x|0)C\gamma_j]\,\mathrm{Tr}[P_+P_{ij}^{3/2}S_s^{\,c_1\,c'}(x|y)(\Gamma_\mu^T)^T S_s^{\,c'\,c_2}(y|0)]\\
&- 2\mathrm{Tr}[S_s^{T\,a_1\,a_2}(x|0)C\gamma_i S_s^{\,b_1\,b'}(x|y)\Gamma_\mu^T S_s^{\,b'\,b_2}(y|0)C\gamma_j]\,\mathrm{Tr}[P_+P_{ij}^{3/2}S_s^{\,c_1\,c_2}(x|0)]\\
&- 2\mathrm{Tr}[S_s^{T\,a_1\,a'}(x|y)\Gamma_\mu^T S_s^{T\,a'\,a_2}(y|0)C\gamma_i S_s^{\,b_1\,b_2}(x|0)C\gamma_j]\,\mathrm{Tr}[P_+P_{ij}^{3/2}S_s^{\,c_1\,c_2}(x|0)]\\
&+ 4\mathrm{Tr}[S_s^{\,a_1\,b'}(x|0)P_+P_{ij}^{3/2}S_s^{\,b_1\,a_2}(x|0)C\gamma_i S_s^{T\,c_1\,c'}(x|y)\Gamma_\mu^T S_s^{T\,c'\,c_2}(y|0)C\gamma_j]\\
&+ 4\mathrm{Tr}[S_s^{\,a_1\,b_2}(x|0)P_+P_{ij}^{3/2}S_s^{\,b_1\,a'}(x|y)\Gamma_\mu^T S_s^{\,a'\,a_2}(y|0)C\gamma_i S_s^{T\,c_1\,c_2}(x|0)C\gamma_j]\\
&+ 4\mathrm{Tr}[S_s^{\,a_1\,b'}(x|y)(\Gamma_\mu^T)^T S_s^{\,b'\,b_2}(y|0)P_+P_{ij}^{3/2}S_s^{\,b_1\,a_2}(x|0)C\gamma_i S_s^{T\,c_1\,c_2}(x|0)C\gamma_j]\,\}\,.
\end{aligned}$$

$$= -2\Big[ \quad + \quad + \quad$$

$$-2 \quad - 2 \quad - 2 \quad \Big] \quad , \tag{C.61}$$

$$\Delta C^{J_\mu^{(s)}J_\nu^{(s)}}_{\Omega^-\bar\Omega^-}(x) = \epsilon_{a_1b_1c_1}\epsilon_{a_2b_2c_2}\sum_{y,z} D_{\mu\nu}(y|z)\,\{$$

$$\begin{aligned}
&- 2\mathrm{Tr}[S_s^{T\,a_1\,a_2}(x|0)C\gamma_i S_s^{\,b_1\,b_2}(x|0)C\gamma_j]\,\mathrm{Tr}[P_+P_{ij}^{3/2}S_s^{\,c_1\,c'}(x|y)\Gamma_\mu^V S_s^{c',c''}(y|z)\Gamma_\nu^V S_s^{\,c''\,c_2}(z|0)]\\
&- 2\mathrm{Tr}[S_s^{T\,a_1\,a_2}(x|0)C\gamma_i S_s^{\,b_1\,b'}(x|y)\Gamma_\mu^V S_s^{b',b''}(y|z)\Gamma_\nu^V S_s^{\,b''\,b_2}(z|0)C\gamma_j]\,\mathrm{Tr}[P_+P_{ij}^{3/2}S_s^{\,c_1\,c_2}(x|0)]\\
&- 2\mathrm{Tr}[S_s^{T\,a_1\,a'}(x|y)(\Gamma_\mu^V)^T S_s^{a',a''}(y|z)(\Gamma_\nu^V)^T S_s^{T\,a''\,a_2}(z|0)C\gamma_i S_s^{\,b_1\,b_2}(x|0)C\gamma_j]\,\mathrm{Tr}[P_+P_{ij}^{3/2}S_s^{\,c_1\,c_2}(x|0)]\\
&+ 4\mathrm{Tr}[S_s^{\,a_1\,b'}(x|0)P_+P_{ij}^{3/2}S_s^{\,b_1\,a_2}(x|0)C\gamma_i S_s^{T\,c_1\,c'}(x|y)(\Gamma_\mu^V)^T S_s^{T\,c',c''}(y|z)(\Gamma_\nu^V)^T S_s^{T\,c''\,c_2}(z|0)C\gamma_j]\\
&+ 4\mathrm{Tr}[S_s^{\,a_1\,b_2}(x|0)P_+P_{ij}^{3/2}S_s^{\,b_1\,a'}(x|y)\Gamma_\mu^V S_s^{a',a''}(y|z)\Gamma_\nu^V S_s^{\,a''\,a_2}(z|0)C\gamma_i S_s^{T\,c_1\,c_2}(x|0)C\gamma_j]\\
&+ 4\mathrm{Tr}[S_s^{\,a_1\,b'}(x|y)\Gamma_\mu^V S_s^{\,b',b''}(y|z)\Gamma_\nu^V S_s^{\,b''\,b_2}(z|0)P_+P_{ij}^{3/2}S_s^{\,b_1\,a_2}(x|0)C\gamma_i S_s^{T\,c_1\,c_2}(x|0)C\gamma_j]\,\}\,.
\end{aligned}$$

$$= -2\Big[ \quad + \quad + \quad + \quad + \quad + \quad$$

$$- 2 \quad - 2 \quad - 2 \quad - 2 \quad -2 \quad - 2 \quad \Big] \,. \tag{C.62}$$

For the proton:

$$
\begin{aligned}
\Delta C^{J_P^{(u)}}_{p\bar{p}}(x) &= \epsilon_{a_1b_1c_1}\epsilon_{a_2b_2c_2}\sum_y \{ \\
&- 2\mathrm{Tr}[S_\ell^{T\,a_1\,a_2}(x|0)C\gamma_i S_\ell^{b_1\,b'}(x|y)(i\gamma_5)S_\ell^{b'\,b_2}(y|0)C\gamma_j]\,\mathrm{Tr}[P_+ S_\ell^{c_1\,c_2}(x|0)] \\
&- 2\mathrm{Tr}[S_\ell^{T\,a_1\,a'}(x|y)(i\gamma_5)S_\ell^{T\,a'\,a_2}(y|0)C\gamma_i S_\ell^{b_1\,b_2}(x|0)C\gamma_j]\,\mathrm{Tr}[P_+ S_\ell^{c_1\,c_2}(x|0)] \\
&+ 4\mathrm{Tr}[S_\ell^{a_1\,b_2}(x|0)P_+ S_\ell^{b_1\,a'}(x|y)(i\gamma_5)S_\ell^{a'\,a_2}(y|0)C\gamma_i S_\ell^{T\,c_1\,c_2}(x|0)C\gamma_j] \\
&+ 4\mathrm{Tr}[S_\ell^{a_1\,b'}(x|y)(i\gamma_5)S_\ell^{b'\,b_2}(y|0)P_+ S_\ell^{b_1\,a_2}(x|0)C\gamma_i S_\ell^{T\,c_1\,c_2}(x|0)C\gamma_j]\,\}\,.
\end{aligned}
\tag{C.63}
$$

$= -2\Big[$ 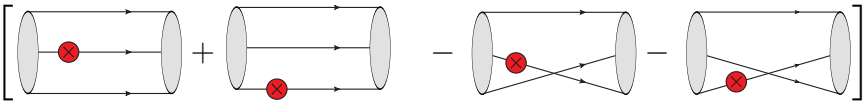 $\Big]$ ,

$$
\begin{aligned}
\Delta C^{J_P^{(d)}}_{p\bar{p}}(x) &= \epsilon_{a_1b_1c_1}\epsilon_{a_2b_2c_2}\sum_y \{ \\
&- 2\mathrm{Tr}[S_\ell^{T\,a_1\,a_2}(x|0)C\gamma_i S_\ell^{b_1\,b_2}(x|0)C\gamma_j]\,\mathrm{Tr}[P_+ S_\ell^{c_1\,c'}(x|y)(i\gamma_5)S_\ell^{c'\,c_2}(y|0)] \\
&+ 4\mathrm{Tr}[S_\ell^{a_1\,b'}(x|0)P_+ S_\ell^{b_1\,a_2}(x|0)C\gamma_i S_\ell^{T\,c_1\,c'}(x|y)(i\gamma_5)S_\ell^{T\,c'\,c_2}(y|0)C\gamma_j]\,\}\,.
\end{aligned}
\tag{C.64}
$$

$= -2\Big[$ 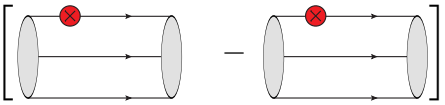 $\Big]$ ,

and for the neutron they are the same but for the replacement $u \leftrightarrow d$.
For the $\Delta^{++}$:

$$
\begin{aligned}
\Delta C^{J_P^{(u)}}_{\Delta^{++}\bar{\Delta}^{++}}(x) &= \epsilon_{a_1b_1c_1}\epsilon_{a_2b_2c_2}\sum_y \{ \\
&- 2\mathrm{Tr}[S_\ell^{T\,a_1\,a_2}(x|0)C\gamma_i S_\ell^{b_1\,b_2}(x|0)C\gamma_j]\,\mathrm{Tr}[P_+ P_{ij}^{3/2} S_\ell^{c_1\,c'}(x|y)(i\gamma_5)S_\ell^{c'\,c_2}(y|0)] \\
&- 2\mathrm{Tr}[S_\ell^{T\,a_1\,a_2}(x|0)C\gamma_i S_\ell^{b_1\,b'}(x|y)(i\gamma_5)S_\ell^{b'\,b_2}(y|0)C\gamma_j]\,\mathrm{Tr}[P_+ P_{ij}^{3/2} S_\ell^{c_1\,c_2}(x|0)] \\
&- 2\mathrm{Tr}[S_\ell^{T\,a_1\,a'}(x|y)(i\gamma_5)^T S_\ell^{T\,a'\,a_2}(y|0)C\gamma_i S_\ell^{b_1\,b_2}(x|0)C\gamma_j]\,\mathrm{Tr}[P_+ P_{ij}^{3/2} S_\ell^{c_1\,c_2}(x|0)] \\
&+ 4\mathrm{Tr}[S_\ell^{a_1\,b'}(x|0)P_+ P_{ij}^{3/2} S_\ell^{b_1\,a_2}(x|0)C\gamma_i S_\ell^{T\,c_1\,c'}(x|y)(i\gamma_5)^T S_\ell^{T\,c'\,c_2}(y|0)C\gamma_j] \\
&+ 4\mathrm{Tr}[S_\ell^{a_1\,b_2}(x|0)P_+ P_{ij}^{3/2} S_\ell^{b_1\,a'}(x|y)(i\gamma_5)S_\ell^{a'\,a_2}(y|0)C\gamma_i S_\ell^{T\,c_1\,c_2}(x|0)C\gamma_j] \\
&+ 4\mathrm{Tr}[S_\ell^{a_1\,b'}(x|y)(i\gamma_5)S_\ell^{b'\,b_2}(y|0)P_+ P_{ij}^{3/2} S_\ell^{b_1\,a_2}(x|0)C\gamma_i S_\ell^{T\,c_1\,c_2}(x|0)C\gamma_j]\,\}\,.
\end{aligned}
$$

$= -2\Big[$ 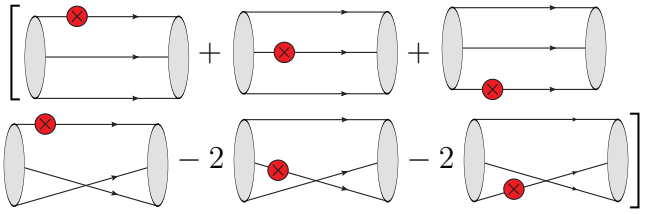 $\Big]$ ,

(C.65)

$$
\begin{aligned}
\Delta C^{J_S^{(u)}}_{\Delta^{++}\bar{\Delta}^{++}}(x) = \epsilon_{a_1b_1c_1}\epsilon_{a_2b_2c_2}\sum_y \{ \\
&- 2\mathrm{Tr}[S_\ell^{T\,a_1\,a_2}(x|0)C\gamma_i S_\ell^{\,b_1\,b_2}(x|0)C\gamma_j]\,\mathrm{Tr}[P_+P_{ij}^{3/2}S_\ell^{\,c_1\,c'}(x|y)S_\ell^{\,c'\,c_2}(y|0)] \\
&- 2\mathrm{Tr}[S_\ell^{T\,a_1\,a_2}(x|0)C\gamma_i S_\ell^{\,b_1\,b'}(x|y)S_\ell^{\,b'\,b_2}(y|0)C\gamma_j]\,\mathrm{Tr}[P_+P_{ij}^{3/2}S_\ell^{\,c_1\,c_2}(x|0)] \\
&- 2\mathrm{Tr}[S_\ell^{T\,a_1\,a'}(x|y)S_\ell^{T\,a'\,a_2}(y|0)C\gamma_i S_\ell^{\,b_1\,b_2}(x|0)C\gamma_j]\,\mathrm{Tr}[P_+P_{ij}^{3/2}S_\ell^{\,c_1\,c_2}(x|0)] \\
&+ 4\mathrm{Tr}[S_\ell^{\,a_1\,b'}(x|0)P_+P_{ij}^{3/2}S_\ell^{\,b_1\,a_2}(x|0)C\gamma_i S_\ell^{T\,c_1\,c'}(x|y)S_\ell^{T\,c'\,c_2}(y|0)C\gamma_j] \\
&+ 4\mathrm{Tr}[S_\ell^{\,a_1\,b_2}(x|0)P_+P_{ij}^{3/2}S_\ell^{\,b_1\,a'}(x|y)S_\ell^{\,a'\,a_2}(y|0)C\gamma_i S_\ell^{T\,c_1\,c_2}(x|0)C\gamma_j] \\
&+ 4\mathrm{Tr}[S_\ell^{\,a_1\,b'}(x|y)S_\ell^{\,b'\,b_2}(y|0)P_+P_{ij}^{3/2}S_\ell^{\,b_1\,a_2}(x|0)C\gamma_i S_\ell^{T\,c_1\,c_2}(x|0)C\gamma_j]\,\}\,.
\end{aligned}
\tag{C.66}
$$

$$= -2\Bigg[$$ 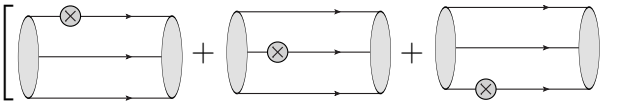 $$+$$  $$+$$ 

$$-2$$ 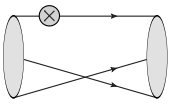 $$- 2$$ 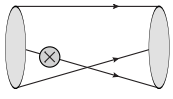 $$- 2$$ 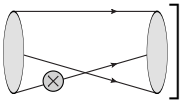 $$\Bigg] \quad ,$$

and

$$
\begin{aligned}
\Delta C^{T_\mu^{(u)}}_{\Delta^{++}\bar{\Delta}^{++}}(x) = \epsilon_{a_1b_1c_1}\epsilon_{a_2b_2c_2}\sum_y \{ \\
&- 2\mathrm{Tr}[S_\ell^{T\,a_1\,a_2}(x|0)C\gamma_i S_\ell^{\,b_1\,b_2}(x|0)C\gamma_j]\,\mathrm{Tr}[P_+P_{ij}^{3/2}S_\ell^{\,c_1\,c'}(x|y)(\Gamma_\mu^T)^T S_\ell^{\,c'\,c_2}(y|0)] \\
&- 2\mathrm{Tr}[S_\ell^{T\,a_1\,a_2}(x|0)C\gamma_i S_\ell^{\,b_1\,b'}(x|y)\Gamma_\mu^T S_\ell^{\,b'\,b_2}(y|0)C\gamma_j]\,\mathrm{Tr}[P_+P_{ij}^{3/2}S_\ell^{\,c_1\,c_2}(x|0)] \\
&- 2\mathrm{Tr}[S_\ell^{T\,a_1\,a'}(x|y)\Gamma_\mu^T S_\ell^{T\,a'\,a_2}(y|0)C\gamma_i S_\ell^{\,b_1\,b_2}(x|0)C\gamma_j]\,\mathrm{Tr}[P_+P_{ij}^{3/2}S_\ell^{\,c_1\,c_2}(x|0)] \\
&+ 4\mathrm{Tr}[S_\ell^{\,a_1\,b'}(x|0)P_+P_{ij}^{3/2}S_\ell^{\,b_1\,a_2}(x|0)C\gamma_i S_\ell^{T\,c_1\,c'}(x|y)\Gamma_\mu^T S_\ell^{T\,c'\,c_2}(y|0)C\gamma_j] \\
&+ 4\mathrm{Tr}[S_\ell^{\,a_1\,b_2}(x|0)P_+P_{ij}^{3/2}S_\ell^{\,b_1\,a'}(x|y)\Gamma_\mu^T S_\ell^{\,a'\,a_2}(y|0)C\gamma_i S_\ell^{T\,c_1\,c_2}(x|0)C\gamma_j] \\
&+ 4\mathrm{Tr}[S_\ell^{\,a_1\,b'}(x|y)(\Gamma_\mu^T)^T S_\ell^{\,b'\,b_2}(y|0)P_+P_{ij}^{3/2}S_\ell^{\,b_1\,a_2}(x|0)C\gamma_i S_\ell^{T\,c_1\,c_2}(x|0)C\gamma_j]\,\}\,.
\end{aligned}
\tag{C.67}
$$

$$= -2\Bigg[$$ 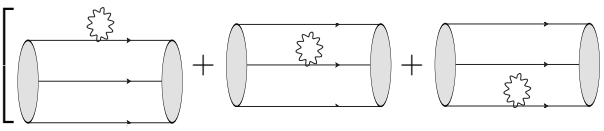

$$-2$$ 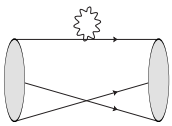 $$- 2$$ 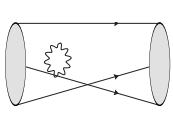 $$- 2$$ 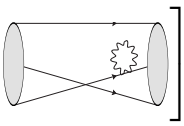 $$\Bigg] \quad ,$$

$$\Delta C^{J_\mu^{(s)} J_\nu^{(s)}}_{\Delta^{++}\bar{\Delta}^{++}}(x) = \epsilon_{a_1 b_1 c_1}\epsilon_{a_2 b_2 c_2} \sum_{y,z} D_{\mu\nu}(y|z)\,\{$$

$$\begin{aligned}
&- 2\mathrm{Tr}[S_\ell^{T\,a_1\,a_2}(x|0) C\gamma_i S_\ell^{b_1\,b_2}(x|0) C\gamma_j]\,\mathrm{Tr}[P_+ P_{ij}^{3/2} S_\ell^{c_1\,c'}(x|y)\Gamma_\mu^V S_\ell^{c',c''}(y|z)\Gamma_\nu^V S_\ell^{c''\,c_2}(z|0)]\\
&- 2\mathrm{Tr}[S_\ell^{T\,a_1\,a_2}(x|0) C\gamma_i S_\ell^{b_1\,b'}(x|y)\Gamma_\mu^V S_\ell^{b',b''}(y|z)\Gamma_\nu^V S_\ell^{b''\,b_2}(z|0) C\gamma_j]\,\mathrm{Tr}[P_+ P_{ij}^{3/2} S_\ell^{c_1\,c_2}(x|0)]\\
&- 2\mathrm{Tr}[S_\ell^{T\,a_1\,a'}(x|y)(\Gamma_\mu^V)^T S_\ell^{a',a''}(y|z)(\Gamma_\nu^V)^T S_\ell^{T\,a''\,a_2}(z|0) C\gamma_i S_\ell^{b_1\,b_2}(x|0) C\gamma_j]\,\mathrm{Tr}[P_+ P_{ij}^{3/2} S_\ell^{c_1\,c_2}(x|0)]\\
&+ 4\mathrm{Tr}[S_\ell^{a_1\,b'}(x|0) P_+ P_{ij}^{3/2} S_\ell^{b_1\,a_2}(x|0) C\gamma_i S_\ell^{T\,c_1\,c'}(x|y)(\Gamma_\mu^V)^T S_\ell^{T\,c',c''}(y|z)(\Gamma_\nu^V)^T S_\ell^{T\,c''\,c_2}(z|0) C\gamma_j]\\
&+ 4\mathrm{Tr}[S_\ell^{a_1\,b_2}(x|0) P_+ P_{ij}^{3/2} S_\ell^{b_1\,a'}(x|y)\Gamma_\mu^V S_\ell^{a',a''}(y|z)\Gamma_\nu^V S_\ell^{a''\,a_2}(z|0) C\gamma_i S_\ell^{T\,c_1\,c_2}(x|0) C\gamma_j]\\
&+ 4\mathrm{Tr}[S_\ell^{a_1\,b'}(x|y)\Gamma_\mu^V S_\ell^{b',b''}(y|z)\Gamma_\nu^V S_\ell^{b''\,b_2}(z|0) P_+ P_{ij}^{3/2} S_\ell^{b_1\,a_2}(x|0) C\gamma_i S_\ell^{T\,c_1\,c_2}(x|0) C\gamma_j]\,\}\,.
\end{aligned}$$

$$= -2\Bigg[ \quad + \quad + \quad + \quad + \quad + \quad$$

$$- 2 \quad - 2 \quad - 2 \quad - 2 \quad -2 \quad - 2 \quad .$$

(C.68)

Moreover by symmetry we have:

$$\begin{aligned}
&\Delta C^{J_P^{(u)}}_{\Delta^{++}\bar{\Delta}^{++}} = \Delta C^{J_P^{(d)}}_{\Delta^{-}\bar{\Delta}^{-}} = \\
&3\,\Delta C^{J_P^{(d)}}_{\Delta^{+}\bar{\Delta}^{+}} = 3\,\Delta C^{J_P^{(u)}}_{\Delta^{0}\bar{\Delta}^{0}} = (3/2)\,\Delta C^{J_P^{(u)}}_{\Delta^{+}\bar{\Delta}^{+}} = (3/2)\,\Delta C^{J_P^{(d)}}_{\Delta^{0}\bar{\Delta}^{0}}
\end{aligned} \tag{C.69}$$

$$\begin{aligned}
&\Delta C^{J_S^{(u)}}_{\Delta^{++}\bar{\Delta}^{++}} = \Delta C^{J_S^{(d)}}_{\Delta^{-}\bar{\Delta}^{-}} = \\
&3\,\Delta C^{J_S^{(d)}}_{\Delta^{+}\bar{\Delta}^{+}} = 3\,\Delta C^{J_S^{(u)}}_{\Delta^{0}\bar{\Delta}^{0}} = (3/2)\,\Delta C^{J_S^{(u)}}_{\Delta^{+}\bar{\Delta}^{+}} = (3/2)\,\Delta C^{J_S^{(d)}}_{\Delta^{0}\bar{\Delta}^{0}}
\end{aligned} \tag{C.70}$$

$$\begin{aligned}
&\Delta C^{T_\mu^{(u)}}_{\Delta^{++}\bar{\Delta}^{++}} = \Delta C^{T_\mu^{(d)}}_{\Delta^{-}\bar{\Delta}^{-}} = \\
&3\,\Delta C^{T_\mu^{(d)}}_{\Delta^{+}\bar{\Delta}^{+}} = 3\,\Delta C^{T_\mu^{(u)}}_{\Delta^{0}\bar{\Delta}^{0}} = (3/2)\,\Delta C^{T_\mu^{(u)}}_{\Delta^{+}\bar{\Delta}^{+}} = (3/2)\,\Delta C^{T_\mu^{(d)}}_{\Delta^{0}\bar{\Delta}^{0}}
\end{aligned} \tag{C.71}$$

# Appendix D

# Pseudo-Bayesian fit

In this section is described how the least-squares fit were implemented in the analysis. We use Bayes theorem [3] in order to find which quantity must be minimized to estimate the free parameters of the fit. The idea is to consider the measured values of the observables and the parameters as independent random variables. As such, we think to the fit as a way of maximizing the *posterior function*, i.e. the probability density function (p.d.f) of getting such parameters given the measured data. In our case the latter are the values extracted from the lattice simulation.
Let's consider a set of observables $y_i$ (with $i = 1, ..., N$) which are function of one or more variables $\vec{x}_i$ (with $\vec{x}_i = (x_i^1, ...., x_i^v)$). The former can be different observables, more points corresponding to the same one, or both. We write the functional relation as

$$y_i = g(\vec{x}_i, \vec{p}) \quad , \tag{D.1}$$

where $\vec{p}$ is the vector of parameters. Note that there's no formal distintion between the $y_i$ and the $\vec{x}_i$, so that we could also write:

$$G(y_i, \vec{x}_i, \vec{p}) = 0 \tag{D.2}$$

Let's now suppose we have a set of measured (or simulated) points $\hat{y}_i$, $\hat{\vec{x}}_i$, with uncertainties $\sigma_{\hat{y}_i}$, $\vec{\sigma}_{\hat{\vec{x}}_i} = (\sigma_{\hat{x}_i^1}, ..., \sigma_{\hat{x}_i^v})$.
Bayes' theorem states that if $f(A|B)$ denotes the p.d.f. of obtaining the result $A$ given $B$, then we have

$$\begin{aligned} f(\vec{p}, y_i, \vec{x}_i | \hat{y}_i, \hat{\vec{x}}_i) &\propto f(\hat{y}_i, \hat{\vec{x}}_i \,|\, \vec{p}, y_i, \vec{x}_i) \;\times\; f(\vec{p}, y_i, \vec{x}_i) \\ &= f(\hat{y}_i | y_i)\, f(\hat{\vec{x}}_i | \vec{x}_i) \;\times\; f(y_i | \vec{x}_i, \vec{p}) f_1(\vec{x}_i) f_2(\vec{p}) \quad . \end{aligned} \tag{D.3}$$

$f(\vec{p}, y_i, \vec{x}_i | \hat{y}_i, \hat{\vec{x}}_i)$ is the p.d.f. that the theoretical values of the independent variables are the $\vec{x}_i$, the ones of the dependent observable are the $y_i$ and that they are reproduced with the ansatz of eq. (D.1) by the parameters $\vec{p}$.
In the second step we used the following observations. For the first term, we note that the $y_i$ and $\vec{x}_i$ are statistically independent variables. Moreover, they are the true values of the measured variables $\hat{y}_i$ and $\hat{\vec{x}}_i$. The latter depend only on the true values, so that the dependence on $\vec{p}$ is removed. In the second term we used Bayes' theorem again, together with the independence between $\hat{\vec{x}}_i$ and $\vec{p}$. The densities $f_1$ and $f_2$ are the "a priori" probability distributions respectively for the $\hat{\vec{x}}_i$ and $\vec{p}$.

We assume the number of points is large enough to approximate the distribution of the measured values with a Gaussian, and impose the functional relation on the true values. In the end we obtain:

$$f(\vec{p}, y_i, \vec{x}_i|\hat{y}_i, \hat{\vec{x}}_i) \propto \exp\left(-\sum_i \frac{(y_i - \hat{y}_i)^2}{\sigma^2_{\hat{y}_i}}\right) \exp\left(-\sum_{i,j} \frac{(x_i^j - \hat{x}_i^j)^2}{\sigma^2_{\hat{x}_i^j}}\right) \times \delta\left(y_i - g(\vec{x}_i, \vec{p})\right) f_1(\vec{x}_i) f_2(\vec{p}) \quad . \tag{D.4}$$

Integrating over all possible values of $y_i$ and $\vec{x}_i$ we obtain the posterior:

$$f(\vec{p}\,|\,\hat{y}_i, \hat{\vec{x}}_i) = \int dy_i d\vec{x}_i f(\vec{p}, y_i, \vec{x}_i|\hat{y}_i, \hat{\vec{x}}_i) \propto \int d\vec{x}_i \exp\left(-\sum_i \frac{(g(\vec{x}_i, \vec{p}) - \hat{y}_i)^2}{\sigma^2_{\hat{y}_i}}\right) \exp\left(-\sum_{i,j} \frac{(x_i^j - \hat{x}_i^j)^2}{\sigma^2_{\hat{x}_i^j}}\right) f_1(\vec{x}_i) f_2(\vec{p}) \quad . \tag{D.5}$$

At this point we should find the $\vec{p}$ that maximizes the above integral. However, instead of solving explicitly this problem, we choose to do the following assumptions. The "a priori" distributions $f_1$ and $f_2$ are supposed to be sufficiently flat in the interval inside which we look for the parameters, so we replace them with constant values. The integrand is replaced everywhere by its maximum value. In practice, what we want to find are the $\vec{p}$ and $\vec{x_i}$ such that the integrand is maximized. This is the same as finding the minimum of:

$$\chi^2 = \sum_i \frac{(g(\vec{x}_i, \vec{p}) - \hat{y}_i)^2}{\sigma^2_{\hat{y}_i}} + \sum_{i,j} \frac{(x_i^j - \hat{x}_i^j)^2}{\sigma^2_{\hat{x}_i^j}} \quad . \tag{D.6}$$

Note that now $\vec{p}$ and $\vec{x}_i$ are on the same footage, being free parameters of the minimization.
The second term in the above equation can be omitted only in the limit $\sigma_{\hat{x}_i^j} \to 0\,, \forall\, i, j$. In this case the second Gaussian in eq. (D.4) is proportional to a delta function, and the quantity to be minimized is:

$$\chi^2 = \sum_i \frac{(g(\hat{\vec{x}}_i, \vec{p}) - \hat{y}_i)^2}{\sigma^2_{\hat{y}_i}} \quad . \tag{D.7}$$

Furthermore in the particular case of a linear ansatz,

$$y_i = a + \sum_j b_j\, x_i^j \quad , \tag{D.8}$$

the integration in (D.5) can be done explicitly, and the function to be minimized is:

$$\chi^2 = \sum_i \frac{(a + \sum_j b_j\, \hat{x}_i^j - \hat{y}_i)^2}{\sigma^2_{\hat{y}_i} + \sum_j b_j^2\, \sigma^2_{\hat{x}_i^j}} \quad . \tag{D.9}$$

The above $\chi^2$ values are given by the sum of squares of $N_{tot}$ random variables following a normal distribution with expectation values 0 and variance 1. Among them, $\nu = N_{tot} - N_{pars}$ are independent, where $N_{pars}$ is the number of parameters in the ansatz. Therefore these are distributed according to a $\chi^2$-distribution with $\nu$ degrees of freedom [114, 115]. In the analysis we write $\chi^2_{d.o.f.} = \chi^2/\nu$ to denote the reduced chi-squared.

# Bibliography


[1] Michael E Peskin and Daniel V Schroeder. *An Introduction to Quantum Field Theory (Boulder, CO*. 1995 (cit. on pp. 2, 7, 9, 13, 19–21, 25, 29, 31, 50, 56, 60).

[2] Leonard S Kisslinger and Debasish Das. "A brief review of dark matter". In: *International Journal of Modern Physics A* 34.27 (2019), p. 1930013 (cit. on p. 2).

[3] Particle Data Group et al. "Review of Particle Physics". In: *Progress of Theoretical and Experimental Physics* 2020.8 (Aug. 2020). 083C01. ISSN: 2050-3911. DOI: 10.1093/ptep/ptaa104. eprint: https://academic.oup.com/ptep/article-pdf/2020/8/083C01/34673722/ptaa104.pdf. URL: https://doi.org/10.1093/ptep/ptaa104 (cit. on pp. 3, 50, 73, 89, 98, 149).

[4] Andrzej Czarnecki, William J Marciano, and Alberto Sirlin. "Precision measurements and CKM unitarity". In: *Physical Review D* 70.9 (2004), p. 093006 (cit. on p. 3).

[5] I S Towner and J C Hardy. "The evaluation of $V_{ud}$ and its impact on the unitarity of the Cabibbo-Kobayashi-Maskawa quark-mixing matrix". In: *Reports on Progress in Physics* 73.4 (Mar. 2010), p. 046301. DOI: 10.1088/0034-4885/73/4/046301. URL: https://doi.org/10.1088/0034-4885/73/4/046301 (cit. on p. 3).

[6] A. Sirlin. "Radiative corrections to $G_V/G_\mu$ in simple extensions of the SU(2) × U(1) gauge model". In: *Nuclear Physics B* 71.1 (1974), pp. 29–51. ISSN: 0550-3213. DOI: https://doi.org/10.1016/0550-3213(74)90254-5. URL: https://www.sciencedirect.com/science/article/pii/0550321374902545 (cit. on p. 3).

[7] Christof Gattringer and Christian Lang. *Quantum chromodynamics on the lattice: an introductory presentation*. Vol. 788. Springer Science & Business Media, 2009 (cit. on pp. 3, 19, 20, 24, 26–30, 34, 45, 46, 105, 138).

[8] A Duncan, E Eichten, and H Thacker. "Electromagnetic splittings and light quark masses in lattice QCD". In: *Physical review letters* 76.21 (1996), p. 3894 (cit. on pp. 3, 133).

[9] GM de Divitiis et al. "Real photon emissions in leptonic decays". In: *arXiv preprint arXiv:1908.10160* (2019) (cit. on p. 3).

[10] D Giusti et al. "First lattice calculation of the QED corrections to leptonic decay rates". In: *Physical review letters* 120.7 (2018), p. 072001 (cit. on p. 3).

[11] CT Sachrajda et al. "Radiative corrections to semileptonic decay rates". In: *arXiv preprint arXiv:1910.07342* (2019) (cit. on p. 3).

[12] G. M. de Divitiis et al. "Leading isospin breaking effects on the lattice". In: *Phys. Rev. D* 87 (11 June 2013), p. 114505. DOI: 10.1103/PhysRevD.87.114505. URL: https://link.aps.org/doi/10.1103/PhysRevD.87.114505 (cit. on pp. 3, 49, 56, 58, 62, 126, 128, 135, 136).

[13] N Carrasco et al. "Up, down, strange and charm quark masses with Nf= 2+ 1+ 1 twisted mass lattice QCD". In: *Nuclear Physics B* 887 (2014), pp. 19–68 (cit. on pp. 5, 58, 81, 93, 99, 100, 102, 125, 126, 128, 129, 131).

[14] Steven Weinberg. *The quantum theory of fields. Vol. 1: Foundations*. Cambridge University Press, 1995 (cit. on pp. 8, 30).

[15] Rafael de la Madrid. "The role of the rigged Hilbert space in quantum mechanics". In: *European Journal of Physics* 26.2 (Feb. 2005), pp. 287–312. DOI: 10.1088/0143-0807/26/2/008. URL: https://doi.org/10.1088/0143-0807/26/2/008 (cit. on p. 8).

[16] Gert Roepstorff. *Path integral approach to quantum physics: an introduction*. Springer Science & Business Media, 2012 (cit. on p. 11).

[17] Joseph Polchinski. *String theory: Volume 1, an introduction to the bosonic string*. Cambridge university press, 1998 (cit. on p. 12).

[18] JC Yoon. "CPT Symmetry and The Equality of Mass and Lifetime". In: *arXiv preprint hep-ph/0503220* (2005) (cit. on pp. 15, 33).

[19] Sylvie Braibant, Giorgio Giacomelli, and Maurizio Spurio. *Particles and fundamental interactions: an introduction to particle physics*. Springer Science & Business Media, 2011 (cit. on p. 16).

[20] Thomas Mannel. "Theory and phenomenology of CP violation". In: *Nuclear Physics-Section B-PS-Proceedings Supplements* 167 (2007), pp. 115–119 (cit. on p. 16).

[21] Roberto D Peccei and Helen R Quinn. "CP conservation in the presence of pseudoparticles". In: *Physical Review Letters* 38.25 (1977), p. 1440 (cit. on p. 16).

[22] Kenneth G. Wilson. "Confinement of quarks". In: *Phys. Rev. D* 10 (8 Oct. 1974), pp. 2445–2459. DOI: 10.1103/PhysRevD.10.2445. URL: https://link.aps.org/doi/10.1103/PhysRevD.10.2445 (cit. on pp. 17, 22).

[23] Rüdiger Achilles and Andrea Bonfiglioli. "The early proofs of the theorem of Campbell, Baker, Hausdorff, and Dynkin". In: *Archive for history of exact sciences* 66.3 (2012), pp. 295–358 (cit. on p. 20).

[24] F. Bloch and A. Nordsieck. "Note on the Radiation Field of the Electron". In: *Phys. Rev.* 52 (2 July 1937), pp. 54–59. DOI: 10.1103/PhysRev.52.54. URL: https://link.aps.org/doi/10.1103/PhysRev.52.54 (cit. on p. 25).

[25] Toichiro Kinoshita. "Mass Singularities of Feynman Amplitudes". In: *Journal of Mathematical Physics* 3.4 (1962), pp. 650–677. DOI: 10.1063/1.1724268. eprint: https://doi.org/10.1063/1.1724268. URL: https://doi.org/10.1063/1.1724268 (cit. on p. 25).

[26] T. D. Lee and M. Nauenberg. "Degenerate Systems and Mass Singularities". In: *Phys. Rev.* 133 (6B Mar. 1964), B1549–B1562. DOI: 10.1103/PhysRev.133.B1549. URL: https://link.aps.org/doi/10.1103/PhysRev.133.B1549 (cit. on p. 25).

[27] Guido Martinelli et al. "A general method for non-perturbative renormalization of lattice operators". In: *Nuclear Physics B* 445.1 (1995), pp. 81–105 (cit. on p. 26).

[28] KG Chetyrkin and A Retey. "Renormalization and running of quark mass and field in the regularization invariant and MS schemes at three and four loops". In: *Nuclear Physics B* 583.1-2 (2000), pp. 3–34 (cit. on p. 26).

[29] JA Gracey. "Three loop anomalous dimension of non-singlet quark currents in the RI' scheme". In: *Nuclear Physics B* 662.1-2 (2003), pp. 247–278 (cit. on p. 26).

[30] Benoit Blossier et al. "Renormalisation constants of quark bilinears in lattice QCD with four dynamical Wilson quarks". In: *arXiv preprint arXiv:1112.1540* (2011) (cit. on p. 27).

[31] Martha Constantinou et al. "Non-perturbative renormalization of quark bilinear operators with N f= 2 (tmQCD) Wilson fermions and the tree-level improved gauge action". In: *Journal of High Energy Physics* 2010.8 (2010), p. 68 (cit. on p. 27).

[32] Roberto Frezzotti et al. "Lattice QCD with a chirally twisted mass term". In: *Journal of High Energy Physics* 2001.08 (2001), p. 058 (cit. on p. 27).

[33] Timothy H Boyer. "Conserved currents, renormalization, and the ward identity". In: *Annals of Physics* 44.1 (1967), pp. 1–10. ISSN: 0003-4916. DOI: https://doi.org/10.1016/0003-4916(67)90261-8. URL: https://www.sciencedirect.com/science/article/pii/0003491667902618 (cit. on p. 27).

[34] Marco Bochicchio et al. "Chiral symmetry on the lattice with Wilson fermions". In: *Nuclear Physics B* 262.2 (1985), pp. 331–355. ISSN: 0550-3213. DOI: https://doi.org/10.1016/0550-3213(85)90290-1. URL: https://www.sciencedirect.com/science/article/pii/0550321385902901 (cit. on p. 27).

[35] M Crisafulli, V Lubicz, and A Vladikas. "Improved renormalization of lattice operators: A critical reappraisal". In: *The European Physical Journal C-Particles and Fields* 4.1 (1998), pp. 145–171 (cit. on p. 27).

[36] T Reisz and HJ Rothe. "Renormalization of lattice gauge theories with massless Ginsparg–Wilson fermions". In: *Nuclear Physics B* 575.1-2 (2000), pp. 255–266 (cit. on p. 27).

[37] PV Ruuskanen and NA Törnqvist. "Unitarity constraints on resonance mixing and the Okubo-Zweig-Iizuka rule". In: *Il Nuovo Cimento A (1965-1970)* 48.4 (1978), pp. 446–460 (cit. on pp. 29, 40).

[38] C. Alexandrou et al. "Baryon spectrum withNf=2+1+1twisted mass fermions". In: *Physical Review D* 90.7 (Oct. 2014). ISSN: 1550-2368. DOI: 10.1103/physrevd.90.074501. URL: http://dx.doi.org/10.1103/PhysRevD.90.074501 (cit. on p. 29).

[39] M. Benmerrouche, R. M. Davidson, and Nimai C. Mukhopadhyay. "Problems of describing spin-(3/2 baryon resonances in the effective Lagrangian theory". In: *Phys. Rev. C* 39 (6 June 1989), pp. 2339–2348. DOI: 10.1103/PhysRevC.39.2339. URL: https://link.aps.org/doi/10.1103/PhysRevC.39.2339 (cit. on p. 30).

[40] Jiunn-Wei Chen et al. "Symmetry properties of nonlocal quark bilinear operators on a Lattice". In: *Chin. Phys. C* 43.10 (2019), p. 103101. DOI: 10.1088/1674-1137/43/10/103101. arXiv: 1710.01089 [hep-lat] (cit. on p. 31).

[41] Palash B Pal. "Dirac, majorana, and weyl fermions". In: *American Journal of Physics* 79.5 (2011), pp. 485–498 (cit. on p. 31).

[42] L. Maiani and M. Testa. "Final state interactions from euclidean correlation functions". In: *Physics Letters B* 245.3 (1990), pp. 585–590. ISSN: 0370-2693. DOI: https://doi.org/10.1016/0370-2693(90)90695-3. URL: http://www.sciencedirect.com/science/article/pii/0370269390906953 (cit. on p. 32).

[43] Shoichi Sasaki. *N* Spectrum in Lattice QCD*. 2000. arXiv: hep-ph/0004252 [hep-ph] (cit. on p. 33).

[44] Frank X. Lee and Derek B. Leinweber. "Negative-parity baryon spectroscopy". In: *Nuclear Physics B - Proceedings Supplements* 73.1-3 (Mar. 1999), pp. 258–260. ISSN: 0920-5632. DOI: 10.1016/s0920-5632(99)85041-5. URL: http://dx.doi.org/10.1016/S0920-5632(99)85041-5 (cit. on p. 33).

[45] S. Romiti and S. Simula. "Extraction of multiple exponential signals from lattice correlation functions". In: *Phys. Rev. D* 100 (5 Sept. 2019), p. 054515. DOI: 10.1103/PhysRevD.100.054515. URL: https://link.aps.org/doi/10.1103/PhysRevD.100.054515 (cit. on p. 34).

[46] G Peter Lepage. "Lattice QCD for novices". In: *Strong Interactions at Low and Intermediate Energies* (1998), pp. 49–90 (cit. on pp. 40, 43).

[47] István Montvay. "Numerical simulation with light Wilson-quarks". In: *Strong and Electroweak Matter 2002*. World Scientific, 2003, pp. 317–321 (cit. on p. 40).

[48] H. Leutwyler. "Chiral perturbation theory". In: *Scholarpedia* 7.10 (2012). revision #138476, p. 8708. DOI: 10.4249/scholarpedia.8708 (cit. on p. 41).

[49] A. Hasenfratz et al. "Goldstone bosons and finite size effects: A numerical study of the O(4) model". In: *Nuclear Physics B* 356.1 (1991), pp. 332–363. ISSN: 0550-3213. DOI: https://doi.org/10.1016/0550-3213(91)90153-O. URL: https://www.sciencedirect.com/science/article/pii/055032139190153O (cit. on p. 42).

[50] M. Luscher. "Volume Dependence of the Energy Spectrum in Massive Quantum Field Theories. 1. Stable Particle States". In: *Commun. Math. Phys.* 104 (1986), p. 177. DOI: 10.1007/BF01211589 (cit. on pp. 42, 56).

[51] M. Luscher. "Volume Dependence of the Energy Spectrum in Massive Quantum Field Theories. 2. Scattering States". In: *Commun. Math. Phys.* 105 (1986), pp. 153–188. DOI: 10.1007/BF01211097 (cit. on pp. 42, 43).

[52] B. Pozsgay and G. Takacs. "Form-factors in finite volume I: Form-factor bootstrap and truncated conformal space". In: *Nucl. Phys. B* 788 (2008), pp. 167–208. DOI: 10.1016/j.nuclphysb.2007.06.027. arXiv: 0706.1445 [hep-th] (cit. on p. 42).

[53] B. Pozsgay and G. Takacs. "Form factors in finite volume. II. Disconnected terms and finite temperature correlators". In: *Nucl. Phys. B* 788 (2008), pp. 209–251. DOI: 10.1016/j.nuclphysb.2007.07.008. arXiv: 0706.3605 [hep-th] (cit. on p. 42).

[54] Thomas A Degrand and Carleton DeTar. *Lattice methods for quantum chromodynamics*. World Scientific, 2006 (cit. on pp. 42, 43).

[55] Gilberto Colangelo, Stephan Dürr, and Christoph Haefeli. "Finite volume effects for meson masses and decay constants". In: *Nuclear Physics B* 721.1-3 (2005), pp. 136–174 (cit. on pp. 42, 87).

[56] Claude W. Bernard. "Feynman rules for gauge theories at finite temperature". In: *Phys. Rev. D* 9 (12 June 1974), pp. 3312–3320. DOI: 10.1103/PhysRevD.9.3312. URL: https://link.aps.org/doi/10.1103/PhysRevD.9.3312 (cit. on p. 42).

[57] Fernando Romero-López et al. "Relativistic N-particle energy shift in finite volume". In: *Journal of High Energy Physics* 2021.2 (2021), pp. 1–52 (cit. on p. 43).

[58] G. Peter Lepage. "The Analysis of Algorithms for Lattice Field Theory". In: *Theoretical Advanced Study Institute in Elementary Particle Physics*. June 1989 (cit. on p. 44).

[59] Michael L Wagman. "Statistical Angles on the Lattice QCD Signal-to-Noise Problem". In: *arXiv preprint arXiv:1711.00062* (2017) (cit. on p. 44).

[60] Stephan Güsken. "A study of smearing techniques for hadron correlation functions". In: *Nuclear Physics B - Proceedings Supplements* 17 (1990), pp. 361–364. ISSN: 0920-5632. DOI: https://doi.org/10.1016/0920-5632(90)90273-W. URL: https://www.sciencedirect.com/science/article/pii/092056329090273W (cit. on p. 45).

[61] M. A. Clark and R. Babich. "High-efficiency Lattice QCD computations on the Fermi architecture". In: *2012 Innovative Parallel Computing (InPar)*. 2012, pp. 1–9. DOI: 10.1109/InPar.2012.6339591 (cit. on p. 45).

[62] M Foster, Christopher Michael, UKQCD collaboration, et al. "Quark mass dependence of hadron masses from lattice QCD". In: *Physical Review D* 59.7 (1999), p. 074503 (cit. on pp. 46, 132).

[63] Gerard LG Sleijpen, Henk A Van der Vorst, and Diederik R Fokkema. "BiCGstab (l) and other hybrid Bi-CG methods". In: *Numerical Algorithms* 7.1 (1994), pp. 75–109 (cit. on p. 46).

[64] Peter Young. "Jackknife and bootstrap resampling methods in statistical analysis to correct for bias". In: *Statistical Science* 11 (1996), pp. 189–228 (cit. on p. 47).

[65] Avery McIntosh. "The Jackknife estimation method". In: *arXiv preprint arXiv:1606.00497* (2016) (cit. on p. 47).

[66] Gilberto Colangelo et al. "Review of lattice results concerning low-energy particle physics". In: *The European Physical Journal C* 71.7 (2011), pp. 1–76 (cit. on p. 49).

[67] GM De Divitiis et al. "Isospin breaking effects due to the up-down mass difference in lattice QCD". In: *Journal of High Energy Physics* 2012.4 (2012), pp. 1–30 (cit. on pp. 49, 50, 61, 131).

[68] Nazario Tantalo. *Isospin Breaking Effects on the Lattice*. 2013. arXiv: 1311.2797 [hep-lat] (cit. on pp. 49, 53).

[69] Heinz J Rothe. *Lattice Gauge Theories: An Introduction Third Edition*. Vol. 74. World Scientific Publishing Company, 2005 (cit. on p. 51).

[70] Roberto Frezzotti and Giancarlo Rossi. "Chirally improving Wilson fermions 2. Four-quark operators". In: *Journal of High Energy Physics* 2004.10 (2004), p. 070 (cit. on pp. 52, 82).

[71] Martha Constantinou et al. "B K-parameter from N f= 2 twisted mass lattice QCD". In: *Physical Review D* 83.1 (2011), p. 014505 (cit. on p. 52).

[72] Sz Borsanyi et al. "Ab initio calculation of the neutron-proton mass difference". In: *Science* 347.6229 (2015), pp. 1452–1455 (cit. on pp. 52, 57, 121).

[73] Remi Baron et al. "Light meson physics from maximally twisted mass lattice QCD". In: *Journal of High Energy Physics* 2010.8 (2010), pp. 1–41 (cit. on pp. 53, 81).

[74] Heinz Neudecker Jan R. Magnus. *Matrix differential calculus with applications in statistics and econometrics*. Rev. ed. Wiley Series in Probability and Statistics. John Wiley, 1999. ISBN: 9780471986324; 0471986321; 047198633X; 9780471986331 (cit. on p. 54).

[75] J Gasser and GRS Zarnauskas. "On the pion decay constant". In: *Physics Letters B* 693.2 (2010), pp. 122–128 (cit. on p. 56).

[76] Shumpei Uno and Masashi Hayakawa. "QED in Finite Volume and Finite Size Scaling Effect on Electromagnetic Properties of Hadrons". In: *Progress of Theoretical Physics* 120.3 (Sept. 2008), pp. 413–441. ISSN: 0033-068X. DOI: 10.1143/PTP.120.413. eprint: https://academic.oup.com/ptp/article-pdf/120/3/413/5203205/120-3-413.pdf. URL: https://doi.org/10.1143/PTP.120.413 (cit. on pp. 56, 57).

[77] Zohreh Davoudi and Martin J Savage. "Finite-volume electromagnetic corrections to the masses of mesons, baryons, and nuclei". In: *Physical Review D* 90.5 (2014), p. 054503 (cit. on pp. 56, 57, 115).

[78] E. Hilf and L. Polley. "NOTE ON THE CONTINUUM THERMAL WILSON LOOP WITH SPACE PERIODIC BOUNDARY CONDITIONS". In: *Phys. Lett. B* 131 (1983), pp. 412–414. DOI: 10.1016/0370-2693(83)90529-4 (cit. on p. 57).

[79] Z. Fodor et al. "Quantum electrodynamics in finite volume and nonrelativistic effective field theories". In: *Physics Letters B* 755 (2016), pp. 245–248. ISSN: 0370-2693. DOI: https://doi.org/10.1016/j.physletb.2016.01.047. URL: https://www.sciencedirect.com/science/article/pii/S0370269316000642 (cit. on p. 57).

[80] Sinya Aoki et al. "Perturbative renormalization factors of bilinear quark operators for improved gluon and quark actions in lattice QCD". In: *Physical Review D* 58.7 (1998), p. 074505 (cit. on p. 58).

[81] Chris Bouchard et al. "On the Feynman-Hellmann theorem in quantum field theory and the calculation of matrix elements". In: *Physical Review D* 96.1 (2017), p. 014504 (cit. on p. 60).

[82] Arjun Singh Gambhir. "Disconnected Diagrams in Lattice QCD". PhD thesis. The College of William and Mary, 2017 (cit. on p. 62).

[83] Roger Dashen. "Chiral SU(3) $\bigotimes$ SU(3) as a Symmetry of the Strong Interactions". In: *Phys. Rev.* 183 (5 July 1969), pp. 1245–1260. DOI: 10.1103/PhysRev.183.1245. URL: https://link.aps.org/doi/10.1103/PhysRev.183.1245 (cit. on p. 62).

[84] Dao-Neng Gao, Mu-Lin Yan, and Bing-An Li. "Dashen's theorem and electromagnetic masses of the mesons". In: *arXiv preprint hep-ph/9612258* (1996) (cit. on p. 62).

[85] Véronique Bernard, Ulf-G Meißner, and Akaki Rusetsky. "The $\Delta$-resonance in a finite volume". In: *Nuclear physics B* 788.1-2 (2008), pp. 1–20 (cit. on p. 73).

[86] G. Ecker. "The Pion - nucleon interaction as an effective field theory". In: *Chin. J. Phys.* 32 (1994), pp. 1303–1316. arXiv: hep-ph/9407240 (cit. on p. 74).

[87] Steven C. Pieper et al. "Realistic models of pion-exchange three-nucleon interactions". In: *Physical Review C* 64.1 (June 2001). ISSN: 1089-490X. DOI: 10.1103/physrevc.64.014001. URL: http://dx.doi.org/10.1103/PhysRevC.64.014001 (cit. on p. 74).

[88] Bao-Jun Cai et al. "Critical density and impact of $\Delta(1232)$ resonance formation in neutron stars". In: *Physical Review C* 92.1 (July 2015). ISSN: 1089-490X. DOI: 10.1103/physrevc.92.015802. URL: http://dx.doi.org/10.1103/PhysRevC.92.015802 (cit. on p. 74).

[89] A. Mucke et al. "On photohadronic processes in astrophysical environments". In: *Publ. Astron. Soc. Austral.* 16 (1999), p. 160. DOI: 10.1071/AS99160. arXiv: astro-ph/9808279 (cit. on p. 74).

[90] Y. Iwasaki. "Renormalization group analysis of lattice theories and improved lattice action: Two-dimensional non-linear O(N) sigma model". In: *Nuclear Physics B* 258 (1985), pp. 141–156. ISSN: 0550-3213. DOI: https://doi.org/10.1016/0550-3213(85)90606-6. URL: https://www.sciencedirect.com/science/article/pii/0550321385906066 (cit. on p. 81).

[91] Y Iwasaki. "Renormalization group analysis of lattice theories and improved lattice action: two-dimensional non-linear O (N) sigma model". In: *Nuclear Physics B* 258 (1985), pp. 141–156 (cit. on p. 81).

[92] Roberto Frezzotti et al. "Reducing cutoff effects in maximally twisted LQCD close to the chiral limit". In: *Journal of High Energy Physics* 2006.04 (2006), p. 038 (cit. on p. 82).

[93] Gilbert Colangelo and Stephan Dürr. "The pion mass in finite volume". In: *The European Physical Journal C-Particles and Fields* 33.4 (2004), pp. 543–553 (cit. on p. 87).

[94] Gilberto Colangelo and Andreas Fuhrer. "Finite volume effects for nucleon and heavy meson masses". In: *Physical Review D* 82.3 (2010), p. 034506 (cit. on pp. 88, 96).

[95] V Bernard et al. "The mass of the $\Delta$ resonance in a finite volume: fourth-order calculation". In: *Journal of High Energy Physics* 2009.06 (2009), p. 061 (cit. on p. 89).

[96] Alexander Semke and MFM Lutz. "Quark-mass dependence of the baryon ground-state masses". In: *Physical Review D* 85.3 (2012), p. 034001 (cit. on p. 89).

[97] Matthias FM Lutz et al. "Finite volume effects in the chiral extrapolation of baryon masses". In: *Physical Review D* 90.5 (2014), p. 054505 (cit. on p. 89).

[98] A. Semke and M. F. M. Lutz. "Baryon self energies in the chiral loop expansion". In: *Nucl. Phys. A* 778 (2006), pp. 153–180. DOI: 10.1016/j.nuclphysa.2006.07.043. arXiv: nucl-th/0511061 (cit. on p. 89).

[99] Szabolcs Borsanyi et al. "High-precision scale setting in lattice QCD". In: *JHEP* 09 (2012), p. 010. DOI: 10.1007/JHEP09(2012)010. arXiv: 1203.4469 [hep-lat] (cit. on p. 90).

[100] Constantia Alexandrou et al. "Low-lying baryon spectrum with two dynamical twisted mass fermions". In: *Physical Review D* 80.11 (2009), p. 114503 (cit. on pp. 95, 97).

[101] Constantia Alexandrou et al. "Light baryon masses with dynamical twisted mass fermions". In: *Physical Review D* 78.1 (2008), p. 014509 (cit. on pp. 96, 132).

[102] J. Martin Camalich, L. S. Geng, and M. J. Vicente Vacas. "Lowest-lying baryon masses in covariant SU(3)-flavor chiral perturbation theory". In: *Phys. Rev. D* 82 (7 Oct. 2010), p. 074504. DOI: 10.1103/PhysRevD.82.074504. URL: https://link.aps.org/doi/10.1103/PhysRevD.82.074504 (cit. on pp. 96, 98).

[103] J. Gasser, H. Leutwyler, and M.E. Sainio. "Sigma-term update". In: *Physics Letters B* 253.1 (1991), pp. 252–259. ISSN: 0370-2693. DOI: https://doi.org/10.1016/0370-2693(91)91393-A. URL: https://www.sciencedirect.com/science/article/pii/037026939191393A (cit. on p. 96).

[104] Luis Alvarez-Ruso et al. "Nucleon mass and pion-nucleon sigma term from a chiral analysis of lattice QCD data". In: *Physical Review D* 88.5 (2013), p. 054507 (cit. on p. 96).

[105] IP Cavalcante et al. "Pion-$\Delta$ $\sigma$-term". In: *Physical Review C* 72.6 (2005), p. 065207 (cit. on p. 98).

[106] Anastassios Vladikas. "Three topics in renormalization and improvement". In: *Les Houches Summer School: Session* 93 (2011), pp. 161–222 (cit. on p. 104).

[107] Andrea Shindler. "Twisted mass lattice QCD". In: *Physics Reports* 461.2-3 (2008), pp. 37–110 (cit. on p. 105).

[108] A. B. Gridnev et al. "The K-matrix approach to the Delta - resonance mass splitting and isospin violation in low-energy pi-N scattering". In: *Phys. Atom. Nucl.* 69 (2006), pp. 1542–1551. DOI: 10.1134/S1063778806090122. arXiv: hep-ph/0408192 (cit. on p. 122).

[109] V. B. Ganenko et al. "INVESTIGATION OF PHOTOPRODUCTION OF POSITIVE PIONS ON DEUTERIUM. (IN RUSSIAN)". In: *Yad. Fiz.* 29 (1979), pp. 565–571 (cit. on p. 122).

[110] Roberto Frezzotti, Giancarlo Rossi, and Nazario Tantalo. "Sea quark QED effects and twisted mass fermions". In: *arXiv preprint arXiv:1612.02265* (2016) (cit. on p. 129).

[111] R Frezzotti et al. "First direct lattice calculation of the chiral perturbation theory low-energy constant *ell_7*". In: *arXiv preprint arXiv:2107.11895* (2021) (cit. on p. 129).

[112] Constantia Alexandrou et al. "Quark masses using twisted mass fermion gauge ensembles". In: *arXiv preprint arXiv:2104.13408* (2021) (cit. on p. 129).

[113] D Giusti et al. "Leading isospin-breaking corrections to pion, kaon, and charmed-meson masses with twisted-mass fermions". In: *Physical Review D* 95.11 (2017), p. 114504 (cit. on pp. 133, 136).

[114] Henry Scheffé. "H. Cramér, Mathematical methods of statistics". In: *Bulletin of the American Mathematical Society* 53.7 (1947), pp. 733–735 (cit. on p. 150).

[115] Alan Stuart, Maurice G Kendall, et al. *The advanced theory of statistics*. Griffin, 1963 (cit. on p. 150).